Stable Strontium Isotope Fractionation in Marine and Terrestrial Environments

By
Emily Isabel Stevenson
St John's College

June 2012

Supervised by K.W Burton, I.J Parkinson

Department of Earth Sciences
University of Oxford
Oxford

The thesis submitted for the degree of Doctor of Philosophy to the University of Oxford

Both strontium and strontianite are named after Strontian, a village in Scotland near which the mineral was first discovered

Stable Strontium Isotope Fractionation in Marine and Terrestrial Environments

Emily I Stevenson

St John's College Oxford

Trinity Term 2012

The work reported in this thesis applies a new isotope tracer, stable strontium isotopes ($\delta^{88/86}Sr$), to address questions concerning changes in global climate that occur in response to continental weathering processes, and to constrain the modern marine geochemical Sr cycle.

Stable Sr isotopes are a relatively new geochemical proxy, and as such their behaviour needs to be understood in differing forms of marine calcium carbonate, the archives from which records of past stable Sr variability in the oceans can be constructed. Foraminifera, coccoliths and corals (both aragonite and high Mg calcite) acquire $\delta^{88/86}Sr$ values lighter than that of modern day seawater, (approximately 0.11, 0.05, 0.2 and 0.19 ‰ lighter than seawater at ~25°C respectively) providing a measureable offset which can be used to constrain the modern Sr outputs from the ocean and provide a better understanding of the modern Sr cycle.

Using foraminifera as a sedimentary archive the first marine $\delta^{88/86}Sr$ record of seawater over the last two glacial cycles has been constructed, and used to investigate changing carbonate input and output over this 145 kyr period. Modelling of the large excursion of $\delta^{88/86}Sr$ to heavier values during Marine Isotope Stage (MIS) 3, reveals that this is more likely to be due to local changes in seawater or post-depositional alteration, rather then whole ocean changes.

In the terrestrial environment $\delta^{88/86}Sr$ has been measured in the dissolved load of rivers from the Himalaya. It is found that, in general, rivers draining carbonate catchments possess lighter isotopic $\delta^{88/86}Sr$ values than those from rivers draining silicates. Covariations of either $\delta^{88/86}Sr$ vs. $\delta^{30}Si$ or $\delta^{88/86}Sr$ vs. 1/[Sr] can be used to distinguish between rivers draining different catchment areas.

Stable Strontium Isotope Fractionation in Marine and Terrestrial Environments

Emily I Stevenson

St John's College Oxford

Trinity Term 2012

This thesis discusses the application of a new geochemical tracer, stable strontium isotopes, to investigate if this system can be used to provide new information on key geological processes such as continental weathering and the variation in the balance of silicate to carbonate input to the oceans both today and in the past. This is important because the weathering of silicate rocks leads to the net drawdown of carbon dioxide, a greenhouse gas, from the atmosphere into the oceans, over million year time scales, and has consequences for the global carbon cycle.

The mass dependent fractionation of stable strontium isotopes has only recently begun to be developed due, principally, to analytical advances in mass spectrometry, the relative mass deference between two of the stable Sr isotopes studied here (^{88}Sr and ^{86}Sr) is small and observable variation requires measurements at the parts per million level. The combination of thermal ionisation mass spectrometry (TIMS) and double-spike (DS) techniques used in the analysis of samples in this thesis allows these small variations to be resolved.

The marine radiogenic strontium isotope record ($^{87}Sr/^{86}Sr$) is the most commonly used proxy record to constrain the geologic history of chemical weathering variations over time. This is recorded in marine sedimentary records, and is thought reflect either changes in the balance of continental weathering relative to input from hydrothermal exchange at mid-ocean ridges over time. However, interpretations of changes in continental weathering using the radiogenic strontium geochemical cycle is problematic because changes in the input flux cannot be

distinguished from changes in composition, and the extent of removal accompanying carbonate sedimentation cannot be readily quantified. Stable strontium isotopes ($\delta^{88/86}$Sr) precipitated in marine carbonates have been shown to be lighter than that of seawater (Fietzke and Eisenhauer, 2006) providing a measureable Sr output from the oceans, enabling the completion of Sr mass balance equations and providing better constraints on the Sr geochemical cycle. This thesis builds on this initial finding to explore the degree of mass dependent $\delta^{88/86}$Sr fractionation from seawater into modern marine biogenic calcites, specifically in different species of foraminifera (chapter three) and coccolithophores (chapter five), and also, but to a lesser extent, in corals (both high Mg calcite and aragonite; chapter two), and offsets in $\delta^{88/86}$Sr of approximately 0.02, 0.05, 0.19 and 0.20 ‰ at ~25°C, respectively, have been determined. An attempt was made to quantify $\delta^{88/86}$Sr fractionation from seawater in inorganically precipitated calcite, however, it was not possible to complete this part of the project and this is summarised in appendix 7.

Investigating the influences of temperature on the fractionation of $\delta^{88/86}$Sr in marine calcium carbonates suggests there is little variability in the planktic foraminifera *G. sacculifer* (samples from core-tops in the South Atlantic ocean; $\delta^{88/86}$Sr ~0.09 ‰; temperature range of ~18-28 °C) whereas coccolithophores (culture study) show a strong negative correlation with temperature (range of 10-25 °C) and growth-rate, consistent with a kinetic isotope fractionation of Sr aquo-complexes. The aragonitic corals analysed, precipitated in the ocean at either 26 or 4 °C, are statistically indistinguishable from each other suggesting little temperature dependence, however more data are required to complete this finding. These results contribute to the on-going scientific research into the processes of biomineralisation and how such organisms incorporate trace metals and isotopes into marine calcium carbonate, specifically the results conclude that $\delta^{88/86}$Sr in coccolithophores can be used as a proxy for growth-rate.

The investigations of $\delta^{88/86}$Sr variation in different species of modern foraminifera illustrate that choice of shell size in planktonic foraminifera is a practical issue of importance in the design or methodological procedures for paleoceanographic work, and care should be made to choose a single size fraction taken from a single species. Where using one species is not possible it would be best to pick from the smaller size fraction where inter species offsets appear to be smaller (c.f. 250-355μm).

Today the $\delta^{88/86}$Sr value of seawater is ~0.38‰ but has this varied in the past? If so, are variations in seawater composition observed on glacial time periods, perhaps in response to increases in carbonate weathering from sea-level low stands, as has been suggested by Krabbenhöft et al., (2010). Chapter four presents a record of $\delta^{88/86}$Sr preserved in the tests of the foraminifera *Globigerinoides ruber* over the past 145 kyr; and an excursion of ~120ppm to heavier $\delta^{88/86}$Sr values in MIS 3 is found, however there is little variation associated with glacial growth and/or retreat. A simple model of $\delta^{88/86}$Sr variation over the last glacial cycle, incorporating a three-fold increase in shelf carbonate weathering, suggests that $\delta^{88/86}$Sr is insensitive to changes in input over glacial-interglacial time periods; therefore the interpretation of the excursion lends its self to potential post-depositional diagenetic alteration.

Constraining the balance of carbonate to silicate weathering is important for determining the contribution of weathering to the long-term drawdown of carbon dioxide from the atmosphere. By investigating $\delta^{88/86}$Sr variability in the dissolved load of rivers in the Himalaya, draining both silicate, carbonate and mixed carbonate and silicate lithologies, the potential of stable strontium isotopes to be used as tracers of weathering processes has been investigated. The Himalaya is an active orogeny and notorious for having a complex weathering regime, made difficult to interpret with traditional weathering proxies such radiogenic Sr isotopes and elemental (metal/Ca) ratios due to regional metamorphism and the

non-conservative behaviour of Ca. In this preliminary study it is found that rivers draining carbonate catchments acquire lighter isotopic $\delta^{88/86}Sr$ values ($\delta^{88/86}Sr = 0.26\pm0.2$) than those from river draining silicates $\delta^{88/86}Sr = 0.34\pm0.1$).

There is a strong seasonal shift of $\delta^{88/86}Sr$ to heavier values after the monsoon that is less pronounced in the silicate catchments. Some of the small variations we observe between monsoonal seasons may be caused by input from precipitation, groundwater, vegetation or the precipitation of secondary mineral phases, but each of these reservoirs and minerals needs to be fully characterised. However, preliminary data suggests that through the use of plots of either $\delta^{88/86}Sr$ vs. $\delta^{30}Si$ or $\delta^{88/86}Sr$ vs. 1/[Sr] it may be possible to distinguish between different rivers draining different catchment areas, allowing $\delta^{88/86}Sr$ isotopes to be used as a tracer of weathering processes when combined with other elemental or isotope techniques.

The results from this thesis have greatly improved our knowledge of stable Sr isotope behaviour in a variety of marine carbonates, both in the modern ocean and in the past. This information has contributed detail both on biomineralisation of Sr and Ca as well as helping to constrain the geochemical cycle of Sr by allowing the Sr carbonate output of the oceans to be constrained. This is important so that correct interpretations can be made on the relative contributions of silicate and carbonate weathering from the continents to the oceans both today and in the past and may, in the future, help constrain interpretations of carbon drawdown from the atmosphere due to chemical weathering.

Acknowledgements

Firstly I would like to thank Kevin and Ian. Thank you for putting your faith in a chemist, you have both given me a great amount of your time, experience and support, great advice both in and out of the laboratory and helped me understand new concepts and theories, all of which I am truly grateful for. You have both been inspirational and I hope I will do you both proud in the future.

A big thank you to my co-supervisors; Ros Rickaby for welcoming me into her research group and her helpful feedback, Pallavi Anand who helped me see that foraminifera were so much more than just 'microscopic pop-corn', Eric Oelkers in Toulouse, as well as Gideon Henderson who helped me out in my final year.

For either providing samples, data or helping with analytical work I'd like to thank Fatima Mokadem, Chris Pearce, Michael Hermoso, Allison Stephenson-Haus, Therese Flaathen-Loe, Ed Hathorne, Rachael James, Başak Kisakürek, Tristan Horner, Bastian Georg, Steve Wyatt, Philip Pogge Von Strandmann, Philip Holdshop, Geoff Nowell, Sam Hammond and Jon Tyler. Chelsea, my partner in stable strontium, amazeballs.

To my colleagues at the University of Oxford both past and present who have always been helpful, supportive, there to write a letter of recommendation when I needed it or gladly initiating me into the incredibly social side of geochemistry: Helen Williams, Julie Prytulak, Chris Siebert, Alex Thomas, Ros Armytage, Alex Halliday, Katie Egan, Laura Gregory, Giovanni Fontana and Dave Cook. Also, to other members of the departmental support staff, TOILET-, Ocean BUG- and Climotope- groups, Thermo engineers and lab managers, you've certainly made the last four years insightful and amusing and I thank you.

The completion of a successful University of Oxford D.Phil. would not be possible without a more than healthy work-life balance; to that extent I'll miss the well-trodden path from the

department to the Lamb and Flag, 340 m (2008-2010) 440 m (2010-2012). The location of many celebrations, commiserations, group meetings and BGC ‘gossips’ as Herr Moso would put it.

Aisha and Jodi; for all the parties, great weekends and the times you listened to me; you guys have been the best friends, flatmates and inspirational colleagues, I hope we end up in the same department again some day.

Tristan, Al, and Phil; I have thoroughly enjoyed our scientific discussions just as much as the late night ones in the PT. You always took the time to help me out when I was stuck or confused and were never condescending about my lack of geological background; I am truly thankful and will miss you (and the burrito club) when I’m gone.

Chris Pearce, you helped me out more than you can ever know in Toulouse, not only are you thoughtful, selfless and kind you are a great laugh and friend too. I have thoroughly enjoyed your company wherever we’ve been in the world; I cannot think of a greater person, thank you.

I would also like to thank my two examiners Conall Mac Niocaill and Derek Vance for a thoroughly stimulating and dare I say it, enjoyable, viva and for their constructive feedback.

Finally this Thesis is dedicated to Paul and my parents who have felt the brunt of my emotional attachment to this project, from anguish and despair to excitement and elation. It is a triumph of human patience (and tolerance) on your behalf that has really me seen through this past four years. Thank you.

This work has been supported by the Natural Environmental Research Council.

Glad to be part of ‘The Oxford Isotope Laboratory for Earth Tracers’, Iceland, 2010. Left to right: Dr R. Armytage, E.I. Stevenson, Dr L. Gall, Dr C. R. Pearce, Dr J. Prytulak, Dr P. S. Savage, K. Hibbert.

CHAPTER ONE

Introduction

Summary

The work reported in this thesis is concerned with the isotope fractionation between two of the four stable isotopes of the element Strontium, ^{86}Sr and ^{88}Sr. The following chapter outlines the concepts of isotope behaviour, and the mechanisms by which fractionation can occur. Studies of the isotope composition of radiogenic strontium ($^{87}Sr/^{86}Sr$) in a range of terrestrial reservoirs have highlighted the potential for the Sr isotope system for yielding information on global weathering processes and chronology. However, the radiogenic $^{87}Sr/^{86}Sr$ isotope ratio has limitations in its use for interpreting the global Sr cycle, some of which can potentially be overcome by utilising the ratios of two other stable strontium isotopes ($^{88}Sr/^{86}Sr$), which additionally reveal information on carbonate precipitation and dissolution in the oceans. Studies using Sr stable isotopes are relatively new, made possible by improvements in high-precision mass spectrometry techniques. In this regard a brief review of the different analytical techniques used to measure stable Sr isotopes is given, with particular emphasis on the application of TIMS-double-spike technique.

1.1 Isotope fractionation

Isotope geochemistry is an area of geology that utilises the relative and absolute concentrations of elements and their isotopes in the Earth and Solar System. Atoms comprise of a dense central nucleus of positively charged protons and electrically neutral neutrons surrounded by a cloud of negatively charged electrons. Each atom is classified on the basis of the number of protons and neutrons in its nucleus; the number of protons determines the chemical element, and the number of neutrons determines the isotope of the element. Measurements of the variations in the abundance of isotopes of a given element can provide an insight into chemical processes; from revealing the ages of rocks and providing tracers for geochemical cycles, to the details of chemical reactions. In terms of the isotopes themselves the field of isotope geochemistry uses both stable and radiogenic isotopes with respect to the processes by which the isotopes are fractionated and formed. Stable isotope geochemistry is concerned with variations of the isotope compositions of elements arising from physicochemical processes whilst radiogenic isotope geochemistry is largely concerned with nuclear processes.

1.1.1 Stable isotope fractionation

Many elements have more than one isotope, and the small differences in the relative abundance between the isotopes of a given element results in variations that can act as informative tracers of geological processes. Stable isotopes are thought to fractionate via kinetic or equilibrium processes; in general equilibrium isotope effects arise from the difference in vibrational energies between isotopes (Urey, 1947) whereas kinetic isotope fractionation generally arises from the difference in velocities of the isotopes. Fractionation between two isotopes can be thought of as a chemical reaction in which isotopes can be

exchanged between different phases containing the same element, for example in the isotopic exchange reaction of carbon dioxide and the bicarbonate ion:

$$^{13}CO_2 + H^{12}CO_3^- \leftrightarrow {}^{12}CO_2 + H^{13}CO_3^- \qquad [1.1]$$

$$K_{eq} = \frac{\left[{}^{12}CO_2\right]\left[H^{13}CO_3^-\right]}{\left[{}^{13}CO_2\right]\left[H^{12}CO_3^-\right]} \qquad [1.2]$$

In this reaction isotopic equilibrium is reached when there is a balance between the rate of the forward and backward reactions. If either CO_2 or HCO_3^{2-} accepted ^{13}C or ^{12}C without discrimination K_{eq} should equal 1 (unity). However in practice we find K_{eq} in this reaction is slightly greater than 1 implying that there is a preference for ^{12}C to be bound in CO_2 and ^{13}C to be bound in HCO_3^{2-}. The difference in the behaviour between heavy and light isotopes is a quantum mechanical phenomenon that arises from the vibrational energy of connecting atoms and the bond that joins them. In a simple model (the Harmonic Oscillator), consider a diatomic molecule (e.g. H_2) where two atoms are held together via a chemical bond, each atom is subject to combined attractive and repulsive forces from the other such that they vibrate around their position at rest. There is an optimum rest distance between the two atoms, which is a trade off between the attractive and repulsive forces, that defines a minimum point in a Potential Energy well, known as the zero point energy (ZPE):

$$ZPE = \tfrac{1}{2}h\nu \qquad [1.3]$$

As the bond contracts and expands around the rest position due to the combined attractive and repulsive forces, the potential energy of the bond increases in discrete quanta (energy levels) as the bond length between the atoms increases or decreases until the bond is broken (dissociation of the atoms). The energy of the bond is related to the vibrational frequency, *v*,

of the bond is dependent on the mass of the atoms as shown below, where *h* is Planks constant and the vibrational energy, *v*:

$$v = \frac{1}{2\pi}\sqrt{\frac{k}{\mu}} \qquad [1.4]$$

and μ is the reduced mass (m_1 and m_2 are the masses of the isotopes 1 and 2 respectively) given by:

$$\mu = \frac{m_1 m_2}{m_1 + m_2} \qquad [1.5]$$

this illustrates that the vibrational frequency of an atom is related to its mass. Heavier isotopes have a larger mass and therefore a lower vibrational energy. When the heavier isotope of an element replaces that of the lighter in a molecule during an exchange reaction (see equation 1.1) the overall energy of the molecule decreases as there is a small increase in mass (from the heavier isotope); this decreases the overall vibrational energy of the molecule forming a stronger bond. This is sometimes referred to as the Rule of Bigeleisen (1965) whereby the heavier isotope goes preferentially into the compound with the stronger bonds; in the case of equation 1.1 this means that ^{13}C is preferentially bound in HCO_3^-. (For a more detailed description the readier is referred to the works of Urey, 1947)

Kinetic effects are usually associated with an array of unidirectional processes occurring under conditions of incomplete isotopic exchange in physical processes, for example diffusion, evaporation and freezing. At a given temperature, all the molecules in an ideal gas have the same average kinetic energy (*E*) that is a function of temperature (*T*), (note in this case v refers to velocity and not vibration and *k* is the Boltzmann constant):

$$E = \tfrac{3}{2}kT = \tfrac{1}{2}mv^2 \qquad [1.6]$$

The ratio of the velocities of the heavy and light isotopes (of the same element, v_1 and v_2) are related to their respected masses (m_1 and m_2) according to:

$$\frac{\sqrt{3kT/m_1}}{\sqrt{3kT/m_2}} = \frac{v_1}{v_2} \qquad [1.7]$$

At a given temperature, the velocity of the lighter isotopes is slightly faster than that of the heavier isotopes. This leads to physical, kinetic isotope fractionation between different phases in a reaction. Differences in the bond strength between lighter or heavier isotopes bonded to a molecule also affect the kinetics of reactions. Since lighter isotopes form weaker bonds (higher vibrational energy) these molecules will react more readily and in a unidirectional process will be concentrated in the product which is another effective way of fractionating isotopes.

Isotope fractionations are the largest for light elements and for isotopes with large mass differences as the magnitude of fractionation is related by $(m_{heavy}-m_{light})/(m_{light}m_{heavy})$ often simplified to $\Delta m/m^2$ where m is the average atomic mass of the element. The fractionation between two isotopes is commonly given in the delta notation, δ, and in parts per thousand (mille; ‰).

$$\delta^{H/L}X = \left(\frac{\left({}^{H}X/{}^{L}X\right)_{sample}}{\left({}^{H}X/{}^{L}X\right)_{standard}} - 1 \right) \times 1000 \qquad [1.8]$$

where X is the element of interest and H and L are the heavy and light isotopes respectively. Note that stable isotopes are reported as normalized to a standard.

1.1.2 Radiogenic isotope variation

Isotopes can also be formed by radioactive decay of a parent isotope by a variety, or series, of different decay mechanisms that result in the loss of elementary particles to form new isotopes. The time it takes for one isotope to decay another is a statistically predictable process as the rate of decay is taken to be constant; this means that radiogenic isotopes can be used as a precise and accurate means for the measurement of time. Conversion of a parent isotope to a daughter isotope is described by the following equation;

$$-\frac{dN}{dt} = \lambda N \qquad [1.9]$$

where $-dN/dt$ is the nuclear decay rate, N is the total number of radioactive atoms present, and λ is the first-order decay constant in units of inverse time. Integration of this equation gives the classic first order decay equation

$$N = N_0 e^{-\lambda t} \qquad [1.10]$$

where N_0 is the decay constant for that nuclide. This equation allows the calculation of the total number of radioisotope atoms remaining after a given amount of time (t).

1.2. Strontium

Strontium (symbol Sr, atomic weight 87.62, atomic number 38) belongs to the family of divalent alkaline earth metals, so called as the oxides of elements in this group give basic alkaline solutions. It was so named after being discovered in the ores taken from lead mines in the Scottish village of Strontian, (see page ii). Strontium has four naturally occurring stable isotopes of ^{84}Sr, ^{86}Sr, ^{87}Sr and ^{88}Sr, and also has a radioactive isotope ^{90}Sr, which is formed as a by-product of nuclear fission.

1.2.1 Radiogenic strontium isotopes

The ^{87}Sr stable isotope also has a radiogenic component due to the beta decay of ^{87}Rb which has a half life of 48.8 byr (Faure and Mensing, 2005), this means that over time, in a given Rb and Sr bearing mineral, the concentration of ^{87}Sr will increase relative to the original ^{87}Sr value. The number of ^{87}Sr daughter atoms produced by the decay of ^{87}Rb in a rock or mineral since its formation *t* years ago is given by substitution into the radioactive decay equation (Equation 1.11):

$$^{87}Sr = {}^{87}Sr_i + {}^{87}Rb\,(e^{\lambda t} - 1) \qquad [1.11]$$

where $^{87}Sr_i$ is the number of ^{87}Sr atoms initially present. It is however difficult to measure precisely the absolute abundance of a given nuclide. Mass spectrometers can measure isotope ratios to very high accuracy and precision, and so it is more convenient to work with isotope ratios by dividing by the number of atoms of ^{86}Sr (which is a stable isotope and therefore remains constant with time).

$$(^{87}Sr/^{86}Sr)_p = (^{87}Sr/^{86}Sr)_i + (e^{\lambda t} - 1)\,(^{87}Rb/^{86}Sr) \qquad [1.12]$$

The present-day Sr isotope ratio $(^{87}Sr/^{86}Sr)_p$ is measured by mass spectrometry, and the $^{87}Rb/^{86}Sr$ ratio can be calculated from the measured concentrations of Rb and Sr. If the initial ratio $(^{87}Sr/^{86}Sr)_i$ is known or can be estimated then *t* can be determined, if it is assumed that the system has been closed to Rb and Sr mobility from the time *t* to the present.

The trace elements Rb and Sr are geochemically similar to the major elements K and Ca respectively, minerals with high Rb/Sr, and K/Ca ratios, (such as biotite or alkali feldspar) evolve to radiogenic $^{87}Sr/^{86}Sr$ isotope compositions over relatively short timescales (i.e. 10 Myr or less). Once released into the hydrosphere, Sr retains its isotope composition without significant fractionation by geochemical or biological processes. Rubidium is highly

incompatible during melting relative to Sr, consequently the Earth's mantle has a low Rb concentration relative to Sr, therefore, mantle-derived rocks have a very low Rb/Sr ratio and evolve to relatively unradiogenic $^{87}Sr/^{86}Sr$ compositions. In contrast continental rocks such as granites and shales are Rb-rich and evolve to higher ^{87}Sr concentrations over time and thus radiogenic $^{87}Sr/^{86}Sr$ ratios.

Many natural radiogenic isotopes in seawater are sensitive to changes in the balance of input from continental weathering (via rivers, groundwaters and aeolian input) against that from hydrothermal exchange at mid-ocean ridges, yielding information on both long- (millions of years: e.g. $^{87}Sr/^{86}Sr$) and short- (thousands of years: e.g. $^{187}Os/^{188}Os$) time scales (the reader is referred to the review by Frank (2002) for a more in-depth discussion of different radiogenic isotope systems). Of these, the rubidium-strontium (^{87}Rb-^{86}Sr) radiogenic isotope system is the most widely used and variations in seawater $^{87}Sr/^{86}Sr$ ratios on both long and short timescales are thought reflect changing continental input through time (e.g. Brass, 1976; Hess et al., 1986; Hoddell et al., 1990; Capo and DePaolo, 1990; Hodell et al., 2007). Consequently, variations in the $^{87}Sr/^{86}Sr$ isotope composition of seawater over time reflect changes the balance of input from the weathering of carbonate and silicate continental rocks, and that derived from hydrothermal exchange at mid-ocean ridges, as illustrated in Figure 1.1 (e.g. Palmer and Edmond, 1986). Strontium is present in the oceans at a concentration of approximately 90 μmol kg^{-1} with a residence time of ≥2.5 million years in the ocean (e.g. Hodell et al., 1990, Richter and Turekian 1993) which is long compared with the mixing rate of the ocean, ~10^3 years (e.g. Veizer, 1989). The modern-day $^{87}Sr/^{86}Sr$ value of seawater is 0.70917 (e.g. Vance et al. 2009; Allègre et al., 2010).

The average modern riverine $^{87}Sr/^{86}Sr$ has a value of 0.71144 (e.g. Vance et al., 2009) and largely reflects the input of Sr derived from continental weathering of carbonate and silicate rocks. Carbonate rocks typically possess lower $^{87}Sr/^{86}Sr$ ratios (0.708; Allègre et al., 2010)

similar to seawater values while silicate rocks typically have more radiogenic $^{87}Sr/^{86}Sr$ ratios (0.721; e.g. Allègre et al, 2010).

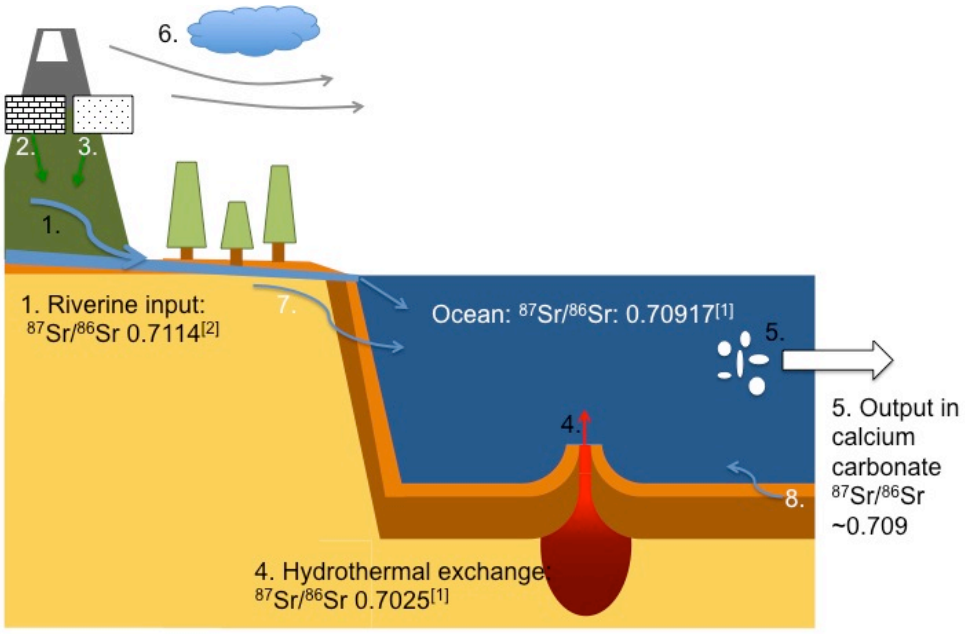

Figure 1.1. The radiogenic Sr cycle in the modern ocean showing the primary inputs: riverine (**1**) (which represents a balance of carbonate (**2**) $^{87}Sr/^{86}Sr$-=0.708[2] and silicate (**3**) $^{87}Sr/^{86}Sr$ =0.721[2] sources) and hydrothermal exchange (**4**) and the primary output of strontium via the precipitation of marine carbonates (5). There are also inputs associated with digenesis (**8**), ground water (**7**) as well as input from rain, dust, and melt water (**6**). $^{87}Sr/^{86}Sr$ values from [1] Allègre et al. (2010) and [2] Vance et al. (2009).

The hydrothermal input reflects Sr exchange with oceanic crustal rocks and these have a lower $^{87}Sr/^{86}Sr$ composition $^{87}Sr/^{86}Sr$ = 0.7025 (Vance et al., 2009), because their isotope composition reflects that of the mantle source, which has evolved to relatively unradiogenic compositions due to the preferential depletion of Rb relative to Sr over time (see above). The major output of Sr in the oceans is through precipitation in carbonate minerals, such as the shells and skeletons of marine calcifiers, in which it substitutes for calcium (Ca). More significantly, during the measurement of $^{87}Sr/^{86}Sr$ ratio, instrumental mass fractionation is corrected for via internal normalisation of the $^{87}Sr/^{86}Sr$ ratio to a fixed $^{88}Sr/^{86}Sr$ value of 8.375209 (Nier et al., 1938) removing any natural mass fractionation in the Sr isotope ratios.

Marine calcium carbonate $^{87}Sr/^{86}Sr$ ratios therefore directly record the seawater $^{87}Sr/^{86}Sr$ ratio from which they precipitated.

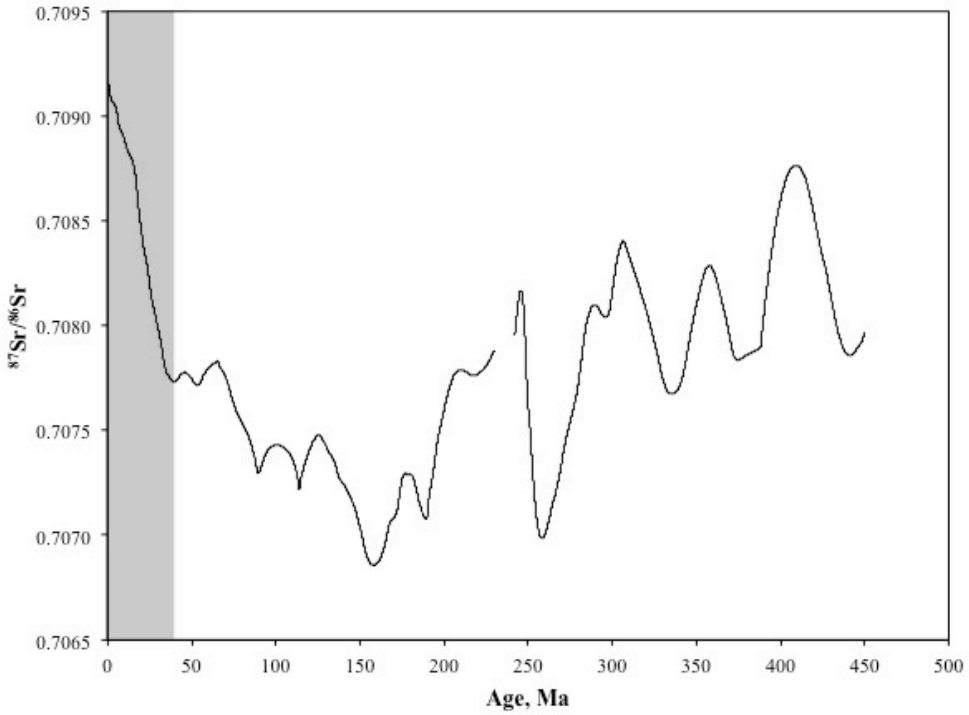

Figure 1.2 Marine $^{87}Sr/^{86}Sr$ record over the last 500 Myr, of which the Phanerozoic extends to 542 Myr. The shaded grey area highlights the last 40 Myr increase of Sr in the oceans to more radiogenic values. Sr curve constructed from the LOWESS 3 data set; McArthur et al. (2001)

The Phanerozoic $^{87}Sr/^{86}Sr$ isotope curve, Figure 1.2, is thought to reflect the evolution of Sr in the oceans from about 540 million years ago to the present (Burke et al., 1982; Veizer et al., 1989). In many cases, variations in the curve have been attributed to changes in the intensity of continental weathering that must have consequences for the consumption of CO_2 and global climate as the long-term weathering of silicate based rocks consumes atmospheric CO_2. Over the past 40 Myr the $^{87}Sr/^{86}Sr$ seawater record shows a monotonic and rapid increase and indicates a significant shift to more radiogenic values over the past 40 Myr, (highlighted area in Figure 1.2). This has been linked by some to intensified continental weathering caused by orogenesis, in particular uplift and weathering of the Himalaya-Tibet plateau commencing around 40 Ma (Raymo et al., 1988, Richter et al, 1992). While others

too have related this shift to the onset of glaciation in the Late Eocene (the transition from so-called 'greenhouse to icehouse conditions') resulting in an increase in both physical and chemical weathering rates (Armstrong, 1971; Hoddell et al., 1990; Blum and Erel, 1995). However, changes in the Sr isotope record cannot be simply used to quantitatively reconstruct the relationship between chemical weathering fluxes and climate. This is partly because the balance of continental and hydrothermal input to the oceans remains poorly constrained (e.g. Davis et al., 2003; Vance et al., 2009), but more significantly because it is rarely possible to distinguish changes caused by variations in the total flux of strontium to the oceans from those caused by variations in the isotope composition of riverine input (e.g. Richter et al., 1992; Derry and France-Lanord, 1996; Quade et al., 1997).

The $^{87}Sr/^{86}Sr$ composition of seawater is thus sensitive to the balance of Sr sources from the continent, which can very in flux and composition over time. However, for the $^{87}Sr/^{86}Sr$ ratio, marine carbonates have the same $^{87}Sr/^{86}Sr$ ratio as seawater therefore Sr output in oceanic carbonates is ignored (a zero term) with regard to $^{87}Sr/^{86}Sr$ evolution, although implicit in Sr mass balance, see equation 1.13).

$$\frac{dR_{SW}}{dt} = \left[\frac{JSr_{RIV}(R_{RIV} - R_{SW})}{Sr_{SW}}\right] + \left[\frac{JSr_{HYD}(R_{HYD} - R_{SW})}{Sr_{SW}}\right] + \left[\frac{JSr_{DIA}(R_{DIA} - R_{SW})}{Sr_{SW}}\right] - \left[\frac{JSr_{CARB}(R_{CARB} - R_{SW})}{Sr_{SW}}\right]$$

[1.13]

where J is the flux and R is the $^{87}Sr/^{86}Sr$ ratio of the riverine ($_{RIV}$), hydrothermal ($_{HYD}$) diagenetic ($_{DIA}$) input and carbonate ($_{CARB}$) outputs in the ocean with respect to the concentration of Sr in seawater (Sr_{SW}) over time. Secondly, as a consequence of the difficulty in constraining weathering intensity in the past, for example, due the release of radiogenic Sr from rapidly weathering mineral phases (Blum, 1995; Vance et al., 2009) and from carbonate bearing minerals with very radiogenic values in the Himalaya, Sr budgets from weathering

products cannot be quantitatively evaluated. Changes in the fluxes of continental weathering to the oceans over glacial-interglacial cycles in the Quaternary have been suggested to result in imbalances in oceanic Sr budgets forcing this element out of steady state (e.g. Vance et al., 2009). However, without any constraint on the Sr output flux in the oceans, interpretations are based on careful measurement of all the Sr inputs into the oceans, which remain the subject of debate. Potential uncertainties include the influence of glacial retreat (Vance et al., 2009), poorly constrained estimates for the flux of hydrothermal Sr input to the oceans (e.g. Davis et al., 2003), the role of arc-island weathering (Allègre et al., 2010), hydrothermal processes on the flanks of mid ocean ridges (Hess et al., 1991) and groundwater run-off (Basu et al., 2001).

It is clear that there are limitations in quantifying the Sr marine budget with just $^{87}Sr/^{86}Sr$ isotopes alone, therefore another method is required to assess the output fluxes and composition of Sr in the oceans.

1.2.2. Stable strontium isotopes

Traditionally utilised stable isotope systems are typically elements that have a low mass (i.e. mw <40, e.g. H, C and O isotope systems), as atomic number increases the degree of isotopic variation will decrease as the relative mass difference between the isotopes decreases. The small mass difference between ^{88}Sr and ^{86}Sr, 1.16% (calculated as $\Delta m/m$, see section 1.1.1) suggests that variations are likely to be small, requiring very high precision measurements to detect small changes in isotope composition. Conventionally the $^{88}Sr/^{86}Sr$ ratio is taken to be a constant ($^{88}Sr/^{86}Sr = 8.375209$) and used to correct for instrumental mass fractionation during the measurement of $^{87}Sr/^{86}Sr$ isotopic ratios. Internal normalisation enables the measurement of $^{87}Sr/^{86}Sr$ ratios to a very high precision. Nevertheless, stable Sr isotope

variations have been known to exist since the late 1970's. Nucleosynthetic variations in $^{84}Sr/^{86}Sr$ variations were found by Papanastassiou et al. (1978) in inclusions EK I-4-I and CI of the Allende chondritic meteorite. Patchett et al. (1980a) and Patchett et al. (1980b) discovered the first mass dependent $^{88}Sr/^{86}Sr$ variations, in chrondrules and refractory inclusions of the Allende meteorites, with the $^{88}Sr/^{86}Sr$ ratio depleted up to 2.8‰ when compared with bulk meteorites and terrestrial samples.

More recently Fietzke and Eisenhauer (2006) found a significant fractionation of $\delta^{88/86}Sr$ (Equation 1.14) accompanying precipitation of aragonitic $CaCO_3$ from seawater;

$$\delta^{88/86}Sr = \left(\frac{\left({}^{88}Sr/{}^{86}Sr \right)_{samp}}{\left({}^{88}Sr/{}^{86}Sr \right)_{standard}} - 1 \right) * 1000 \qquad [1.14]$$

this was observed in both natural warm water coral samples (*Pavona clavus*) and experimentally precipitated inorganic aragonite. This is a significant finding as it showed a measureable offset in stable strontium isotopes of marine carbonates to lighter values then seawater, a fractionation that is unable to be resolved using traditional $^{87}Sr/^{86}Sr$ isotopes (see section 1.2.1). Therefore, in principle, when $^{87}Sr/^{86}Sr$ and $\delta^{88/86}Sr$ data are taken together it is possible to assess all of the input and output fluxes of Sr in the ocean as shown in Equation 1.13.

As calcium carbonate is significantly lighter than seawater in $\delta^{88/86}Sr$ space it begs the question; have there been significant changes in the stable strontium isotope composition of seawater over time? Global changes in Sr inputs to, or outputs from, seawater could all have a significant affect on the $\delta^{88/86}Sr$ seawater value. For example, changes in the balance of silicate to carbonate weathering from the continents, changes in carbonate productivity and sedimentation in the oceans, or even changes in the flux of weathering of shelf carbonates

due to sea level low stands during glacial periods, could all change the $\delta^{88/86}$Sr composition of seawater. Section 1.3 discusses the possible applications of the $\delta^{88/86}$Sr proxy in the marine and terrestrial environment.

Since the work of Fietzke and Eisenhauer (2006) other carbonate samples and standards have been measured and shown to have a lighter isotopic composition than seawater, these data are summarized in Figure 1.3.

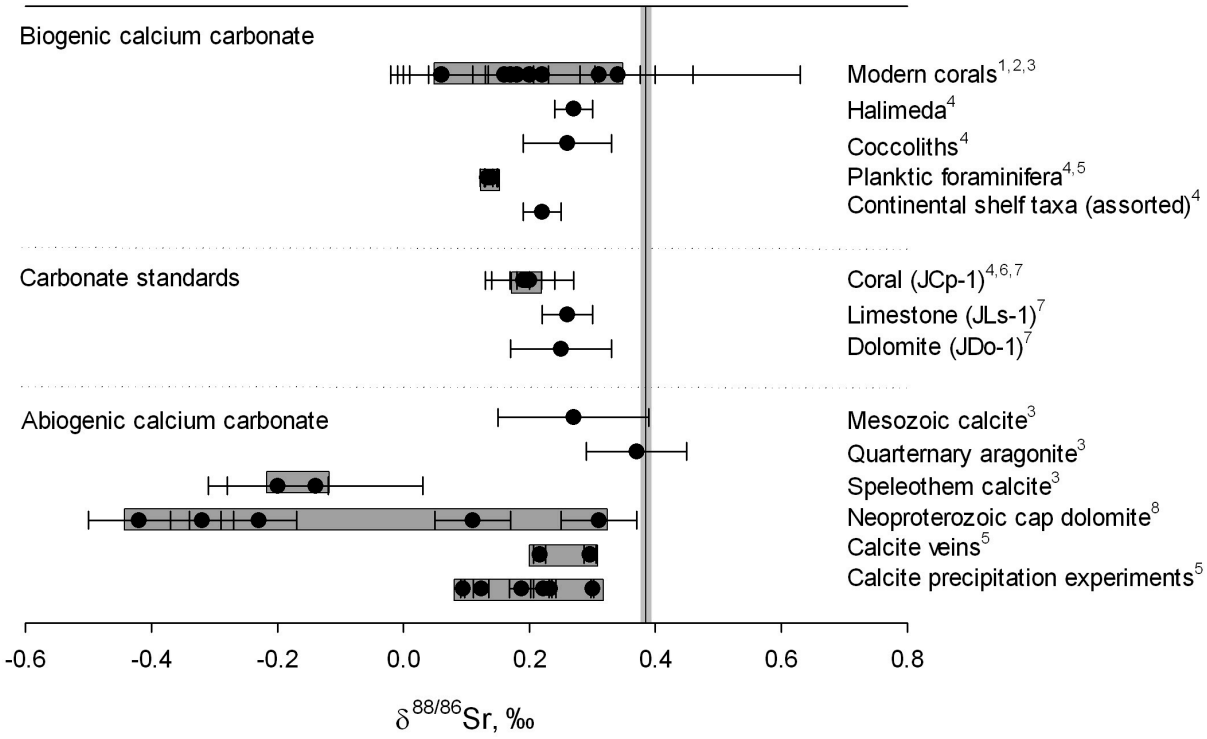

Figure 1.3. Range of stable strontium isotopes data in carbonates currently in the literature; [1] Fietzke and Eisenhauer, 2006; [2] Ruggeberg et al., 2008; [3] Halicz et al., 2008; [4] Krabbenhoft et al., 2010; [5] Bohm et al., 2012; [6] Ohno et al., 2008; [7] Ohno and Hirata, 2007. The IAPSO (seawater standard, grey band from Fietzke and Eisenhauer, 2006) is shown for reference.

1.3 The stable strontium isotope proxy; application to marine and terrestrial environments

Since the onset of this research project the investigation of the $\delta^{88/86}Sr$ proxy has led to its application not only in the marine environment (e.g. Fietzke and Eisenhauer 2006; Rüggeberg et al., 2008; Krabbenhöft et al., 2010, Böhm et al., 2012) but also in terrestrial (e.g. Halicz et al., 2008; Ohno et al., 2008; DeSouza et al., 2010) and extraterrestrial environments (Moynier et al., 2010; Chariler et al., 2012), as well as archeology (e.g. Knudson et al., 2010). However its application to extraterrestrial (high-temperature) processes is beyond the scope of this thesis and the reader is referred to the recent works of Moynier et al. (2011) and Charlier et al. (2012).

1.3.1 The marine environment

When dissolved Sr reaches the marine environment it largely follows Ca in its geochemical behavior; trace amounts of Sr are incorporated into the $CaCO_3$ shells and skeletons of marine calcifiers in place of Ca as they construct their shells/skeletons from seawater reflecting the external environment in which they lived enabling the construction of marine archives (as shown for the $^{87}Sr/^{86}Sr$ ratios in seawater).

Coccoliths, foraminifera and corals are commonly used as marine archives for paleoclimate reconstructions and quantification of marine conditions, such as temperature, salinity, nutrient content and pH. Fietzke and Eisenhauer (2006) observed the $\delta^{88/86}Sr$ fractionation from seawater in both the coral and inorganic aragonite to be temperature dependent; as temperature increased, $\delta^{88/86}Sr$ trended towards heavier values approaching that of seawater.

The biogenic coral exhibited a significantly greater (six-fold) temperature dependence than that seen in inorganic aragonite, suggesting a marked biological (vital) effect on the fractionation. A study by Rüggeberg et al. (2008) found a similar temperature dependence in the cold-water coral *Lophelia pertusa* and it was suggested that $\delta^{88/86}$Sr isotopes in corals could be used as a new proxy for reconstruction of intermediate ocean water temperatures. As stable strontium isotope ratios are fractionated from seawater in coral aragonite, we might expect to see a fractionation in other marine calcite archives. If stable strontium isotopes fractionate to a similar degree in foraminifera and coccolithophores we can use these marine calcifiers to construct the first marine records of changes in past seawater $\delta^{88/86}$Sr composition. In order to produce a faithful $\delta^{88/86}$Sr record of past ocean chemistry it is important to understand the controls on $\delta^{88/86}$Sr varies in a given archive i.e. how it may vary with growth rate (shell size), elucidate the nature of any temperature dependent fractionation and investigate if the $\delta^{88/86}$Sr ratio varies between different species.

Foraminifera are unicellular zooplankton found throughout the ocean, which develop shells (tests) generally made of calcareous material. Under favorable conditions, in the oceans, the tests are preserved as fossils, and have been present since Cambrian times making them ideal for use in the construction of tong-term marine records. Planktonic foraminiferal tests are composed of extremely pure calcite, typically about 99% by weight $CaCO_3$, with trace elements such as Mg, Sr, Ba and Cd comprising the remaining 1% (Lea, 1999). The distribution and abundance of planktonic foraminiferal species is strongly linked to surface water properties and thus different species have distinct temporal and geographic ranges. Chapter three of this thesis is concerned with the investigation of $\delta^{88/86}$Sr fractionation in foraminiferal calcite. Many studies (eg. Schmidt et al., 2003; Schmidt et al., 2004(a); Schmidt et al., 2004(b)) have shown that sea surface temperatures (SSTs) appear to be the most important factor controlling shell composition, diversity and shell size, therefore this is a key

parameter than needs to accounted for when investigating $\delta^{88/86}Sr$ behaviour in foraminiferal calcite.

Coccolithophores are a group of unicellular phytoplankton (algae), which, at some point in their life cycle, are covered in plates, knows as coccoliths. These are microscopic calcareous plates or disks, often oval and intricately patterned or ornamented. Calcitic coccoliths account for the greater part of oceanic carbonate sedimentation worldwide (Lowenstam and Weiner, 1989), and therefore play an important role in the output of Sr from the oceans and the global Sr cycle. Chapter five of this thesis investigates $\delta^{88/86}Sr$ fractionation in different species coccolithophores with regards to temperature and growth rate. Coccoliths have existed for, at least, the past 170 Myr and therefore also present a potential archive of past variations in seawater $\delta^{88/86}Sr$.

Krabbenhöft et al. (2010) presented the first quantification of the marine Sr budget with both radiogenic $^{87}Sr/^{86}Sr$ and stable $\delta^{88/86}Sr$ strontium isotopes, where the outputs of Sr in different forms of marine calcium carbonate could be quantified. Combining species-dependent $CaCO_3$ burial rates from Schiebel (2002) and measurements of $\delta^{88/86}Sr$ in common marine $CaCO_3$ (tropical corals, green algae (Halimedia), foraminifera and coccoliths as well as an estimation of other continental shelf and slope taxa (i.e. mussels, starfish etc. assuming two-thirds are composed of aragonite and one third calcite)) they estimate a modern-day $\delta^{88/86}Sr$ burial flux-weighted average of 0.21±0.02‰. Taking this estimate, along with the other primary modern day Sr inputs, Krabbenhöft et al. (2010) attempted to quantify the Sr budget of the global ocean (Figure 1.4). The modern Sr day input is a balance between the riverine input and hydrothermal exchange and on figure 1.4 both lie on the red mixing line, the composition of their calculated modern input is closer in composition to the riverine value suggesting that this is the predominant Sr input source. Seawater and carbonate $\delta^{88/86}Sr$ both lie on a mass dependent isotope fractionation line (blue in figure 1.4) but take the same

radiogenic $^{87}Sr/^{86}Sr$ values; where the mixing and fractionation lines intercept defines the isotope composition of the combined Sr inputs into the ocean which is significantly different from the calculated input value of Krabbenhöft et al. (2010), Figure 1.4.

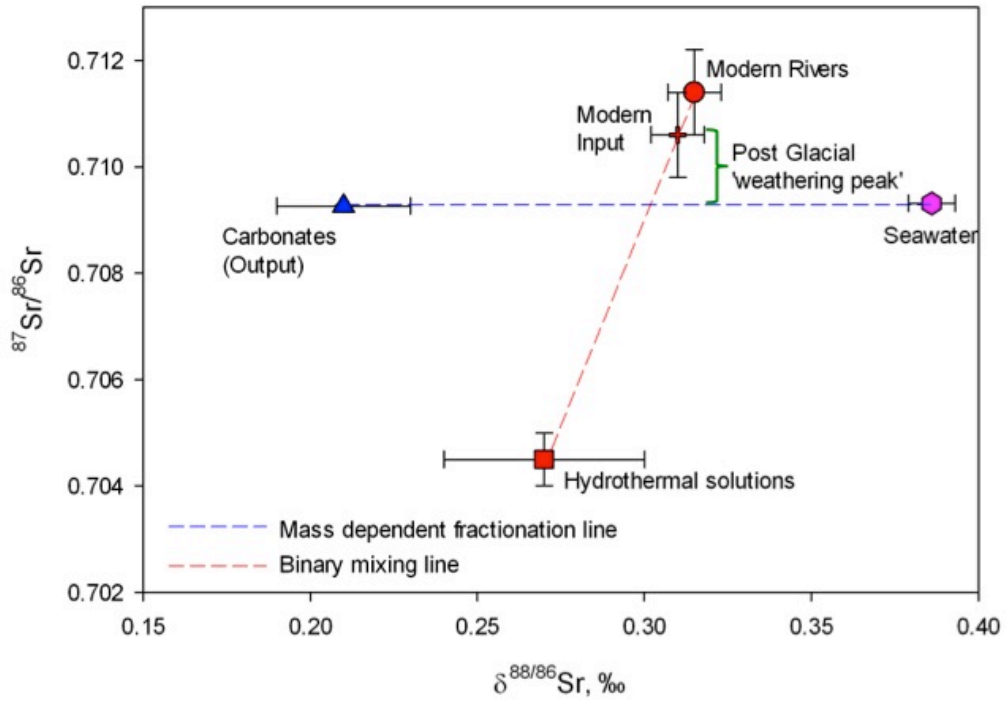

Figure 1.4 Triple isotope plot showing the flux-weighted average Sr isotope values of rivers, hydrothermal fluids (inputs, red), and marine carbonates (output, blue) in seawater. The $(^{87}Sr/^{86}Sr, \delta^{88/86}Sr)_{Seawater}$ and the $(^{87}Sr/^{86}Sr, \delta^{88/86}Sr)_{Carbonates}$ values define a mass-dependent fractionation line, whereas $(^{87}Sr/^{86}Sr, \delta^{88/86}Sr)_{Rivers}$ and $(^{87}Sr/^{86}Sr, \delta^{88/86}Sr)_{HydEnd}$ values define a binary mixing line. The weathering peak is the difference between modern $(^{87}Sr/^{86}Sr, \delta^{88/86}Sr)_{input}$ and $(^{87}Sr/^{86}Sr, \delta^{88/86}Sr)_{Intercept}$. Plot is reproduced from Krabbenhoft et al., 2010.

This has been taken to be indicative of disequilibrium between inputs and outputs because at isotope equilibrium the inputs should equal the outputs. The observation of Krabbenhöft et al. (2010) that the modern input is offset from the intercept was taken to be consistent with similar conclusions based on the radiogenic $^{87}Sr/^{86}Sr$ isotope composition of seawater where it is suggested that the modern continental weathering rates are higher than the long term average mean (Vance et al., 2009). In this case the difference between the input and intercept values is attributed to a 'post glacial 'weathering peak'' where the modern ocean has not yet recovered from the increase in continental weathering from the last glacial maximum (LGM)

(Vance et al., 2009). Thus, the conclusions of Krabbenhöft et al. (2010) may provide additional evidence that the modern-day ocean is out of equilibrium with regards to Sr cycling; chapter four investigates $\delta^{88/86}$Sr variations in seawater over the last two glacial cycles.

1.3.3 The terrestrial environment

Quantifying the release of cations from the continents due to chemical weathering is of fundamental importance for understanding the link between the lithosphere, hydrosphere and atmosphere, including the long-term carbon cycle (deSouza et al., 2010 and references therein). For example, weathering of primary minerals causes atmospheric CO_2 drawdown, and in this regard, $^{87}Sr/^{86}Sr$ data from river catchments have been used to discriminate between carbonate and silicate weathering sources, for the investigation of relative mineral weathering rates, as well as for the identification of the sources of base cations in streams. However, such interpretations are limited by complexities such as Sr release from rapidly weathered mineral phases (e.g. Blum, 1995; White et al., 1999; Olivia et al., 2004) or radiogenic carbonates, which may mask the characteristic fingerprints of carbonate and silicate rocks (e.g. Palmer and Edmond 1992; Quade et al., 1997). By applying the $\delta^{88/86}$Sr proxy to an actively weathering environment, it may be possible to circumvent some of the ambiguity associated with the information provided by the radiogenic ratio as $\delta^{88/86}$Sr only undergoes mass dependent fractionation. The application of the $\delta^{88/86}$Sr to the terrestrial environment is not been extensive, and only a few studies have been undertaken thus far (Halicz et al., 2008; Ohno et al., 2008; de Souza et al., 2010).

Halicz et al. (2008) measured calcite cave-speleothems (from Pleistocene caves in the Judea Mountains, see Figure 1.3) and soils (terra rossa soil representing soil covering the

Pleistocene caves; $\delta^{88/86}Sr$ = -0.17‰) that were found to possess much lighter $\delta^{88/86}Sr$ compositions than marine carbonates and seawater. It was suggested by these authors that soil formation processes (pedogenesis) could be responsible for the fractionation and that $\delta^{88/86}Sr$ in speleothem calcite could potentially be used to trace soil production processes in high-chronological resolution throughout the late Pleistocene period.

Stable strontium isotope fractionation has been observed in a Neoproterozoic cap-carbonate measured from the Doushantuo Formation in China, $\delta^{88/86}Sr$ analysis showed very negative values from the base (-0.4‰) shifting to heavier values of ~0.32‰ at the top (Ohno et al., 2008). Comparing these light values to those of biological and inorganic carbonate, which range from 0.2-0.3‰, Ohno et al. conclude that there is no reservoir present on Earth with a $\delta^{88/86}Sr$ value as low as that found at the base of the cap carbonate. These results were attributed to kinetic isotope effect that occurs due to deposition at high precipitation rates associated with climatic warming after a glacial event (see Ohno et al. (2008) for a more detailed discussion).

The study of de Souza et al. (2010) reported $\delta^{88/86}Sr$ values for a variety of geological materials (including soils, waters and vegetation) present in the Damma Glacier forefield, in Switzerland. They found evidence for mass dependent stable strontium isotope fractionation during assimilation of Sr into plant roots (~0.02‰, *Rhododendron*) from surrounding soils (~0.37‰), with significantly lower $\delta^{88/86}Sr$ ratios found in floral and foliar tissues (-0.23 and 0.08‰ respectively). Measurement of gneiss, mylonite and granite revealed average $\delta^{88/86}Sr$ values of 0.26, 0.15 and 0.23‰, respectively.

Each of these studies concluded that $\delta^{88/86}Sr$ has the potential to be used as a tracer for secondary weathering processes and/or soil paedogenesis but suggest that more precise analytical techniques need to be used. Strontium isotopes are a potentially powerful tool to

help us understand and constrain the Sr exogenic cycle (and by proxy the Ca cycle), and a potential tracer of weathering processes strontium is virtually unique in that its isotope composition records analytically resolvable information about both the source of Sr ($^{87}Sr/^{86}Sr$) and the mass-fractionation processes ($\delta^{88/86}Sr$) it has witnessed (DeSouza et al., 2010).

Chapter six of this thesis applies the $\delta^{88/86}Sr$ proxy to the dissolved load of Himalayan River waters. The Himalaya is an active orogenic belt with contributions to the river load from both carbonate and silicate lithologies, as well as inputs from other parts of the hydrological cycle such as rain, glacial melt and groundwater.

1.4 Measurement of stable strontium isotopes

Measurement of the small differences between the masses of ^{88}Sr and ^{86}Sr require that high precision mass spectrometry techniques are used. Mass spectrometry is a method used to separate ions (charged atoms) from a sample based on their mass/charge ratio and the machine consists of three main components: an ion source (for the generation of an ion beam), a electromagnet (to separate ion based on their molecular mass), and a collector (to determine the abundance of each atomic mass). For the measurement of strontium isotopes there are two common methods currently used, Thermal Ionisation Mass Spectrometry (TIMS) and Multi Collector – Inductively Coupled Plasma – Mass Spectrometry (MC-ICP-MS). The principal difference between these instruments lies in how they produce ion beams for analysis; TIMS thermally ionizes solid samples, whereas MC-ICP-MS produces ion beams by introduction of an element in a plasma.

1.4.1 MC-ICP-MS with sample standard bracketing.

In the initial study of $\delta^{88/86}$Sr fractionation in carbonates (Fietzke and Eisenhauer, 2006) MC-ICP-MS was used in combination with a standard bracketing (SSB) technique with an external precision of ~±50ppm. The MC-ICP-MS technique produces large but relatively constant mass fractionation which makes SSB an appealing method for measuring Sr isotopes, where a normalization factor is derived from the isotope composition of the standards which is then used to correct the isotopic ratio of the sample. In general the precision of Sr measurements obtained by this method is limited by isobaric interferences of Kr present in the argon gas on both ^{84}Sr and ^{86}Sr, and assumes that the sample and standard fractionate in a similar manner. Nowell et al. (2007) presented an alternative technique for Sr isotope analyses using a modified SSB method, but corrected for instrumental mass bias 'externally' using admixed zirconium (Zr) isotopes as an additional reference material added to both sample and standards. The certified ^{88}Sr/^{86}Sr of the standard measurement is used to obtain mass bias corrected ^{90}Zr/^{91}Zr in the sample-bracketed standards; their average value is then used to calculate mass bias corrected Sr ratios in the sample. Yang et al., (2008) utilized this method and reported a 2.5-fold improvement in the precision of $\delta^{88/86}$Sr measurement. More recently, Liu et al., (2012) modified the procedure once again to the use of the ^{92}Zr/^{90}Zr isotope pair instead of ^{90}Zr/^{91}Zr resulting in an enhanced precision of the $\delta^{88/86}$Sr ratio by a factor of 1.5. However, external element doping assumes the element of interest and the doping element both fractionate to a similar extent, but this is not always true and also depends on the amount of matrix in solution (e.g. Thirwall, 2002). Both techniques require 100% column yields and high levels of chemical purity, as fractionation may occur during column chemistry.

This method has remained the most commonly used for stable strontium measurement published to date (e.g. Fietzke and Eisenhauer, 2006; Ohno and Hirata, 2007; Halicz et al,, 2008; Ohno et al., 2008; Ruggebürg et al., 2008; Yang et al., 2008; deSouza et al., 2010; Knudson et al., 2010; Moynier et al., 2010; Charlier et al., 2012). Measurement of a $SrCO_3$ standard (NIST-987) analysed by Parkinson (2008; unpublished) compared the precision of MC-ICP-MS-SSB to the TIMS-DS technique and the results are shown Figure 1.5. It is clear that higher precisions can be more readily achieved using the TIMS-DS method which is outlined in the following section.

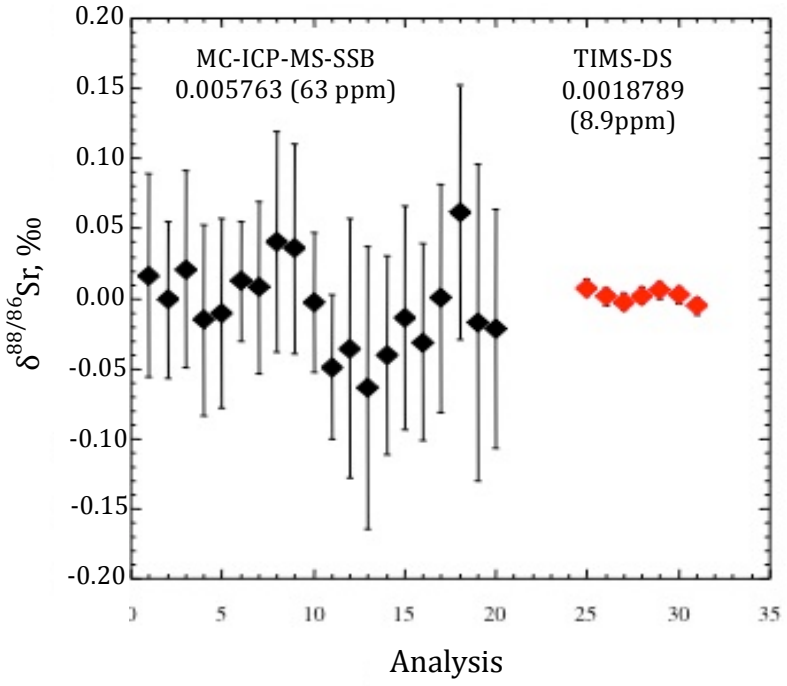

Figure 1.5 Comparison of $\delta^{88/86}Sr$ data collected from MC-ICP-MS-SSB and TIMS-DS. Figure courtesy of I.J. Parkinson. Since this figure was made improvements have been made on MC-ICP-MS $\delta^{88/86}Sr$ measurement, with precisions approaching ±30ppm (Parkinson, unpublished) but this is still not getting close to the precision achievable with TIMS-DS methods.

1.4.1 TIMS with double spike

In 2009 Krabbenhöft et al. published $\delta^{88/86}$Sr data using the TIMS-DS technique and improved on the precision of MC-ICP-MS measurements a factor of 2-3. High precision TIMS analysis in combination with a double spike technique is a well established method for correcting instrumental fractionation in mass spectrometry (e.g. Galer, 1999; Johnson and Beard, 1999; Siebert et al., 2001). It allows both natural and instrumental mass fractionation to be distinguished and has become the preferred method for high-precision stable Sr analysis (Krabbenhoft et al., 2009; Krabbenhöft et al., 2011; Böhm et al., 2012). The TIMS-DS technique benefits from the fact that there are fewer isobaric interferences during Sr measurement and smaller quantities of sample can be measured. The TIMS-DS method has been used throughout this study, principally because it produces stable Sr data to a higher precision data than that for MC-ICP-MS.

The layout of the TIMS and a brief summary of how Sr isotope analysis is performed is given in Figure 1.6. As a consequence of the heating process the ionized Sr progressively experiences significant instrumental mass fractionation, which is greater than that of the natural mass fractionation that is being measured. During the process of ionization the Sr sample becomes enriched in the heavier isotopes as the lighter isotope is preferentially ionized first. This enrichment of lighter isotopes in the vapour phase can be described by the Rayleigh law and is governed by the following equations (Russell et al., 1978);

$$R_T = r_{meas}\left(\frac{m_1}{m_2}\right)^f \qquad [1.15]$$

where r_{meas} is the observed isotope ratio; R_T is the true isotope ratio m_1 and m_2 are the mass for isotopes 1 and 2 and *f* is the *fractionation coefficient*. Typically, in the measurement of the radiogenic ratio, the ^{88}Sr/^{86}Sr ratio is normalised to 8.357209 (Nier, 1938) and used to correct

the other Sr isotope ratios for instrumental mass fractionation. However, since the measurement of the $^{88}Sr/^{86}Sr$ ratio is the objective of this study alternate ways to correct for instrumental mass fractionation must be found.

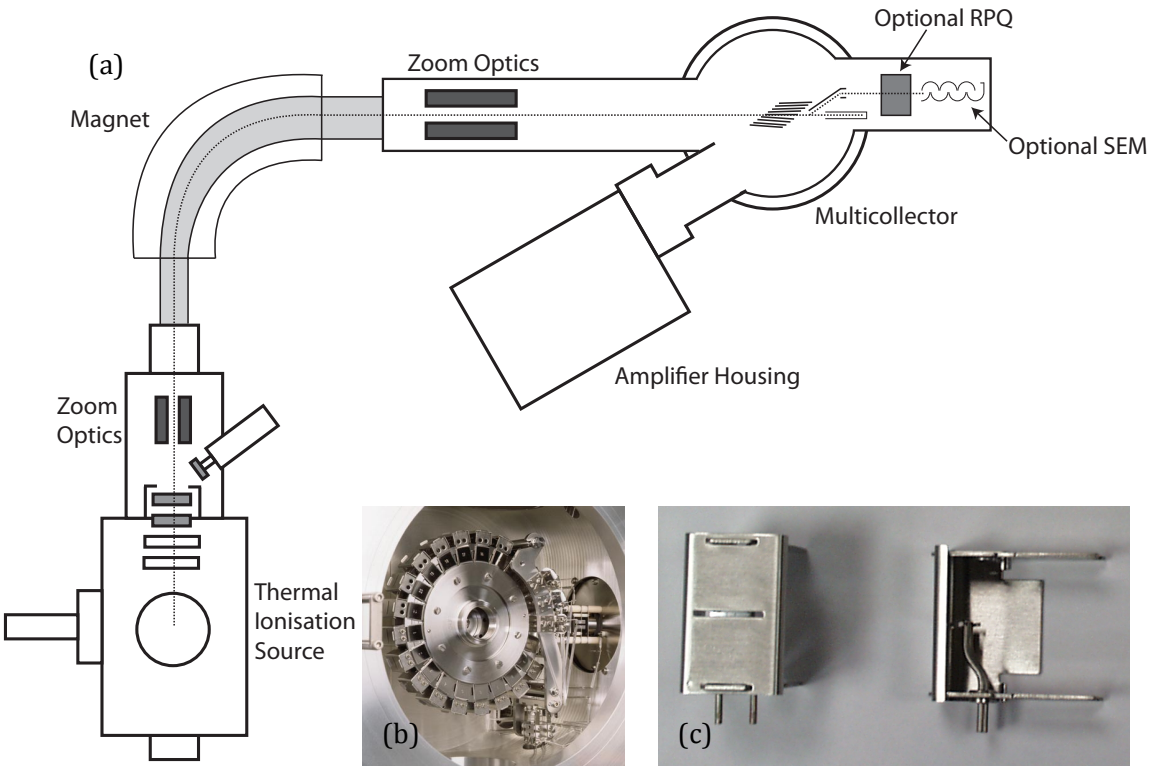

Figure 1.6 Schematic layout of a Thermal ionization Mass Spectrometer (a). Samples are loaded onto Re metal strips then mounted to filament holder (c) then loaded into the TIMS source (b). Samples are heated electrically to high temperatures to initialize ionization until a steady beam of ions is formed. These ions are accelerated by a high electric field which are then focused and optimized using a series of slits and lenses (Zoom optics on the diagram). The ions pass through a magnetic field (magnet) that deflects ions according to their mass-to-charge ratio. The individual ion beams are then detected in the multicollector, each cup is connected to an amplifier where the signal is digitized.

The double spike technique provides a robust method for distinguishing between natural and instrumental mass fractionation (Rudge et al., 2009) where precision is generally only limited by spike calibration and counting statistics (Galer, 1998). To use this method the element of

interest must have four or more isotopes, and a double spike, usually enriched in two isotopes, is prepared and calibrated. A natural sample is split into two portions to which a measured amount of spike is added to a known volume of one of the sample splits. Both the spiked and unspiked samples are measured on a mass spectrometer and the abundance of each isotope measured. In the case of Sr, ^{84}Sr, ^{86}Sr, ^{87}Sr and ^{88}Sr are measured while ^{85}Rb is also monitored, the latter allows for the correction for interferences arising from ^{87}Rb in the sample (assuming a ^{87}Rb/^{85}Rb ratio of 0.385041). If all the isotopes vary only due to mass dependent fractionation then any sample is related to a known standard (Nat) by a fractionation factor f_{nat}, however, when one or more of the isotopes varies through non-mass dependent processes, which is the case for Sr due to the radiogenic ingrowth of ^{87}Sr, then an additional un-spiked measurement of the natural sample is also made (a schematic of the technique can be seen in Figure 1.7).

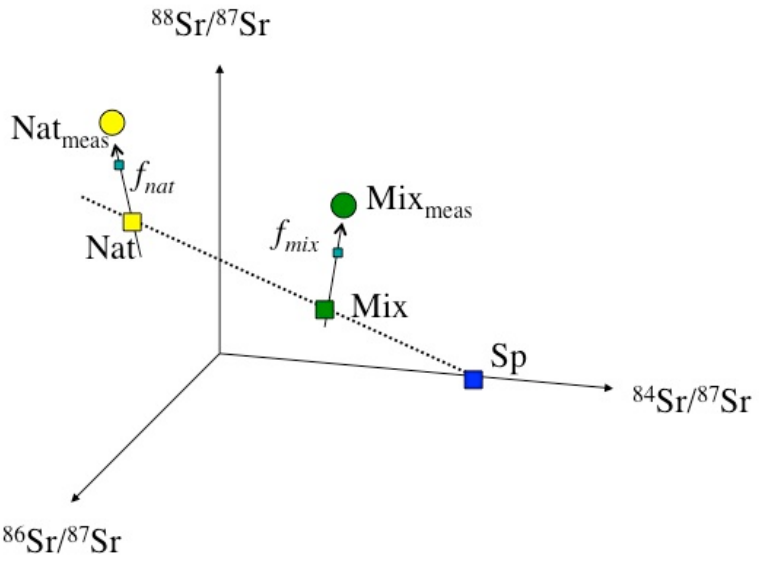

Figure 1.7 Three-dimensional plot illustrating how the double spike technique is applied to isotope systems with more than 4 isotopes. to The dotted line represents a mixing line between the double spike (Sp) and natural sample (Nat) where the sample-spike mix (Mix) plots at an isotopic composition on this line. The arrowed lines represent mass fractionation lines; for Sr isotopes the natural sample and mix sample are measured on TIMS (Nat_{meas} and Mix_{meas}) where f_{nat} and f_{mix} represent the natural and instrumental mass fractionation trends respectively. The double spike inversion mathematics takes the compositions of Nat_{meas}, Mix_{meas} and Sp to determine the unknown f_{mix}, f_{nat}, Mix and the true composition of natural sample, Nat.

From the knowledge of the DS composition it is possible to invert the measurements of the natural sample and spiked sample to obtain the true composition of natural sample corrected for instrumental mass fractionation. This technique also has the advantage of correcting for any fractionation that may occur during column chemistry by addition of the spike to the sample prior to column chemistry, which also means that 100% column yields are not essential. The TIMS-DS technique also has the added benefit of being able to simultaneously determine the concentration of Sr in a sample.

1.5 Thesis structure

Chapter two provides the reader with an overview of the analytical techniques and methods used in this thesis to obtain stable strontium isotope data. Chapter three demonstrates the reliability of using foraminiferal shells in the retrieval of marine stable Sr isotope records. In particular, this is done through an investigation of how $\delta^{88/86}$Sr isotopes behave with respect to changing conditions (such as, temperature, shell size or species variation). This then provides a basis for using foraminifera as an archive of the marine $\delta^{88/86}$Sr record. Chapter four builds on the understanding gained in chapters two and three to produce the first marine record of $\delta^{88/86}$Sr seawater variation on glacial-interglacial time scales (i.e. ~100 kyr) constructed from $\delta^{88/86}$Sr data obtained from foraminiferal shells. In chapter five the $\delta^{88/86}$Sr isotopic composition of coccolithophores as a function of temperature and, by inference, growth rate is investigated through culturing experiments. This is critical as coccolithophores represent one of the largest outputs of Sr in marine biogenic calcite and therefore chemical signals preserved by coccoliths can used both to reconstruct past seawater compositions and provide a more comprehensive understanding of the stable Sr isotope budget of the oceans.

Chapter six applies the $\delta^{88/86}Sr$ proxy to small catchments in the Himalaya with the aim of investigating the $\delta^{88/86}Sr$ variation in the dissolved load of rivers, where the information gathered from small catchment areas allows for a more detailed understanding of Sr behavior during weathering, which can potentially be applied globally. Finally, chapter seven brings together the conclusions from each of the previous chapters, to present an overall view of the applicability of $\delta^{88/86}Sr$ as a new isotope proxy.

CHAPTER TWO

Methods

Summary

This chapter reviews the general methods and techniques used in this thesis. The first part of the chapter outlines the methods used to prepare samples for mass spectrometric analysis as well as the laboratory conditions, preparation of reagents and steps taken to ensure that blanks remain low. The second part of this chapter outlines the mass spectrometric techniques used, and in particular Thermal Ionisation Mass Spectrometry (TIMS) and its application to this project in combination with the double spike (DS) isotope dilution technique.

At this point it is important to make clear, that due to circumstances unforeseen at the start of this research project, three different TIMS had to be utilized; therefore the reproducibility of the measurements and data from both standards and samples will be presented separately for each instrument used.

2.1. Chemical methodology

Three main requirements must be met for analysis of Sr by TIMS (e.g. Charlier et al., 2006):

(1) Strontium must be isolated to high purity from Rb and Ca, since Rb produces a mass interference on ^{87}Sr, and Ca severely impairs Sr ionization and produces ion beam instability;

(2) Yields from the chemical procedures must be as high as possible;

(3) Procedural blanks must be small compared to the amount of Sr in the sample (e.g. <1% of the sample Sr)

2.1.1 Laboratory conditions

All column chemistry and sample preparation for analysis was performed at the Department of Earth Sciences in the University of Oxford. All chemistry was performed under clean laboratory conditions using laminar flow controlled fume hoods.

2.1.2 Cleaning of Savillex™ Teflonware

All Teflonware was thoroughly cleaned before use to remove contaminants. This was accomplished by using strong mineral acids followed by dilution and removal with repeated washings with Ultrapure Milli-Q water (MQ) (18.2 MΩ cm at 25°C, TOC < 10ppb). Acids were either Quartz distilled or Ultra Purity Acids (HCl or HNO_3) purchased from ROMIL™. The following cleaning procedure was followed.

- Rinse x3 with MQ water
- Add 1-2mL 16% HNO_3, put on the lid/cap

- Leave on hot plate for 48-60 hours at ~120°C
- Remove from hot plate and leave to cool
- Rinse at least three times with MQ water
- If storing long term, leave beaker half filled with MQ water but for immediate use the beakers are left to dry at room temperature

Two sets of savillex were used, one for spiked samples and one for unspiked samples. Each savillex beaker was marked with a code on both the lid and container so that the history of each could be tracked if any problems arose.

Eppendorf centrifuge tubes were cleaned by soaking in 2% HNO_3 for up to 24 hours then rinsed three times. Polytetrafluoroethylene (PTFE) pipette tips were rinsed in concentrated nitric acid followed by at least one rinse in MQ water.

2.1.3 Preparation of reagents

Acids: For cleaning teflonware reagent grade concentrated HCl and HNO_3 were used. For all chemistry relating to samples and resin cleaning, concentrated quartz distilled (QD) acids were used which were then diluted to the required molarity with MQ H_2O and titrated to within no more than ±5% of the desired molarity.

2.1.4 Biogenic calcite cleaning

To clean biogenic calcite a method was used modified from that of Barker et al., (2003); individual stages involved are summarized below, sufficient for cleaning approximately 10-15 samples of 1-2mg calcite, at one time. A fresh mixture of alkali buffered 1% H_2O_2 was prepared for each batch of samples. 100µL hydrogen peroxide 30% w/w (reagent grade) is

mixed with 10mL 0.1M sodium hydroxide (reagent grade). This is sufficient for approximately 20 samples.

2.1.4.1 Crushing

Foraminiferal tests are crushed gently using a pestle and mortar with the aim of gently opening the chambers so that any contents can be released in the later cleaning stages. Care is taken not to over crush the tests as this leads to excess loss of sample during cleaning. Following this MQ water is added to the sample to keep the test particles in suspension then excess water is removed; the individual samples are then transferred to acid cleaned 2mL centrifuge tubes.

2.1.4.2 Clay removal

During this stage all samples are treated individually, in order to maximize cleaning effectiveness.

[1] 500µL of MQ H_2O is squirted into the tube and the sample allowed to settle.

[2] The overlying solution is removed with a pipette leaving approximately 10-20 µL of H_2O.

[3] The sample rack is placed in an ultrasonic bath for 1-2 minutes to encourage the release of tightly bound clays from test surfaces.

[4] 500µL of MQ H_2O is sprayed into the tube to agitate the sample and bring loose clays into suspension, then the sample is allowed to settle.

[5] The overlying solution is removed and steps [3] to [4] repeated a further four times.

Methanol is used for further clay removal; the lower viscosity of this reagent should dislodge material still attached to the carbonate tests.

[6] 250 µL of methanol is squirted into each sample tube; the sample rack is placed in an ultrasonic bath for 1-2 minutes.

[7] Treating each sample individually, the methanol removed from each sample then squirted back into the same tube to agitate the sample and bring the clays back into suspension.

[8] The sample is then allowed to settle and the methanol removed.

[9] Steps 7 to 8 are repeated.

[10] Step [4] is repeated and then the overlaying solution removed.

Removal of organic matter

[1] 250 µL of alkali buffered 1% H_2O_2 solution is added to each tube and the rack secured with a lid to prevent tubes popping open under pressure.

[2] The sample rack is placed in boiling water for 10 minutes. At the 2.5 and 7.5 minute mark the rack is removed momentarily and rapped on the bench to release any buildup of gas. After 5 minutes the rack is removed from the boiling water bath and placed in an ultrasonic bath for a few seconds, rapped on the bench then placed back into the boiling water bath.

[3] After 10 minutes the oxidizing reagent is removed using a pipette.

[4] Steps [1] through [3] are repeated

[5] Any remaining oxidizing reagent is removed by filling the centrifuge tube with MQ H_2O and removing after settling. This step is repeated 1-2 times.

At this stage Barker et al., (2003) remove the coarse grained silicates, this stage is only required if silicate were observed in the sample after crushing, however during my work no silicate material was observed, therefore this step was omitted.

2.1.4.3 Weak acid leach

A weak acid is used to remove any adsorbed contaminants from the test fragments.

[1] 250 µL of 0.001M HNO_3 is added to each sample, which is then ultrasonicated for 30 seconds.

[2] The acid is removed from each sample and replaced with 500µL of MQ H_2O. It is important to do this as quickly as possible for all samples to prevent excess dissolution. The water is then removed.

[3] Steps [1] to [2] are repeated.

[4] Using a 10 µL pipette, any remaining solution is removed carefully.

2.1.4.4 Dissolution

500 µL of 0.075M HNO_3 is added to each sample and then placed in an ultrasonic bath to dissolve the carbonate. During this process the tubes are removed in turn and agitated to allow any buildup of CO_2 to escape. When production of CO_2 ceases the sample is removed from the ultrasonic bath and left to settle. Once all samples are dissolved they are placed in clean centrifuge tubes.

During the process of cleaning steps 1 through 5 the loss of material was ~20% of the initial starting weight of the tests.

2.2 Column chemistry

The following section provides details on the preparatory steps and methods used to isolate Sr from other elements, particularly Rb and Ca,

2.2.1 Production of columns

Chromatographic columns were made from shrink-wrap Teflon and a stainless steel mould with a 150µL resin bed and reservoir of between 1.5-2mL. The mould was placed inside a length of shrink-wrap Teflon tubing and heated in a furnace for approximately 15 minutes until the Teflon had taken the shape of the mould. This was then placed in cold water and the

column carefully removed from the mould. The columns were cleaned and stored in ~2% HNO_3. Before use, cleaned columns are removed from the ~2% HNO_3, rinsed in MQ H_2O and left to dry. Frits were made from a circular piece of polypropylene (30µm pore-size) material inserted into the column. These were replaced after approximately 5 column runs, in case of degradation or any potential memory effects.

2.2.2 Resin cleaning

The Sr Spec™ resin (particle size 50-100µm) is cleaned thoroughly before use. 5mL of resin (good for approximately 30 columns) is placed in a 10ml Biorad™ column with a 10mL reservoir attached. 200mL volumes of 6M HCl, MQ, 3M HNO_3 and MQ are passed in sequence until a total of 3.2L has passed through the column. The resin is then extracted and stored, as a slurry, in weak HCl. For column chemistry 150µL Sr Spec™ resin is loaded into the resin bed using a 10-100µL pipette.

2.2.3 Chemical separation

Separation of Sr was carried out using cleaned Sr Spec extraction chromatographic resin (particle size 50–100 µm) supplied by Eichrom Technologies Inc (Darien, Il.) using the separation scheme detailed by Deniel and Pin (2001), and is outlined below.

1. Clean resin with 1mL of 7M HNO_3
2. Condition the column with 1mL of 2M HNO_3
3. Load the sample in 500µL of 2M HNO_3
4. Wash the sample onto the column with four 100µL aliquots of 2M HNO_3
5. Remove Ca and Ba with rinse of 1mL 7M HNO_3
6. Elute Sr in 1.5mL of 0.05M HNO_3

For the column calibration successive 100μL batches of the column elute were analysed to assess the optimum separation of Sr from, Ca and Rb, and also to determine which column fraction contained Sr. Elemental analysis using the ICP-MS was used to determine the quantity of Sr, Ca and Rb in each fraction (Appendix 2 a), demonstrating a good separation of Sr from the other elements.

Following chemical separation the sample is dried down at 120°C in preparation for loading onto Re filaments. It was found that when loading the column with a calcium carbonate matrix not all the calcium was removed, this was evident when running the sample on the TIMS as Ca hampers Sr ionisation; a cursory scan between masses 39 and 45 showed that Ca was indeed present. On this basis it was decided to modify the column procedure to extend the Ca wash-out step from 1mL 7M HNO_3 to 1.5mL 7M HNO_3. This proved successful but was only applied to samples with a calcium carbonate matrix, (see appendix 2 a)

For Sr stable isotopes, like other stable isotope systems, high yield chemistry is required to avoid significant isotope fractionation (Parkinson et al., 2007); Although, the yield from the SrSpec™ separation method is high (~90%; Charlier et al., 2006), when the Sr standard (NBS987) was separated on Sr Spec™ columns and then spiked (after chemistry), the $\delta^{88/86}Sr$ values were 21-93 ppm too light. This fractionation was ascribed to a small amount of heavy Sr isotopes being eluted during washing of the sample on the column. These variations are significantly larger than the analytical reproducibility of the method and therefore indicate that samples need to be spiked prior to chromatographic separation (Parkinson et al., 2007; see also Krabbenhöft, et al., 2009).

2.2.4 Addition of the double spike

The $^{84}Sr/^{87}Sr$ double-spike was prepared at the Open University, by I.J. Parkinson in 2007. Two strontium carbonate spikes enriched in ^{84}Sr and ^{87}Sr respectively were purchased from

Oak Ridge National Laboratories. The spikes where weighed accurately and dissolved in HNO_3 and then mixed to produce an optimal double spike. The concentration of the Sr in the spike was then determined by calibration with a gravimetric NBS 987 solution. The spike has a composition of $^{84}Sr/^{87}Sr = 0.912665$, $^{86}Sr/^{87}Sr = 0.0496697$ and $^{88}Sr/^{87}Sr = 0.223677$.

After dissolution, the solutions are split and one aliquot is spiked. The amount of spike added is determined from knowing the exact weight of the sample and the concentration of Sr within it; it is then left to equilibrate overnight at ~100°C then dried down. The spiked sample is then re-suspended in 500uL of 2M HNO_3 for column chemistry. Concentrations of sample material are determined exactly by ICP-MS or estimated from literature values.

The true isotope composition of the three Sr isotope ratios ($^{84}Sr/^{86}Sr$, $^{87}Sr/^{86}Sr$ and $^{88}Sr/^{86}Sr$), are derived from the results of the spiked and un-spiked run, which are deconvolved using the exponential fractionation law and a Newton-Raphson iterative technique using a macro written by I. J Parkinson based on the equations in Albarède and Beard (2004). Uncertainties on the three Sr isotope ratios are derived using a Monte Carlo simulation that incorporates the uncertainties from the unspiked and spiked analyses.

2.3. Measurement of Sr isotopes

Strontium isotope ratios are routinely measured by both TIMS and Multi Collector-Inductively Coupled Plasma-Mass Spectrometry (MC-ICP-MS) as stated in Section 1.4. However, for this work all measurements were made using TIMS due to the ability to make routine measurements with higher precision.

2.3.1 Preparation of filaments

Strontium samples are loaded onto a thin strip of outgassed rhenium (Re) ribbon (the filament), which is held in place via welding onto filament holders on the filament insert (see Figure 1.4, Chapter 1). The rhenium ribbon used in this study is zone-refined and of high purity (99.98 – 99.999% pure and approximately. 0.04mm thick and 0.7mm wide). The filament is cut to a length of ~2.5cm with ceramic scissors, this is then attached to the filament insert by using the filament-making tool and a spot welder. Once made, all filaments are outgassed in order to remove organics and other contaminants that may be present on the surface of the Re ribbon.

2.3.2 Preparation of Sr activator, TaF_5

An activator is used to increase the ionization efficiency of Sr during TIMS measurement. Approximately 20g TaF_5 is produced following the method outlined in Charlier et al. (2006). 250mg $Ta2O_5$ powder is dissolved in 10mL concentrated HF at 80°C for 7 days. After dissolution is complete, the solution is evaporated to dryness, redissolved in 1mL HF and placed in a centrifuge tube with 6mL MQ H2O. To this, reagent grade ammonia solution is added dropwise until white crystals of $Ta(OH)_5$ are precipitated. When precipitation ceases, the tube is centrifuged and the supernatant, which contains any Sr or Rb, is decanted. The pellet is then resuspended in and centrifuged and the supernatant discarded, and this procedure is then repeated. Finally the pellet is dissolved in water and dried down. The $Ta(OH)_5$ powder is then taken up in 1mL HF and the precipitation cycle repeated. The remaining crystals are weighed. For 300mg $Ta(OH)_5$ crystals the following volumes of reagents are added in this order: 370µL HF; 270µL concentrated H_3PO_4; 2125mL 3M HNO_3 and 16.55mL MQ H_2O. The solution is sealed and placed on a hot-plate to equilibrate.

2.3.3 Sample loading

The dried down Sr eluted from column chemistry is dissolved in 1μL nitric acid ready for loading. Initially, at the start of this project a 2M Nitric acid solution was used but this was increased later on to 7M then concentrated (~16M) nitric acid as it was found that not all of the Sr was dissolving. This is because 200-500ng sample of Sr is very hard to see in a Savillex^{TM} beaker by the naked eye so it was hard to tell if the entire sample had been fully dissolved by the acid. Using the stronger nitric acid allowed for more consistent sample loading.

Three methods of loading were investigated over the course of my research project. Firstly a Hamilton Syringe and cleaned capillary tube were used to transfer the dissolved sample to the filament; I found that the syringe was awkward to use, and not all of the sample was transferred and the activator and/or sample tended to spread out on the filament. Therefore, the sample was not concentrated in the centre of the filament.

Secondly an Eppendorf^{TM} pipette was used to introduce the sample and activator; this was much easier to use and increased the amount of sample transferred, but the droplet would still occasionally spread.

Thirdly a method set out by Charlier et al., (2006) was tried which used parafilm to constraint the droplet. Two dots of parafilm were melted onto the filament, aproximately 2mm apart, in the centre of the filament, which was later removed by melting and evaporation; this proved the best method to use but was only utilized 1 year into the project.

The final loading procedure used was as follows:

1. Dissolve sample in 1μL QD concentrated HNO_3
2. Heat filament to ~1A
3. Place two dots of parafilm onto filament, then take down to 0A
4. Add 0.7μL of TaF_5 activator to the filament
5. Add sample to filament
6. Increase current slowly to 0.8A and leave until droplet has evaporated and filament is dry

7. Increase current slowly until the parafilm starts to smoke, leave at this temperature until no more smoke can be seen
8. Keep increasing temperature slowly and leave at that temperature until all parafilm has gone.
9. Once all parafilm has gone, 'flash' the filament (i.e. increase the temperature until there is a dull red glow from the sample) then immediately take the current down to 0A.

2.3.4 Sample run

Twenty-one sample/standards can be loaded into the TIMS machine at any one time in a sample magazine. Once the sample magazine is loaded into the machine the pumps are turned on to create a vacuum in the ion source. Before a sample is selected and measurement started, vacuum pressures within different areas of the TIMS are checked are checked to confirm that they are have reached the following values;

Fore Vacuum Press: $2x10^{-2}$ mbar
High Voltage Source Press: $2x10^{-7}$ mbar or lower
Ion Getter Press: $5x10^{-9}$ mbar or lower

The amplifier temperature is also checked to be within about ±0.2°C of 36.9°C, variations in this temperature can indicate problems with the vacuum in the amplifier housing.

The cup configuration is then chosen; the exact positioning of the cups varied between instruments but the number of cups used remains the same; in total 6 cups are used to measure ^{84}Sr, ^{85}Rb, ^{86}Sr, ^{87}Sr and ^{88}Sr and a dummy mass. ^{85}Rb is measured to correct for the interference of ^{87}Rb on ^{87}Sr by assuming a constant natural ratio of $^{87}Rb/^{85}Rb = 0.385041$ during sample measurement. At the beginning of each day an amplifier gain was performed to monitor the daily performance of the amplifiers and detect for artifacts.

Once a sample has been selected the following general heating and focusing procedure is used for Sr isotope measurement:

1. Sample heated to 1800mA at 500mA/min
2. Sample heated to 2100mA at 100mA/min, analyzer gate opened.
3. Sample heated to 2300 (and higher) at 50mA/min
4. Fine wheel tuning procedure
5. Focus the beam using the Extraction Left, Extraction Right, Condenser, X-Symmetry and Z-focus lenses.
6. Increase the beam size to ~8V of ^{88}Sr and fine-tune the focus lenses.
7. Peak centre
8. Method set and analysis started.

Exceptions; firstly when the sample appeared unstable or could not be stabilized to a full 8V of ^{88}Sr, in this case the sample would be run at a lower voltage. Secondly, for samples where there appeared to be high amounts of calcium in the sample, because calcium (as mentioned before) inhibits the ionisation of Sr. In this case the filament had to be heated beyond the optimum temperature for Sr analysis in order to remove as much Ca as possible. The filament was then cooled to control the Sr ionisation. Thirdly, if a sample ran out before the measurement finished the analysis was stopped. Each analysis consisted of 54 blocks of 10 cycles, constituting a total of 540 measurements. A peak centre was made at the start of the measurement followed by an amplifier background measured for 30 seconds at the start of the run, and before each block which was then then subtracted online from the sample signal (the background was always less $10^{-5}V$). The idle time between each measurement block was set at 10 seconds and each measurement was integrated for 16.777 seconds. The amplifiers were rotated after each block and always set to rotate to the right; the abundances of the Sr isotopes are variable (see introduction), therefore the decay of the signal from the cup collecting ^{88}Sr may affect the ^{87}Sr data as its relative abundance is much smaller in

comparison. Therefore it is important to always keep the amplifier rotation in the same direction, so that if there is any signal decay it will always affect the same isotope. These effects are minimized by rotating to the right and by placing a dummy mass between ^{88}Sr and ^{84}Sr.

2.4 Reproducibility

In total three different TIMS machines were used at the following establishments; the University of Oxford, The Open University, Milton Keynes and Durham University. Consequently, the reproducibility had to be determined for each instrument, which was achieved by multiple measurements of the Sr standard NBS987 (also known as NIST987 and SRM 987) to determine the mean and the external reproducibility. The TIMS instrument used to run each batch of samples will be referred to in the methods part of each chapter where appropriate. Each instrument yields a slightly different mean $^{87}Sr/^{86}Sr$ for the NBS987 standard, consequently where possible each different data set was obtained form the same instrument.

2.4.1 Strontium Standard Data: NBS 987

The long-term reproducibility (external precision) of NBS987 for each TIMS instrument (Figures 2.1(a), (b) and (c)) where (a) and (b) refer to standards run in the same month but in different magazines.

For the TIMS at Oxford University the long-term average is taken only up to 2009 as we suffered analytical difficulties after this time, hence no more samples where run on this instrument. The average over this period is $^{87}Sr/^{87}Sr$ 0.710291 ±0.000058 (2.s.d., n=44).

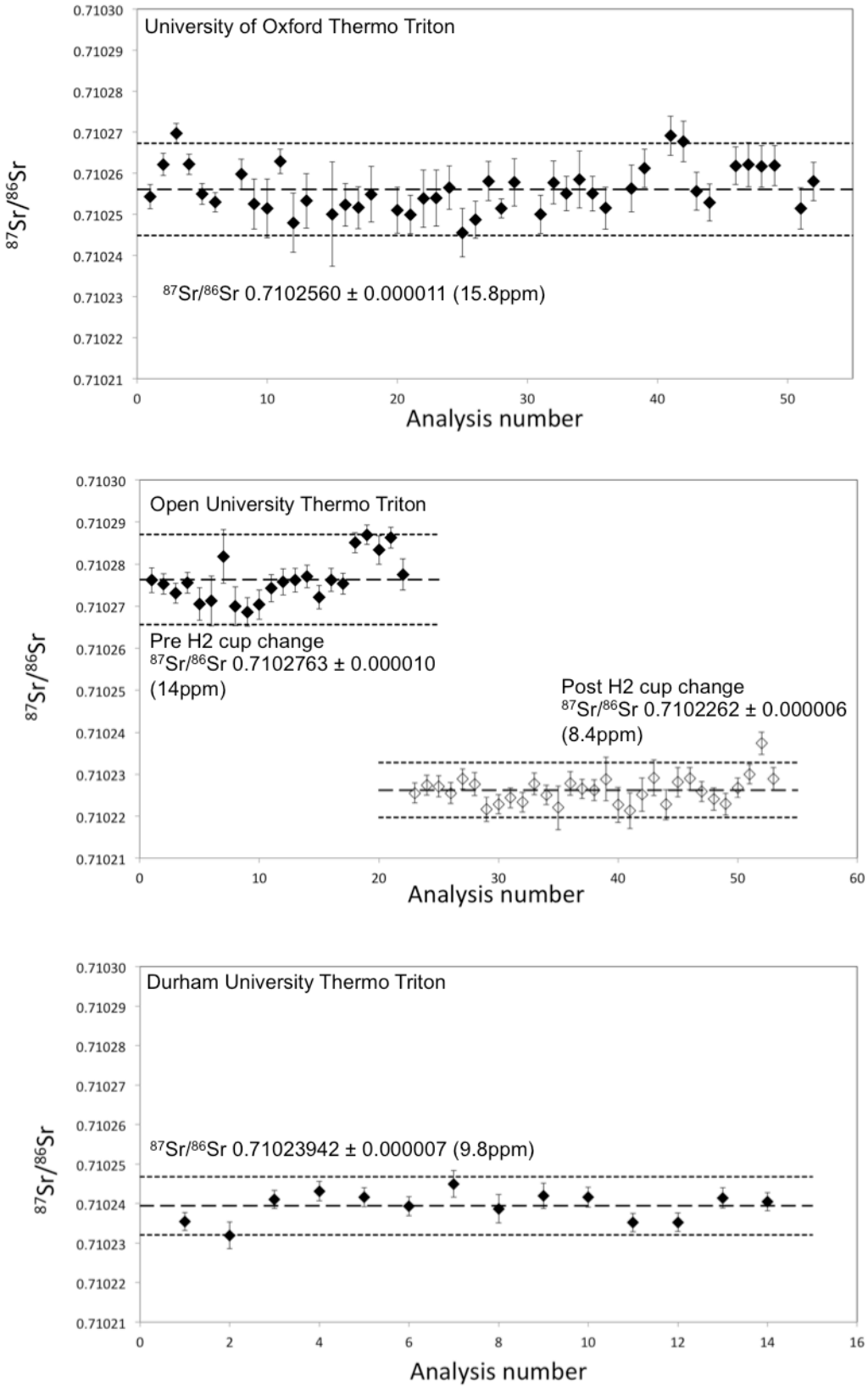

Figure 2.1 Sr standard data (NBS987) from (a) University of Oxford (2008-2009); (b) The Open University (2009-2011); (c) Durham University (2011-2012); where the dashed line represents the long-term average with the 2s.d error envelope. After 2010 at the Open University the H2 cup was replaced. Long term averages are shown separately for pre and post cup change.

The TIMS at the Open University underwent maintenance and all of the high-mass cups were changed in 2010 because cup degradation started to affect the external reproducibility of the standard. Therefore, samples that were analysed for $\delta^{88/86}Sr$ either side of the cup change took into account this change. Before the cup change the long-term $^{87}Sr/^{86}Sr$ average was 0.7102763±0.000010 (2.s.d n=22), after the cup change the long-term average was slightly less radiogenic at 0.7102262±0.000006 (2.s.d n=30). At The University of Durham the external precision over two sessions was $^{87}Sr/^{86}Sr$ =0.7102342±0.000007 (2.s.d n=14).

In all cases the internal precision was better that the external precision

2.4.2 Strontium Reference measurements: IAPSO seawater standard

The IAPSO seawater standard is commonly used as a reference material in the measurement of stable Sr isotopes (e.g. Fietzke and Eisenhauer, 2006; Rüggeburg et al., 2008; Krabbenhöft et al., 2009, Galer et al., 2011 and Böhm et al., 2012). In this study two different batches of IAPSO seawater, P148 (salinity 34.993‰) and P141 (salinity 34.997‰), where measured and these gave resolvably different $\delta^{88/86}Sr$ values; +0.358±0.008 (2.s.d n=5) and +0.397±0.007 (2.s.e n=3) respectively, see Table 1, clearly demonstrating that there is variability between different batches of the IAPSO standard. As a consequence of this Sr stable isotope compositional variability care must be taken when using IAPSO as a reference value, and the batch number clearly needs to be stated. This may well explains some of the variability that has been reported for IAPSO values published by different laboratories, (Figure 2.2). Böhm et al. (2012) recently adopted the '$\Delta^{88/86}Sr_{calc\text{-}aq}$' (Equation 2.1) where calcite samples are reported to a seawater or an aqueous solution representative of seawater, if this standard notation is to be used then it is imperative that the $\delta^{88/86}Sr$ of the solution is stated, especially if samples are taken from different ocean basins (see section 2.5.3 and Figure 2.3).

$$\Delta^{88/86}Sr_{(carb-aq)} = \delta^{88/86}Sr_{carb} - \delta^{88/86}Sr_{aq} \quad [2.1]$$

Batch P141 gives similar $\delta^{88/86}$Sr values to those given in previously published data by Fietzke and Eisenhauer (2006; +0.381±0.010‰), Krabbenhöft et al., (2009; +0.386±0.005‰), Liebetrau et al., (2009; +0.386±0.007‰) and deSouza et al., (2010; +0.39±0.02‰); whereas P148 gives values similar to those of Halicz et al., (2008; +0.35±0.1‰), Knudson et al., (2010; +0.36±0.04‰) and Liu et al., (2011; +0.370±0.026‰). To avoid confusion, the value reported in the following chapters is for Batch 141.

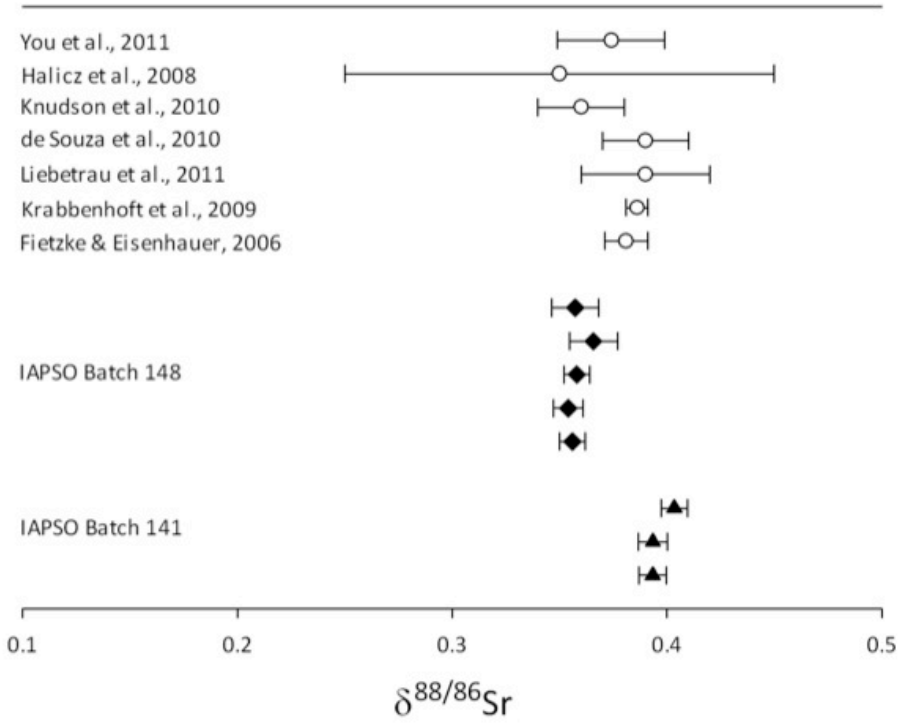

Figure 2.2 IAPSO seawater standard data compared to published studies. Filled data points are from this study, open data points are from the literature; see text for references.

2.4.3 Modern-day seawater samples

Stable strontium isotope data analysed from different locations in the modern Oceans suggests that there may be small differences between individual Ocean basins; $\delta^{88/86}Sr$ from a sample suite from Mokadem et al. (unpublished), Galer et al., (2011) and seawater measured in chapter five show subtle variations between the Atlantic, Pacific, Indian and Southern Ocean's and the English Channel (Figure 2.3). This indicates that, unlike the radiogenic $^{87}Sr/^{86}Sr$ isotope composition, there are resolvable variations in the composition of modern seawater. This suggests that there are significant regional variations in either the input or output of Sr, sufficient to generate stable Sr isotope variations. It is not possible at this stage to say exactly why this is occuring given the very long residence time of Sr in the Ocean but perhaps environmental differences between different oceans, such the predominance of Acantharia (delicate, marine microzooplanktonic protozoa) which have a skeleton of strontium sulfate ($SrSO_4$), may induce local variations.

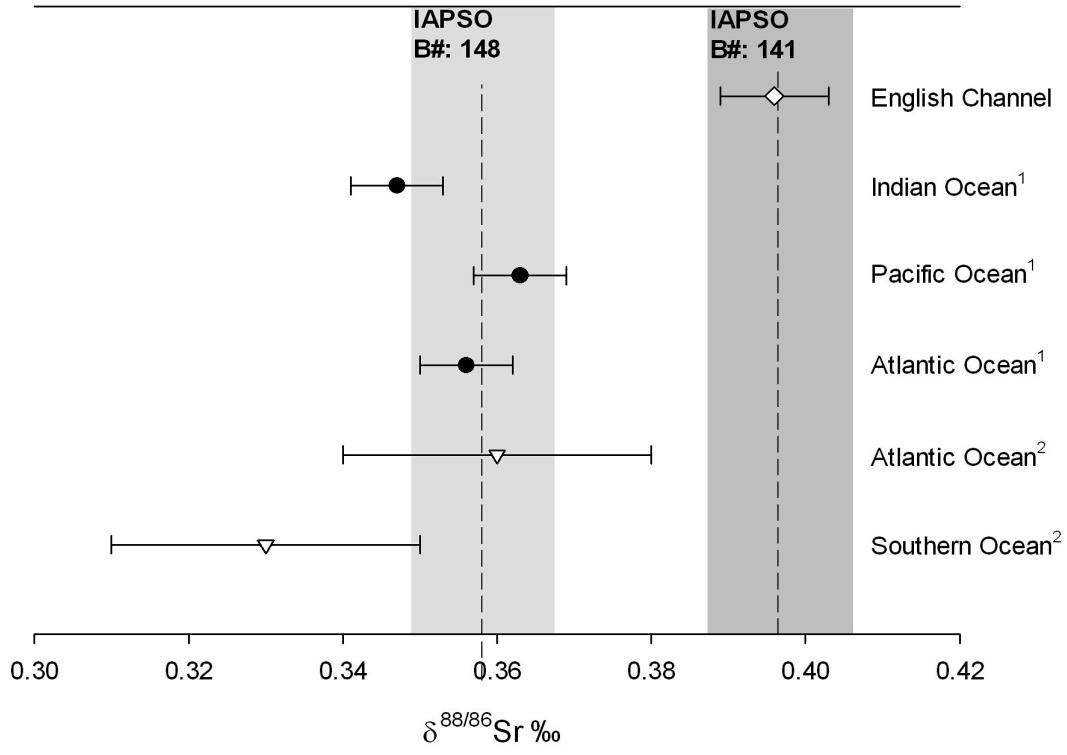

Figure 2.3 Variation in $\delta^{88/86}Sr$ of seawater sampled from different ocean basins. [1] Mokadem et al. (unpublished); [2] Galer et al., 2011. IAPSO is highlighted in grey (dark; Batch No. 141 and light; Batch No. 148. See section 2.5.2 for details)

2.4.4 Biogenic coral, comparison to previous studies

Five corals where also analysed from a suite collected by Robinson et al. (2004), four of these are aragonite and one high-Mg calcite. These samples were analysed to see if the work of previous studies could be reproduced using the DS-TIMS technique, and to produce higher precision data compared to the work of Fietzke and Eisenhauer, 2006; Halicz et al., 2008; Rüggeburg et al., 2008). The corals were cleaned and run for trace element analysis by T. Horner; see appendix 2 (b) for the Sr isotope data.

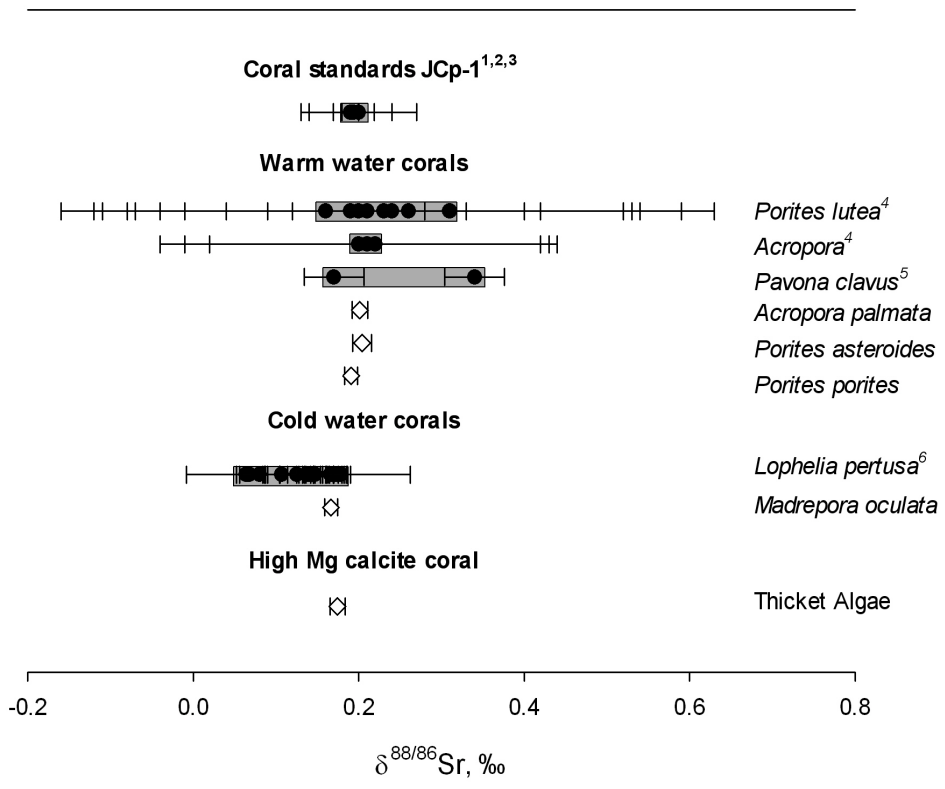

Figure 2.3 Coral $\delta^{88/86}$Sr data measured in this study compared to published studies. Open diamonds are data from this study, filed diamonds are data from other studies (1. Ohno and Hirata (2007); Krabbenhöft et al. (2009); Krabbenhöft et al. (2010) 4. Halicz et al., 2008; 5. Fietzke and Eisenhauer (2006);6. Rüggeberg et al (2008)), grey bars represent total range of data.

Figure 2.3 clearly shows that the corals lie within the range of previous data showing that we can reproduce the data of other published studies, but also to a higher precision. The average error (2.s.e) on each measurement was 9ppm, a great improvement compared to the average error obtained by MC-ICP-MS on corals (~23ppm, Ruggeburg et al., 2008; ~20ppm Fietzke

and Eisenhauer 2006). This is also the first measurement of a high-Mg calcite coral; all the corals studied in the literature are aragonitic.

The warm water corals were precipitated at ~26°C whereas the cold water coral was precipitated at ~4°C, (Sea surface temperatures were obtained from the world ocean atlas 2005; http://www.nodc.noaa.gov/OC5/WOA05/pr_woa05.html). Due to the large variation in temperature between the samples one might expect to see a temperature dependent fractionation of the type published by Fietzke and Eisenhauer (2006) and Rüggeburg et al. (2008). There is no apparent temperature dependent fractionation, however, it is difficult to compare different species growing in contrasting environments.

2.5.5. Blanks

Total procedural blanks (TPB) where spiked with a weighed addition of approximately 0.1g of a highly-enriched single ^{84}Sr spike before column chemistry. Column blanks (CB) are prepared by weighing 0.1g of the ^{84}Sr spike with 2mL 2M HNO_3 (weighted) which is then left to equilibrate overnight at ~100°C and then dried down. The blank is then re-dissolved in 500uL 2M HNO_3 for column chemistry. Typically 500ng of Sr was isolated for TIMS analysis, and the total procedural blank was never greater than 63 pg. Therefore blank contributions are less than 0.0126% of the total measured Sr, which equates to less than 0.15 ppm on the $^{87}Sr/^{86}Sr$ and for any reasonable range of blank values for $^{88}Sr/^{8}6Sr$ <0.03 ppm on the $^{88}Sr/^{86}Sr$ ratio.

CHAPTER THREE

The Sr stable isotope composition of modern planktonic foraminifera: effect of temperature, species and test size variations.

Summary

This chapter presents stable Sr isotope data for a suite of modern day planktonic foraminiferal shells (tests); typically trace element and stable isotope compositions of their carbonate tests are used as proxies for various physical and chemical parameters of seawater and are commonly used to construct marine records such as past seawater temperatures. Through careful measurement of $\delta^{88/86}$Sr in modern planktonic foraminifera we can determine processes that may effect $\delta^{88/86}$Sr fractionation in foraminiferal tests preserved in marine sediments. Quantification of biological and environmental effects on $\delta^{88/86}$Sr will help produce a faithful record of changing seawater $\delta^{88/86}$Sr in the geological past. Tests of *Globigerinoides sacculifer* were picked from core-top samples from seven locations in the South Atlantic Ocean preserving different sea surface temperatures. In order to assess an influence of size fraction, species specific $\delta^{88/86}$Sr isotope were measured in four size fractions from one core top in the South Atlantic Ocean.

3.1. Introduction

Traditionally radiogenic strontium isotopes ($^{87}Sr/^{86}Sr$) recorded in marine calcite have been used for reconstructing past seawater $^{87}Sr/^{86}Sr$ compositions (chapter one). However, recent data from biogenic aragonite has shown that the stable isotopes of Sr ($^{88}Sr/^{86}Sr$) undergo significant fractionation from seawater during calcium carbonate precipitation in both warm- and cold-water corals; during precipitation there is discrimination against the heavier ^{88}Sr isotope such that carbonate (in this case aragonitic corals) $\delta^{88/86}Sr$ values are ~0.2‰ lighter than seawater (Fietzke and Eisenhauer, 2006; Rüggeburg et al., 2008). The preferential incorporation of light Sr isotopes into biogenic calcite from seawater is similar to those of other geochemically similar non-traditional stable isotopes such as $\delta^{44/40}Ca$ (~0.1‰, average *G. sacculifer;* Gussone et al., 2009), and $\delta^{26}Mg$ (~3.9‰, average, mixed foraminiferal species; Pogge Von Strandmann, 2008). Foraminiferal tests preserved in marine sediment cores can provide long term high-resolution marine records, commonly used for precise dating using biostratigraphic, palaeomagnetic or isotope stratigraphic techniques, which can be directly related to other stable isotope, trace metal and palaeoenvironmental information from the same test (shell) material (Burton and Vance 2000). Foraminifera possess high Sr concentrations (typically around 1200-1300 $\mu g\ g^{-1}$) and much of the existing radiogenic Sr ($^{87}Sr/^{86}Sr$) seawater record has been obtained through their measurement (e.g. Brass, 1976; Capo and DePaolo, 1990; Elderfield, 1986; Hess et al., 1986; Hoddell et al., 1990; Hodell et al., 2007, Ando et al., 2010). Just as the $^{87}Sr/^{86}Sr$ ratio in seawater changes over time in response to changing inputs (see chapter one) it is possible that the $\delta^{88/86}Sr$ composition of seawater has also varied in the past. The $\delta^{88/86}Sr$ composition of marine carbonates is light relative to seawater hence variations in $\delta^{88/86}Sr$ over time could reflect changes

in the either the balance of carbonate to silicate weathering on the continent or changes in carbonate productivity and sedimentation in the oceans (see chapters one and four).

Fietzke and Eisenhauer, (2006) demonstrated that the mass dependent $\delta^{88/86}$Sr fractionation of Sr from seawater in both aragonitic corals and inorganic aragonite is temperature dependent, suggesting that $\delta^{88/86}$Sr isotopes in corals could serve as a paleothermometer for past seawater temperatures. Moreover, for corals at least, this temperature dependence has been shown to be species specific (Rüggeberg et al., 2008). In order to construct an archive of past $\delta^{88/86}$Sr in seawater any such temperature dependent variations must be quantified and corrected.

There are only two published studies that have measured the $\delta^{88/86}$Sr compositions of foraminifera. Firstly Krabbenhöft et al. (2010) proposed an average value of +0.14±0.01‰ based on the combined measurements of *G. ruber* and *G. sacculifer.* More recently, Böhm et al. (2012) found average $\delta^{88/86}$Sr for Holocene *G. ruber* and *G. sacculifer* to be statistically indistinguishable at ~0.139 and 0.138‰ respectively. A sample of *G. ruber* taken from the last glacial maximum (LGM) was also shown to be within error of the Holocene samples at ~0.132‰. Strontium is geochemically similar to both Mg and Ca. Previous research has shown that the isotopic composition and degree of fractionation of both Mg and Ca isotopes in foraminifera can depend on shell size, growth rate, temperature at precipitation, carbonate saturation state of the surrounding seawater and also the specific species (e.g. Gussone et al., 2003; Sime et al., 2005; Pogge Von Strandmann, 2008; Gussone et al., 2009; Kisakürek et al., 2011; Wombacher et al., 2011). The purpose of this study is to investigate the influence of temperature, species and/or shell size on stable strontium isotope behavior accompanying the growth of modern planktonic foraminifera with the aim of using sedimentary foraminifera to construct marine records of $\delta^{88/86}$Sr variation.

3.2. Sample settings, GeoB cores

GeoB cores (multi-corer or box core tops) were kindly supplied by the University of Bremen, Geosciences Department and MARUM. See Figure 3.1 and appendix 3 (a) for geographical locations, depths and SST's.

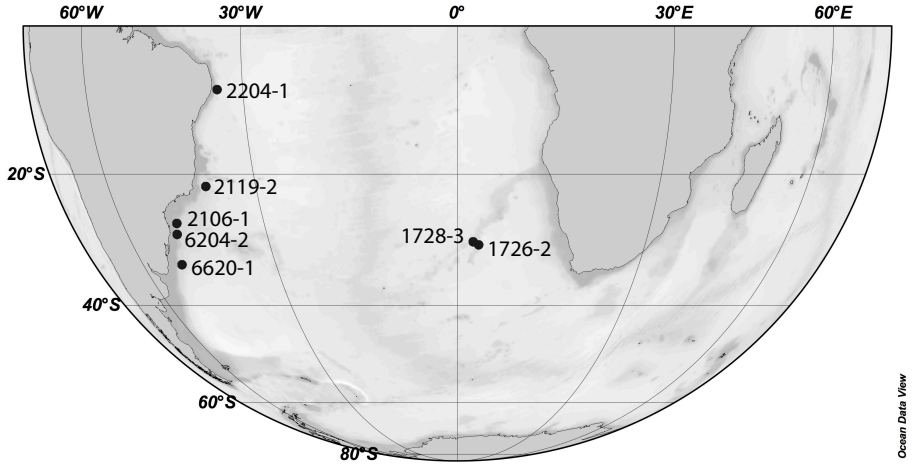

Figure 3.1. Geographical location of GeoB Cores in the South Atlantic Ocean.

3.2.1. Temperature variation

Around 2 mg of *Globigerinoides sacculifer* (without sac) in the 355-400µm size fraction were hand picked from core-top sediments (GeoB multi-corer or box core tops) from the S. Atlantic Ocean. These locations were chosen for their variable mixed layer temperatures and presence of

G. sacculifer, covering a range of ca. 10°C from which to ascertain any resolvable temperature influence on the $\delta^{88/86}$Sr values of foraminiferal calcite. Sea surface temperatures were obtained from the world ocean atlas 2005 (http://www.nodc.noaa.gov/OC5/WOA05/pr_woa05.html). *Globigerinoides sacculifer* was specifically chosen as it is a key mixed layer dwelling species, widely used in paleoceanographic studies and sea-surface temperature reconstructions (e.g. Dueñas-Bohórquez et al., 2011)

3.2.2. Planktonic foraminifera species and shell size.

For one core top sample (GeoB 2204-1, Lat 8° 31' 54.12" S, Lon 34° 1' 24.59 W, (depth 2080, temp 27°C) four different foraminifer species; *Globigerinoides sacculifer*, *Globorotalia menardii, Globigerinoides ruber* and *Globigerinella aequilateralis*, from 250-355μm, 355-400μm, 400-500μm and 500-1000μm, size fractions were hand-picked for $\delta^{88/86}$Sr measurement. See Figure 3.2 for a summary of the different foraminiferal species selected.

3.3. Methods

Foraminifera were cleaned using the method set out by Barker et al. (2003) and prepared for measurement using TIMS at the University of Oxford. See chapter two for details.

Globigerinita sacculifer

Spinose
Symbiotic; dinoflagellate
Lives in photic zone
lunar reproductive cycle
temperature tolerance of
14-31°C

Globigerinita ruber

Spinose
Symbiotic; dinoflagellate
Pink and White forms; pink
larger and prefer warmer water,
white smaller and prefer cooler
water
Shallowest dwelling species
Temperature tolerance of
16-31°C

Globigerinacea aequilateralis

Spinose
Symbiotic; chrysophytes
Temperature tolerance of 11-30°C

Globorotalia menardii

Non-spinose
Highly variable calcite crust
changing with depth
Found mainly below 100m as
adults but juveniles live in
euphotic zone

Figure 3.2 Summary of the different species of foraminifera investigated in this study. Information as summarized from Hemleben (1989) and Martin (1999). Images from the Illustrated Foraminifera Gallery; Illustrated Taxonomy Guide. Hhtp://www.foraminifera.eu

3.4. Results

3.4.1 Temperature dependence

Figure 3.3 illustrates the variation of $\delta^{88/86}$Sr in *G. sacculifer* from South Atlantic core-top samples, reflecting a range in sea surface temperature of ~19 to 28 °C. *Globigerinoides sacculifer* shows no systematic variation with temperature giving an average value of 0.089±0.085‰. All samples are lighter than both IAPSO seawater standards (chapter two) and are, on average, offset from modern seawater by ~0.26‰, raw data is shown in appendix 3 (a). Nevertheless, there is variation in the data of some 0.09‰, which is significantly greater than the analytical uncertainties.

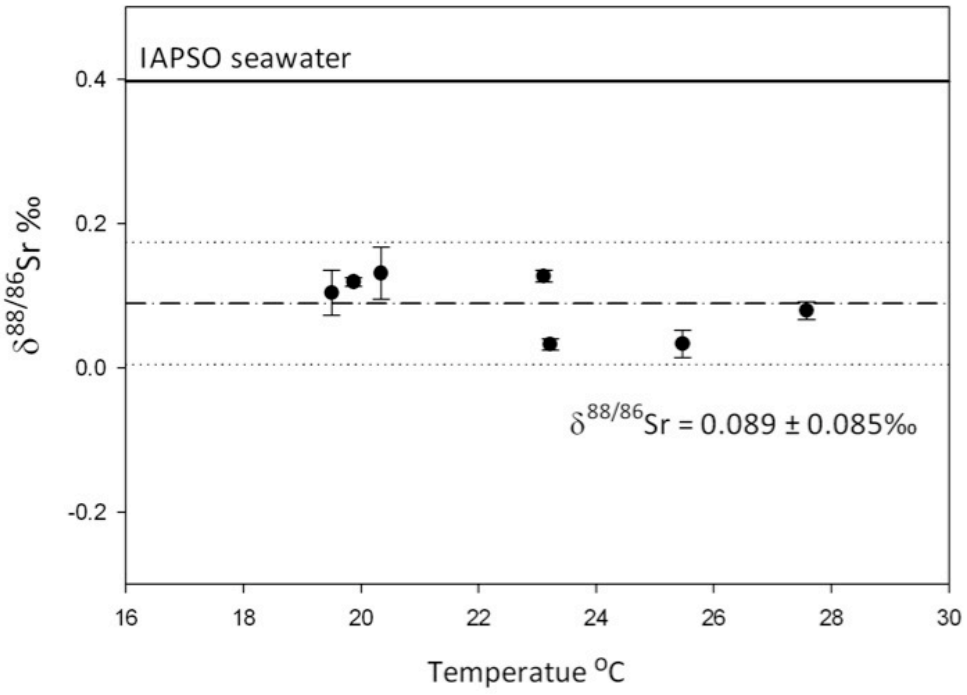

Figure 3.3 $\delta^{88/86}$Sr versus temperature in *G. sacculifer* tests, errors on each data point are 2.s.e. The modern day average of *G. sacculifer* tests is also shown with an error envelope of ± 2.s.d. IAPSO is shown for reference.

3.4.2 Species and shell size effects

Figure 3.3 shows the $\delta^{88/86}$Sr composition of *Globigerinoides sacculifer*, *Globorotalia menardii, Globigerinoides ruber* and *Globigerinella aequilateralis*, from the 250-355μm, 355-400μm, 400-500μm and 500-1000μm, size fractions. It is clear that each species fractionates $\delta^{88/86}$Sr to a different degree with increasing shell size. However, it must be stated that tests were selected from size fractions rather than chosen to be of a set size. Therefore there is an error associated with the actual size of the test as well as $\delta^{88/86}$Sr, but in all cases only whole foraminiferal tests were picked.

Both *G. sacculifer* and *G. menardii* show a positive correlation with test size (R^2=0.91 and R^2= 0.88 respectively), with *G. menardii* tending towards seawater $\delta^{88/86}$Sr values in the largest size fraction (500-1000 μm). In contrast, both *G. ruber* and *G. aequilateralis* show no systematic variation with shell size and average 0.023±0.008‰ and -0.056±0.06‰ respectively. However, there is considerable scatter in the data set of *G. aequilateralis* which is larger then the associated analytical errors.

The smallest size fraction (250-300μm) shows the smallest inter-species variation between *G. sacculifer, G. ruber and G. aequilateralis.* As the size fraction of the test increases inter-species difference become more prominent with offsets increasing between *G. sacculifer, G. ruber and G. aequilateralis* from ~0‰ to ~0.2‰. As the degree of fractionation changes between size fractions this suggests, by preliminary inference, that growth rate between different species influences the degree of $\delta^{88/86}$Sr fractionation.

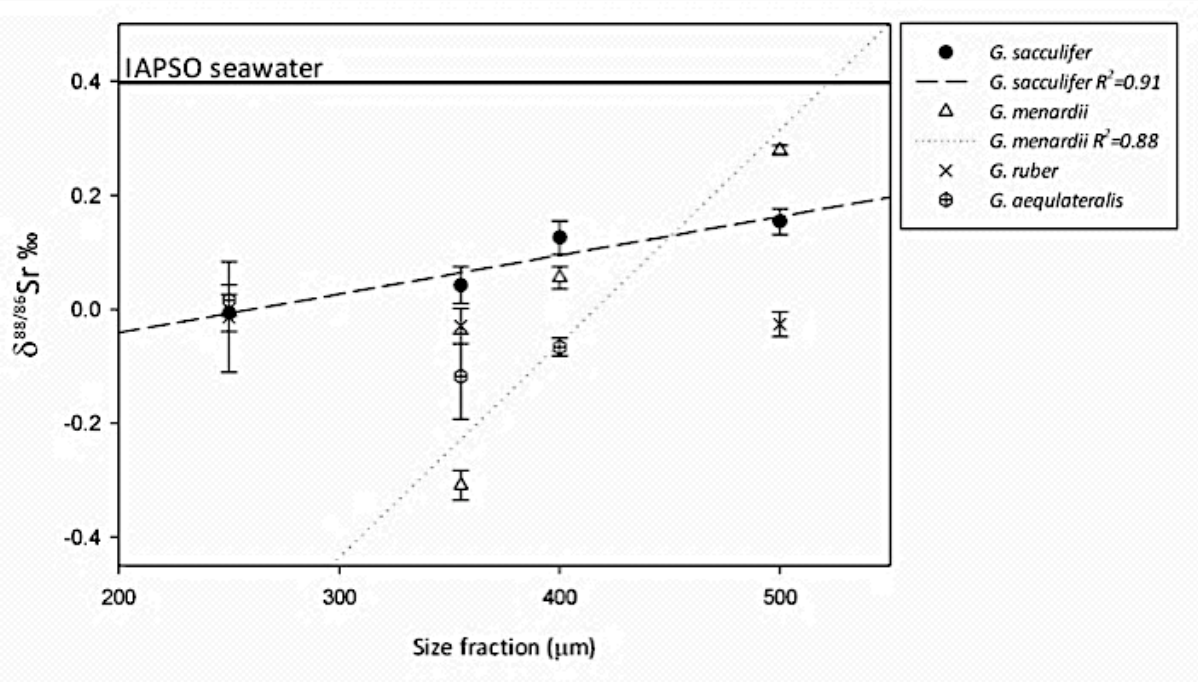

Figure 3.4 $\delta^{88/86}$Sr in different test sizes of various foraminiferal species; *Globigerinoides sacculifer*, *Globorotalia menardii, Globigerinoides ruber* and *Globigerinella aequilateralis*, from the 250-355µm, 355-400µm, 400-500µm and 500-1000µm, size fractions. The IAPSO seawater standard is shown for reference.

In comparison with other studies, Holocene foraminifera *G. ruber* and *G. sacculifer* were measured by Böhm et al. (2012) in the 315-355 µm size fraction showing $\delta^{88/86}$Sr of 0.139 and 0.138‰ which are slightly heavier than the values reported here.

3.5 Discussion

3.5.1 Temperature dependent fractionation

The average $\delta^{88/86}$Sr ratio recorded by G. *sacculifer* at different temperatures is offset from the $\delta^{88/86}$Sr value of seawater by ~0.26‰; this enrichment in lighter isotopes is the same trend seen for both $\delta^{44/40}$Ca and δ^{26}Mg isotopes in *G. sacculifer* as well as that of $\delta^{88/86}$Sr recorded in

inorganic calcite (Böhm et al., 2012), high Mg-calcite coral (chapter two) aragonitic coral (chapter two, Fietzke and Eisenhauer, 2006; Rüggeberg et al., 2006) and inorganic aragonite (Fietzke and Eisenhauer, 2006). The data presented here suggest that there is little temperature dependent fractionation of $\delta^{88/86}$Sr in the planktonic foraminifera *G. sacculifer*. Nevertheless, there is variability in the data ($\delta^{88/86}$Sr = 0.09‰) that is greater than the analytical uncertainty. Böhm et al. (2012) recently published data showing a kinetic isotope fractionation of $\delta^{88/86}$Sr accompanying inorganic calcium carbonate precipitation whereby the heavier isotope is increasingly discriminated against as precipitation rate is increased. If the data set here is regressed a weak negative correlation with temperature (R^2=0.34) is apparent; as temperature increases from 18 to 28°C the growth rate of *G. sacculifer* increases from ~0.24 to 0.38 d^{-1} (growth rate is shown as number of chambers precipitated per day quantified by organic carbon weight, Lombard et al., 2009), this slight decrease in $\delta^{88/86}$Sr temperature (Figure 3.3) could also be in line with a kinetic isotope fractionation effect. However the correlation is weak; a Spearmann-Rank statistical test (R^2=0.54 p=0.78) suggests an insignificant correlation.

Strontium, in general, tends to follow the geochemical behavior of Ca (due to a similar mass and charge). However there is ambiguity in the literature as to whether $\delta^{44/40}$Ca isotope fractionation in *G. sacculifer* is indeed temperature dependent (e.g Nägler et al., 2000; Gussone et al., 2003; Sime et al., 2005; Kasemann et al., 2008). Gussone et al., (2009), published $\delta^{44/40}$Ca data in *G. sacculifer* indicating that there is a bimodal (that is, both sensitive and *in*sensitive) temperature dependence of this species. In most cases Gussone et al., (2003) found that an absence of temperature dependence could be linked to low salinity levels. Under low salinity conditions foraminifera displayed growth limitations, such as smaller test diameter and shorter survival times, and also display little temperature dependent fractionation of $\delta^{44/40}$Ca. Whereas

foraminifera cultured at higher salinities grew to larger sizes, with a higher rate of gametogenesis and showed a strong temperature response. Potentially, differences in the salinities of the core-top locations where *G. sacculifer* was sampled, or other differences in environmental conditions between each location could explain some of the variability in the data ($\delta^{88/86}Sr$ = 0.09‰) beyond than the analytical uncertainties. Constraining the effects of differing environmental growth conditions of foraminifera in the future through culturing studies will perhaps elucidate if temperature dependent $\delta^{88/86}Sr$ fractionation in *G. sacculifer* is affected by additional environmental parameters such as salinity.

The kinetic isotope effect of $\delta^{88/86}Sr$ in inorganic calcite observed by Böhm et al. (2012) is explained by the discrimination against heavy strontium isotopes during crystal formation occurring at the surface of the crystal under non-equilibrium conditions. Böhm et al. (2012) argue that equilibrium fractionation of $\delta^{88/86}Sr$ into calcite does not discriminate between either Sr isotope ($\Delta^{88/86}Sr_{eq(carb\text{-}aq)}$=-0.03±0.09‰; $\Delta^{88/86}Sr_{eq(carb\text{-}aq)}= \delta^{88/86}Sr_{sample}-\delta^{88/86}Sr_{fluid)}$), and they conclude that the increase in discrimination against the heavier isotope with growth rate must be due to a kinetic isotope fractionation. Böhm et al. (2012) propose that the dehydration of lighter Sr^{2+} ions is more favorable, as the vibrational energy in $Sr\text{-}H_2O_{(n)}$ bonds is higher in the aquo-complex for the lighter isotope (c.f. chapter one). Therefore the heavier isotope is preferentially discriminated against as Sr is incorporated into the calcite lattice.

Fietzke and Eisenhauer (2006) employed a similar argument to explain the temperature dependent fractionation first observed for $\delta^{88/86}Sr$ in inorganic aragonite and corals except that, in the case of their samples, the heavier isotope became increasingly incorporated into the calcite structure as temperature increased (6-fold stronger fractionation in the coral compared to inorganic aragonite). In similar studies, Nägler et al., (2000) and Gussone et al. (2003) find that

for Ca isotopes two kinetic fractionations are observed during mineralization (biomineralisation) into inorganic (biogenic) aragonite that are dependent on the speciation of Ca^{2+}; firstly a weaker temperature dependent fractionation of the Ca^{2+} with a full, or even double layer hydrate shell, and secondly a 15 times stronger fractionation for the unhydrated, pure, Ca^{2+} ion. During biomineralisation the foraminifer test is precipitated from a calcification fluid, where Ca is derived from a mixture of endocytosis and cytosolic pathways; the Ca isotopic composition of the these reservoirs is controlled by a number of processes such as fractionation during biological Ca cell and membrane transport and the mixing of different Ca sources and reservoirs (Gussone et al., 2009). If isotopic fractionation takes place in more than one location it is possible that there may be a mixture of both kinetic and vital (biological) effects determining the extent of $\delta^{88/86}Sr$ fractionation observed during biomineralisation. If it assumed that a kinetic isotope effect is taking place during incorporation of $\delta^{88/86}Sr$ at the surface of the foraminifera, akin to that occurring during the precipitation of inorganic calcite (Böhm et al., 2012), there may be a competing isotope effect stemming from biomineralisation (vital effect), that is observed during the precipitation of coralline aragonite (Fietzke and Eisenhauer, 2006; Rüggeberg et al., 2008) as temperature increases, such that overall we see little temperature dependent fractionation in foraminifera as the different fractionation mechanisms compete. In any event, this is a highly speculative interpretation as it involves the comparison of aragonite to calcite, in order to fully interpret the trend observed here further work regarding $\delta^{88/86}Sr$ fractionation in foraminifera during the biomineralisation process needs to be undertaken. However, for the moment this remains the only data of its kind, and future work may reveal the effects that both internal (biological/vital) and external (environmental e.g. salinity) have on $\delta^{88/86}Sr$ incorporation and fractionation with temperature.

In this preliminary study, the absence of a significant temperature dependent fractionation in *G. sacculifer* emphasizes its use as a potential marine archive for constructing $\delta^{88/86}$Sr seawater variations in the past, as there is no apparent need for a temperature correction.

3.5.2. Shell size and species effects

The data presented in Figure 3.4 argues for a strong inter-species control on $\delta^{88/86}$Sr fractionation that becomes more significant as test size increases. Trace element incorporation in foraminiferal calcite does not occur at thermodynamic equilibrium (Elderfield and Ganssen, 2000; Rosenthal et al., 2000), but rather under biological control by the organism (e.g. Erez, 2003, and above), thus species-specific effects are to be expected. In particular, the data indicates that for some species there are both kinetic and species dependent effects if test size can be related to growth rate. The measured inter-species differences in $\delta^{88/86}$Sr and offsets from the seawater value indicate that the biological (vital) effect is a significant source for Sr stable isotope variability. In the following section the influence of shell morphology, secondary calcite formation and environmental habitat of the foraminifera studied will be addressed.

In the smallest size fraction *G. sacculifer*, *G. aequilateralis* and *G. ruber* have similar $\delta^{88/86}$Sr values (Figure 3.4). If the regression from *G. menardii* is extrapolated to smaller test sizes it can be assumed that it will acquire much lighter value than the other foraminifera measured. The main morphological difference between these species is that *G. sacculifer, G. ruber and G. aequilateralis* are all spinose and *G. menardii* is non-spinose (Figure 3.2). The spinose foraminifera studied here are mainly surface dwellers, living in the upper most part of the water column (0-50m). Most shallow dwelling species harbor symbiotic organisms (dinoflagellates in

the case of *G. sacculifer* and *G. ruber*; chrysophytes in the case of *G. aequilateralis* (Hemleben et al., 1989)) and typically have small thin walled porous tests in order to remain afloat in the photic zone, whereas deeper dwelling species (such as *G. menardii*) have dissolution resistant features such as thick test walls and rope-like keels that decrease their buoyancy (Martin, 1999). These results could suggest that during the early stages of ontogeny the spinose foraminifera may have similar growth rates and/or mode of biomineralisation and fractionate $\delta^{88/86}$Sr to a similar extent (Spindler et al., 1984; Hemleben et al., 1985) where as the non-spinose *G. menardii* fractionates Sr to a different extent, potentially explaining to the extrapolated offset observed in the $\delta^{88/86}$Sr value of *G. menardii* in the smaller size fraction. In addition, for some species changes in the depth habitat during ontogeny (growth from juvenile to adult individuals) in the water column may influence their $\delta^{88/86}$Sr composition. In the smallest size fraction we find the smallest inter-species variation between *G. sacculifer, G. ruber and G. aequilateralis*, these species live in a narrow depth habitat range and experience a similar initial growth rate (in the small size fraction) which is supportive of the observation that all three species have similar initial $\delta^{88/86}$Sr for the small size fraction.

Individuals from smaller size fractions may also have thinner calcite shells than those in the larger size fractions; and for species that experience a significant range in depth of habitat during their life cycle a substantial proportion (~50 %) of their shell may have been deposited at greater depths (Lohmann, 1995). *G. menardii* is known to inhabit deeper water depths during the later the stage of their growth than *G. ruber*, *G. sacculifer* and *G. aequilateralis* (Kemle-von Mucke and Oberhänsli, 1999).

The effect of increasing shell size is different for each species studied; for those species that respond to differences in shell size (*G. sacculifer* and *G. menardii*), and by inference growth rate,

the relationship is always the same, that is, with increasing shell size the heavy isotope is preferentially incorporated into the foraminiferal calcium carbonate, whereas *G. ruber* and *G. aequilateralis* show no measurable variation with shell size. Both *G. menardii* and *G. sacculifer* are known to deposit additional layers of calcite at later stages in life, which can be morphologically different to the primary test calcite. One feature of the globorotaliids, such as *G. menardii*, is that they produce calcite both in the surface waters where they live for some of their life cycle, and also at depth as they sink to the seafloor at the end of their life cycle. This calcite is added in the form of additional chambers or as a calcite crust (Sime et al., 2005). In particular *G menardii* is characterized by its variable calcite crust which has been interpreted as indicating a changing habitat (e.g. from shallow to deep water) during its life cycle (Hemleben et al., 1989). Foraminiferal tests are composed of several calcite layers termed ontogenetic and gametogenic calcite which formed at different times during their life cycle. For *G. sacculifer* the surface of the shell becomes thickened by an additional deposition of gametogenic calcite, up of 28% by weight to the pre-gametogenic shell (Bé, 1980). It is worthwhile considering that gametogenic calcite makes up a considerable percentage of the total amount of calcite in *G. sacculifer*. Of the continual surface dwellers studied it is the only one that shows a positive relationship with shell size.

Globigerinoides ruber and *G. aequilateralis* do not display a positive correlation with size fraction. It could be that the formation of new calcite in these species is minimal compared to the other two species, but there is a greater variability in *G. aequilateralis* compared to *G. ruber* which could also potentially be due to a morphologically different form of calcite. A more detailed study is required to investigate intra-test $\delta^{88/86}$Sr variability within single foraminifera,

as well as $\delta^{88/86}$Sr variation in secondary test calcite such as that possibly present in *G. sacculifer* and *G. menardii.*

The isotopically heavier $\delta^{88/86}$Sr values of *G. menardii* in the larger size fractions might yield true seawater stable Sr values, and thus could be used to construct past seawater records directly without the necessity to correct for any offsets.

3.6 Conclusions

The results show that for *G. sacculifer*, at least, there is little systematic temperature dependent variation of $\delta^{88/86}$Sr, yielding an average $\delta^{88/86}$Sr value of 0.089±0.09‰ (2.s.d, n=7). Both *G. sacculifer* and *G. menardii* show positive variations with shell size with heavier compositions in the larger size fractions. By contrast *G. aequilateralis* and *G. ruber* show little systematic variation.

The observed $\delta^{88/86}$Sr variation with different species of foraminifera (and also in shell size) could be due to type of foraminiferal shell precipitated (e.g. spinose vs non-spinose) or perhaps small differences in ecological depth habitat or shell construction (e.g. the addition of secondary calcite such as gametogenic versus ontogenic calcite). The depth of habitat may play a significant role, such that shallow and deeper seawater dwelling foraminifera occupy habitats that vary slightly in environmental parameters beyond those of simply differences in temperature. In particular, the data suggests that for some species there are both kinetic and species dependent effects, while the measured inter-species differences in $\delta^{88/86}$Sr and offsets

from the seawater value indicate that the biological (vital) effect is a significant source of Sr stable isotope variability.

In summary, the data presented here show that the stable isotope composition of foraminifera may vary depending on the species involved. The choice of shell size in planktonic foraminifera is a practical issue of importance in the design or methodological procedures for paleoceanographic work, and care should be made to choose a single size fraction taken from a single species. Where using one species is not possible it would be best to pick from the smaller size fraction where inter species offsets from each other are smaller (c.f. 250-355μm).

CHAPTER FOUR

The stable strontium isotope composition of seawater during glacial and interglacial transitions

Summary

Variations in the stable isotope composition of seawater over time could reflect either changes in (1) the balance of carbonate to silicate weathering on the continents (2) carbonate productivity and sedimentation in the oceans or (3) the amount of shelf carbonate weathering associated with sea level low-stands. Using the knowledge gained in chapter three, a record of $\delta^{88/86}Sr$ preserved in *Globigerinoides ruber* (white) tests covering the last 145 ka is produced. The data indicate that there is resolvable change in the $\delta^{88/86}Sr$ composition of seawater of 120ppm over the last two glacial cycles. However the variation observed does not co-vary with glacial retreat and growth, possibly due to local variations in seawater or whole ocean changes. The reasons behind these conclusions are discussed.

4.1 Introduction

The information obtained in chapter three indicates that planktic foraminifera, preserved in ocean sediments, can be used to reconstruct records of the $\delta^{88/86}$Sr isotope composition of seawater in the past. The chemical evolution of the oceans over time is controlled by a range of biological and sedimentary processes, and records of changing seawater chemistry potentially provide us with a means of determining changes in the balance of inputs to- and outputs from- the oceans. Over glacial-interglacial time periods the growth and retreat of ice sheets, and associated fall in sea-level, is likely to have influenced the composition of material delivered to the oceans from the continents.

The $\delta^{88/86}$Sr isotopic composition of calcium carbonate (both inorganic and biogenic) is lighter than that of most continental rocks and modern day seawater (e.g. Fietzke and Eisenhauer, 2006; Halicz et al., 2008; Ohno et al., 2008; Rüggeburg et al., 2008; DeSouza et al., 2010; Krabbenhöft et al., 2010; Böhm et al., 2012). Therefore, any change in the balance of carbonate to silicate weathering delivered from the continents since the last glacial maximum (LGM), likewise any change in carbonate formation and sedimentation in the oceans, may have influenced the $\delta^{88/86}$Sr composition of seawater.

During glacial intervals much of the continental crust was covered with large ice sheets decreasing the surface area of continental crust available for weathering (about 25% of the continental surface (Kump and Alley, 1994)). Significantly more of the ice covered continental surface comprised ancient shield rocks exposed at high-latitudes, rather than carbonates, and those shield rocks usually possess radiogenic Sr isotope compositions. Available data suggests that the $^{87}Sr/^{86}Sr$ signal from rivers draining glaciated terrains is more radiogenic than non-

glaciated, 0.71177 and 0.71134, respectively (Vance et al., 2009). Although some of this difference simply reflects the age of the terrains being weathered (evolving to more radiogenic $^{87}Sr/^{86}Sr$ compositions over time) it may also be due to the scarcity of carbonates in such shield terrains, in which case it can be anticipated that during glacial intervals the proportion of carbonate weathering from the continents delivered to the oceans would be greater. Moreover, it has been suggested that the decrease in the weathering flux from the continents to the oceans during glacial intervals is likely to be, at least partly, balanced by the exposure of readily weathered shelf carbonates accompanying a fall in sea level (Foster and Vance, 2006; Gibbs and Kump, 1994; Vance et al. 2009). Stoll and Schrag (1998) suggest that the Sr flux from the exposure and weathering of aragonite on continental shelves during the last glacial maximum may have been up to ten times greater than the modern global river input. On this basis it has been estimated that the glacial weathering signal from weathering of this carbonate possessed a $\delta^{88/86}Sr$ value of 0.23‰, compared to the present-day global river average of 0.31‰ (Krabbenhoft et al. 2010). Taken together, these observations suggest that the relative proportion of carbonate weathering may have increased during glacial intervals, potentially shifting the composition of weathered material delivered to the oceans to lighter stable Sr isotope compositions.

However, it has also been argued that during deglaciation the retreat of the continental ice-sheets would leave significant quantities of fresh finely grained minerals in soils and glacial tills that are highly susceptible to chemical weathering (e.g. Blum and Erel, 1995; Vance et al. 2009). Indeed, the study of Vance et al. (2009) suggests that the present-day imbalance of Sr inputs to the ocean, can be accounted for by a post-glacial pulse in chemical weathering some 70% greater than the steady state weathering rate. In this case the weathering flux of Sr during deglaciation

may have been dominated by the weathering of silicates, possessing relatively heavier $\delta^{88/86}Sr$ isotope compositions. Glacial climate cycles are thought by some to have been accompanied by changes in carbonate production and sedimentation in the oceans, with biological productivity and carbonate preservation being the key controls on carbonate sedimentation (Anderson et al., 2008). Calcium carbonate abundance tends to be at a maximum during later parts of glacial periods and deglaciation, and at a minimum during times of continental ice sheet growth (e.g. Hodell et al., 2001). In this case, the precipitation and sedimentation of $CaCO_3$ may drive seawater to heavier $\delta^{88/86}Sr$ values during these parts of the glacial cycle. Taken together, these observations suggest that the relative proportion of both carbonate weathering and carbonate sedimentation may have varied during glacial intervals, potentially shifting the composition of the oceans to stable Sr isotope compositions that differ from those of the present-day.

On the timescale of an individual glacial-interglacial cycle (i.e. ~100 kyr over the past ~900 kyr), the very long residence time of Sr (ca. 2.5 Ma or longer) (Hodell et al., 1990; Richter and Turekian, 1993) in the oceans necessitates significant changes in the flux or composition of material delivered by continental weathering in order to cause a measurable change in the composition of seawater (Richter and Turekian, 1993). By comparison, work involving very high-precision radiogenic Sr isotope measurements on foraminifera by Henderson et al. (1994) and more recently Ando et al. (2010) has found no resolvable variation in the $^{87}Sr/^{86}Sr$ ratio at the ±13 ppm and ± 9 ppm (2σ) level of precision, respectively, of those studies. However, for Sr stable isotopes, the composition of different water masses presented in chapter two, Figure 2.3 indicates that, unlike the radiogenic $^{87}Sr/^{86}Sr$ isotope composition, there are resolvable variations in the composition of modern seawater.

This chapter presents high precision $\delta^{88/86}Sr$ isotope data for the planktic foraminifera *Globigerinoides ruber* through the last glacial cycle (145,000 years) from Ocean Drilling Program (ODP) Site 758 in the north-east Indian ocean. This site is of particular interest because it preserves not only a global record of variations in seawater composition accompanying climate change, but also the local effects of erosion from the Himalaya-Tibet region that are seen in other radiogenic isotope systems. Much of the previous work on $^{87}Sr/^{86}Sr$ variations over the Quaternary has been undertaken on samples from this site (Dia et al., 1991; Clemens et al., 1993; Henderson et al., 1994), enabling a direct comparison with the data from those studies. Moreover, The sea surface temperature (SST) at this site shows little annual variation since the last glacial ±2(~1ºC) (Wyrtki, 1973), and thus any potential temperature dependent $^{86}Sr/^{88}Sr$ fractionation is likely to be negligible.

These data show that there are resolvable variations in the $\delta^{88/86}Sr$ isotope composition of seawater, preserved by these foraminifera, but that these variations do not simply covary with the oxygen isotope record in the same way as Nd and Os isotope records from the same samples.

4.2 Sample location

The foraminifera *Globigerinoides ruber* were taken from sediment samples from ODP site 758 which is located at the northern end of the Ninetyeast ridge (5°23'N, 90°21'E; 2925 m water depth), in the North East Indian Ocean, and lies about 1000 m above the Bengal fan (Figure 4.1). The sediment is primarily biogenic pelagic $CaCO_3$ (35 to 65% $CaCO_3$) but fine-grained terrigenous silts and clays predominantly sourced by rivers in the north and east of the Bay of Bengal, and volcanic tephra from Toba, in northern Sumatra, are also present (Shipboard

Scientific Party, Site 758, 1989). Sedimentary foraminifera are the archive of choice to this particular project as they can potentially provide a high-resolution record and contain high concentrations of Sr (typically 1300µg/g), but more importantly there are also high precision radiogenic strontium records from a foraminiferal archive to compare to, from the same core (e.g. Ando et al., 2010).

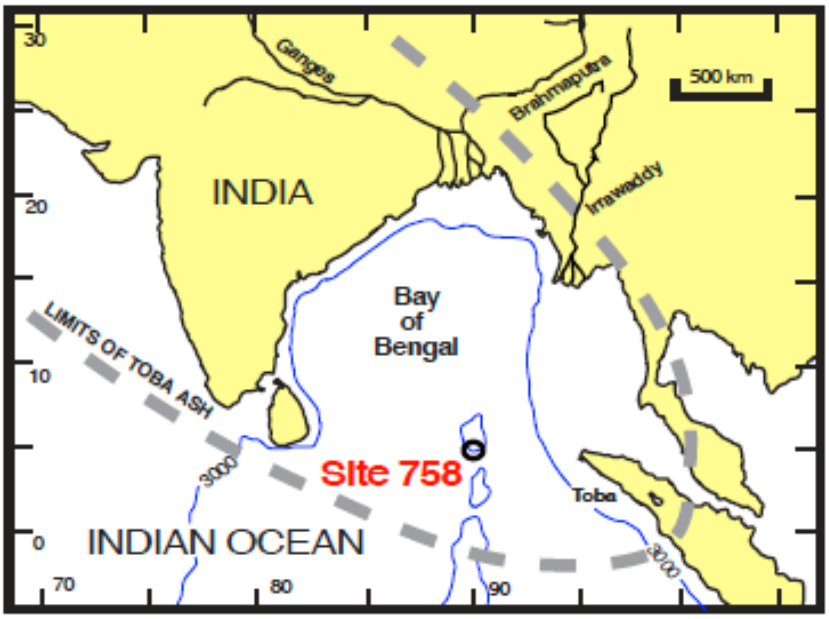

Figure 4.1; Map showing the location of site 758 with the limits of the Toba ash, courtesy of Burton et al. (2010)

General circulation models indicate that during the last glacial maximum (LGM) the presence of Northern hemisphere ice sheets, caused a migration of the Inter-Tropical Convergence Zone (ITCZ) (Chiang and Bitz, 2005; Broccoli et al., 2006), reducing monsoonal rainfall and runoff over the Indian subcontinent, which resulted in a decrease in the input of freshwater from the Ganges-Brahmaputra (Cullen, 1981; Duplessy, 1982) and increasing precipitation over the Irrawaddy drainage basin and the Andaman Sea .

Since the LGM both local variations in riverine input to the Bay of Bengal, and global variations in weathering and erosion, are likely to have had a marked impact on a number of radiogenic

isotopes that serve as tracers of continental weathering. For Nd, both dissolved and suspended material carried by the Ganges and Brahmaputra are characterized by relatively unradiogenic isotope compositions (e.g. Goldstein et al., 1984; Goldstein and Jacobsen, 1987; Allegre et al., 2010), resulting in a north-south gradient in the surface waters of the Bay of Bengal (Amakawa et al., 2000). The Nd isotope variations preserved in planktic foraminifera from site 758 demonstrate the existence of significant variations on glacial-interglacial timescales, that show a close correspondence with the oxygen isotope record (Farrell and Janacek, 1991) suggesting a process controlling the Nd isotopes that responds in phase with global climate cycles (Burton and Vance, 2000). These variations were originally attributed to a change in the flux or composition of Nd from the Ganges-Brahmaputra into the Bay of Bengal (Burton and Vance, 2000), although more recent work with sampling across the Bay has attributed the Nd isotope variations to a shift from the modern dominance of unradiogenic Nd from the Ganges-Brahamputra to the more radiogenic Nd sources of Arakan coastal rivers and Irrawaddy during the LGM (Stoll et al., 2007).

The Os isotope composition of the Brahmaputra is not particularly radiogenic (Sharma et al., 1999) but the Ganges possesses $^{187}Os/^{188}Os$ ratios that range from 1.6 to 2.9 (Sharma et al., 1999; Levasseur et al., 1999), significantly more radiogenic than estimates for global average riverine input ($^{187}Os/^{188}Os \approx 1.38$; e.g. Levasseur et al., 1999; Peucker-Ehrenbrink, 2002) or modern seawater itself ($^{187}Os/^{188}Os = 1.07\pm0.07$; Levasseur et al., 1998; Woodhouse et al., 1999). This raises the possibility that any change in the riverine flux into the Bay of Bengal during the LGM may have had an affect on the Os isotope composition of seawater. Recent Os isotope data for planktic foraminifera from Site 758 does indeed show covariations with the oxygen, and Nd, isotope record, suggesting a response that is linked to climate change (Burton et al., 2010).

However, for Os the variations cannot be explained by changes in the local riverine flux alone, rather such excursions (seen here and in the other major oceans (e.g. Oxburgh, 1998; Oxburgh et al., 2007) to relatively unradiogenic $^{187}Os/^{188}Os$ during glacial intervals are consistent with a global decrease in the input of radiogenic continental material, reflecting cooler temperatures and reduced continental runoff.

It is well established that the Sr isotope compositions of Himalayan rivers, particularly those of the Ganges-Brahmaputra system, are extremely radiogenic (e.g. Krishnaswami et al., 1992; Galy et al., 1999). Over recent glacial-interglacial cycles it has been shown that glacial sediments are systematically characterized by more radiogenic $^{87}Sr/^{86}Sr$ compositions than those seen in interglacial sediments (Colin et al., 1999; 2006). This has been attributed to an increase in physical erosion in the highlands and efficient transport in the floodplains during glacial stages, due to an increase in the extent of mountain glaciers and a fall in sea level (Colin et al., 2006).

A compilation of global river data (Pearce et al., 2010) reveals that the rivers draining into the Bay of Bengal i.e. Ganges and Brahamaputra, have $\delta^{88/86}Sr$ compositions of 0.38 and 0.47‰ respectively, heavier than that of $\delta^{88/86}Sr$ of the modern Indian Ocean (~+0.35‰; Mokadem, unpublished). Preliminary $\delta^{88/86}Sr$ data taken from the Himalaya suggests that river waters draining carbonate-based lithologies have a lighter stable isotope composition than of silicate ($\delta^{88/86}Sr_{carb}$ = 0.34±0.1‰ (2.s.d, n=16) and $\delta^{88/86}Sr_{sil}$ = 0.26±0.2‰ (2.s.d, n=15); chapter six). Therefore an increase in the relative proportion of carbonate weathering into rivers draining the Himalayas could potentially drive inputs to lighter values, and vice-versa for an increase in silicate weathering.

4.3 Methods

Globigerinoides ruber (white, whole), in the 212-300 μm size fractions, were hand-picked from twenty-eight down-core samples covering the last 145 ka. Shells were picked from the smaller size fraction and in a strict range as data from chapter three showed that there can be a significant effect on the fractionation of stable strontium isotopes depending on the shell size picked. Approximately 100-150 individual *G. ruber* shells were picked from each sample to obtain a total weight of 1-1.5mg of foraminifera. The foraminiferal shells were cleaned following the method outlined by Barker et al. (2003), then run on the TIMS at the Open University, Milton Keynes. Methods for cleaning the foraminifera, column chemistry and TIMS analysis are outlined in chapter two. The section of core from which the foraminifera where taken contains a major ash layer ~34cm thick corresponding to the eruption of the youngest Toba tuff at 74±2 ka (e.g. Farrell and Janacek, 1991), which dispersed an extensive ash fall deposit over much of the Bay of Bengal (see Figure 4.1).

4.4 Results

4.4.1 Temperature variations

The Mg/Ca data for *N. dutertrei*, *G. menardii* and *G. conglobatus* are shown in Figure 4.2. these indicate that the temperature variations at this locality, over the past 35 kyr at least, are no greater than 1-2°C, consistent with the SST reconstructions of Prell et al. (1980) and Cullen (1981), which show no significant temperature variation at this site.

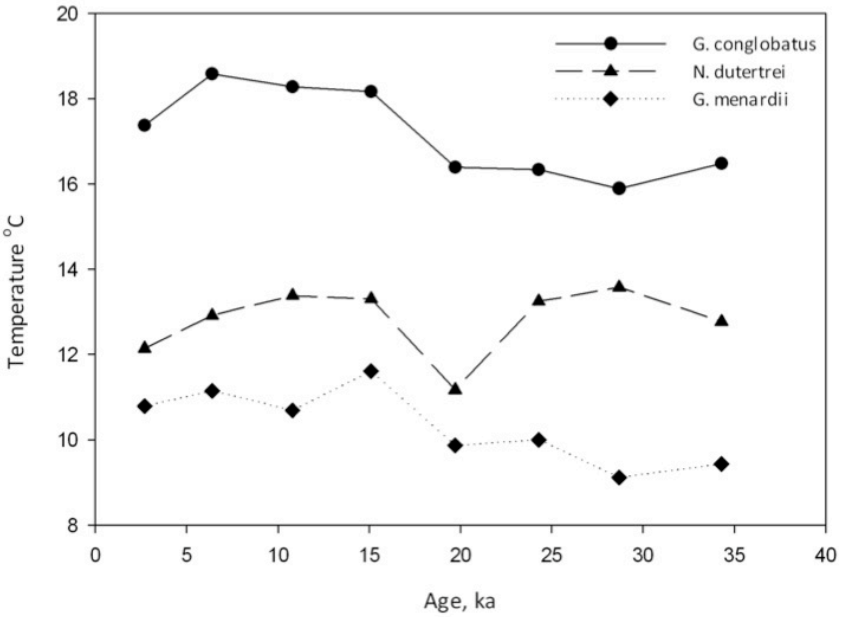

Figure 4.2 Temperature variations over the last 35 kyr constructed from Mg/Ca data for *N. dutertrei*, *G. menardii* and *G. conglobatus* taken from the same ODP758A core-top splits, of 1-2°C (Burton, unpublished), the raw data is shown in appendix 4 (a).

4.4.2 Strontium stable isotope variations.

The $\delta^{88/86}$Sr isotope data for by *G. ruber*, given Table 4.1 show a total variation of the order of 150ppm (Figure 4.2). However, the variations observed do not correlate with the timing of glacial retreat and growth as indicated by the δ^{18}O curve (e.g. Farrell and Janacek, 1991). Rather there is a distinct shift to heavier values around 40 ka, with excursions to lighter values at ~18, 24, 60 and 80 Ka. This pattern of change closely corresponds to the δ^{13}C record from the same core (Chen and Farrell, 1991). The Younger toba tuff, representing the on-land equivalent of the Toba ash layer found in these sediments, gives a $\delta^{88/86}$Sr value of -0.19±0.13 (Charlier et al., 2012)

Core, section, interval, cm 121-758A-	ODP depth, mbsf	Composite depth	$\delta^{18}O$ age[§] Ma	Age Ka	$\delta^{13}C$[§]	Interpolated MS k (10^{-6}) (CGS)[§]	$^{88}Sr/^{86}Sr$	2.s.e	$\delta^{88/86}Sr$,‰	2.s.e, ‰
1H-1, 1	0.01	0.01	0.00055	0.55	1.56	2.5	8.37559	0.00009	0.105	0.011
1H-1, 11	0.11	0.11	0.006	6	1.6	5.23	8.37557	0.00017	0.103	0.02
1H-1, 21	0.21	0.21	0.01033	10.33	1.49	6.2	8.37662	0.00008	0.161	0.01
1H-1, 31	0.31	0.31	0.01467	14.67	1.41	8.07	8.37529	0.00009	0.069	0.01
1H-1, 41	0.41	0.41	0.019	19	1.6	9.77	8.376	0.00008	0.095	0.036
1H-1, 51	0.51	0.51	0.02386	23.86	1.66	8.9	8.37566	0.0001	0.114	0.012
1H-1, 61	0.61	0.61	0.02871	28.71	1.71	10.53	8.3759	0.00006	0.069	0.013
1H-1, 71	0.71	0.71	0.03357	33.57	1.58	10.53	8.37589	0.00012	0.141	0.015
1H-1, 81	0.81	0.81	0.03843	38.43	1.68	6.7	8.37618	0.00008	0.176	0.009
1H-1, 91	0.91	0.91	0.04329	43.29	1.57	7.57	8.37633	0.00007	0.194	0.009
1H-1, 101	1.01	1.01	0.04814	48.14	1.64	3.63	8.37618	0.00013	0.175	0.015
1H-1, 111	1.11	1.11	0.053	53	1.53	6.2	8.37611	0.00008	0.168	0.01
1H-1, 121	1.21	1.21	0.0578	57.8	1.4	4.67	8.37553	0.00009	0.098	0.011
1H-1, 131	1.31	1.31	0.0626	62.6	1.39	8.47	8.37579	0.00007	0.069	0.008
1H-1, 141	1.41	1.41	0.067	67	1.67	9.5	8.37593	0.00009	0.086	0.011
1H-2, 1	1.51	1.51	0.071	71	1.19	15.03	8.37636	0.00008	0.138	0.01
ASH	1.61	1.61				50.9				
ASH	1.71	1.71				35.9				
ASH	1.81	1.81				31.27				
IH2, 41	1.91	1.91	0.07614	76.14	1.45	12.23	8.37634	0.00005	0.135	0.006
ASH	2.01	2.01				113.5				
1H-2, 61	2.11	2.11	0.07871	78.71	1.57	5.57	8.37628	0.00007	0.127	0.008
1H-2, 71	2.21	2.21	0.08	80	1.48	5.07	8.37569	0.00006	0.058	0.007
1H-2, 81	2.31	2.31	0.0895	89.5	1.41	4.8	8.37616	0.00007	0.114	0.009
1H-2, 91	2.41	2.41	0.099	99	1.48	10.17	8.37599	0.00007	0.093	0.008
1H-2, 101	2.51	2.51	0.10667	106.67	1.26	13.63	8.3762	0.00008	0.118	0.009

Core, section, interval, cm 121-758A-	ODP depth, mbsf§	Composite depth§	$\delta^{18}O$ age§ Ma	Age Ka	$\delta^{13}C$§	Interpolated MS k (10^{-6}) (CGS)§	$^{88}Sr/^{86}Sr$	2.s.e	$\delta^{88/86}Sr$,‰	2.s.e, ‰
1H-2, 111	2.61	2.61	0.11433	114.33	1.16	13.8	8.37631	0.0001	0.131	0.012
1H-2, 121 c	2.71	2.71	0.122	122	1.07	11.53	8.3763	0.00008	0.13	0.01
1H-2, 131	2.83	2.81	0.12633	126.33	1.06	12.83	8.37595	0.00007	0.088	0.008
1H-2, 141	2.91	2.91	0.13067	130.67	1.1	14.4	8.37631	0.00007	0.131	0.008
1H-3, 1	3.01	3.01	0.135	135	1.2	10.9	8.37595	0.00008	0.088	0.009
1H-3, 11	3.11	3.11	0.1422	142.2	1.39	11.53	8.37619	0.00008	0.118	0.01
Toba Ash*									-0.19	0.13

Table 4.1 Site 758A Composite records of sample location, depth, age, mean $\delta^{13}C$, magnetic susceptibility and $\delta^{86/88}Sr$ data for *G. ruber*.
All data except Sr data for *G. nuber* Farrell and Janecek, 1991

§ The chronostratigraphy here is based on the correlation of the site 758 oxygen isotope record from planktonic foraminifera Globigerinoides sacculifer (Farrell and Janacek, 1991) to the global average oxygen isotope record, the SPECMAP stack (ref. Imbrie et al., 1984). This chronostratigraphy is consistent with the biostratigraphic data (Shipboard Scientific Party, Site 758, 1989)

c Composite sample taken

* Data from Charlier et al. (2012)

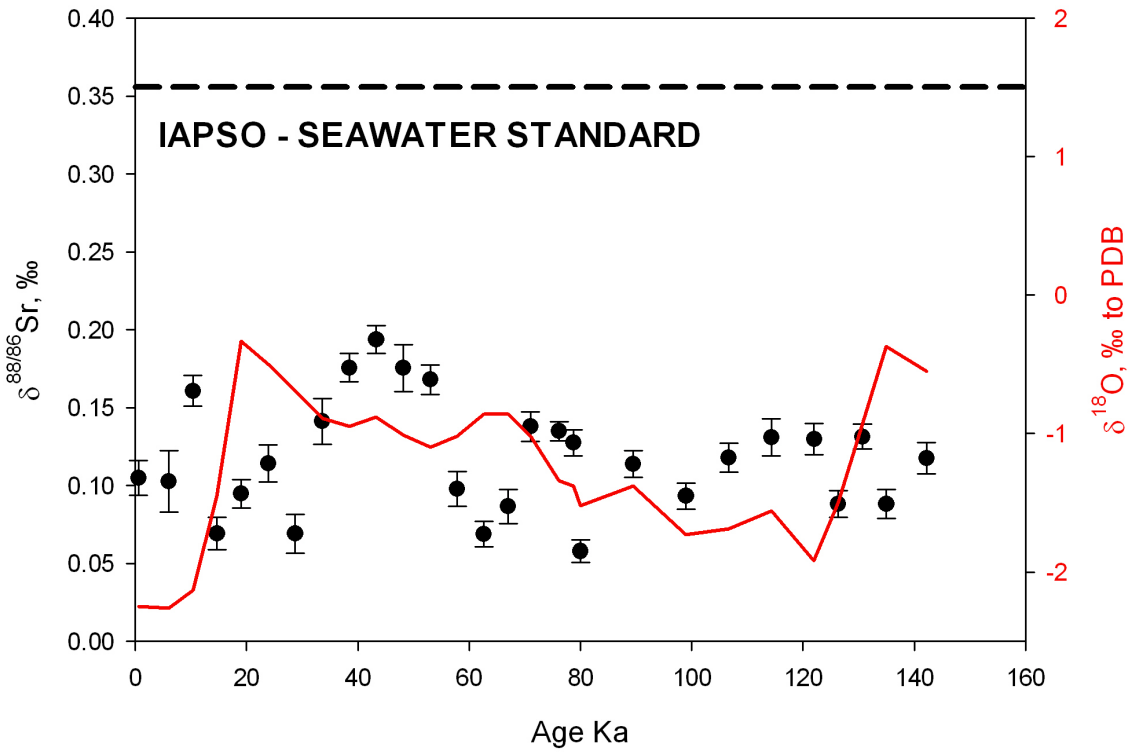

Figure 4.3 $\delta^{88/86}$Sr versus age plot covering 145 ka. At the 75ppm level $\delta^{88/86}$Sr =0.118±0.075‰ (2sd). IAPSO seawater standard is shown for reference The δ^{18}O curve (in red) from Farrell and Janacek (1991).

4.5 Discussion

The Sr stable isotope record preserved by *Globigerinoides ruber* (white, whole), in the 212-300 μm size fraction show clearly resolved variations of ~120ppm (Figure 4.3) much greater than the analytical uncertainty of ± 7-15 ppm. These data, unlike radiogenic Os and Nd, do not show variations that closely follow the oxygen isotope record (Burton and Vance, 2000; Burton et al., 2010). These variations could potentially arise as a consequence of a number of different effects including temperature and size effects, sedimentary diagenesis, local variations on seawater composition or whole ocean changes. Each of these will be considered in the following discussion.

4.5.1 Temperature and size effects

The Sr stable isotope composition of the core top (~550 yr) sample yields a $\delta^{88/86}$Sr value of +0.105±0.01‰, suggesting an offset from measured values for seawater in the Indian ocean of~ 0.25‰. This is consistent with the data for this species given in chapter three. The data for this species suggest that there is no significant effect with variations in shell size. Moreover, all of the samples studied here were taken from a restricted size range of 212-300 μm. However, the effect of temperature of precipitation for this species is not known. This raises the possibility that some of the variation seen in the 145 ka record might be due to variations in temperature. Sea surface temperature (SST) reconstructions of Prell et al. (1980) and Cullen (1981), show no significant temperature variation (<1°C) at this site, which is further confirmed by the shorter 40 kyr Mg/Ca data for *N. dutertrei*, *G. menardii* and *G. conglobatus*, of 1-2°C given in appendix 4 (a), suggesting that the shifts observed are unlikely to be due to variations in temperature.

4.5.2 Diagenesis and sedimentary contamination

The cleaning procedure adopted in this study (outlined in chapter 2) is primarily aimed at the removal of adhering clays and sediment particles and organic material on the surfaces of the foraminifera, but not the removal of secondary Fe-Mn oxyhydroxide coatings. The bulk sediment shows a typical Mn peak (see Table 1, Fig. 2a; Burton & Vance, 2000) commonly attributed to the precipitation of diagenetically mobilised Mn^{2+} at the oxic/ post-oxic boundary (e.g. Boyle, 1983). In sediments such as these, early diagenesis is driven by the oxidation of organic material leading to the dissolution of Fe-Mn oxyhydroxide phases under sub-oxic conditions. During this process Fe^{2+} and Mn^{2+} are released into pore waters and migrate upwards re-precipitating at the oxic/post-oxic boundary (e.g. Thomson et al, 1993). Such diagenetic mobilization has been

shown to significantly fractionate rare earth elements (e.g. Elderfield and Sholkovitz, 1987), and may well have resulted in Sr mobility and modification of the Sr stable isotope record at the site studied here.

As a consequence of the relatively high Sr concentration in foraminiferal calcium carbonate, it might be argued that the Sr isotope signal preserved in the calcite would dominate that of the Fe-Mn oxyhydroxide coating. However, Sr elemental data for foraminifera that have been cleaned using the full oxidative-reductive cleaning technique (for the removal of both organic material and Fe-Mn oxyhydroxide coatings) differs from those that have not been cleaned (Appendix 4 (b)) suggesting that Sr in the Fe-Mn coating may have some affect on the $\delta^{88/86}$Sr record. However, the $\delta^{88/86}$Sr variations show no clear relationship with the Mn elemental record in the bulk sediment, or indeed with the Sr in the uncleaned foraminifera. Taken together these data suggest that the $\delta^{88/86}$Sr variations cannot be explained by the mobilization of Sr and precipitation onto Fe-Mn coatings.

Alternatively, it is possible that some of the Sr stable isotope variations result from the presence of a signal acquired from volcanic ash, which possesses a relatively light $\delta^{88/86}$Sr isotope composition of -0.19±13 (Charlier et al., 2012). Magnetic susceptibility (MS) is primarily a measure of the concentration of magnetizable material, and variations in pelagic sediments usually reflect the ratio of biogenic to lithogenic material. However, a significant exception to this at site 758 is the presence of mafic volcanic ash (see Farrell and Janacek, 1991), and variations in the MS of the bulk at depths both above and below the ash layer corresponding to the eruption of the youngest Toba tuff at 74±2 ka minor amounts of ash disseminated in the sediments (Farrell and Janacek, 1991). In this case the magnetic susceptibility can be used as a proxy for the presence of ash, but there is no covariation either of $\delta^{88/86}$Sr isotope composition or

Sr concentration of foraminifera or the Sr concentration of the bulk sediments, suggesting that this element is not strongly influenced by the presence of volcanic ash (appendix 4(c)).

Taken together, these observations suggest that the $\delta^{88/86}$Sr isotope composition of *Globigerinoides ruber* preserved over the past 145 kyr have not been significantly affected by diagenesis or the secondary mobilization of Sr.

4.5.3 Shell preservation

Variations in the proportion of foraminiferal assemblages downcore in ODP-758A can reflect changes in preservation on the sea floor as the tests of some species of foraminifera are more susceptible to dissolution than others with systematic increase in the abundance of foraminiferal species with thick skeletons at the expense of less resistant species (Peterson and Prell, 1985a). The preservation of planktonic foraminifera in the deep ocean is controlled by the saturation state of the bottom waters and interstitial pore waters with respect to calcium carbonate (Chen and Farrell, 1991). The foraminifer lysocline (FL) is the depth at which the dominant type of foraminifera shifts in surface sediments from 'soluble' to 'resistant' species, known as the Resistant Species Ratio (RSP), (Berger, 1968). Values of RSP less than 30% are considered to lie above the FL, therefore the foraminiferal assemblage is assumed to primarily reflect fluctuations in foraminifera input from surface waters and thus ecological factors, whereas those exceeding than 30% are assumed to be significantly influenced by $CaCO_3$ dissolution. During the period 140 ka to 20 ka, the RSP%, as estimated by Chen and Farrell, (1991), exceeded 30%, rising to as high as 60% in some periods, see Figure 4.6 indicating a significant influence of dissolution. The coarse fraction (wt% $CaCO_3$ >150μm) is also considered to be a reliable index of relative dissolution intensity (e.g. Berger, 1970), where low coarse fractions represent times of enhanced

dissolution, which are observed over the period 40-140 kyr as shown in Figure 4.4. Taken together, the RSP% and coarse fraction data suggests that the dissolution of foraminifera is likely to have been an additional cause of variation in foraminiferal abundance in the 145 kyr record.

Figure 4.4 Percentage abundance of A. Resistant species ratio (RSP%). Arrow shows the modern foraminifera lysocline as defined by the 30% RSP level (see text) B. Coarse fraction (wt%>150μm) and $\delta^{18}O$ (‰ to PDB from G. sacculifer) from ODP 758A. Taken from Chen and Ferrell (1991)

The data of Spero et al. (1997) was taken to suggest that the $\delta^{13}C$ and $\delta^{18}O$ ratios of foraminiferal calcite shells decreases with increasing seawater $[CO_3^{2-}]$. A decrease in $[CO_3^{2-}]$ is associated with an increase in acidity and thus enhances the potential for shell/test dissolution. For the samples studied here a strong co-variation of the $\delta^{13}C$ and $\delta^{88/86}Sr$ data is observed, as $\delta^{13}C$ shifts towards

lighter values so does the $\delta^{88/86}$Sr, which might suggest that as the propensity for dissolution increases, the heavier $\delta^{88/86}$Sr isotope (^{88}Sr) is becoming mobile, Figure 4.5.

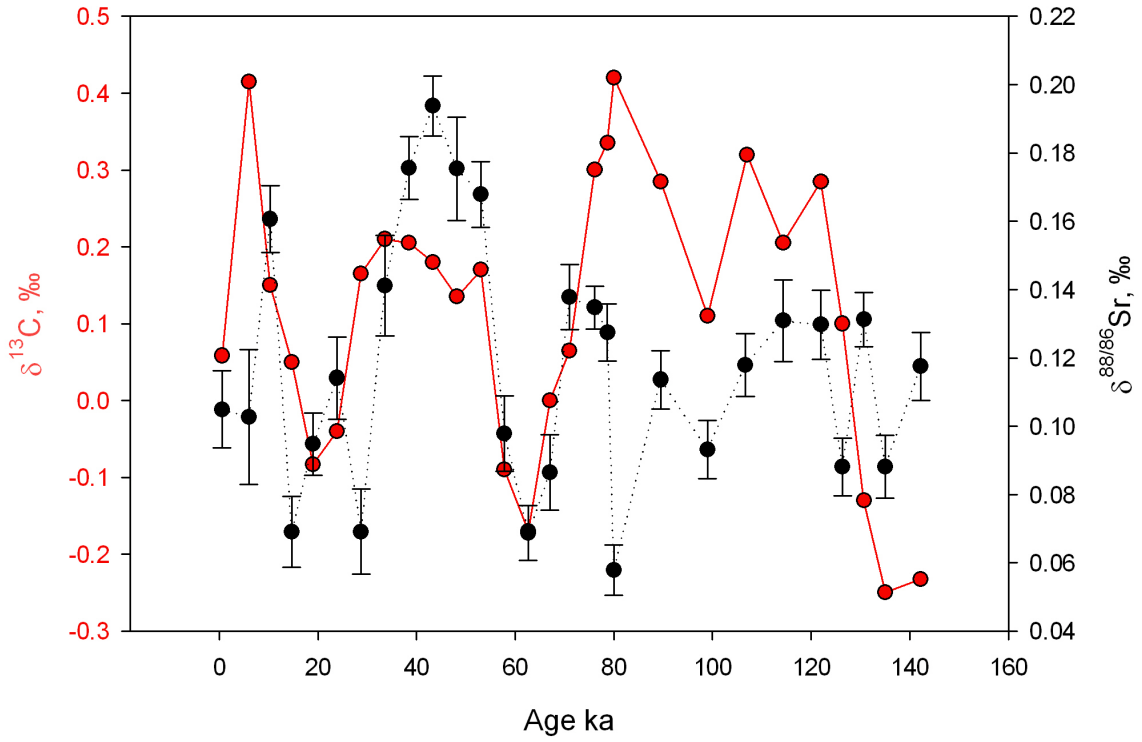

Figure 4.5 Plot of $\delta^{88/86}$Sr versus age covering 145 ka with the δ^{13}C curve from Farrell and Janecek, 1991

4.5.4 Local variations in seawater chemistry

Alternatively it may be that the variations in $\delta^{88/86}$Sr isotope composition preserved over the past 145 kyr at this site relate either directly to local changes in the Sr stable isotope composition of seawater, or are an indirect consequence of variations in water chemistry that have affected the signal preserved by foraminifera.

Variations in the abundance of different species of foraminifera can provide some indication of variations in the source of the water. *Pulleniatina obliquiloculata* is a tropical subsurface dwelling planktonic foraminifera, the abundance of which is closely related to subsurface

seawater temperatures (SSST) and the depth of the thermocline (An and Jian, 2009). Chen and Farrell (1991) found a anonymously high proportions of *P. obliquiloculata* between 35-60 ka (~MIS 3), as shown in Figure 4.6, in the same core, which coincides extremely well with the shift to heavy values seen in $\delta^{88/86}$Sr. The high abundance in *P. obliquloculata* is greater than that in core tops from the modern Indian Ocean, but is similar to that found in modern core top samples from the western tropical Pacific, (Chen and Farrell, 1991) suggest that at this period in the northeastern Indian Ocean seawater conditions were closer to those in the modern Western tropical Pacific, rather than the modern Indian Ocean.

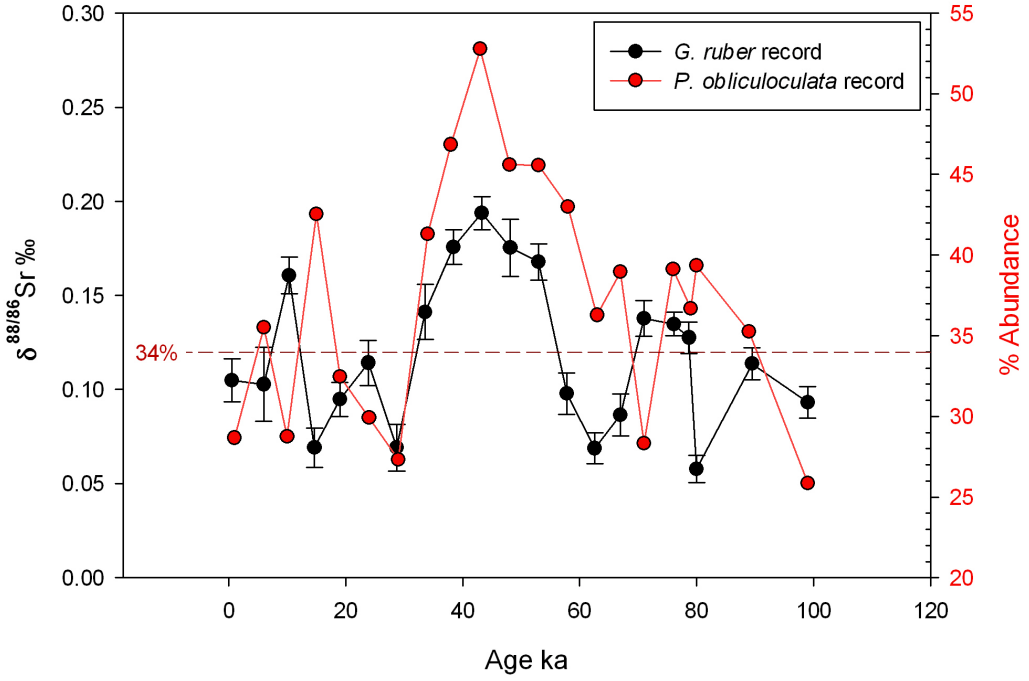

Figure 4.6 Plot of percent abundance of *P. obliquloculata* in 758 for the last 100 ka, 34% is the average modern day abundance of this species in the Indian Ocean (Cullen and Prell, 1984).

Six species of foraminifera remain the most abundant in the core over the time interval studied here (Chen and Ferrell, 1991), and their variations in abundance are shown in Figure 4.7. As stated above, the abundance of foraminifera can be related to surface water conditions (e.g.

Cullen, 1984; Chen and Farrell, 1991), with the most important factors controlling their abundance including sea-surface temperature (SST), salinity and productivity. Both *G. sacculifer* and *G. ruber* are shallow dwelling species that are often found in sediments underlying the warm waters of tropical oceans, and due to their thinner tests, are more susceptible to dissolution, the abundance of which decreases during MIS 3, whereas the abundance of the dissolution resistant species *P. obliquiloculata* and *G. menardii* increases, suggesting their abundance may be influenced by dissolution.

The decrease in the abundance of *N. dutertrei* (panel (c) in Figure 4.5) was has been attributed to changes in salinity or productivity at site 758 (Chen and Farrell, 1991), where increases in abundance could be due to either decreasing salinity or by regional fluctuations in the ratio of evaporation to precipitation. This suggests that the decrease in the abundance of *N. dutertrei* may be associated with enhanced advection of warmer, more saline, waters to this region. Chen and Farrell (1991) also suggest that higher percentages of *P. obliquiloculata* are more common in interglacials when throughflow between the tropical Indian and Pacific Oceans was greatest; in contrast, during glacial times sea water low stands restricted the exchange of water between these two regions.

The Indonesian Throughflow (ITF) is thought to play an important role in global ocean circulation as it provides a low-latitude pathway for warm, fresh water to move from the Pacific to the Indian Ocean (e.g. Gordon et al., 2003). During MIS 3 sea-level fluctuations reached magnitudes of 35±12m (Dürkop et al., 2008), and planktic foraminiferal oxygen isotope and palaeoproductivity studies have been taken to indicate high variability in ITF outflow during MIS 3 (Holbourn et al., 2005). It is not known whether variations in salinity affect the $\delta^{88/86}Sr$ recorded in foraminifera, and this is one aspect of Sr stable isotope chemistry that merits

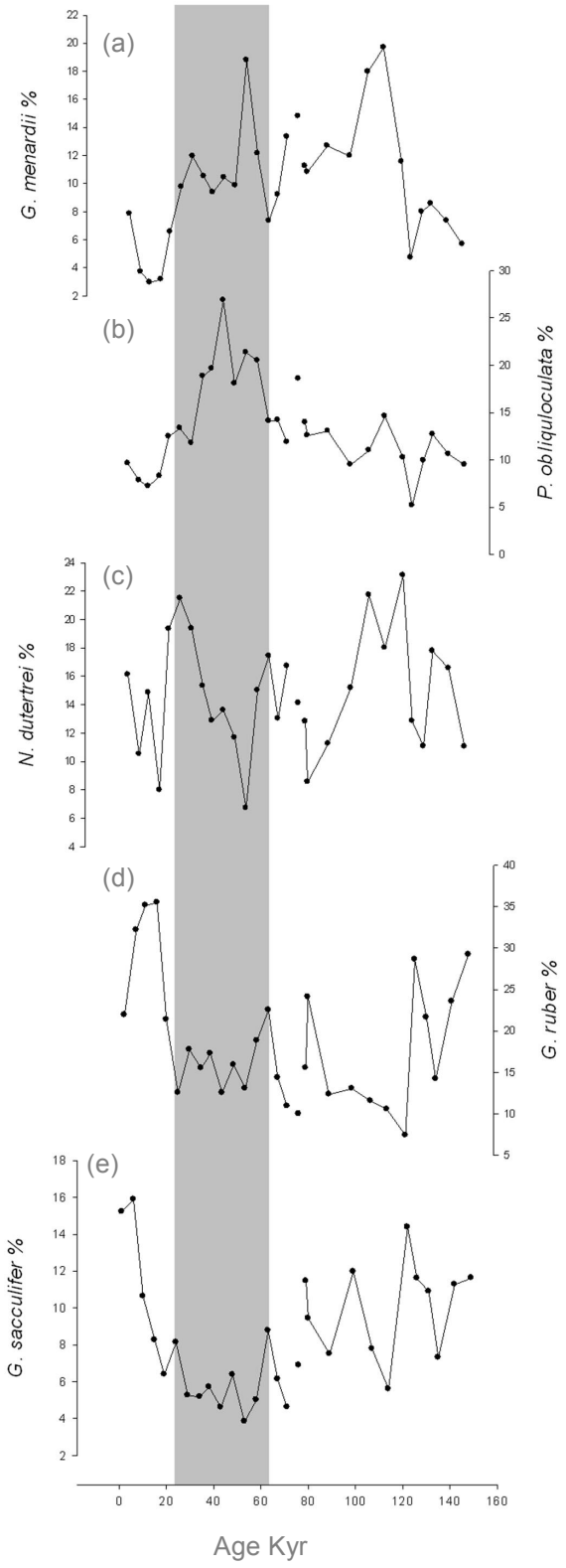

Figure 4.7 Percent abundance as a function of total foraminiferal species taken from Chen and Farrell, 1991 for (a) *G. menardii*, (b) *P. obliquiloculata*, (c) *N. dutertrei (d) G. ruber, and (e)G. sacculifer*. The shaded grey area highlights the timing of the $\delta^{88/86}Sr$ excursion

investigation in the future. The excursion observed in this study is significant, but at this stage it is not clear whether the variations in $\delta^{88/86}$Sr in the 145 ka record could be due to a simple change in water mass alone. The $\delta^{88/86}$Sr data from a single modern seawater sample from the Pacific Ocean yields a value that is slightly heavier that of a single Indian Ocean seawater sample (see chapter 2, Figure 2.4). The variations in the $\delta^{88/86}$Sr isotope composition of seawater at this locality could possibly be due to the increased advection of Pacific water into the Indian Ocean through the Indonesian gateway, thereby accounting for the shift to heavy values seen around 35-60 ka. However, the limited existing data (i.e. 2 samples) indicates a subtle $\delta^{88/86}$Sr difference between the Indian and Pacific Ocean ($\delta^{88/86}$Sr = 0.347±0.006 and 0.363±0.006 ‰, 2.s.e respectively; (illustrated in Figure 2.4, chapter two) that cannot account for the order of change we observe in the record. Further measurements are needed to quantify the magnitude of the difference in the $\delta^{88/86}$Sr isotope composition between the Indian and Pacific Ocean.

4.5.5 Whole ocean changes

While local changes in seawater chemistry may account for some, if not all, of the $\delta^{88/86}$Sr variation observed, it is also possible that these variations reflect whole ocean changes in the composition of $\delta^{88/86}$Sr. Strontium is a conservative element, well mixed in the oceans, with a residence time of > 2.5 Ma (Hodell et al., 1990; Richter and Turekian, 1993) that is much longer than the mixing time of the oceans ~10^3 yr (e.g. Veizer, 1989) and necessitates significant changes in the flux or composition of material delivered by continental weathering in order to cause a measurable change in the composition of seawater (Richter and Turekian, 1993).

Higher temperatures and runoff enhance chemical weathering and increase metal transport to the oceans via rivers; therefore, it is reasonable to assume that during glacial intervals when

temperatures are cooler and continental runoff is lower that the weathering flux to the oceans will be reduced. Recent data for radiogenic osmium isotopes ($^{187}Os/^{188}Os$) indicates shifts of 10% through the last glacial maximum that must have involved changes in the flux and/or composition of material delivered to the oceans by continental weathering (Burton et al., 2010). Crucially, for Sr stable isotopes, there is evidence to suggest that there was also a change in the balance of carbonate to silicate weathering since the LGM, as presented in section 4.1. These observations suggest that the relative proportion of carbonate weathering will have increased just before glacial intervals due to a drop in sea level, and then also during glacial intervals, shifting the composition of weathered material delivered from the continents to lighter stable Sr isotope compositions. The effect on the $\delta^{88/86}Sr$ value of seawater can be modeled assuming a three-fold change in the Sr flux occurred during a glacial cycle. This can be accomplished using a mass balance equation, 4.1

$$\frac{dR_{SW}}{dt} = \left[\frac{JSr_{RIV}(R_{RIV} - R_{SW})}{Sr_{SW}}\right] + \left[\frac{JSr_{HYD}(R_{HYD} - R_{SW})}{Sr_{SW}}\right] + \left[\frac{JSr_{DIA}(R_{DIA} - R_{SW})}{Sr_{SW}}\right] - \left[\frac{JSr_{CARB}(R_{CARB} - R_{SW})}{Sr_{SW}}\right]$$

[4.1]

where R_{RIV}, R_{HYD}, R_{DIA} and R_{CARB} are the $^{88}Sr/^{86}Sr$ or $^{87}Sr/^{86}Sr$ ratios and JSr_{RIV}, JSr_{HYD}, JSr_{DIA} and JSr_{CARB} are the riverine, hydrothermal, diagenetic input and carbonate output fluxes respectively. R_{RIV} and Sr_{SW} are the Sr isotope ratio and concentration of seawater. Input values and fluxes are from Vance et al. (2009) and Krabbenhoft et al. (2010), with the additional increase in carbonate weathering incorporated into the diagenetic flux. However, the modeling made some key assumptions. Firstly that Equation 6.1 is steady-state with respect to the Sr concentration in seawater if the carbonate output flux is equal to the input fluxes for Sr, so any

model that has dramatic increases in the input fluxes requires marine carbonates to remove considerably more Sr. Although, Lear et al. (2003) suggest Sr concentrations have increased by a factor of two over the last 40 Ma, short term changes in the Sr concentration of marine carbonates are equivocal. However, Equation 6.1 can be easily modified to allow both increases and decreases in the Sr concentration of the oceans. Secondly, a three-fold increase in the weathering of carbonate platforms makes the model very sensitive to the $\delta^{88/86}$Sr of both the weathered carbonate and the carbonate output as both these reservoirs are isotopically light.

Figure 4.8 illustrates the effect on the $\delta^{88/86}$Sr ratio of seawater over the last glacial cycle (20 ka) for a variety of weathering fluxes. The data from Vance et al, (2009) allow the calculation of a long term Sr flux data set that explains the 70 ppm Ma^{-1} shift in $^{87}Sr/^{86}Sr$ over the last 1 Ma, which can be simply modified to give short term 30 and 70% increases in the weathering flux. Additionally the data from (Krabbenhoft et al. 2010) can be modeled with a short-term non-steady state concentration model whereby 90, 70, 50 and 30% of the Sr is not removed by the carbonate output flux over this 20kyr period. The consequences of these models for the Sr ocean concentration are minor due to the long residence time of Sr in the oceans. There are two clear conclusions from the modeling; firstly $\delta^{88/86}$Sr is highly insensitive (<0.003‰) to short term changes in the weathering fluxes, even if they are large, and therefore no measurable changes in $\delta^{88/86}$Sr are expected on a glacial-interglacial cycle. This is not surprising because the compositions of the various end-member reservoirs are only 0.2‰ different in composition. The effect of making the model non-steady state with respect to Sr concentration is that less light $\delta^{88/86}$Sr is removed and so seawater evolves to slightly lighter $\delta^{88/86}$Sr. Secondly the $^{87}Sr/^{86}Sr$ ratio of the modeled seawater compositions are much more sensitive to the addition of a three-fold increase in carbonate that is slightly unradiogenic compared to seawater. In fact all of the

models that involve such a large increase in carbonate weathering produce a decrease in seawater $^{87}Sr/^{86}Sr$ of ~10 ppm. Such shifts are both measurable and are not observed in the record (Mokadem et al., unpublished, Ando et al., 2010). In fact, such models go against the overall shift of increasing $^{87}Sr/^{86}Sr$ over the last six glacial cycles.

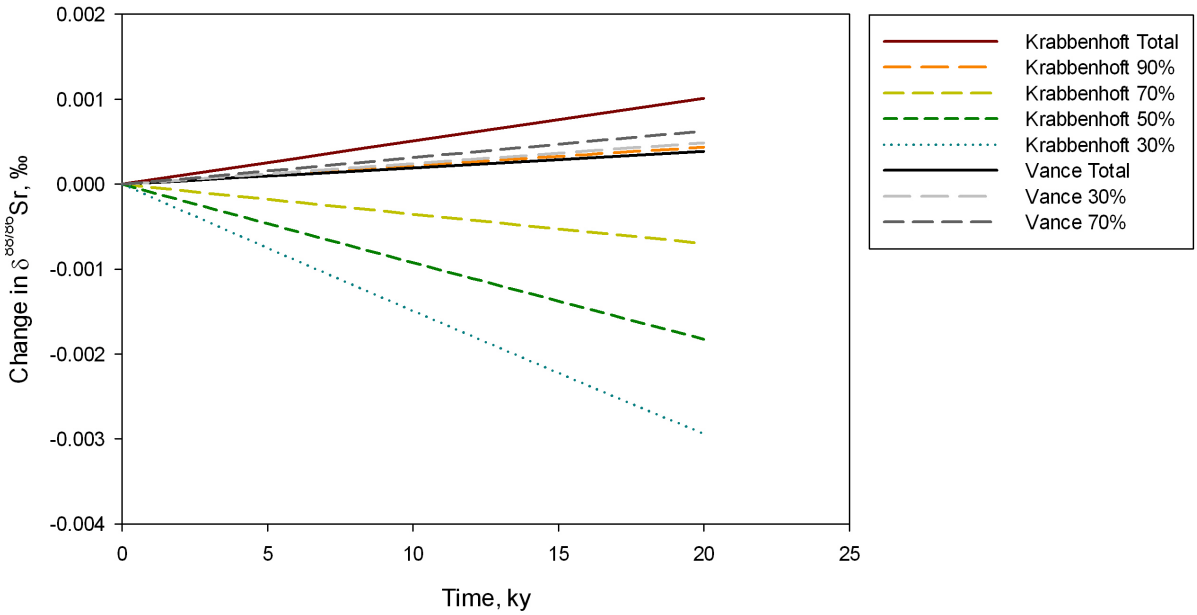

Figure 4.8 Modelled evolution of $\delta^{88/86}Sr$ over the last 20 ka based on figures published by Krabbenhoft et al. (2010) and Vance et al. (2009) with percentages referring to the proportion of silicate weathering that constitutes a non-steady state weathering regime, see text for details.

It was not possible to measure the unspiked $^{87}Sr/^{86}Sr$ data from the samples prepared due to a lack of sample therefore true $\delta^{88/86}Sr$ data were obtained from the DS measurement and an assumption that the $^{87}Sr/^{86}Sr$ ratio in seawater does not vary. This has been confirmed by recent high precision $^{87}Sr/^{86}Sr$ measurements in foraminifera over this 145 kyr period (Mokadem et al., submitted; Ando et al., 2010). However, in order to take account of possible variations, such as the 100 kyr variation suggested by Vance et al. (2010), the data were also deconvolved with the $^{87}Sr/^{86}Sr$ ratio decreasing by ~7ppm per 100 kyr; there was no significant difference between the samples deconvolved using the modern day and cyclical values of $^{87}Sr/^{86}Sr$ in the $\delta^{88/86}Sr$ values.

4.6 Conclusions

Data from *G. ruber* over the last two glacial cycles shows resolvable variations, with a large excursion during MIS 3. However, it is not clear whether the $\delta^{88/86}Sr$ variations are due to local changes in seawater or are due to global ocean changes, however modeling suggests that it is not the latter suggestion as $\delta^{88/86}Sr$ was shown to by insensitive (<0.003‰) to short term changes in the weathering fluxes. Although weathering of carbonate platforms is likely during glacial periods, the level of increased flux is likely to be considerably smaller than that described in (Krabbenhoft et al. 2010). Furthermore, Models that require a post-glacial increase in weathering flux, produce shifts in $^{87}Sr/^{86}Sr$ that are at the limits of our current measurement capability and are not observed in high-precision $^{87}Sr/^{86}Sr$ records through the last glacial cycle (Ando et al., 2010; Mokadem et al., submitted). Whilst we cannot ignore the large excursion it is possible it could be due, in part, to digenetic effects; leeching experiments in the future may determine if this is indeed the case.

The residence time of Sr in the ocean and the modeling by Parkinson (unpublished) suggest that we should not see excursions of this size on a global scale, further confirming that if anything the scatter we observe in our data is most likely related to post depositional digenic effects or perhaps local changes in seawater.

Future work should apply the $\delta^{88/86}Sr$ proxy to investigations of changing oceanic carbonate chemistry over periods longer than the residence time of Sr in the ocean such as the mass carbonate dissolution events at the Paleocene-Eocene Thermal Maximum (PETM) ~55 million years ago (e.g Zachos et al., 2005) or the Caribbean carbonate crash (CCC) ~12-10 Myr (e.g. Roth et al., 2000).

CHAPTER FIVE

Stable strontium isotope fractionation in coccolithophores: Proxy for coccolithophore growth rate and implications for the marine Sr cycle

Summary

This chapter investigates the behaviour of stable strontium isotopes in coccolithophores. Coccolithophores are one of the most abundant marine calcifiers and represent a large output of Sr from seawater, potentially influencing the $\delta^{88/86}$Sr mass balance in the modern oceans. In this study the controls on stable Sr isotope composition for the species *Emiliania huxleyi, Coccolithicus pelagicus and Gephryocapsa oceanica* are investigated. Each species has been cultured under controlled laboratory conditions at a range of temperatures (10- 25°C) in two different nutrient (varying N to P) media. The coccoliths were cleaned and $\delta^{88/86}$Sr, Sr/Ca, δ^{18}O and δ^{13}C measured. All species show a temperature dependent fractionation, which is related to the temperature controlled growth rate. As temperature increases, so does growth rate and Sr/Ca, while $\delta^{88/86}$Sr shifts to lighter values, indicative of a kinetic isotope fractionation.

The results from these experiments indicate that coccolithophore calcite incorporates Sr with a very light $\delta^{88/86}$Sr isotope composition, as low as ~0‰, driving the overall marine Sr output budget to lower values than previously considered.

5.1 Introduction

Marine calcareous carbonate is the largest sink for Sr in the global ocean and as such plays an important role in the Sr isotope cycle. Stable strontium isotopes ($\delta^{88/86}$Sr) are fractionated from seawater during precipitation of marine calcium carbonate, this has been shown to be the case for both coral and inorganic aragonite (e.g. Fietzke and Eisenhuer 2006; Rüggeberg et al., 2008) as well as for different calcite-forming foraminifera (Chapter 3). However, there are no published studies to date that explore $\delta^{88/86}$Sr fractionation in coccolithophores; one of the most important pelagic calcifying organisms present in the oceans (Ra et al., 2010). Coccolithophores are unicellular marine phytoplankton; they are distributed worldwide, more abundant than foraminifera, and in oligotrophic regions comprise up to 70 wt.% of the calcareous sediments (Baumann et al., 2004). These organisms produce tiny and intricate calcite scales called coccoliths, intracellularly, to cover the cell exterior. Consequently, for the strontium cycle at least, coccolithophores comprise a large proportion of the output flux of Sr from the oceans, and exert a considerable influence over global biogeochemical cycles, such as the global carbon and calcium cycles.

Coccolith shells preserved in marine sediments potentially provide key geochemical information on past seawater chemistry and seawater temperatures. Both the organic and inorganic remains of the coccolithophore can be used for paleoceanographic interpretation (surmised in Table 5.1; Stoll and Ziveri (2004) and references therein) however, many of these proxies are influenced by other environmental factors and/or vital (biological) effects that hamper their interpretation. In particular the work of Stoll and Schrag (2000) suggested that Sr/Ca ratios in coccolithophores could be used as indicators of calcification rate, as the Sr/Ca ratios are strongly correlated with coccolithophore growth rate.

Indicator	Inferred primary control	Secondary influences	Limitations
U_{37}^{K} (alkenone undersaturation)	Temperature	Physiology or growth rate?	
$\varepsilon^{13}C$ alkenone	pCO2	Cell growth rate and cell size	Requires estimation of ^{13}C of dissolved inorganic carbon
Sr/Ca	Productivity/ coccolithophoriod growth rate	Temperature and seawater Sr/Ca	Long term records (>106 yr) mat require correction for changing seawater Sr/Ca
Mg/Ca	Temperature	Species-specific effects	Requires thorough cleaning of Mg from non-carbonate fractions
$\delta^{18}O$	Temperature and $\delta^{18}O$ of seawater	Vital effects	
$\delta^{13}C$	$\delta^{13}C$ of dissolved inorganic carbon	Vital effects	May require seperation of monospecific samples, assumption of constant vital effects, and inference of vital effects for extinct species

Table 5.1: Common proxies an their limitations in coccolithophores, reproduced from Stoll and Ziveri (2004).

However, aside from seawater Sr/Ca changing the Sr content, other environmental parameters may affect the partitioning of Sr/Ca, including temperature (e.g Stoll et al., 2002a) and changes in light-intensity (Stoll et al., 2002b). Uncertainties in the nature of vital (biological) effects in coccolithophores and a variety of marine calcifying organisms, have hampered palaoceanographic analysis of isotopic proxies which need to be quantified before an accurate interpretation of records can be achieved. In particular, though the primary effects and mechanisms of precipitation are comprehended, there are gaps in understanding with respect to biologically induced calcite formation (e.g. Gussone et al., 2006).

The stable isotope behaviour of Mg ($\delta^{26/24}Mg$) and Ca ($\delta^{44/40}Ca$) in coccoliths has been investigated (e.g. Gussone et al., 2006; Ra et al., 2010; Müller et al., 2011) with a view to elucidating the physiological control over Ca or Mg elemental and isotope fractionation during the process of calcification in biomineralisation, as well as reconstructing the Ca budget of the ocean (e.g. De La Rocha and De Paolo, 2000). Quantifying elemental

fractionation during biomineralisation can improve our knowledge and understanding of proxy behaviour and their utility in the interpretation of marine records. Due to the small size of coccoliths, (1-20μm across), separating them from bulk sediments can be difficult, unlike foraminifera individuals cannot be 'separated' and this has hindered their use as geochemical archives. However, recent advances such as the Minoletti technique (Minoletti et al., 2008) offer the potential for size and species separation of coccolithophores. Laboratory cultures represent a useful model system with which to explore the controls on the chemistry of coccoliths and are a crucial step in applying coccolith-based paleoproxies to past environmental conditions. To test whether coccoliths exert a significant biological effect on the uptake of stable strontium isotopes in comparison to corals (Fietzke and Eisenhauer, 2006, Rüggeburg et al., 2008), foraminifera (chapter 3) or inorganic calcite (Böhm et al., 2012); three coccolithophoroid species have been cultured at four different temperatures (10, 15, 20 and 25°C) and in two different nutrient media with differing nitrogen to phosphorus ratios.

The coccolithophores chosen for this study were *Emiliania huxleyi, Coccolithius* pelagicus (ssp. braarudii) *and Gephryocapsa oceanica*. *E. huxleyi* is one of the most numerically abundant coccolithophores in the modern ocean, and both *E. huxleyi* and *C. braarudii* have been present in the marine sediment record for about 270 thousand years and 65 million years, respectively (Müller et al., 2011) which makes them a potentially valuable archive for constructing records of seawater chemistry. Despite being one of the most abundant coccolithophores, *E. Huxleyi* is one of the smaller coccolithophorids, whereas both *C. pelagicus* and *G. oceanica* are larger in size and are significant contributors to carbonate sediments at both high and low latitudes, respectively.

The data collected in this study provides information on the modern day Sr cycle with regards to inputs and outputs from the ocean. With traditional radiogenic Sr isotopes ($^{87}Sr/^{86}Sr$) the

output flux of Sr from the oceans cannot be assessed (although implicit in mass balance equations, see Equation 5.1) as the $^{87}Sr/^{86}Sr$ ratio of carbonates is the same as that of seawater (see chapter 1). Stable strontium isotopes in marine calcium carbonate are lighter than modern day seawater (e.g. Fietzke and Eisenhauer, 2006; Rüggeburg et al., 2008; Krabbenhöft et al., 2010; Böhm et al., 2012), consequently the stable Sr fractionation enables an assessment of the modern day output flux of Sr from the oceans, and taken with $^{87}Sr/^{86}Sr$ can be used to assess the mass balance of Sr in the ocean both today and, eventually, in the past.

$$\frac{dR_{SW}}{dt} = \left[\frac{JSr_{RIV}(R_{RIV} - R_{SW})}{Sr_{SW}}\right] + \left[\frac{JSr_{HYD}(R_{HYD} - R_{SW})}{Sr_{SW}}\right] + \left[\frac{JSr_{DIA}(R_{DIA} - R_{SW})}{Sr_{SW}}\right] - \left[\frac{JSr_{CARB}(R_{CARB} - R_{SW})}{Sr_{SW}}\right]$$

[5.1]

where R is the Sr ratio of interest, J is the flux of the in-/out- put of the riverine, hydrothermal, diagenetic input and carbonate output fluxes respectively, and Sr_{SW} is the concentration of Sr in seawater.

In summary, this chapter presents Sr stable isotope data for cultured coccolithophores, these experiments were aimed at investigating the temperature dependency, and hence growth rate effect, on Sr stable isotope incorporation into coccolith calcite.

5.2 Methods

5.2.1 Laboratory Culturing

Dilute batch cultures of monoclonal *Emiliania huxleyi, Gephyrocapsa oceanica,* and *Coccolithus pelagicus* sp. *braarudii* (strains RCC 1211, RCC 1314, RCC 1202) from the Roscoff Culture Collection (http://www.sb-roscoff.fr/Phyto/RCC) were produced out at the University of Oxford. Each species was cultured at four temperatures (10, 15, 20, and 25 °C) with two replicate cultures at each temperature. Batch cultures were carried out in 600 mL Nunc® polystyrene flasks, using aged English Channel seawater; each culture was enriched in trace metals, EDTA, nitrate, phosphate and vitamins following the method described in Probert and Houdan (2004). Trace metal and chelator enrichments were added corresponding to K and K/6 (appendix 5a; Keller et al., 1987). Nitrate and phosphate concentrations were adjusted as follows: 576 $\mu mol.L^{-1}$ and 100 $\mu mol.L^{-1}$ nitrate for K and K/6 respectively and 36 $\mu mol.L^{-1}$ and 6.25 $\mu mol.L^{-1}$ phosphate for K and K/6 respectively. f/2 level of vitamins was used (appendix 5a; Guillard, 1975). The media was bubbled with atmospheric air for 24 hours and the pH was corrected to 8.2 (total scale) by addition of 0.2 M NaOH.

The cultures were slowly acclimatised (0.5 $°C.day^{-1}$) to the appropriate temperature and maintained in their exponential phase of growth for at least 10 generations before the experiments were started. Cultures were illuminated by daylight fluorescent bulbs at a light intensity of 200 $\mu mol\ photons.m^{-2}.s^{-1}$, corresponding to the mean photic zone irradiance value, with a 14/10 light/dark cycle.

Cell concentrations of *G. oceanica* were measured using a Beckman Coulter Counter II. The initial cell density at inoculation was about 200 $cells.mL^{-1}$. Aliquots of the culture medium were sampled at the beginning and the end of the experiments, filtered through a 0.22 µm syringe filter and kept at 4 °C.

There culturing experiments for *C. pelagicus* at 25°C or *E. huxleyi* at 10°C were not successful.

Cultures were harvested when cell density reached ~ 150,000 cells mL^{-1} for *G. oceanica* and *E. huxleyi* and 12,000 cells mL^{-1} for *C. pelagicus*. At this stage, the algal population was still in the exponential growth phase. Cocoliths are isolated from seawater via vacuum filtration for analysis.

5.2.2 TIMS analysis

For Sr stable isotope analysis the coccoliths were cleaned and prepared as outlined in Chapter 2 prior to measurement using TIMS.

5.2.3 Trace elemental analysis

Organic matter was removed from the coccoliths using the following technique; 20mL 10% H_2O_2 (neutralised to pH 8 using 5M NaOH) was added to each sample, these were then left in a 60°C oven for 12h. Each sample was then centrifuged and the overlying solution removed. The coccolith pellet was washed three times by re-suspending in 30mL de-ionised water (pH adjusted to 7), centrifuged and the liquid removed. The pellet was left to dry down in an oven at 60°C overnight. The samples were weighed and dissolved in 2M HNO3, and aliquot was taken, dried down and re-suspended in 2mL 1% HNO_3 to make 10ppm Ca solutions for analysis on a Thermo Scientific ELEMENT ICP-MS

Sr/Ca ratios were measured and analysed using matrix-matched standards. Standards were prepared from multiple element ICP standards diluted to 0.1, 0.5, 1, 5 and 10ppm Ca with 0.1, 0.5, 1, 5 and 10ppb Sr respectively, diluted in the same 2% HNO_3 matrix as the samples.

5.2.4 Stable isotope ($\delta^{13}C$ and $\delta^{18}O$) analysis

Coccolithophores were prepared and analysed for $\delta^{18}O$ and $\delta^{13}C$ isotopes measurements on an IsoPrime High Performance Stable Isotope Ratio MS at the Université Pierre et Marie Curie (UPMC), Paris.

5.2.5 Calculation of growth rate

For *G. oceanica* growth rate data is approximated from cell densities at the beginning and end of the experiment, cell growth rate (μ_{cocco}, unit d^{-1}):

$$\mu_{cocco} = \frac{\ln c_1 - \ln c_0}{\Delta t} \qquad [5.2]$$

where c_0 and c_1 denote the cell densities at the beginning and end of the experiment, and Δt is the duration of the incubation in days. For *E. huxleyi* and *C. pelagicus,* (where cell density data was not available) growth rate is calculated using the final weight of biomass at the end of the experiment (GR, unit mg d^{-1}). This was also calculated for *G. oceanica* for comparison.

$$GR = \frac{BM_f}{\Delta t} \qquad [5.3]$$

where BM_f is the final biomass at the end of the experiment.

5.3 Results

5.3.1 Stable Sr isotopes

The $\delta^{88/86}$Sr isotope composition of the growth medium (prepared from English channel seawater) is 0.396±0.007‰ (2.s.e) and is within the range of the IAPSO seawater standard +0.397±0.007‰ (2.s.e n=3) (Batch P141: Salinity 34.997). The $^{87}Sr/^{86}Sr$ ratio of the seawater is 0.709173±0.000003 (2.s.e.); the stable Sr values of both the seawater and coccoliths were deconvolved from spike measurements using this value for $^{87}Sr/^{86}Sr$, assuming that there was no fractionation during calcite precipitation.

Stable Sr isotopes were analysed in coccoliths precipitated from the nutrient replete media (K), all species studied (*E. huxleyi, G. oceanica and C. pelagicus*) show a negative correlation with temperature (see Figure 5.1 and Table 5.2) with *G. oceanica and C. pelagicus* having a stronger temperature dependency than *E. huxleyi*. (*G. oceanica* ~-0.024‰/°C (R^2=0.95)*; C. pelagicus* ~-0.025‰/°C (R^2=0.90); *E. huxleyi* ~-0.012‰/°C (R^2=0.75)*,* Figure 5.1).

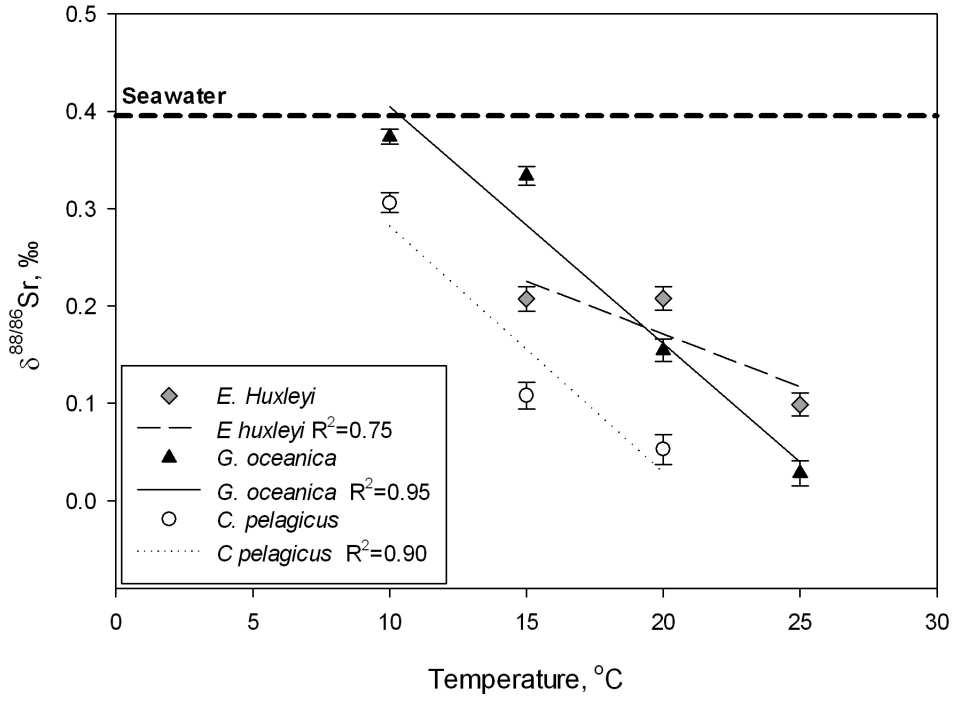

Figure 5.1: Temperature dependent fractionation of $\delta^{88/86}$Sr in cultured coccolithophores. The seawater $\delta^{88/86}$Sr values are given in the thick dashed line for comparison.

Coccolithophore species	Temperature, °C	Nutrients	$^{88}Sr/^{86}Sr$	2 s.e.	$\delta^{88/86}Sr$ ‰	2s.e. ‰	$\Delta^{88/86}Sr_{(calc\text{-}aq)}$ ‰	Growth rate (GR)(mg d^{-1}))
Emiliania huxleyi	15	K	8.37695	0.0001	0.207	0.012	-0.189	1.69
	20	K	8.37695	0.0001	0.208	0.012	-0.188	2.62
	25	K	8.37604	0.0001	0.099	0.012	-0.297	2.46
Coccolithicus pelagicus	10	K	8.37834	0.0001	0.306	0.008	-0.022	1.18
	15	K	8.37800	0.0001	0.108	0.010	-0.062	1.89
	20	K	8.37650	0.0001	0.053	0.011	-0.241	2.31
Gephryocapsa oceanica	10	K	8.37544	0.0001	0.374	0.013	-0.368	0.70
	15	K	8.37777	0.0001	0.334	0.010	-0.090	2.40
	20	K	8.37612	0.0001	0.155	0.014	-0.288	2.95
	25	K	8.37565	0.0001	0.028	0.015	-0.343	4.20
Seawater medium			8.37852	0.0001	0.396	0.007	0	

Table 5.2 $\delta^{88/86}Sr$ ‰, Sr/Ca and growth rate data for coccolithophores in K media. See text for details of growth-rate calculations

5.3.2 Sr/Ca ratios

The Sr/Ca ratios were analysed in coccoliths precipitated from both the nutrient media (K and K/6), all species studied (*E. huxleyi, G. oceanica and C. pelagicus*) show a positive correlation with temperature, Figure 5.2 (a), and the range of Sr/Ca is consistent with other studies (e.g. Rickaby et al., 2002; Stoll et al., 2002(a); Stoll et al., 2002(b); Stoll et al., 2007). The same trend is observed for the Sr/Ca data in the nutrient deplete media (K/6) however, for every species there is an offset of about 0.1-0.2 mmol/mol, between K and K/6 with coccoliths precipitating from the nutrient replete media (K) incorporating less Sr than coccoliths precipitating from nutrient deplete media (K/6). Calcium is a biologically important element whereas Sr is not, and it appears that when nutrients are abundant, coccolithophores have a greater ability to distinguish between Sr and Ca, however, the offset is small and despite being consistent more work needs to be done to confirm this observation.

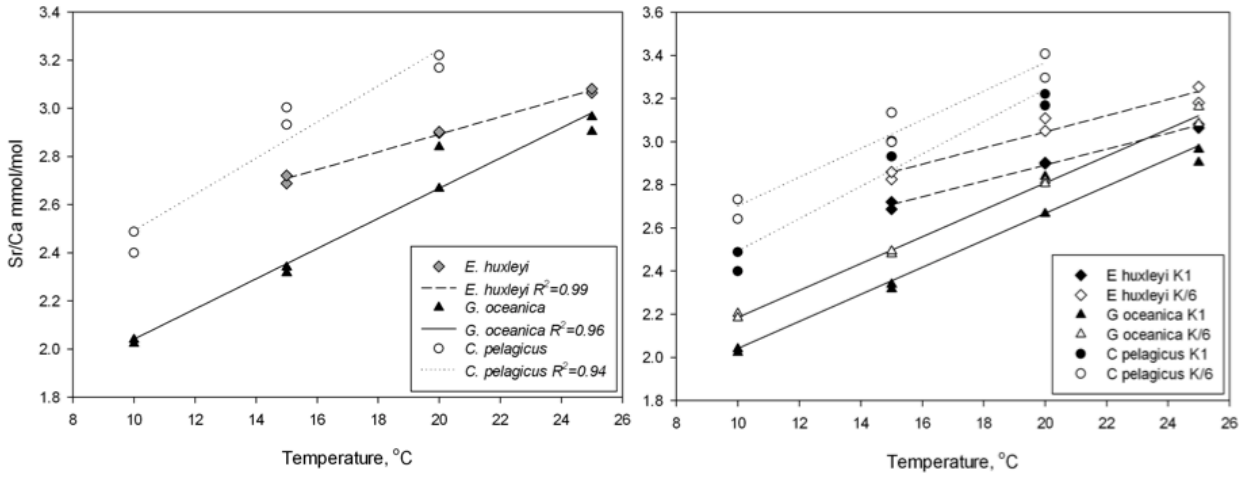

Figure 5.2 (a): Temperature dependent fractionation Sr/Ca in cultured coccolithophores. Each data point is from a separate experiment; each experiment was run in duplicate (R1 and R2). (b): Temperature dependent fractionation Sr/Ca in cultured coccolithophores in two both nutrient media (K, filled symbols; K/6 open symbols). Each data point is from a separate experiment; each experiment was run in duplicate (R1 and R2).

Strontium incorporation into calcite can be calculated from the empirical strontium distribution coefficient, K_D^{Sr}, calculated from:

$$K_D^{Sr} = \frac{\left([Sr] / [Ca] \right)_{calcite}}{\left([Sr] / [Ca] \right)_{solution}} \quad [5.4]$$

The K_D^{Sr} from the K media show a significant negative correlation with $\delta^{88/86}Sr$, and by adopting the $\Delta^{88/86}Sr_{(carb\text{-}aq)}$ notation of Böhm et al. (2012) ($\Delta^{88/86}Sr_{(carb\text{-}aq)} = \delta^{88/86}Sr_{calc} - \delta^{88/86}Sr_{aq}$) it is possible to compare these results with the fractionation of $\delta^{88/86}Sr$ in inorganically precipitated calcite, see Figure 5.3. These results show that the $\delta^{88/86}Sr$ isotope conposition becomes more fractionated as the concentration of Sr increases in the coccolithophore shell:

E. huxleyi $\Delta^{88/86}Sr_{(cocco\text{-}sw)} = -2.66 * K_D^{Sr} + 0.65$ (R^2=0.74) [5.5]

G. oceanica $\Delta^{88/86}Sr_{(cocco\text{-}sw)} = -3.40 * K_D^{Sr} + 0.79$ (R^2=0.96) [5.6]

C. pelagicus $\Delta^{88/86}Sr_{(cocco\text{-}sw)} = -2.97 * K_D^{Sr} + 0.71$ (R^2=0.99) [5.7]

By comparison, the correlation for inorganically precipitated calcite is $\Delta^{88/86}Sr_{(carb\text{-}aq)} = -1.50$ (±0.7) $* K_D^{Sr} +$ -0.09 (± 0.09) (R^2=0.89; Böhm et al. (2012), indicating that $\delta^{88/86}Sr$ is less strongly fractionated as the concentration of Sr increases. However variations in the data for inorganic calcite arise directly from precipitation rate, whereas those here are deduced from a temperature dependence and by inference growth rate. Differences between the strength of the dependency of $\delta^{88/86}Sr$ with Sr concentration between these studies could otherwise be considered as due to vital (biological) effects.

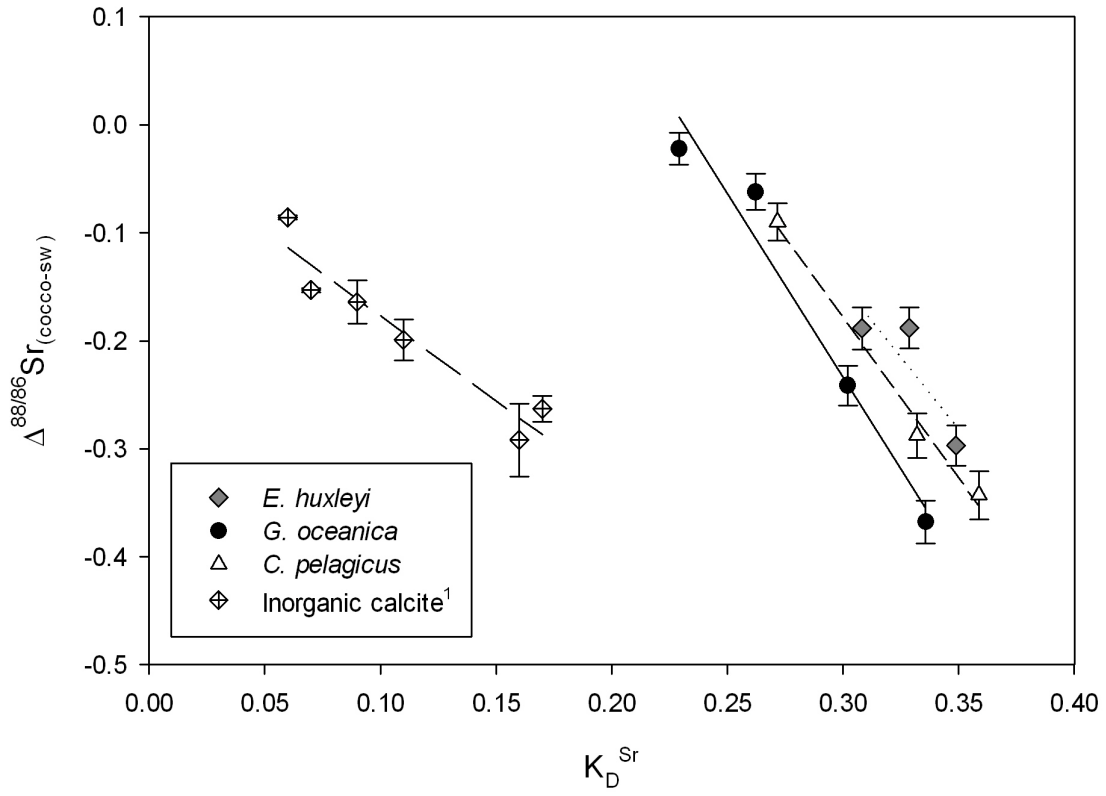

Figure 5.3: Sr concentration dependent fractionation of $\Delta^{88/86}Sr_{(cocco-sw)}$ vs, K_D^{Sr}; as the concentration of Sr increases $\delta^{88/86}Sr$ isotopes become more fractionated from seawater as a larger proportion of the lighter isotope is incorporated. [1] Böhm et al., 2012

5.3.3 $\delta^{18}O$ and $\delta^{13}C$ stable isotopes

All species display a negative correlation with $\delta^{18}O$ as would be expected with a temperature dependent fractionation; *G. oceanica, C. pelagicus* and *E. huxleyi* are all offset from the equilibrium value but still exhibit the same sensitivity to temperature, suggesting they are under equilibrium fractionation control, see Figure 5.4(a)

Coccolithus pelagicus and *E. huxleyi* show a negative correlation with $\delta^{13}C_{calcite}$-$\delta^{13}C_{DIC}$ (where calcite is the coccolith calcite and DIC is the dissolved inorganic carbon from seawater), G. oceanica does not. 5.4(b)

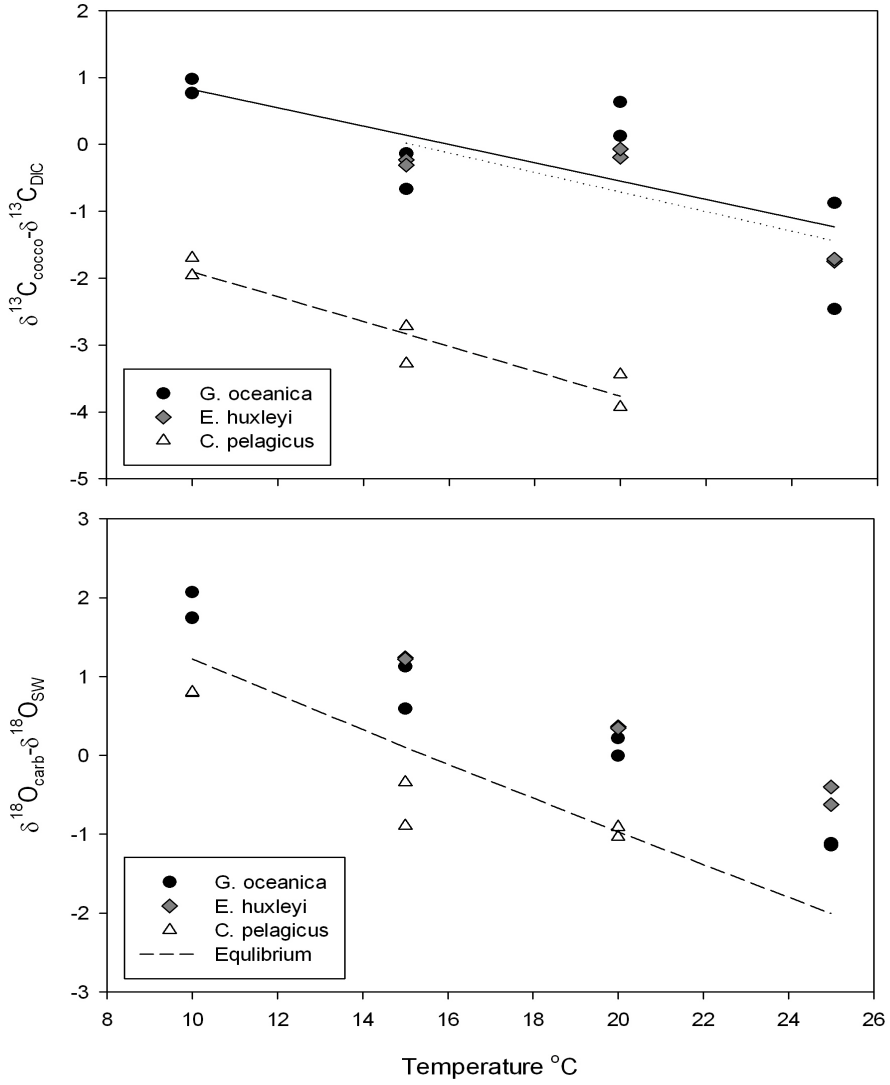

Figure 5.4 (a) plot of $\delta^{18}O$ versus temperature; the equilibrium fractionation line is plotted for comparison. (b) Plot of $\delta^{13}C$ versus temperature, only C. pelagicus shows a significant correlation.

5.4. Discussion

5.4.1 Biological fractionation of $\delta^{88/86}Sr$

The $\delta^{88/86}Sr$ isotopic composition of cultured coccolithophores is lighter than the seawater from which they precipitated, as is the case for $\delta^{88/86}Sr$ in other marine calcifiers (e.g. Fietzke and Eisenhauer, 2006; Rüggeberg et al., 2008; Chapter 3) as well as that seen for $\delta^{44/40}Ca$ and

$\delta^{26/24}$Mg isotope ratios in coccolithophores (e.g Gussone et al., 2006; Ra et al., 2010). There is a significant temperature dependent fractionation of $\delta^{88/86}$Sr for each of coccolithophore species studied, with increasing discrimination against the heavier Sr isotope as temperature (and growth rate) increase (Figure 5.1 and 5.5), a similar trend to that observed for $\delta^{88/86}$Sr fractionation during inorganic calcite precipitation (Böhm et al., 2012).

There is a clear negative correlation of growth rate with $\delta^{88/86}$Sr indicating that as growth rate increases $\delta^{88/86}$Sr becomes more fractionated which is also the same trend seen for temperature. Sr/Ca has also been used as a growth rate proxy (e.g. Stoll and Schrag 2000); in general, $\delta^{88/86}$Sr is negatively correlated with both growth rate and Sr/Ca; supporting a temperature control on growth rate (Figure 5.5).

Coccoliths are produced intracellularly, therefore there are potentially two main steps during coccolith growth where $\delta^{88/86}$Sr can be fractionated; firstly, during uptake from seawater from which the element is sequestered (Figure 5.6 point 1.) and secondly, through partitioning of the isotopes between the seawater, coccolithophore and the internal pool from which the coccolith is produced (Figure 5.6 point 2.). Both of these stages depend on kinetic, thermodynamic and biological effects. Gussone et al. (2006) summarise the processes of Ca uptake from seawater to precipitation of Ca in the coccolith: firstly dissolved Ca is thought to be dehydrated at the cell surface and transported through Ca-selective channels into the cell. The Ca^{2+} ions that enter the cytoplasm are rehydrated and removed via Ca pumps into cell organelles, coccolith vesicles or out of the cell, as illustrated in Figure 5.6); taken to indicate that almost all of the Ca entering the coccolith vesicle is incorporated into the coccolith. If this is assumed to also be the case for Sr then no $\delta^{88/86}$Sr fractionation would occur at the site of precipitation (Figure 5.6 point 2.) and therefore occurs at during the incorporation from seawater at the cell membrane.

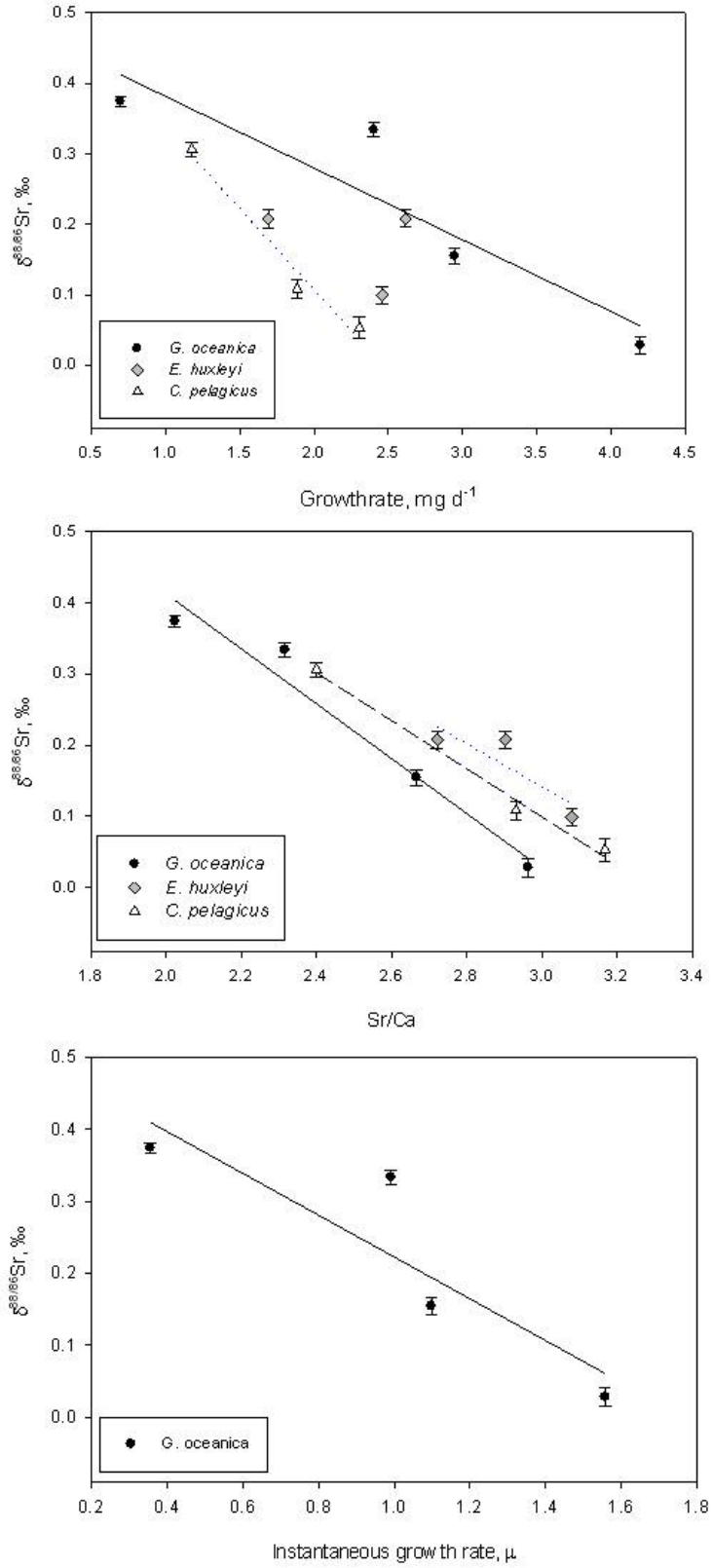

Figure 5.5. Plot of $\delta^{88/86}$Sr fractionation with different proxies of coccolithophore growth rate; a) $\delta^{88/86}$Sr versus growth rate (mg d^{-1}); (b) $\delta^{88/86}$Sr versus Sr/Ca; (c) $\delta^{88/86}$Sr versus instantaneous growth rate (μ)

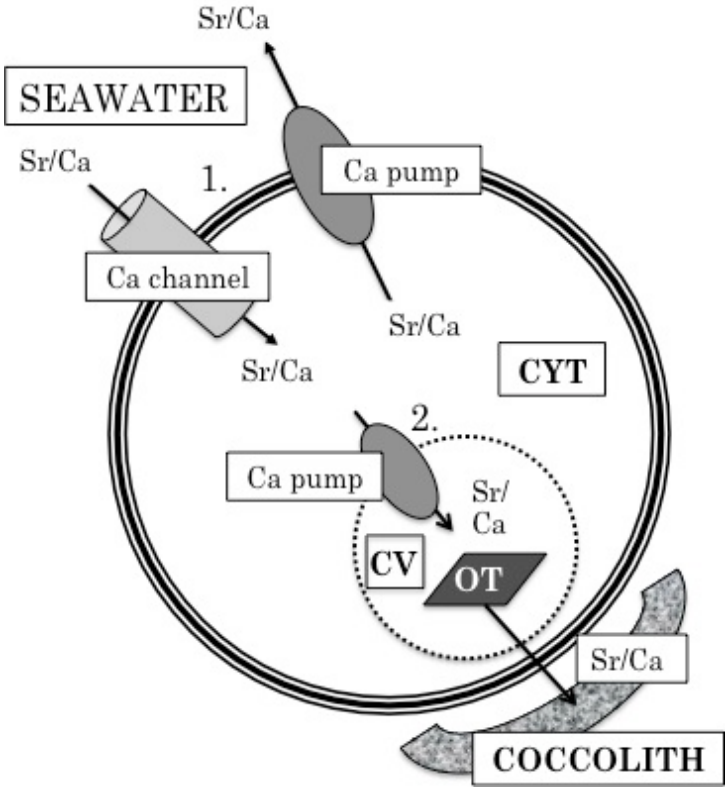

Figure 5.6: Possible locations of Sr (and Ca) fractionation in coccolithophores. 1. Uptake from seawater into the coccolith cytoplasm (CYT) and 2. Fractionation during precipitation of the coccolith in the coccolith vesicle (CV); OT is the organic template used by the coccolith to produce the intricate coccolith shape. Modified from Rickaby and Schrag (2002).

Fractionation of $\delta^{88/86}Sr$ into inorganic calcite is considered to occur via a temperature dependent kinetic isotope fractionation (Böhm et al., 2012) whereby the heavier isotope is increasingly discriminated against as temperature increases. Böhm et al. (2012) suggest that the dehydration of Sr^{2+} ions at the mineral surface is the primary mechanism for the enrichment of light Sr isotopes at the calcite mineral surface. In a chemical reaction where a bond must be broken it is expected that the rate of bond breaking, hence the rate of reactions will be higher for the lighter isotopic species (De Paolo, 1999 and references therein). It is likely, therefore, that the kinetics of dehydration favour the lighter isotope and it is possible that this process is responsible for the fractionation seen in coccolithophores by analogy with that suggested by Böhm et al. (2012) for inorganic calcite precipitation, this is this is

consistent with the relationship between $\Delta^{88/86}Sr_{(cocco\text{-}sw)}$ and K_D^{Sr} seen in both inorganic and coccolith calcite in Figure 5.3.

This conclusion is also supported by the Sr/Ca data, because as temperature (and growth rate) increase Sr/Ca also increases. Stoll et al. (2002(b)) suggest that temperature-induced Sr/Ca variation may be related to the same kinetic effects seen for inorganic calcites, and the constancy of the temperature-Sr/Ca slope for coccoliths and other biogenic calcites (e.g. foraminifera; Lea et al., 1999) and inorganic calcites (e.g. Lorens 1981; Tesoriero and Pankow, 1996) is suggestive of trends away from thermodynamic effects on Sr partitioning i.e as temperature increases a higher proportion of Sr is trapped in the interior of the crystal as specificity for Ca decreases. However, in the case of growth rate the Sr exchange co-efficient in coccolithophores cannot be explained by kinetics alone and biological effects must exert the dominant control on Sr/Ca partitioning. Rickaby et al. (2002) proposed that the growth rate incorporation of Sr/Ca is linked by differential pumping rates of Ca relative to Sr ions across the cellular membranes (which supply ions for photosynthetic carbon fixation and calcification and derived energy from photosynthetic products). Taken together, these observations suggests that selectivity against Sr in channel or carrier transport occurs but as the temperature increases the amount of pumping increases, thus increasing the possibility of 'mistakes' i.e. the incorporation of Sr over Ca, of which the Sr is isotopically light as the lighter (^{86}Sr) isotope is more reactive than the heavier isotope (^{88}Sr) and therefore preferentially incorporated into the coccolith shell, this interpretation is also consistent with the correlation between Sr/Ca and growth rate. Figure 5.5.

A similar kinetic isotope fractionation of stable strontium isotopes appears to occur in plants $\delta^{88/86}Sr$ measurements of *R. ferrugineum* and *Vaccinium* (deSouza et al., 2010) revealed that floral and foliar plant organs are strongly enriched in lighter Sr isotopes, the opposite to trend to that observed for Ca isotopes, in which the heavier isotopes are concentrated in such plant

tissues (e.g. Page et el. 2008). deSouza et al. (2010) suggest that the kinetic fractionation occurs during transport of Ca and Sr in the plant xylem to foliar and floral tissues, and it is the allocation of Ca and Sr to these organs where fractionation occurs rather than within them. These authors further speculate that the plant stem may represent a 'residual' pool of Sr and Ca, where removal of Ca by xylem unloading during transport is associated with a kinetic isotope fractionation that progressively enriches the transportation stream in heavier Ca isotopes. By comparison, this effect is negligible for Sr due to a combination of its higher mass and smaller loss of Sr during xylem unloading. In contrast, the foliar and floral tissues represent the 'product' of element transfer, and these tissues receive a large proportion of isotopically heavy Ca in the xylem, but discrimination against Sr during transfer to these tissues results in only a small proportion of xylem Sr, of which a kinetic isotope fractionation would be recorded as a light Sr signature in the floral and foliar tissues.

For both $\delta^{88/86}$Sr or Sr/Ca *E. huxleyi* consistently shows a weaker temperature dependency compared to both *G. oceanica and C. pelagicus* arguing for a strong species dependent fractionation of Sr. *Emiliania huxleyi* is much smaller than both *G. oceanica and C. pelagicus* and therefore has a larger surface area to volume ratio, and this may result in a smaller affect on the fractionation of Sr/Ca, and $\delta^{88/86}$Sr, entering the coccolith. Rickaby et al. (2002) also point out that *E. hyxleyi* is very different to most other common species of coccolithophores in that it potentially has a faster metabolism and that the entire coccolith appears to be formed by a single growth cycle of crystal units. Any one of these factors, or perhaps some other not considered, could explain why *E. huxleyi* has a smaller temperature dependence than the other species of coccolithophore studied here. The difference in the fractionation of trace metal (TM) isotopes and traditional stable isotopes (δ^{13}C and δ^{18}O) with growth rate (temperature) suggests the they are being controlled by different mechanisms, whereby

kinetics are controlling the TM isotope fractionation into the carbonate whereas equilibrium mechanisms dominate the fractionation of $\delta^{13}C$ and $\delta^{18}O$.

The negative correlation of $\delta^{88/86}Sr$ with temperature in coccolithophores is the opposite to that seen observed for $\delta^{44/40}Ca$ (e.g. Langer et al., 2007) and $\delta^{26/24}Mg$ (Ra et al., 2002) in that as temperature increases $\delta^{88/86}Sr$ becomes more fractionated from the composition of seawater. Calcium and Sr are geochemically similar and would be expected to exhibit analogous behaviour (deSouza et al., 2010). However, since $\delta^{88/86}Sr$ and $\delta^{44/40}Ca$ show different senses of temperature dependence this suggests that they are fractionated by different mechanisms and that there is a strong biological control exerted by the coccolithophore in favour of the uptake of the nutrient Ca over the biologically unimportant element Sr. The direction of temperature dependency observed is at odds with $\delta^{88/86}Sr$ data obtained for other marine calcifiers. Fietzke and Eisenhauer (2006) and Rüggeburg et al., (2008) find a positive correlation of $\delta^{88/86}Sr$ with temperature in aragonitic corals, and in this thesis no temperature dependence of $\delta^{88/86}Sr$ during calcite precipitation in the foraminifera *G. sacculifer* is observed (chapter 3). Unlike foraminifera and corals, coccolithophores precipitate their shells intracellularly, a preliminary inference then is that the different temperature dependencies for different organisms is due to the way in which Ca, hence Sr, is transported across the membrane.

The immediate conclusion is that the $\delta^{88/86}Sr$ isotope composition of coccolithophores has the potential to be used as a proxy for growth rate. Despite the difficulty of separating coccoliths from bulk sediments, analytical advances are being made in microfiltering and settling techniques (e.g. Minoletti et al., 2008; Stoll and Ziveri, 2002) to separate near monospecific fractions of coccoliths. As a consequence of developments such as these coccolithophores could potentially be used as archives for past seawater $\delta^{88/86}Sr$ records of productivity or

temperature. If all coccolithophore species show the same negative correlation (as is shown by the three species examined in this study) perhaps analysis of bulk coccoliths would be possible rather than monospecific species, however more culture studies would be needed to confirm if this is indeed the case.

5.4.2 Implications for Stable Sr mass balance in the oceans

The significant result from this work with regard to Sr mass balance in the oceans is that the coccoliths, which represent an important calcite output have a stable isotope composition that is lighter than seawater (Figure 5.1), and at higher temperatures (~25°C) have $\delta^{88/86}$Sr values significantly lighter than that for other published marine calcifiers (Fietzke and Eisenhauer, 2006; Ohno and Hirata, 2008; Rüggeburg et al., 2008; Krabbenhöft et al., 2010; Böhm et al., 2012) this has implications for the mass balance of inputs and outputs of Sr in the modern oceanic Sr cycle. Traditional radiogenic Sr data (^{87}Sr/^{86}Sr) do not allow investigations the effects of calcite output fluxes on Sr as correction for instrumental mass fractionation removes any mass dependent variations in ^{87}Sr/^{86}Sr ratios for seawater and precipitated carbonate have the similar values, even though the carbonate output flux is implicit in Sr mass balance equations. By contrast, the mass dependent fractionations of stable Sr isotopes during carbonate precipitation allow quantification of the output flux of Sr from the oceans. Krabbenhoft et al. (2010) were estimated the modern Sr output flux, (see Table 5.3). By compiling the average carbonate burial flux from their data: coccoliths, planktonic foraminifera and ⅓rd of the total continental shelf and slope taxa (mussels, starfish, etc.) a total carbonate output flux is averaged at ~47*10^9 mol/yr of which coccoliths account for ~22% with an average $\delta^{88/86}$Sr value of 0.26‰ (Table 5.2), resulting in a total carbonate flux weighted average $\delta^{88/86}$Sr of 0.24‰ of biogenic calcite polymorphs of calcium carbonate.

Carbonate sediment type	$CaCO_3$ deposition (10^{12} mol/yr)	$CaCO_3$ polymorph	Mean (mmol/mol)	Sr Burial Flux mol/yr)	$\delta^{88/86}$Sr ‰ ($2\sigma_m$)
Reef corals	~6.0(20%)	Aragonite	~9.0	~54(31%)	0.19(1)
Halimedia	~1.5(5%)	Aragonite	~11	~16(9%)	0.27(3)
Coccoliths	~5.0(16%)	Calcite	2.2	~11(6%)	0.26(7)
Planktic foraminifera	~6.0(20%)	Calcite	1.4	~8(5%)	0.14(1)
Continental shelf and slope taxa	~13.0(39%)	Aragonite and Calcite	~6.6	~85(49%)	0.22(3)
Total carbonates	~32.0(100%)			~174(100%)	
Average					0.22(2)
Sr burial flux weighted average					0.21(2)

Table 5.2: Sr fluxes and $\delta^{88/86}$Sr isotope values, reproduced from Krabbenhöft et al. (2010)

Together coccoliths and foraminifera make up the predominant mass of calcite on the sea floor and studies have revealed variable patterns of carbonate sedimentation and accumulation produced by planktic foraminifera and coccolithophores, respectively (Baumann et al., 2004 and references therein). For example, mass estimates for coccolith carbonate burial in surface sediments in the South Atlantic Ocean suggest that coccoliths are the major carbonate contributors to most mid-Atlantic Ridge sediments, exceeding up to 70 wt.-% (c.f. Baumann et al., 2004). This, in turn, changes the balance of the calcite output flux from the oceans and has consequences for the absolute mass balance of Sr outputs both in the modern day ocean and in the past. For example, the predominance of significant coccolith blooms in the oceans may drive the local (or even whole ocean) seawater $\delta^{88/86}$Sr values to heavier compositions. The data obtained here illustrates that in warmer tropical waters (~25°C) the local output of Sr in coccoliths can be driven to $\delta^{88/86}$Sr compositions of almost 0‰, driving the total calcite output flux to 0.19‰, some 0.07‰ lighter than the average proposed by Krabbenhöft et al. (2010). Indeed it may be possible that there are small local variations between different water masses, for example, Galer et al. (2011) find surface waters of the Southern Ocean show subtle changes in the $\delta^{88/86}$Sr composition along a single

transect ($\delta^{88/86}Sr$ = 0.33±0.02‰), however these data are just within error of those in deep waters. These authors also found that the composition of the Southern Ocean tends to be isotopically lighter, overall, than that of the North Atlantic ($\delta^{88/86}Sr$ = 0.36±0.02‰), see Figure 5.7. These subtle differences suggest that biology may be exerting a strong controle on the $\delta^{88/86}Sr$ that locally, at least, is at odds with the long residence time of Sr in the oceans (>2.5 Myr). Another possible explanation of local variations in the $\delta^{88/86}Sr$ composition of seawater is the presence of Acantharia, a marine protozoa, which precipitates its skeleton as strontium sulfate ($SrSO_4$). The $SrSO_4$ skeletons of the Acantharia are highly prone to dissolution in the water column after death and on the deep sea floor, and they are therefore rare as fossils (Galer et al., 2011).

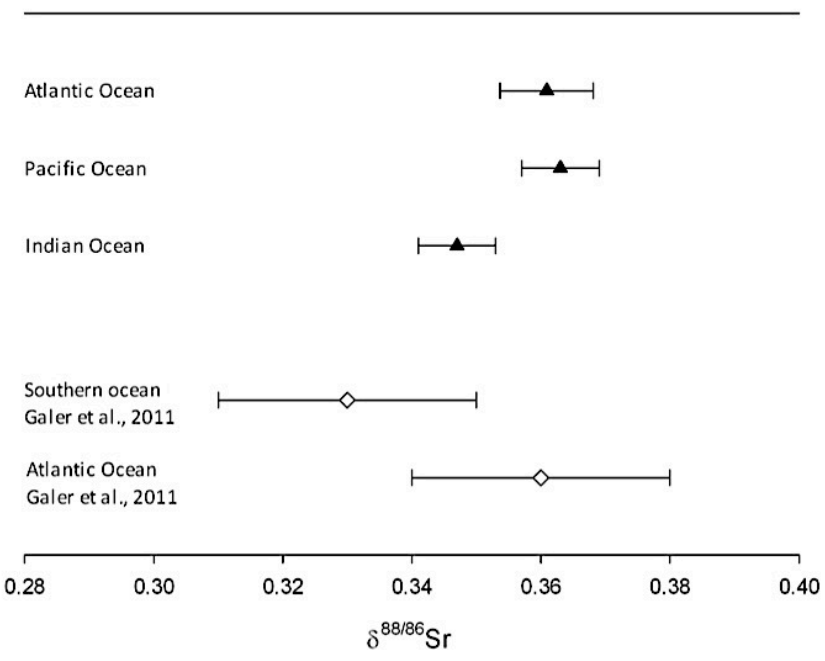

Figure 5.7: $\delta^{88/86}Sr$ isotopic composition of modern day seawater; Atlantic, Pacific and Indian Ocean data from Mokadem et al., (unpublished).

While Krabbenhöft et al., (2010) have made an initial assessment of the modern day inputs and outputs of oceanic Sr, the results obtained here show that more data are required to properly assess all of the modern day output fluxes and actual stable Sr isotope signatures of

marine organisms. The work here contributes to the on-going investigation of global modern day $\delta^{88/86}Sr$ values along with those being undertaken to characterise the $\delta^{88/86}Sr$ of riverine, dust and precipitation inputs (Krabbenhöft et al., 2010; Pearce et al., 2010; Pearce et al., 2011).

An interesting corollary to this work would be an investigation into the variation of $\delta^{88/86}Sr$ isotopes in seawater records accompanying the advent and proliferation of coccolithophores in the cretaceous. This would be important for establishing the extent to which coccolithophore calcite could drive seawater $\delta^{88/86}Sr$ ratios to differing values when they are at their most proliferate.

5.5 Conclusions

The $\delta^{88/86}Sr$ isotope composition of coccolithophores is significantly lighter than seawater, as temperature increases so does growth rate and with this comes a greater discrimination against the uptake of the heavier isotope. The degree of fractionation with temperature and growth rate is species dependent, and most likely associated with the dehydration of Sr aquo-complexes during uptake from seawater by the coccolithophore rather than due to a fractionation process during coccolith production within the coccolithophore itself. Taken together, the $\delta^{88/86}Sr$ and K_D^{Sr} data argues strongly for a kinetic isotope fractionation that increases with temperature, $\Delta^{88/86}Sr_{(cocco\text{-}sw)}$ and K_D^{Sr} are negatively correlated but have a greater degree of fractionation than inorganic calcite, possibly due to a vital effect. It is proposed that $\delta^{88/86}Sr$ could be used as an indicator of coccolith growth rate. This work also provides some insight into the strong biological control of Ca uptake during biomineralisation in coccolithophores.

A significant conclusion from this work is that the coccolithophores, which represent a significant output of Sr from the oceans, have a stable isotope composition that is significantly lighter than previously thought (c.f. Krabbenhöft et al., 2010) and can be driven to values as low as 0‰ in tropical waters (>20°C). This has important implications for the local seawater $\delta^{88/86}$Sr value and also interpretation of the current mass balance of Sr outputs from the ocean and the modern-day Sr cycle.

CHAPTER SIX

The behaviour of radiogenic and stable strontium isotopes in Himalayan Rivers

Summary

This chapter investigates the behaviour of Sr stable isotopes in rivers to determine the information that is revealed on weathering processes. Both $\delta^{88/86}Sr$ and $^{87}Sr/^{86}Sr$ ratios have been analysed in the dissolved load of rivers and tributaries draining both silicate and carbonate dominated catchment areas in the Himalaya. The Himalaya is an active orogenic belt, which has a complex weathering regime, made difficult to interpret with traditional weathering proxies such radiogenic Sr isotopes and element-to-calcium ratios due to regional metamorphism and the non-conservative behaviour of Ca. These preliminary data indicate that, in general, rivers draining carbonate catchments possess lighter isotopic $\delta^{88/86}Sr$ values than those from rivers draining silicates. There is a strong seasonal shift of $\delta^{88/86}Sr$ in the waters draining carbonates to heavier values after the monsoon, that is less pronounced in the silicate catchments. An inverse correlation is observed between $\delta^{88/86}Sr$ and $\delta^{30}Si$ suggesting that the isotope behaviour of both elements is controlled by similar processes.

6.1 Introduction

Chemical weathering of silicates exerts a control on global climate, through its effect on atmospheric CO_2 levels, which in turn can drive temperature changes by modifying greenhouse warming via a feedback loop (e.g. Walker et al., 1981). On >10,000-year timescales silicate weathering leads to the drawdown of CO_2 (e.g. Walker et al., 1981) and on millennial timescales changes in the flux of alkalinity affects the calcium carbonate saturation state of the oceans, and hence their uptake of CO_2 (e.g. Archer et al., 2000). Chemical weathering regulates global climate by converting the atmospheric greenhouse gas carbon dioxide (CO_2) to bicarbonate ions, which along with metals, are transported to the oceans by rivers where the CO_2 is fixed by formation of carbonates (e.g. Berner, 2003). On the continents the weathering of silicate and carbonate rocks provides a net drawdown of CO_2 as indicated by the simplified reactions in Equations 6.1 and 6.2 respectively:

$$CaSiO_3 + 2CO_2 + 3H_2O \rightarrow Si(OH)_4 + Ca^{2+}_{(aq)} + 2HCO^-_{3(aq)} \quad [1] \qquad [6.1]$$

$$CaCO_3 + CO_2 + H_2O \rightarrow Ca^{2+}_{(aq)} + 2HCO^-_{3(aq)} \qquad [6.2]$$

$$Ca^{2+}_{(aq)} + 2HCO^-_{3(aq)} \rightarrow CaCO_{3(s)} + CO_2 + H_2O \qquad [6.3]$$

The weathering of carbonates will have an effect on the balance of CO_2 in the atmosphere via the consumption of one molecule of CO_2 (Equation 6.2) but only on a time scale which is similar to the residence time of HCO_3^- in the oceans (100,000 yr, Viers et al., 2003), but over geological time periods (>10^6 yr) the weathering of carbonates on land has no net effect on atmospheric CO_2 as one molecule of CO_2 is eventually removed from the oceans, via precipitation, to the atmosphere (Equation 6.3). In contrast, the weathering of silicate rocks transforms two molecules of CO_2 from the atmosphere to HCO_3^- in rivers leading to

[1] Weathering of Mg silicates also leads to drawdown of atmospheric CO_2, leading to precipitation of dolomite in rivers and the oceans

precipitation in the oceans (Equation 6.3), providing a sink of CO_2. Therefore quantifying the release of cations from continents due to chemical weathering is of fundamental importance for understanding the long-term carbon cycle and the links between the lithosphere, hydrosphere and atmosphere (deSouza et al., 2010).

Many natural radiogenic isotopes in seawater are sensitive to changes in the balance of input from continental weathering (via rivers, groundwaters and aeolian input) against that from hydrothermal exchange at mid-ocean ridges, yielding information on both long- (millions of years: e.g. $^{87}Sr/^{86}Sr$) and short- (thousands of years: e.g. $^{187}Os/^{188}Os$) time scales (the reader is referred to the review by Frank (2002) for a more in-depth discussion of different radiogenic isotope systems). Of these, the rubidium-strontium (^{87}Rb-^{86}Sr) radiogenic isotope system is the most widely used and variations in seawater $^{87}Sr/^{86}Sr$ ratios on both long and short timescales are thought reflect changing continental input through time (e.g. Brass, 1976; Hess et al., 1986; Hoddell et al., 1990; Capo and DePaolo, 1990; Hodell et al., 2007). The traditional radiogenic strontium ($^{87}Sr/^{86}Sr$) system has been applied to weathering catchments to discriminate between contributions from carbonates, silicates and evaporites (Gaillardet et al., 1999b). In general, rivers draining silicate catchments usually possess relatively radiogenic $^{87}Sr/^{86}Sr$ compositions while carbonates possess relatively unradiogenic compositions ($^{87}Sr/^{86}Sr$ = 0.721 and 0.708 for silicate and carbonate catchments, respectively, e.g. Allègre et al., 2010). It is widely held that carbonate weathering is the dominant source of Sr in river runoff (75%: Brass, 1976; 67%: Berner and Rye, 1992; 78%: Veizer and Mackenzie, 2003). Consequently, variations in the $^{87}Sr/^{86}Sr$ isotope composition of seawater over time reflect changes in the balance of input from the weathering of carbonate and silicate continental rocks, and that derived from hydrothermal exchange at mid-ocean ridges (e.g. Palmer and Edmond, 1986).

The Cenozoic record of radiogenic Sr isotopes in seawater is now well established, and indicates a significant shift to more radiogenic values over the past 40 Myr, (Figure 1.2, chapter one). This has been linked by some to intensified continental weathering caused by orogenesis, in particular the uplift and weathering of the Himalaya-Tibet plateau commencing around 40 Ma (Raymo et al., 1988, Richter et al, 1992). While others to have related this shift to the onset of glaciation in the Late Eocene (the transition from so-called "greenhouse to icehouse conditions") resulting in an increase in both physical and chemical weathering rates (Armstrong, 1971; Hoddell et al., 1990; Blum and Erel, 1995). However, changes in the Sr isotope record cannot be simply used to quantitatively reconstruct the relationship between chemical weathering fluxes and climate. This is partly because the balance of continental and hydrothermal input to the oceans remains poorly constrained (e.g. Davis et al., 2003; Vance et al., 2009), but more significantly because it is rarely possible to distinguish changes caused by variations in the total flux of strontium to the oceans from those caused by variations in the isotope composition of riverine input (e.g. Richter et al., 1992; Derry and France-Lanord, 1996; Quade et al., 1997). One unusual aspect of some lithologies in the Himalaya is that during metamorphism diffusional exchange of strontium between co-exisiting silicates and carbonates has imparted a radiogenic $^{87}Sr/^{86}Sr$ isotope composition to the carbonates. Consequently, the weathering of such carbonates releases unusually radiogenic $^{87}Sr/^{86}Sr$ compositions to the river waters (Oliver et al., 2003). Similarly, Jacobsen et al., (2002) considered that previous Sr isotope studies in the Himalaya had underestimated the overall input of carbonate dissolution, primarily because (1) carbonate bedrock in the Himalaya has a wide range of Ca/Sr and $^{87}Sr/^{86}Sr$ ratios that cannot be adequately defined by a single end-member in conventional mass-balance equations, and (2) Ca^{2+} behaves non-conservatively during transport in Himalayan stream waters. As a consequence, it is extremely difficult to distinguish between silicate and carbonate sources of

Sr in the Himalaya-Tibet region, and this is reflected in several studies that have come to different conclusions on the predominance of silicate or carbonate weathering (e.g. Blum et al., 1998; Krishnaswami et al., 1992).

Rivers are the dominant source of many elements and isotopes to the ocean and are influenced by climatic, hydrological and erosional processes as well as vegetation and relief, however, for Sr the primary control is thought to be the rock type being weathered (Tipper et al., 2012 and references therein). Compared to major elements, the trace elements (<1mg L^{-1}) in natural waters are much more readily fractionated by weathering and transport processes, and these fractionations give clues for understanding the nature and intensity of the weathering and transport processes (Gaillardet et al., 2003).

Both natural and experimental studies have shown that during the crystallisation of $CaCO_3$, the light isotopes of strontium (^{86}Sr) are preferentially incorporated into this phase (e.g. Fietzke and Eisenhauer, 2006; Krabbenhoft et al., 2010; Böhm et al., 2012) over the heavier isotope (^{88}Sr). In principle, two processes could influence the $\delta^{88/86}Sr$ ratio in the dissolved load of rivers; firstly the chemical weathering of calcium carbonate (Equation 6.2) will yield a light stable isotope composition in river waters relative to that of silicate weathering phases as the lighter isotope is preferentially released. Secondly, the precipitation of secondary carbonates during weathering (Equation 6.3) could drive the residual waters to isotopically heavy compositions.

The application of stable Sr isotopes in the weathering environment has seen little work thus far and only a few studies exist (Halicz et al., 2008; Ohno et al., 2008; de Souza et al., 2010). In particular, at this stage it is still not known (1) to what extent the stable strontium isotope signal from carbonates differs from that of silicates (2) the degree to which diffusional equilibration of Sr in carbonates with silicates also affects the Sr stable isotope system and

(3) the magnitude of the fractionation of stable Sr isotopes that occurs during the precipitation of other secondary phases, for example, clays which can substitute other divalent cations such as Mg and Ca.

This study presents radiogenic and stable strontium data for rivers draining carbonate, silicate and mixed catchments in the Himalaya-Tibet region. The Himalayan orogenic belt comprises four main tectonic units, from North to South these are; (i) The Tibetan Sedimentary Series (TSS), (ii) The High Himalayan Crystalline Series (HHCS), (iii) the Lesser Himalayan Series (LHS) and (iv) the sub-Himalayan sediments. These four units provide a contrast between the weathering of silicates (HHCS) versus carbonates (TSS and LHS), and at both high and low altitudes. Chemical weathering rates are generally low for the high altitude rivers which are fast-flowing under cold temperature conditions, whereas rivers at low altitudes have higher chemical weathering rates due to higher water temperatures and slower flow rates. The Southern Himalayan flank and plain are exposed to significant monsoonal precipitation (1-4 m yr^{-1}) (Galy and France-Lanord, 1999), and the influence of the summer monsoon has also been investigated by comparing samples taken from similar catchments in both the spring and autumn.

These preliminary results indicate that, in general, rivers draining carbonate catchments possess lighter isotopic $\delta^{88/86}Sr$ values than those silicate catchments, but there is no strong shift between the $\delta^{88/86}Sr$ isotope signal from carbonate and silicate draining rivers. Rivers that show evidence for diffusional equilibration of ^{87}Sr in the LHS region of the Himalaya (recorded in the $^{87}Sr/^{86}Sr$ ratios), are also those that possess the lightest $\delta^{88/86}Sr$ isotope signals. Correlations of $\delta^{88/86}Sr$ with mineral saturation states (predicted by PHREEQC) indicate the heavier Sr isotopes are preferentially incorporated into clay minerals and other Mg-bearing phases, similar to the behaviour of Mg isotopes.

6.2 Samples

Himalayan river waters were obtained from a suite collected in the Nepalese Himalaya (Kisakürek et al., 2005). Catchments were selected so as to sample both carbonate and silicate lithologies at both high (2000-4000m) and low (550-1300m) altitudes. The following catchments were chosen for Sr isotope measurement; locations and lithological details are from Kisakürek et al (2005) and are also given in Figure 6.1 and appendix 6 (a)

(a) Tributaries of the Marsyangdi and Modi Khola: These rivers drain mainly carbonates of the TSS at higher altitudes (2900 to 4000m), whilst at altitudes between 2000m and 2600m, Formation II HHCS (calc-silicates gneissic rocks) provide an additional source.

(b) Tributaries of the Dudh Khosi (eastern Nepal): These rivers drain mainly Formation I HHCS (predominantly a 129vapora biotite-sillimanite gneiss) at altitudes of 800-1000m

(c) Tributaries of the Indrawati (central Nepal): These rivers drain mainly Formation I HHCS (predominantly a pelitic biotite-sillimanite gneiss) at altitudes of 800-1000m

(d) Tributaries of the Bhote Khosi (central Nepal): These rivers drain mainly the LHS calc-silicates at altitudes of between 800-1300m

Samples were also taken from the Melamchi Khola and Likhu Khola, which are both low altitude (925m and 572m respectively) rivers draining HHCS catchments.

Samples were selected on the basis of their Ca/Na vs. Mg/Na ratios (Figure 6.2) to distinguish between carbonate, silicate and evaporate lithologies (see Gaillardet et al., 1999b).

Figure 6.1 Geological map of the sampling area reproduced with permission from Kisakürek et al., (2005). Samples were taken from both (a), (b), (c) and (d) covering the TSS and HHCS FII, High altitude HHCS FII, Low altitude HHCS and LHS respectively. STDZ: South Tibetan Detachment Zone, MCT: Main Central Thrust, MBT: Main Boundary Thrust.

Carbonate rocks contain very little Na, therefore the Ca/Na ratios of carbonate rocks is very high (<2000 mol/mol in limestones and dolomites from the TSS and the LHS; Oliver et al., 2003) compared with the much lower Ca/Na (<0.7 mol/mol HHCS; Jacobson et al., 2002) for catchments draining silicates; silicates also tend to have a higher concentration of Mg compared to carbonates (with the exception of dolomites) (Gaillardet et al., 1999b).

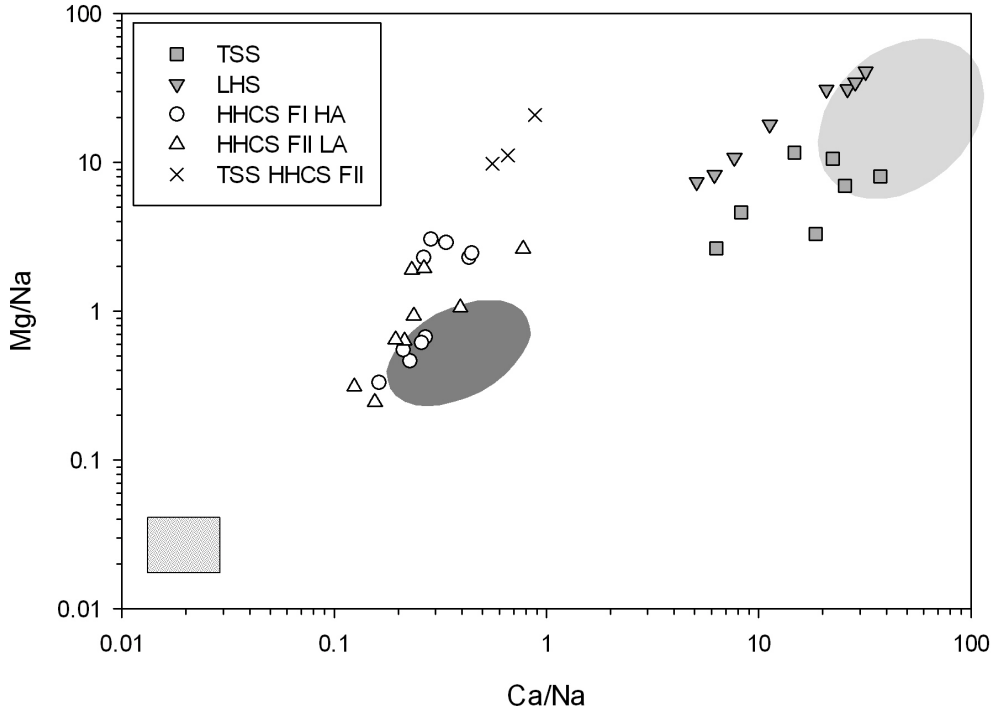

Figure 6.2 Ca/Na versus Mg/Na values analysed by Kisakürek et al. (2005) for the samples selected. The range of mineral Mg/Na and Ca/Na data defined by Gaillardet at al., 1999b for evaporites (dotted square) silicates (dark grey region) and carbonates (pale grey region) are also shown for reference.

These samples were originally sampled for lithium isotope analysis (δ^7Li, Equation 6.4) by Kisakürek et al. (2005), where it was found that most of the dissolved Li is sourced by the dissolution of silicate minerals even in carbonate dominated terrains. It was found that isotope composition of the suspended load is nearly always lighter than the corresponding bedload probably reflecting the presence of secondary phases. There is considerable overlap in the δ^7Li composition of the dissolved load from the carbonate-silicate catchments, suggesting that the main control on the Li isotope chemistry of the dissolved load is not the

bedrock lithology, but rather weathering reactions involving the formation of secondary minerals. On the basis of these results Kisakurek et al. (2005) concluded that δ^7Li has the potential to be used as a proxy for global silicate weathering processes when combined with Li concentration data in the oceans.

Where δ^7Li is given by:

$$\delta^7 Li = \left[\frac{(^7 Li /^6 Li)_{\text{sample}}}{(^7 Li /^6 Li)_{\text{standard}}} - 1 \right] * 1000 \qquad [6.4]$$

6.3 Methods

The river waters were sampled and treated as outlined in Kisakürek et al. (2005). The dissolved load was sampled for $\delta^{88/86}$Sr analysis, which was collected 30cm below the surface of the river then filtered through a 0.45μm cellulose acetate filter. A volume of each sample was dried down to provide 500μg Sr. Each sample was treated as outlined in chapter two for spiking, column chemistry and TIMS analysis. The spiked samples were deconvolved to find their true $\delta^{88/86}$Sr values using the natural (^{87}Sr/^{86}Sr) data measured by Kisakürek et al. (2005).

Both trace element data (measured by ICP-MS at the Open University, Milton Keynes) and radiogenic Sr data (^{87}Sr/^{86}Sr, measured by TIMS at the Open University Milton Keynes) were provided by Kisakürek et al. (2005).

6.4 Results

6.4.1 Radiogenic Sr isotopes

Radiogenic isotope data and strontium concentration data is provided and interpreted by Kisakürek et al. (2005), and is presented in Table 6.1 and Figure 6.3.Tributaries draining the TSS and FII HHCS with TSS have low $^{87}Sr/^{86}Sr$ ratios (0.7145-0.7335) and the highest concentrations of Sr (>398 nmol/L) while tributaries draining the LHS have very radiogenic $^{87}Sr/^{86}Sr$ ratios (0.7947 to 0.8630) and intermediate concentrations of Sr (150-338nmol/L). Tributaries draining FI HHCS have intermediate $^{87}Sr/^{86}Sr$ ratios (0.7269-0.7577), with the majority of analyses clustering around 0.735-0.7557. Concentrations of Sr in rivers that drain FI HHCS decrease with increasing altitude.

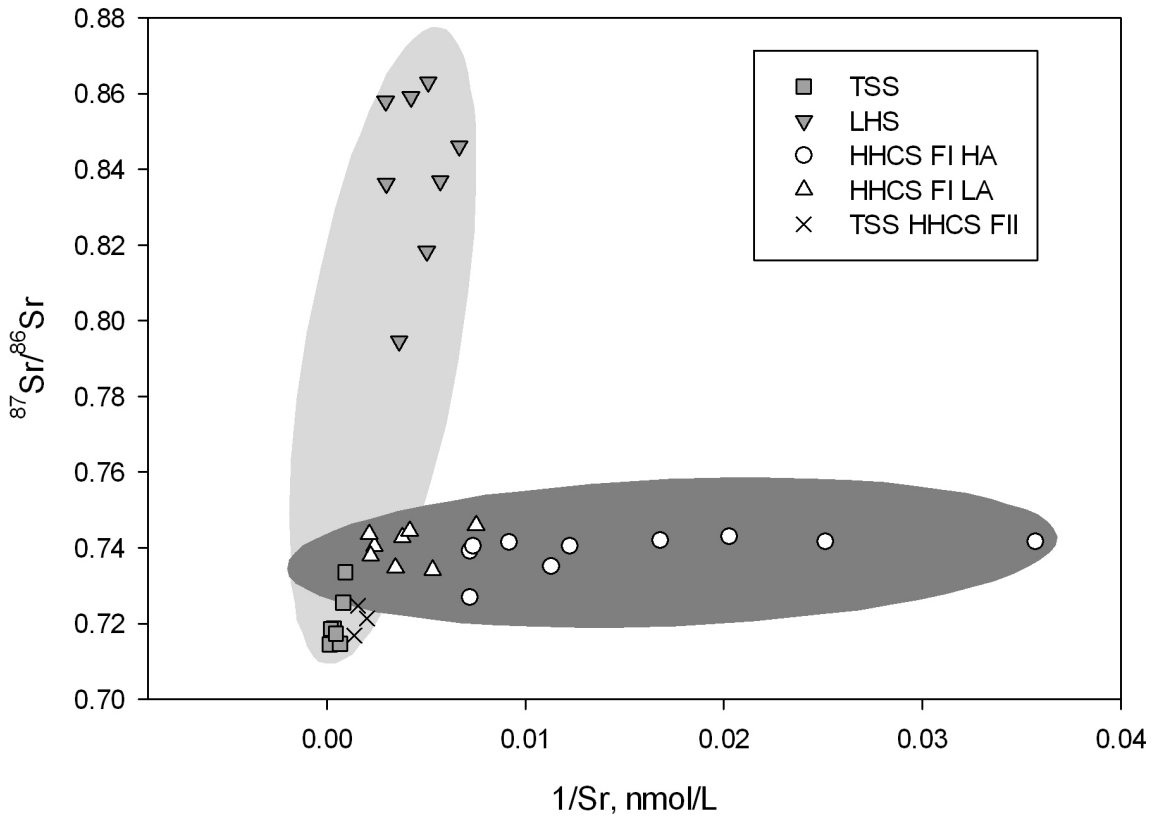

Figure 6.3. Plot of $^{87}Sr/^{86}Sr$ versus 1/[Sr] composition of river waters draining carbonate and silicate catchments. Pale grey highlights the carbonate array whilst the darker highlights the silicate for this sample set.

Table 6.1 Stable Sr isotopes for all river waters sampled. Radiogenic Sr ratios and Sr concentration data from Kisakürek et al., 2005. Where S refers to spring and A refers to autumn i.e. pre and post monsoon respectively.

Sample	Lithology	$\delta^{88/86}Sr$	error (2.s.e)	$^{87}Sr/^{86}Sr$	Sr (nmol/l)
Dudh Khosi and its tributaries					
S3	FI (HHCS)	0.449	0.008	0.739155	139
A15	FI (HHCS)	0.365	0.014	0.740521	136
S1	FI (HHCS)	0.32	0.009	0.742036	59.5
S4	FI (HHCS)	0.34	0.009	0.74163	39.8
S5	FI (HHCS)	0.41	0.011	0.741465	109
A13	FI (HHCS)	0.342	0.012	0.726904	139
A14	FI (HHCS)	0.362	0.006	0.735069	88.5
A18	FI (HHCS)	0.386	0.011	0.740455	81.6
Indrawati and its tributaries					
	FI (HHCS)	0.315	0.012	0.734735	289
A10	FI (HHCS)	0.39	0.013	0.734202	188
S7	FI (HHCS)	0.356	0.009	0.742816	263
S8	FI (HHCS)	0.278	0.007	0.744484	240
A11	FI (HHCS)	0.274	0.008	0.74037	416
A12	FI (HHCS)	0.294	0.008	0.737967	455
Tributaries of the Marsyangdi					
	TSS	0.254	0.007	0.718708	2870
S18	TSS	0.238	0.021	0.718554	4960
S19	TSS	0.261	0.007	0.714545	6360
S20	TSS	0.295	0.007	0.725465	1230
S21	TSS	0.294	0.007	0.71466	1510
S22	TSS FII (HHCS)	0.427	0.016	0.724709	638
S24	TSS FII (HHCS)	0.392	0.011	0.721328	496
S25	FI (HHCS)	0.299	0.008	0.745972	133
Tributaries of the Modi Khola					
	TSS	0.314	0.03	0.733491	1070
A2	TSS	0.347	0.006	0.717273	2190
A3	TSS FII (HHCS)	0.354	0.011	0.716848	713
Tributaries of the Bhote Khosi					
	LHS	0.344	0.009	0.859081	236
S10	LHS	0.277	0.009	0.794646	274
S11	LHS	-0.028	0.016	0.858024	338
S12	LHS	0.279	0.013	0.863043	196
A6	LHS	0.378	0.015	0.846215	150
A7	LHS	0.338	0.014	0.836867	175
A8	LHS	0.207	0.009	0.836219	334
A9	LHS	0.05	0.018	0.818365	199
Likhu Khola					
	FI (HHCS)	0.279	0.01	0.743622	469

6.4.2 Stable Sr isotopes

The full range of $\delta^{88/86}Sr$ is shown in Figure 6.4.

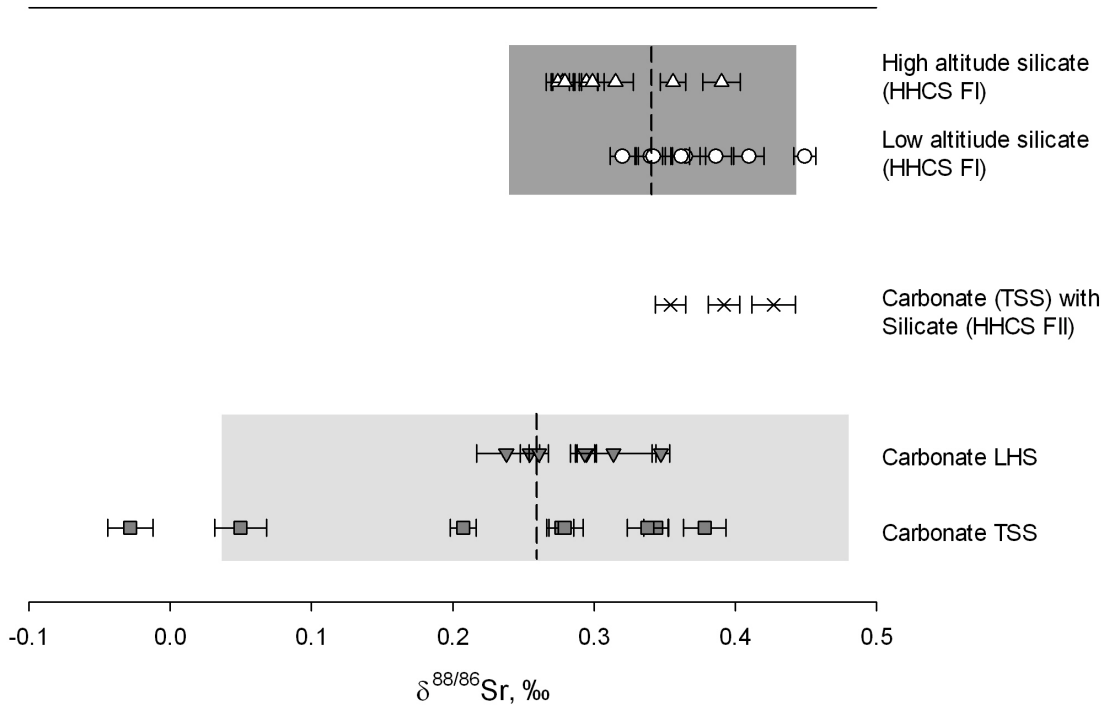

Figure 6.4: Range of $\delta^{88/86}Sr$ data for all river samples analysed. The average $\delta^{88/86}Sr$ is shown for both carbonate and silicate draining rivers as a dashed line with the 2.s.d error range in pale grey for carbonates and dark grey for silicates.

There is considerable overlap between the silicate and carbonate draining tributaries but, in general, the HHCS tributaries take heavier values ($\delta^{88/86}Sr$ = 0.34±0.1‰ (2.s.d, n=16)) than the carbonates (LHS and TSS; $\delta^{88/86}Sr$ = 0.26±0.2‰ (2.s.d, n=15)), and in particular samples with an input from Formation II (FII) calc-silicates HHCS have the heaviest $\delta^{88/86}Sr$ values ($\delta^{88/86}Sr$ = 0.39±0.07‰ (2.s.d, n=3)). The greatest range in $\delta^{88/86}Sr$ is found in the low altitude carbonate lithology (LHS), while the HHCS and TSS draining tributaries have more limited $\delta^{88/86}Sr$ values. The rivers draining the TSS with an additional input from HHCS FII, in general, possess heavier $\delta^{88/86}Sr$ values compared to rivers draining predominantly HHCS FI silicates. The FII HHCS are primarily calc-silicate gneissic rocks, whereas the samples from

the HHCS (referred to in the previous paragraph) are dominated by silicates, predominantly a pelitic biotite-sillimanite gneiss, the difference in composition could be responsible for the small difference in $\delta^{88/86}$Sr we observe between the different types of silicate bedrock. However, specific bedrocks surrounding the sampled tributaries have not been measured; therefore interpretation with regard to bedrock weathering is limited.

Figure 6.5 shows the relationship between $\delta^{88/86}$Sr and Sr concentration, while much of the data shows similar isotope compositions and concentrations, there are two distinct trends to observe, firstly, that carbonates tend to have high Sr concentrations with a wide range of $\delta^{88/86}$Sr values; secondly, silicates have a much narrower range of $\delta^{88/86}$Sr values that extend to much lower concentrations in 1/Sr space.

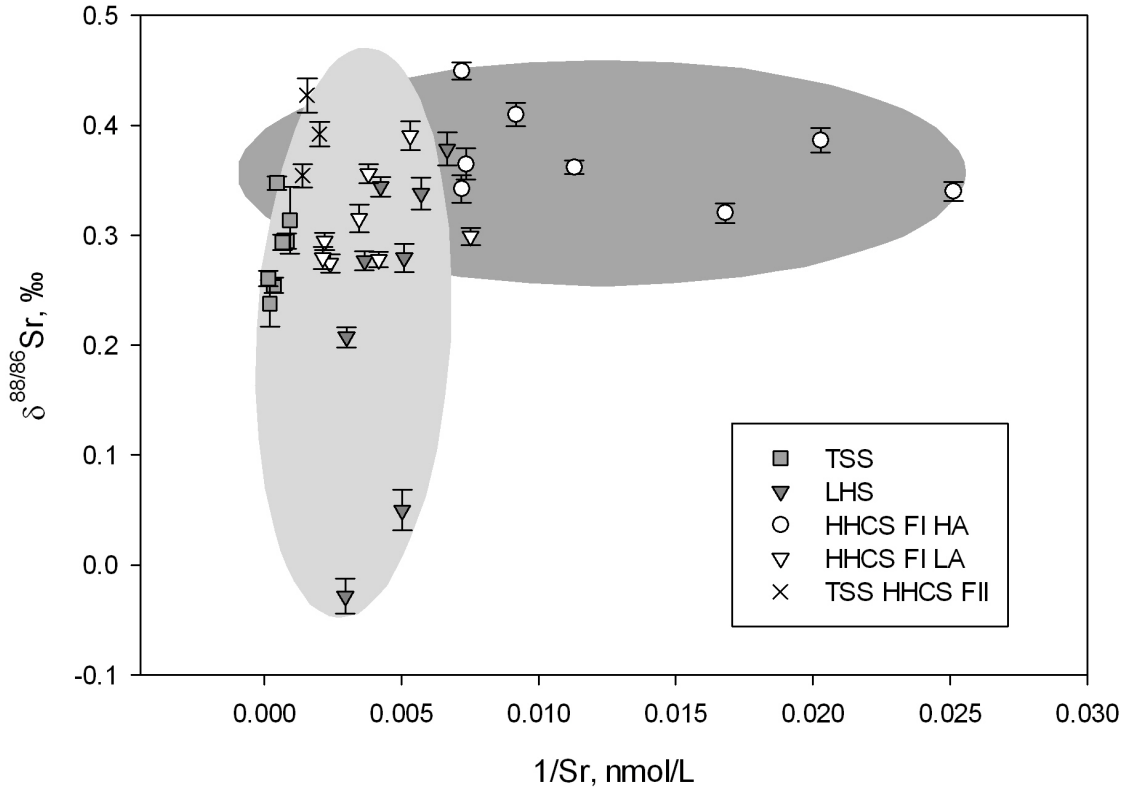

Figure 6.5. Plot of stable Sr isotopes versus 1/[Sr] (concentration data from Kisakürek et al., 2005). HA and LA refer to High altitude and low altitude samples respectively.

Figure 6.6 shows the $\delta^{88/86}Sr$ versus $^{87}Sr/^{86}Sr$ composition, this theoretically reveals both the source of Sr in the dissolved load ($^{87}Sr/^{86}Sr$) and the amount of mass fractionation is has undergone ($\delta^{88/86}Sr$) however we observe no co-variation but little is expected as they are affected by different processes.

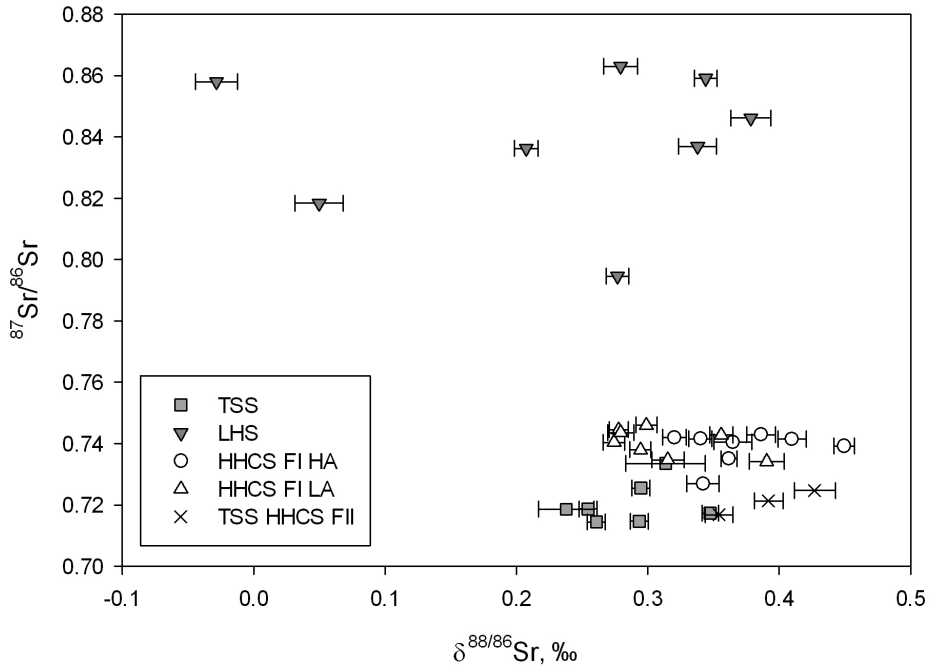

Figure 6.6. Plot of both radiogenic Sr and stable Sr showing source variation ($^{87}Sr/^{86}Sr$) degree of mass fractionation ($\delta^{88/86}Sr$) for each sample in the different catchment areas.

For the carbonate draining tributaries (Figure 6.7a) heavier $\delta^{88/86}Sr$ values in rivers are consistently observed in those samples taken after the monsoon. For the rivers draining silicate catchments (Figure 6.7b) the monsoon seems to have little effect on the $\delta^{88/86}Sr$ ratios.

It is interesting to note that the two lightest values observed (samples S11 and A9 in the LHS) were both samples from the same area within the LHS suggesting that there is perhaps a different weathering regime delivering the dissolved load of the river sampled for this area compared to other regions within the LHS.

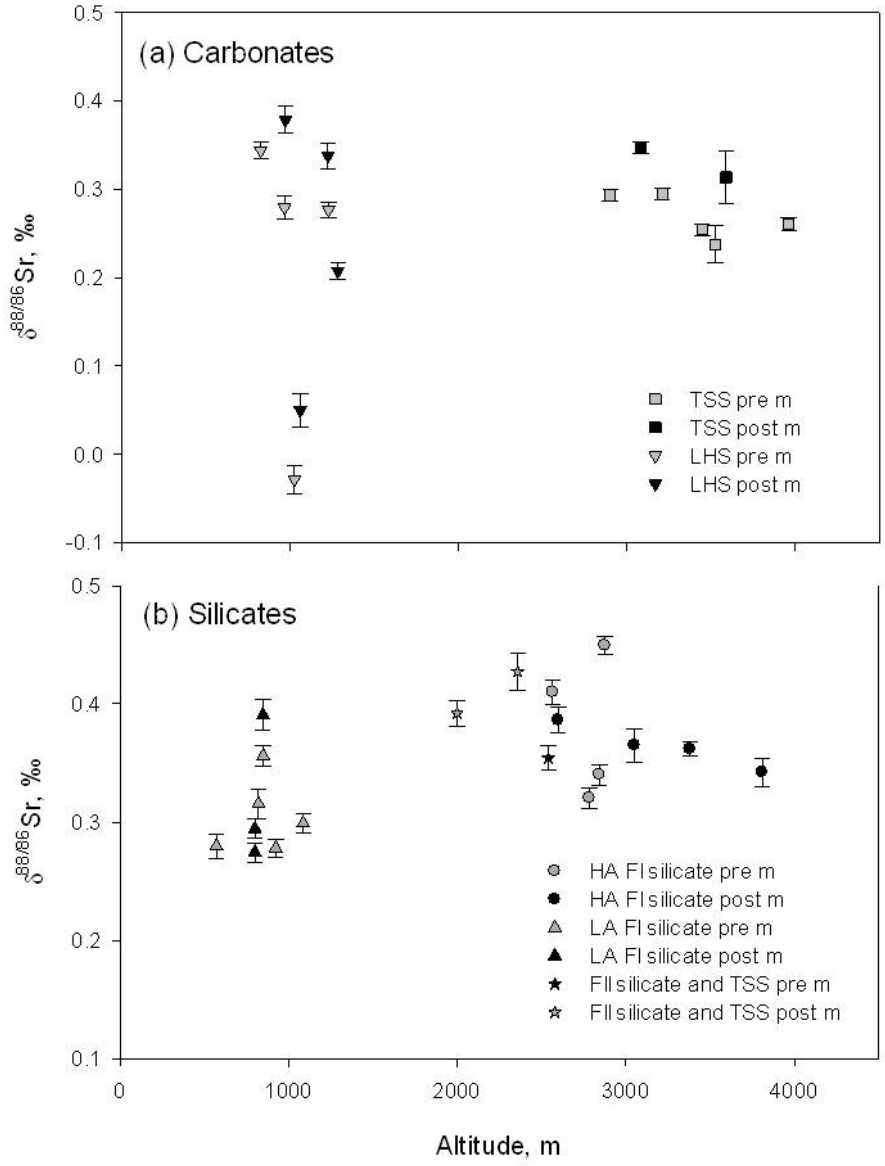

Figure 6.7 Pre- and post- monsoon data for rivers draining (a) carbonates and (b) silicates; samples from a mixed catchment draining the TSS with HHCS FII are also shown; m refers to the monsoon. In the carbonate draining rivers, samples taken after the monsoon are consistently heavier then those taken before, however this is not eh case in the silicate draining rivers.

6.4.3 Saturation state calculations

Mineral saturation states can be calculated using the PHREEQC program, (Pankhurst and Appelo, 1999) using measured concentration data from the dissolved load, as well as in-situ pH and temperature from Kisakürek et al. (2005). The Saturation Index (SI) is given on a log scale where negative values (<0) are undersaturated and positive values (>0) are

oversaturated (0 represents saturation) with respect to different mineral phases. Overall uncertainties are on the order of 1-2 SI units -(Stefansson et al., 2001). The SI of different minerals has been calculated for samples taken after the monsoon where all alkalinity data is available. The results for specific mineral phases are summarised in appendix 6 (b).

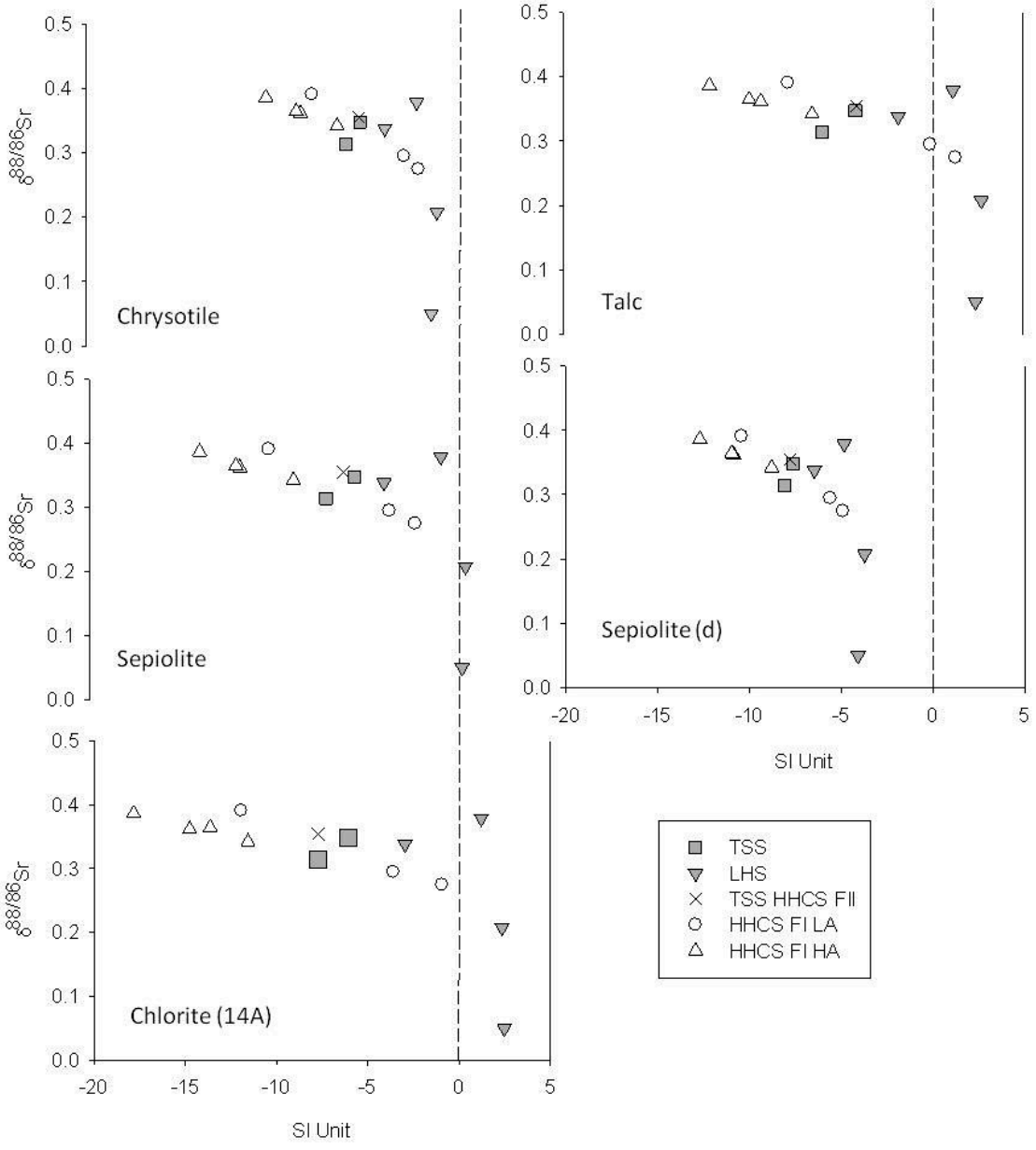

Figure 6.8 PHREEQC calculation of saturation index versus stable strontium isotopes for Mg- bearing silicate minerals and clays. Correlations are observed between silicate draining rivers (open symbols) and SI for Mg-bearing Si mineral phases predicted by PHREEQC, see text and appendix 6 (b) for more information.

There is a significant negative correlation of $\delta^{88/86}Sr$ from the HHCS at both altitudes with all possible Mg bearing minerals considered using the PHREEQC program (Figure 6.8). There is also a weak positive correlation of HHCS draining tributaries with Al bearing silicates and a weak negative correlation with carbonates (appendix 6b). The carbonate draining river waters show no correlation with any of the precipitating or dissolving mineral phases predicted by PHREEQC. The PHREEQC program uses elemental and thermodynamic data and predicts the theoretical stability of minerals in waters of such compositions, however, it takes no account of other variables such as precipitation kinetics. In this case, it should be recognised that perhaps not all of the mineral phases predicted by PHREEQC will actually be present in the rivers catchments themselves. Nevertheless, the strong correlation of $\delta^{88/86}Sr$ with all Mg bearing minerals predicted to be present still remains notable. The negative correlation is consistent with the behaviour of Mg isotopes (e.g Pogge Von Strandmann et al., 2008) and suggests that as the Mg-bearing phases are precipitating they are driving the residual waters to lighter Sr values, indicating the minerals contain predominately isotopically heavy Sr; this will be addressed further in the discussion.

6.5 Discussion

6.5.1 Radiogenic Sr isotopes

Tributaries draining the TSS and FII HHCS with TSS possess $^{87}Sr/^{86}Sr$ compositions that are within the range previously reported for carbonates within the TSS (0.7090-0.7519; Jacobson et al., 2002). Tributaries draining the LHS have very radiogenic $^{87}Sr/^{86}Sr$ ratios and intermediate concentrations of Sr (150-338nmol/L) indicative of Sr isotope exchange

between carbonates and silicates during Himalayan metamorphism (Palmer and Edmond, 1989; Bickle et al., 2001; Oliver et al., 2003). Tributaries draining FI HHCS have intermediate $^{87}Sr/^{86}Sr$ ratios with the majority of $^{87}Sr/^{86}Sr$ compositions clustering around 0.735-0.7557; these values are at the low end of the range typically seen for silicate rocks in the HHCS (0.7290-0.8029; Jacobson et al., 2002) and probably reflect Sr from relatively unradiogenic carbonate rocks (0.7111-0.7458; Jacobson et al., 2002). All the radiogenic Sr-isotope data are in close agreement with those reported previously for rivers draining these lithologies (Oliver et al., 2003; Galy et al., 1999). This interpretation of $^{87}Sr/^{86}Sr$ behaviour in these rivers closely follows that of Kisakurek et al. (2005) who undertook the $^{87}Sr/^{86}Sr$ measurements reported here.

6.5.2 Stable Sr isotopes

The data indicates little $\delta^{88/86}Sr$ significant difference between silicate and carbonate catchments, as illustrated in Figure 6.3. However, silicates (HHCS FI) tend towards heavier $\delta^{88/86}Sr$ values (0.34±0.10‰ (2.s.d n=16)) whilst carbonates $\delta^{88/86}Sr$ tends towards lighter values (0.26±0.22‰ (2.s.d n=15)). The region with the most consistent heavy $\delta^{88/86}Sr$ values is found in catchments draining both the TSS with an additional input from the HHCS FII (calc-silicates), 0.39±0.07‰ (2.s.d n=3).

Both natural and experimental studies have shown that during the crystallisation of $CaCO_3$, the light strontium isotopes are preferentially incorporated into this phase (e.g. Fietzke and Eisenhauer, 2006; Krabbenhoft et al., 2010; Böhm et al., 2012). Therefore, in principle, the chemical weathering of calcium carbonate will potentially yield a lighter stable isotope composition relative to that of silicate weathering phases. In this sense we might expect a correlation between $\delta^{88/86}Sr$ with $^{87}Sr/^{86}Sr$ since silicates possess relatively radiogenic values

whilst carbonates have relatively unradiogenic ratios ($^{87}Sr/^{86}Sr$ = 0.721 and 0.708 respectively, Allègre et al., 2010). The radiogenic $^{87}Sr/^{86}Sr$ ratios of the LHS are consistent with these rock types having experienced regional metamorphism and so are elevated to radiogenic ratios through equilibration of carbonates with coexisting silicates, hence a correlation between stable and radiogenic isotopes would not be expected. In contrast for the rivers draining the carbonates of the TSS it might be anticipated that relatively unradiogenic $^{87}Sr/^{86}Sr$ compositions would be accompanied by relatively light $\delta^{88/86}Sr$ ratios.

Despite the minor differences between tributaries draining silicate and carbonate dominated catchments, there are, however, resolvable shifts in $\delta^{88/86}Sr$ within a single catchment area where rock type varies, which are not seen in the radiogenic $^{87}Sr/^{86}Sr$ ratios. For samples taken from the Marsyangdi river catchment (S17-25) the sample furthest west drains the high altitude TSS (S17-21), as the flow moves towards the South East the river tributaries have an additional input from the Formation II (FII) HHCS (S22-24) and further south East again the tributary changes to Formation I (FI) HHCS only (S25). With regard to the $^{87}Sr/^{86}Sr$ ratio (Figure 6.8, panel (a)) there is no obvious indication of a change in lithology when the TSS catchment begins to drain HHCS FII silicates, however, as with typical $^{87}Sr/^{86}Sr$ ratios, when the catchment becomes predominantly silicate (in this case HHCS FI) the radio becomes more radiogenic. With the $\delta^{88/86}Sr$ ratio we see a clear resolvable variation between the two different silicate inputs, with the FII HHCS retaining a heavier $\delta^{88/86}Sr$ signature than the HHCS FI (Figure 6.8, panel (b)). Further measurement of $\delta^{88/86}Sr$ of the bedrock surrounding the Marsangdi (and other locations) may elucidate the nature of the relationship between the source type of silicate rock and the dissolved phase of the rivers.

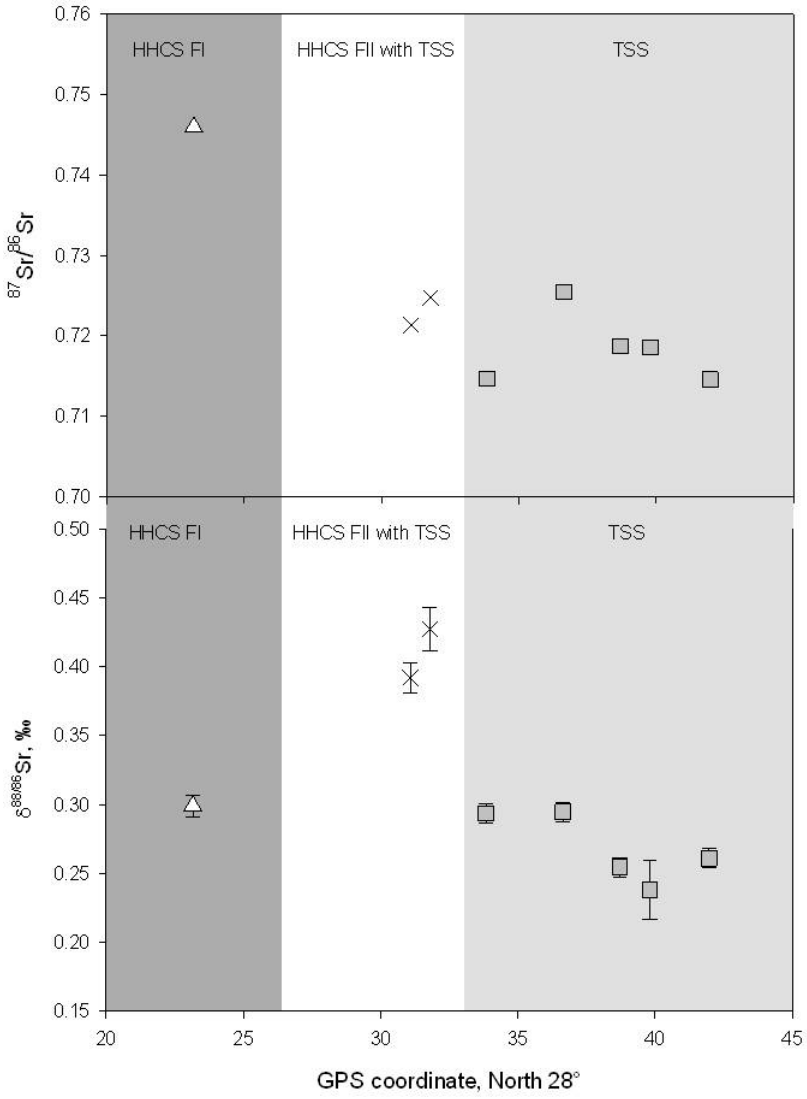

Figure 6.9 Comparison of (a) $^{87}Sr/^{86}Sr$ and (b) $\delta^{88/86}Sr$ strontium data taken from the dissolved load of the Marsyangdi and surrounding tributaries as a function of location along the river.

6.5.3 Seasonal variations in $\delta^{88/86}Sr$

Himalayan rivers exhibit seasonal variations in the relative magnitudes of the silicate and carbonate weathering fluxes, suggesting a climatic sensitivity of the weathering process that may ultimately be controlled by the local hydrology (Tipper et al., 2006c). Carbonate weathering has a greater sensitivity to runoff because of the faster dissolution kinetics of carbonate relative to silicate. In the high Himalaya, rain, ice and snow are thought to control

discharge of the largest rivers (e.g. Bookhagen, 2012). There are currently no other published studies in the literature that explore $\delta^{88/86}$Sr fractionation in the Himalaya or localised catchment areas let alone in relation to seasonal changes so much of the discussion here draws on comparison with similar isotope systems, such as $\delta^{44/40}$Ca and δ^{26}Mg, or else on $\delta^{88/86}$Sr data taken from other geographical locations. Pearce et al. (2011) and Pearce (Pers. Comm.) presented data for the $\delta^{88/86}$Sr composition of precipitation, dust and ice and assess their impact on the $\delta^{88/86}$Sr of rivers and the global Sr cycle.

The primary Sr isotope signal from rock and mineral dissolution may also be fractionated by processes including weathering and incorporation into biomass, and the formation of secondary minerals during weathering. In the following sections the potential influence of precipitation, aeolian input, vegetation, groundwater and Mg-bearing secondary minerals (based on PHREEQC calculations) will be discussed.

Location	Input	$\delta^{88/86}$Sr (‰)	Error (‰)	Error type*
Azores	Rain	0.329	0.007	2.s.e
China	Rainwater	0.203	0.007	2.s.e
	Dust	0.261	0.011	2.s.e
	River	0.355	0.038	2.s.d n=3
Congo	Rainwater	0.064	0.006	2.s.e
	River	0.285	0.054	2.s.d n=2
Greenland	Ice	0.101	0.007	2.s.e
	River	0.331	0.251	2.s.d n=5
Iceland	Ice	0.252	0.008	2.s.e
	River	0.354	0.425	2.s.d n=10
Kansas	Dust	0.174	0.008	2.s.e
New Zealand	Dust	0.249	0.006	2.s.d n=3
Paris	Rainwater	0.219	0.016	2.s.d n=3
	River	0.285	0.007	2.s.e

Table 6.2 Summary of $\delta^{88/86}$Sr values for dust, ice, rainwater and river water in differing geographical locations; where data is available, dust, ice and rain water input is lighter in $\delta^{88/86}$Sr composition than the corresponding river water. Data from Pearce et al. (2011) and Pearce (Pers. Comm.) * Error type refers to either 2.s.e of a single measurement or 2.s.d of an average of sample measurements.

6.5.3.1.Precipitation

The monsoon has a significant affect at all the locations sampled in the LHS and TSS where monthly precipitation between seasons increases from 100 mm in the spring up to 600 mm in the autumn. In contrast, for the HHCS we see very little variation between the spring and autumn seasons with only a slight increase in precipitation of up to 10 mm (values given in Kisakürek, 2005, and taken from Chalise et al., 1996). The $\delta^{88/86}$Sr ratios shift to heavier values after the monsoon in both the LHS and TSS catchments.

Rain waters from a variety of geographical locations (Congo, China, Iceland and France, Pearce Pers. Comm.), yield a range of $\delta^{88/86}$Sr isotope compositions, but in every case rainwater possesses lighter $\delta^{88/86}$Sr values than river waters from the same locations, Table 6.2, and appendix 6 (c). Although these rainwaters are not necessarily representative of precipitation in the Himalaya, if the trend is observed in these other areas also applies then it can be anticipated that rain waters will be lighter than most of the river waters measured in this study. In particular, the input from this source following the monsoon would drive river compositions to lighter values, rather than to heavier values as is observed.

Glacial ice is also ubiquitous in the Himalaya, and any rise in temperature could result in the rivers receiving an increased input from glacial melting. Preliminary data for glacial ice measured from Greenland and Iceland indicates $\delta^{88/86}$Sr values of ~0.10‰ and 0.25‰, respectively. On the basis that such ice should contain a significant proportion of seawater derived Sr, Pearce et al. (2011) suggested that $\delta^{88/86}$Sr isotopes might be fractionated by freeze thaw processes. Alternatively the $\delta^{88/86}$Sr isotope signal of the ice may be dominated by Aeolian inputs, either derived locally or far-field in origin. If it is assumed that Himalayan glacial input is similarly light then this would also drive river waters to lighter values, rather than to heavy values as observed in the LHS and TSS. However, while we have a poor

quantitative understanding of atmospheric and glacial inputs, we know that both rainwater and glacial inputs have low Sr contents; therefore the monsoonal correlations could be inferred as an increase in weathering that overwhelms any rainwater input.

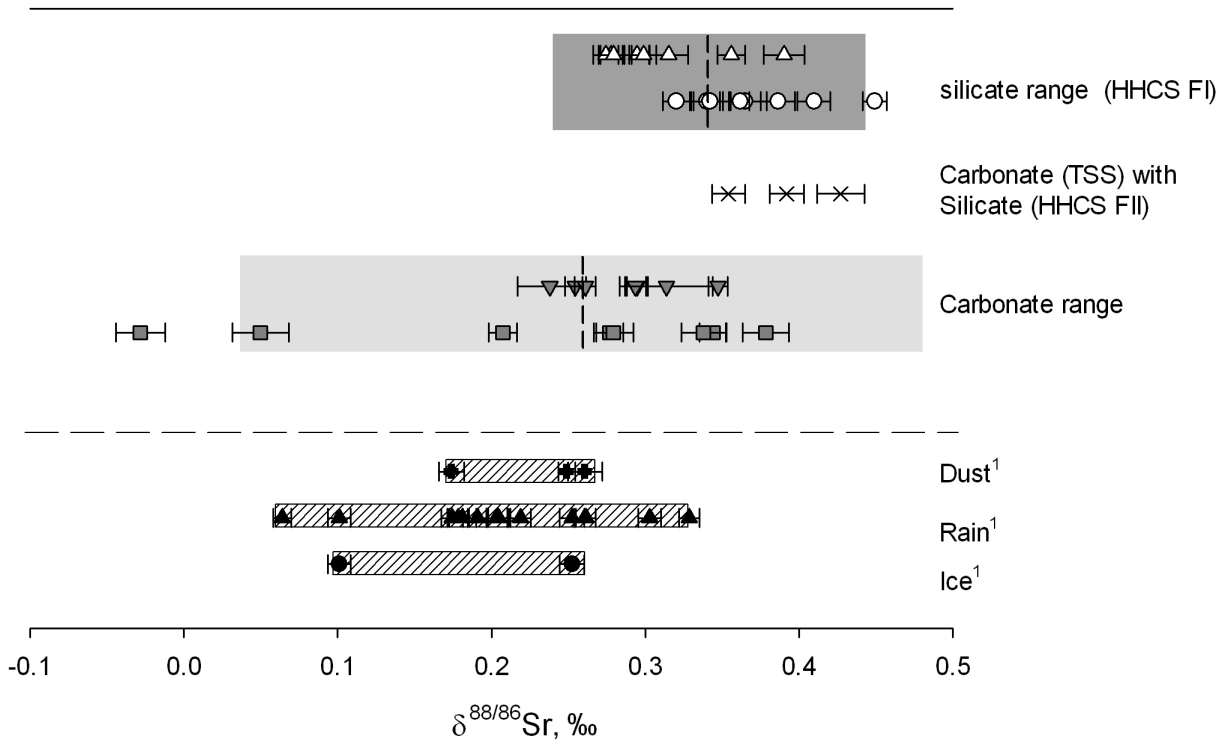

Figure 6.10 Range of hydrological and aeolian inputs from [1] Pearce et al. (2010) and Pearce (Pers. Comm) compared to the range of $\delta^{88/86}$Sr values reported in this study.

Overall, these observation suggest that precipitation, from rain, snow or glacial melting, is not the major cause of the variations observed in the Himalayan rivers, and in particular the post-monsoon shift to heavy $\delta^{88/86}$Sr isotope compositions. Nevertheless, given that such precipitation is likely to acquire much of its Sr from seawater (with a $\delta^{88/86}$Sr value of ~0.36‰) some contribution from this source to the rivers studied here cannot be completely ruled out.

6.5.3.2 Aeolian input

The input of dust from continental weathering and erosion could also have an impact on the $\delta^{88/86}$Sr dissolved in the river waters, but again for the samples that have been measured thus far (from Kansas, China and New Zealand, Pearce, Pers. Comm.) it has also been shown that dust is generally isotopically light compared to average riverine values, and cannot account for the post-monsoon shift to heavy values. Aeolian input may well contribute to the overall chemistry of the rivers; for example, the dissolution of dust in water may affect mineral saturation state and therefore clay formation. But as with glacial input, other processes may overwhelm the contribution from dust.

Therefore, for both precipitation and dust the samples that have been measured thus far have relatively light $\delta^{88/86}$Sr values, and cannot account for the post-monsoon shift of the dissolved phase of Himalayan rivers to relatively heavy values. Nevertheless, it is clear that the observations and interpretations given above are based on $\delta^{88/86}$Sr measurements from other locations and cannot be necessarily assumed to be representative of the hydrological inputs into the Himalaya. Further, study would greatly benefit from measurement of these key inputs in the Himalaya including precipitation, glacial melt, and dust.

6.5.3.3 Vegetation

DeSouza et al. (2010) measured the $\delta^{88/86}$Sr ratios in soils and plant materials in the vicinity of the Damma Glacier in Switzerland, and $\delta^{88/86}$Sr isotopes, like those of $\delta^{44/42}$Ca, are fractionated during incorporation into plants with roots, stems, flowers and leaves (of the genii *R. ferrugineum* and *Vaccinium*) all possessing isotope compositions that are isotopically lighter than the soils from which they grow by 0.2‰-0.5‰. Strontium isotope ratios, like

those of Ca, are fractionated during uptake from the dissolved load in soils into plant roots. This in turn leaves the pore waters surrounding the roots enriched in heavy $\delta^{88/86}$Sr isotopes. Clay minerals within the soil also preferentially adsorb lighter $\delta^{88/86}$Sr isotopes (consistent with a kinetic isotope fractionation) onto their surface, further driving the Sr in residual soil water pools to heavier values.

6.5.3.4 Groundwater

Annual groundwater fluxes in the Himalaya are greater in volume than the contribution from ice- and snowmelt (Andermann et al., 2012). Therefore, it is conceivable that groundwater is a significant source of heavy $\delta^{88/86}$Sr isotopes to low altitude rivers. For Ca stable isotopes direct measurements of ground waters has shown them to be characterised by a heavy $\delta^{44/40}$Ca composition in the Marsyangdi and Bhot Kosi regions (both TSS) of the Himalaya (Tipper et al., 2006c). Groundwater also constitutes a significant source of Sr in the Bengal Basin, Basu et al. (2000) suggest that the strontium flux in sub-surface flowing groundwater's of the Ganges-Brahmaputra (G-B) delta in the Bengal Basin is equal in magnitude to the dissolved strontium flux carried to the oceans by the G-B river waters. Following the monsoon, river discharge increases by up to 200 m^3s^{-1} and 500 m^3s^{-1} in the LHS and TSS, respectively, and up to 250 m^3s^{-1} in the HHCS (values given in Kisakurek (2005) taken from Chalise et al. (1996)). The relative contributions of groundwater to Himalayan rivers and its likely Sr stable isotope composition are difficult to estimate, however, it seems likely that this is a significant hydrological source that may have the potential to effect the compositional changes seen in post-monsoon waters. In a study by Tipper et al. (2006a), visible discharges from cold springs in the Bhote catchment (LHS) are associated with shallow pools from groundwater seepage resulting in massive travertine deposits. The travertine is isotopically

light with respect to $\delta^{44/42}$Ca and δ^{26}Mg isotopes (an average $\delta^{44/42}$Ca of 0.21 ± 0.07‰ and average δ^{26}Mg is − 3.45 ± 0.86‰), the lightest isotopic values observed in the region. It can be anticipated that the precipitation of travertine (calcium carbonate) will have a similar affect on Sr stable isotopes, preferentially incorporating the light isotopes, and driving the residual waters to heavy $\delta^{88/86}$Sr values. Tipper et al. (2006a) suggest that this groundwater may contribute a significant flux of dissolved elements to the Bhote catchment and the dissolved load of Himalayan rivers. Again $\delta^{88/86}$Sr data is needed to properly characterise this potential source of Sr to Himalayan rivers.

6.5.3.5 Mg-bearing secondary minerals

The program PHREEQC was used to calculate mineral saturation states from the dissolved load of river waters. These calculations indicate that $\delta^{88/86}$Sr is strongly correlated with Mg-bearing secondary minerals and carbonates in rivers draining the HHCS, whereas no correlation was found between $\delta^{88/86}$Sr and either carbonate or silicate minerals in the TSS or LHS, appendix 6 (a). Correlations of $\delta^{88/86}$Sr with mineral saturation states (predicted by PHREEQC) appear to indicate that the heavier Sr isotopes are preferentially incorporated into clay minerals and other Mg-bearing phases, similar to the behaviour of Mg isotopes (e.g. Tipper et al., 2006c; Opfergelt et al., 2010). Strontium, like both Mg and Ca, is a divalent cation and will likely substitute in the same way as these elements, either directly into the mineral structure or absorbed onto mineral surfaces. An investigation into δ^{26}Mg fractionation in glacial streams (Tipper et al., 2012), found large seasonal changes in the isotope composition of stream waters with a shift to heavier δ^{26}Mg values immediately after the melt season. A number of interpretations were made to account for this behaviour but one similar to the process of $\delta^{88/86}$Sr fractionation observed with PHREEQC calculations is the

suggestion that if Mg ion-exchange and sorption (desorption) processes are occurring then the heavier Mg isotope would have to be preferentially adsorbed onto clay-mineral surfaces.

The carbonate draining rivers show no correlation with any of the mineral phases predicted by PHREEQC, although any inferences based on this observation are somewhat limited by the number of samples analysed, particularly in the TSS (N=2).

Some of the minor variations we observe between monsoonal seasons may be caused by input from precipitation, dust, groundwater, vegetation or the precipitation of secondary mineral phases, but each of these reservoirs and minerals must be fully characterised and the balance of input from each established in order to fully interpret the data. It may be that in the carbonate catchments the increase in $\delta^{88/86}$Sr after the monsoon could be due to an increase in weathering and the precipitation of secondary weathering minerals, such as calcite, which would drive $\delta^{88/86}$Sr in the dissolved load of rivers to heavier values.

6.5.4 Comparison with δ^{7}Li isotope data for the same samples

The study of Kisakürek et al. (2005) found a significant overlap of the δ^{7}Li composition of the dissolved load of rivers draining both silicate and carbonates, as is the case for $\delta^{88/86}$Sr. Consequently, it was suggested that the composition of the bed rock is not the main control on Li systematics, rather the Li isotope and elemental signature of the rivers is determined by fractionation during weathering. The data presented here for Sr isotopes also indicates that the hydrological cycle may have a significant affect on $\delta^{88/86}$Sr systematics, in addition to the dissolution of primary phases and precipitation of secondary clays and Mg-bearing silicates. A seasonal effect was also observed for Li isotopes, with δ^{7}Li values shifting to lighter values

after the monsoon. This was considered to result from increased weathering intensity (increased primary mineral dissolution relative to secondary mineral formation) but only in the HHCS, silicate-draining, rivers. By comparison, the $\delta^{88/86}$Sr values trend towards heavier values after the monsoon but only in carbonate draining rivers. Lithium and Sr have differing geochemical properties, in part due to different ionic radii and valency, and so differing behaviour during weathering might be expected; however when used together, each has the capacity to respond to weathering process, leaving a diagnostic signal in natural waters.

6.5.5 Comparison with δ^{30}Si ratios on the same samples

Silicon isotope measurements (δ^{30}Si; Equation 6.5) have also been made by Georg (unpublished) for some of the Himalayan river samples studied here. The $\delta^{88/86}$Sr data show a negative correlation with δ^{30}Si, illustrated in Figure 6.11.

Where δ^{30}Si is given by:

$$\delta^{30}Si = \left[\frac{(^{30}Si/^{28}Si)_{\text{sample}}}{(^{30}Si/^{28}Si)_{\text{standard}}} - 1 \right] * 1000 \qquad [6.5]$$

River waters draining the TSS with an additional input from the HHCS FII possess heavy $\delta^{88/86}$Sr values and light δ^{30}Si, whereas, despite a small amount of overlap, those draining the HHCS possess intermediate δ^{30}Si and $\delta^{88/86}$Sr values, and rivers sampled from the TSS have heavy δ^{30}Si values and lighter $\delta^{88/86}$Sr values. These data suggest that at some level rock type, or the response of secondary minerals to the initial chemistry of the waters, does indeed exert a control on Sr and Si stable isotope compositions. Georg et al. (2006) suggested that the Si isotope composition of high mountainous catchments, such as those in the Swiss Alps, reflects the mixing of soil/groundwater and high discharge waters originating from

precipitation and snow melt, where the underlying dominant mass fractionation process is the formation of clay, which incorporates lighter Si isotopes. If this is true of the $\delta^{30}Si$ in the dissolved load in the Himalayan river samples studied here, the inverse correlation between $\delta^{30}Si$ and $\delta^{88/86}Sr$ suggests that they are being affected by similar processes. The PHREEQC calculations showed correlations between $\delta^{88/86}Sr$ and the saturation states of clays and Mg-bearing minerals (appendix 6 (b)), and the same mineral phases that are though to fractionate Si isotopes, although in the case of Si, the lighter isotope is preferentially incorporated.

There is also a trend between 1/[Sr] and 1/[Si] (Figure 6.12), which appears to show two arrays, the first is predominantly carbonate as illustrated by the TSS trend, and the other is silicate as shown by the HHCS FI trend. Interestingly the LHS, which has been inferred to have undergone regional metamorphism (sections 6.4.2 and 6.5.1) lies within the observed silicate trend.

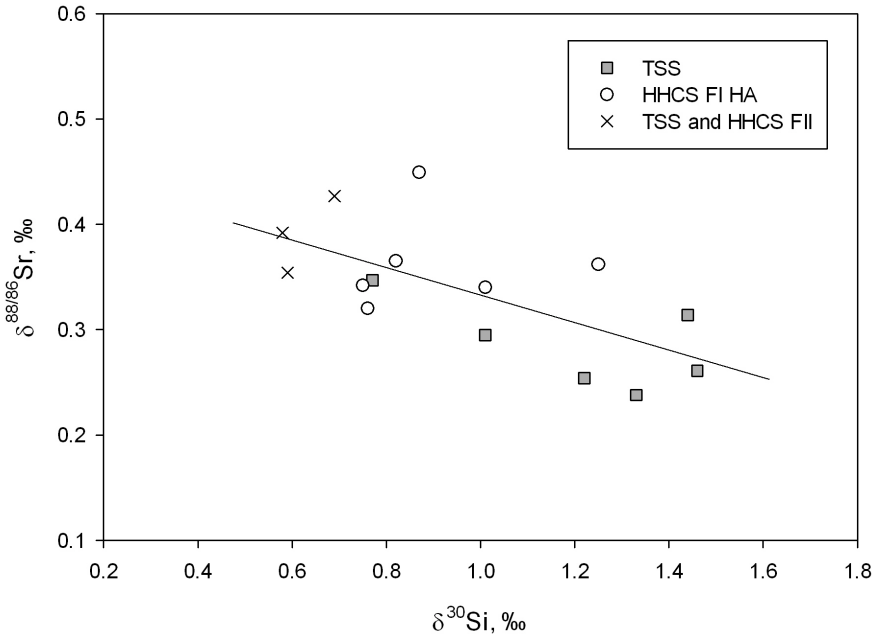

Figure 6.11 Correlation between both $\delta^{30}Si$ and $\delta^{88/86}Sr$ for the dissolved load of Himalayan rivers. $\delta^{30}Si$ data from Georg (unpublished)

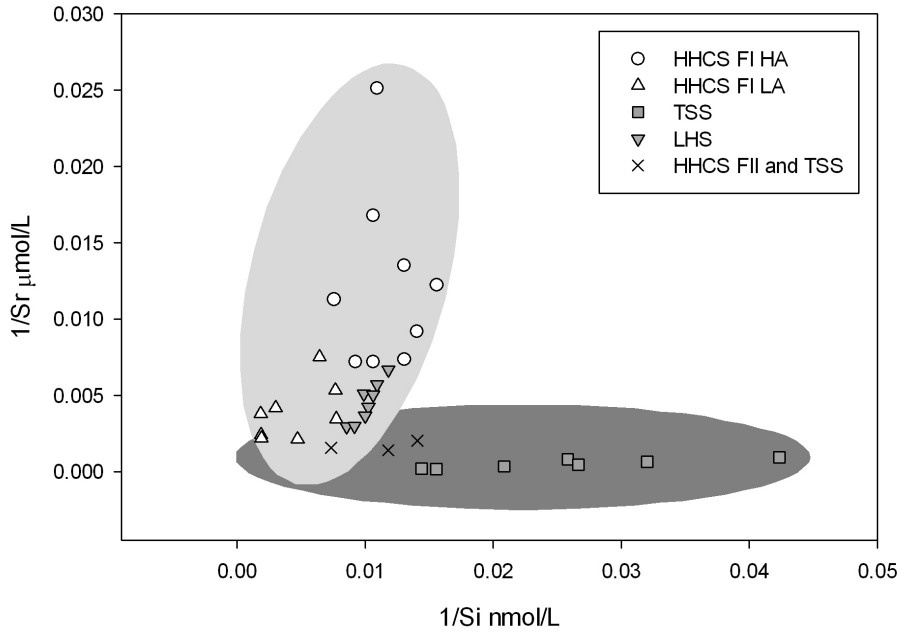

Figure 6.12 Plot of 1/[Si] and 1/[Sr], data from Kisakürek (2005). Pale grey highlights the silicate array whilst the darker grey highlights the carbonate.

6.6 Conclusions

In this preliminary study of Himalayan rivers we find that, in general, those rivers draining carbonate catchments possess lighter $\delta^{88/86}$Sr isotope compositions than those draining silicate terrains, with small variations in the $\delta^{88/86}$Sr of 0.1-0.2‰. However, the sources of many these waters can be distinguished on the basis of geochemical data such as 1/Sr vs. $\delta^{88/86}$Sr (Figure 6.4) and $\delta^{88/86}$Sr vs. δ^{30}Si (Figure 6.11) in the dissolved load.

The relationship between 1/Sr and $\delta^{88/86}$Sr illustrates that rivers draining either carbonate or silicate catchments may be distinguished based on their 1/Sr and $\delta^{88/86}$Sr compositions. Further work of rivers in other areas will confirm if this trend is consistent and general for Sr stable isotopes.

The relationship between $\delta^{88/86}$Sr and δ^{30}Si suggests that these stable isotope systems are responding to the same process during weathering, most likely the preferential incorporation

of light Si, and heavy Sr, into secondary clays and other Mg-bearing phases. This covariation also indicates that despite this fractionation, differences between rock types are preserved, indicating that rock type likely controls the initial isotope composition of Sr and Si liberated by weathering, while weathering processes themselves drive the composition to lighter or heavier values.

The question remains as to what extent stable Sr isotopes in carbonates in the dissolved load of are affected by diffusional exchange with coexisting silicates during regional metamorphism? In this study the LHS is the region most affected by such silicate-carbonate exchange yielding highly radiogenic $^{87}Sr/^{86}Sr$ ratios in carbonate. In this study the stable isotope $\delta^{88/86}Sr$ ratios possess a wide range of values that include some of the lightest measured, suggesting that much of the primary signal from carbonate weathering is retained. Further measurement may reveal whether the $\delta^{88/86}Sr$ ratio is actually decoupled from the processes of radiogenic Sr exchange between carbonates and silicates.

A strong seasonal shift of $\delta^{88/86}Sr$ to heavier values after a monsoon is observed in carbonate catchments, and is much less pronounced in the silicate catchments. Some of the small variations we observe between monsoonal seasons may be caused by input from precipitation, groundwater, vegetation or the precipitation of secondary mineral phases, but each of these reservoirs and processes has yet to be fully characterised for Sr stable isotopes.

Correlations of $\delta^{88/86}Sr$ with mineral saturation states (predicted by PHREEQC) indicate that the heavier Sr isotopes are preferentially incorporated into clay minerals and other Mg-bearing phases, in much the same way as Mg isotopes (e.g. Tipper et al., 2006c; Opfergelt et al., 2010). Such behaviour is also reflected in the correlation of $\delta^{88/86}Sr$ and $\delta^{30}Si$ suggesting that both isotope systems are affected by the same processes. Strontium, like Mg and Ca, is a

divalent cation and will likely substitute in the same way into specific minerals and on mineral surfaces.

This is a preliminary study and more work needs to be undertaken to fully characterise and quantify the hydrological and bedrock inputs to the rivers. But as such this study does reveal that $\delta^{88/86}$Sr isotopes have the potential to be used as a weathering tracer that reacts to seasonal variations in hydrology, that may occur in response to variations in input (precipitation, groundwater and dust) and/or secondary weathering processes.

CHAPTER SEVEN

CONCLUSIONS

Conclusions

This thesis has investigated the behaviour of stable strontium isotopes, to see if they can be used to elucidate key information on processes such as continental weathering, and variations in the balance of silicate to carbonate input to the oceans both today and in the past. This is important because it is the weathering of silicate rocks that leads to the net drawdown of carbon dioxide, a greenhouse gas, from the atmosphere into the oceans, over million year time scales, which has consequences for the global carbon cycle.

Investigation of the mass dependent fractionation of stable strontium isotopes has only recently received wider interest, in part, due to analytical advances in mass spectrometry, and in part, because the systematic variations documented in recent studies were not widely anticipated. Nevertheless, the relative mass deference between the stable Sr isotopes studied here (^{88}Sr and ^{86}Sr) is small and the observed variations require measurements at the parts per million level. The combination of thermal ionisation mass spectrometry (TIMS) and double-spike (DS) techniques used in the analysis of samples in this thesis allows these small variations to be resolved.

7.1 Stable Strontium isotopes in the marine environment

The marine radiogenic strontium isotope record ($^{87}Sr/^{86}Sr$) is the most commonly used proxy record to constrain the geologic history of chemical weathering variations over time. This is recorded in marine sedimentary archives, and is thought reflect either changes in the balance of continental weathering relative to input from hydrothermal exchange at mid-ocean ridges over time. However, interpretations of changes in continental weathering using the radiogenic strontium geochemical cycle is because changes in the input flux cannot be distinguished from changes in composition, and the extent of removal accompanying carbonate sedimentation cannot be readily quantified. Stable strontium isotopes ($\delta^{88/86}Sr$) precipitated in marine carbonates have been shown to be lighter than that of seawater (Fietzke and Eisenhauer, 2006) providing a measureable Sr output from the oceans, enabling the completion of Sr mass balance equations and providing better constraints on the Sr geochemical cycle. This thesis builds on this initial finding to explore the degree of mass dependent $\delta^{88/86}Sr$ fractionation from seawater into modern marine biogenic calcites, specifically in different species of foraminifera (chapter three) and coccolithophores (chapter five), and also, but to a lesser extent, in corals (both high Mg calcite and aragonite; chapter two), and offsets in $\delta^{88/86}Sr$ of approximately 0.02, 0.05, 0.19 and 0.20 ‰ at ~25°C, respectively, have been determined. An attempt was made to quantify $\delta^{88/86}Sr$ fractionation from seawater in inorganically precipitated calcite, however, it was not possible to complete this part of the project and this is summarised in appendix 8.

Investigating the influences of temperature on the fractionation of $\delta^{88/86}Sr$ in marine calcium carbonates suggests there is little variability in the planktic foraminifera *G. sacculifer* (samples from core-tops in the South Atlantic ocean; $\delta^{88/86}Sr$ ~0.09 ‰; temperature range of ~18-28 °C) whereas coccolithophores (culture study) show a strong negative correlation with

temperature (range of 10-25 °C) and growth-rate, consistent with a kinetic isotope fractionation of Sr aquo-complexes. The aragonitic corals analysed, precipitated in the ocean at either 26 or 4 °C, are statistically indistinguishable from each other suggesting little temperature dependence, however more data are required to complete this finding. These results contribute to the on-going scientific research into the processes of biomineralisation and how such organisms incorporate trace metals and isotopes into marine calcium carbonate, specifically the results conclude that $\delta^{88/86}$Sr in coccolithophores can be used as a proxy for growth-rate.

The investigations of $\delta^{88/86}$Sr variation in different species of modern foraminifera illustrate that choice of shell size in planktonic foraminifera is a practical issue of importance in the design or methodological procedures for paleoceanographic work, and care should be made to choose a single size fraction taken from a single species. Where using one species is not possible it would be best to pick from the smaller size fraction where inter species offsets appear to be smaller (c.f. 250-355μm). The range of $\delta^{88/86}$Sr of calcium carbonates measured in this project is summarised in Figure 7.1

Today the $\delta^{88/86}$Sr value of seawater is ~0.38‰ but has this varied in the past? If so, are variations in seawater composition observed on glacial time periods, perhaps in response to increases in carbonate weathering from sea-level low stands, as has been suggested by Krabbenhöft et al., (2010). Chapter four presents a record of $\delta^{88/86}$Sr preserved in the tests of the foraminifera *Globigerinoides ruber* over the past 145 kyr; and an excursion of ~120ppm to heavier $\delta^{88/86}$Sr values in MIS 3 is found, however there is little variation associated with glacial growth and/or retreat. A simple model of $\delta^{88/86}$Sr variation over the last glacial cycle, incorporating a three-fold increase in shelf carbonate weathering (Parkinson, unpublished), suggests that $\delta^{88/86}$Sr is insensitive to changes in input over glacial-interglacial time periods; therefore the interpretation of the excursion lends its self to local seawater changes.

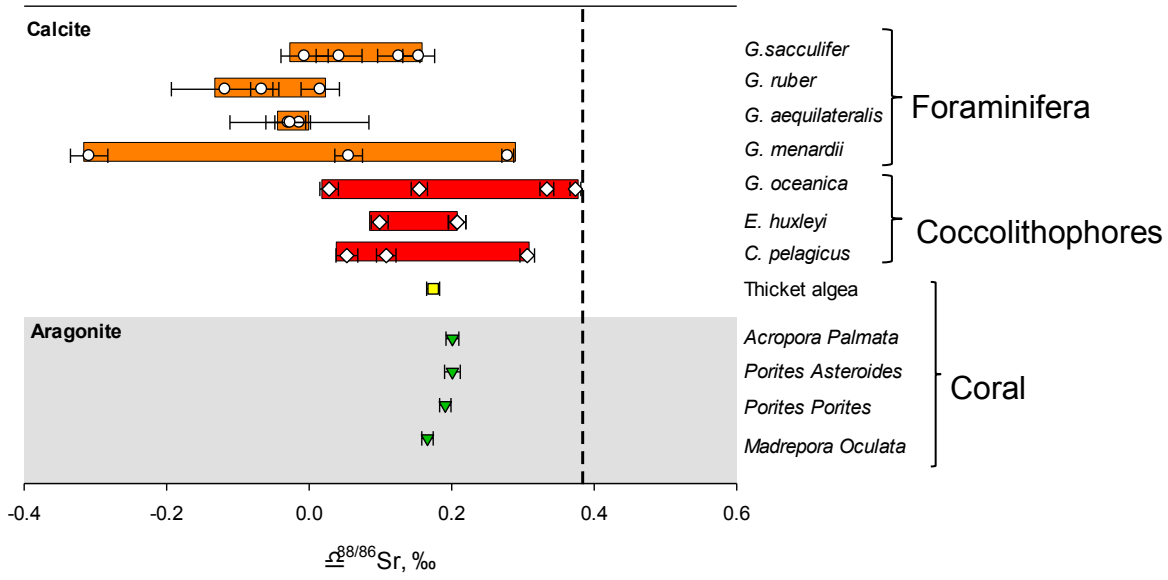

Figure 7.1 summary of biogenic calcites analysed in this study, the coloured bars represent influences on the $\delta^{88/86}$Sr ratio arising from size fraction or temperature respectively. The dashed line represents the IAPSO seawater standard Batch No 141.

7.2 Stable strontium isotopes in the terrestrial environment

Constraining the balance of carbonate to silicate weathering is important for determining the contribution of weathering to the long-term drawdown of carbon dioxide from the atmosphere. By investigating $\delta^{88/86}$Sr variability in the dissolved load of rivers in the Himalaya, draining both silicate, carbonate and mixed carbonate and silicate lithologies, the potential of stable strontium isotopes to be used as tracers of weathering processes has been investigated. The Himalaya is an active orogeny and notorious for having a complex weathering regime, made difficult to interpret with traditional weathering proxies such radiogenic Sr isotopes and elemental (metal/Ca) ratios due to regional metamorphism and the non-conservative behaviour of Ca. In this preliminary study it is found that rivers draining carbonate catchments tend to lighter isotopic $\delta^{88/86}$Sr values ($\delta^{88/86}$Sr = 0.26±0.2) than those from river draining silicates $\delta^{88/86}$Sr = 0.34±0.1), illustrated in Figure 7.2.

There is a strong seasonal shift of $\delta^{88/86}$Sr to heavier values after a monsoon that is less pronounced in the silicate catchments. Some of the small variations we observe between monsoonal seasons may be caused by input from precipitation, groundwater, vegetation or the precipitation of secondary mineral phases, but each of these reservoirs and minerals be fully characterised.

However, preliminary data suggests that through the use of plots of either $\delta^{88/86}$Sr vs. δ^{30}Si or $\delta^{88/86}$Sr vs. 1/[Sr] it may be possible to distinguish between different rivers draining different catchment areas, allowing $\delta^{88/86}$Sr isotopes to be a useful tracer of weathering when combined with other elemental or isotope techniques.

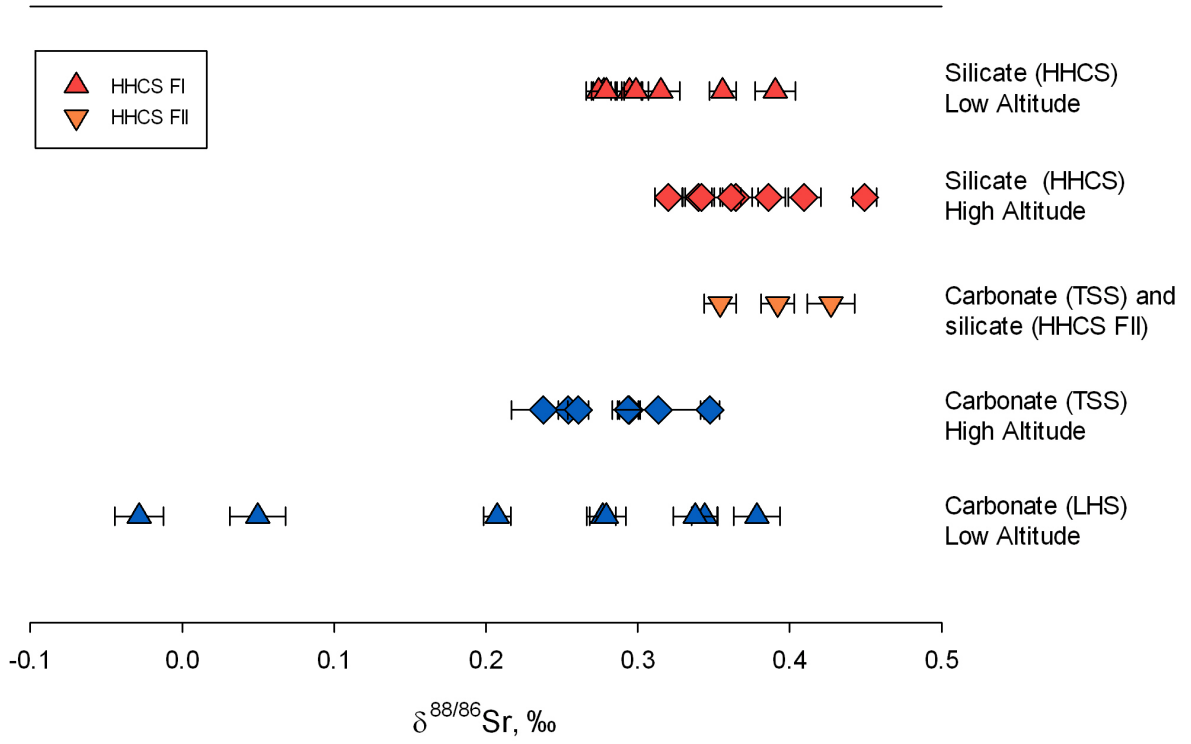

Figure 7.2 summary of the dissolved load of rivers draining different catchments in the Himalaya, in general silicates tend to take heavier $\delta^{88/86}$Sr ratios than carbonate draining rivers.

7.3 Stable strontium isotopes in global cycles

Based on the work of Krabbenhöft et al., 2010, and the results of the above experiments an estimate of the modern calcite $\delta^{88/86}$Sr output of 0.14 ‰ or a flux weighted average of 0.16 ‰ (Table 7.1) at ~25°C can be made, however, this may change with decreasing temperature.

The results from this thesis have greatly improved our knowledge of stable Sr isotope behaviour in a variety of marine carbonates, both in the modern ocean and in the past. This information has contributed detail both on biomineralisation of Sr and Ca as well as helping

Carbonate Sediment type	$CaCO_3$ deposition (10^{12} mol/yr)	$CaCO_3$ polymorph	Sr Burial Flux (10^9 mol/yr)	$\delta^{88/86}$Sr ‰ ($2\sigma_m$) Krabbenhoft et al., 2010	$\delta^{88/86}$Sr ‰ This Study (25-26°C)
Reef corals	~6.0(20%)	Aragonite	~54(31%)	0.19(1)	0.198
Halimedia	~1.5(5%)	Aragonite	~16(9%)	0.27(3)	NA*
Coccoliths	~5.0(16%)	Calcite	~11(6%)	0.26(7)	0.076
Planktic foraminifera	~6.0(20%)	Calcite	~8(5%)	0.14(1)	0.033
Continental shelf and slope taxa	~13.0(39%)	Aragonite and Calcite	~85(49%)	0.22(3)	0.15
Total carbonates	~32.0(100%)		~174(100%)		
Average				0.22(2)	0.14
Sr burial flux weighted average				0.21(2)	0.16

Table 7.1 Sr fluxes and $\delta^{88/86}$Sr isotope values, reproduced from Krabbenhöft et al. (2010), the results from this study are highlighted in the final column. *Halimedia were not measured in this study so the value from Krabbenhöft et al. (2012) was used in its place.

to constrain the geochemical cycle of Sr by allowing the Sr carbonate output of the oceans to be constrained. This is important so that correct interpretations can be made on the relative contributions of silicate and carbonate weathering from the continents to the oceans both today and in the past, and will help with interpretations of the carbon cycle.

Figure 7.3 illustrates the emerging components of the modern day $\delta^{88/86}$Sr cycle, with on-going work outlined here and elsewhere (For example, Pearce et al., 2011; Böhm et al., 2012 and Krabbenhöft et al., 2012) contributing to the full characterisation of the global Sr cycle

(both $^{87}Sr/^{86}Sr$ and $\delta^{88/86}Sr$) so that complete and accurate interpretations can be made on the mass balance of Sr in the modern day oceans and in the past, especially with regards to the monotonic and rapid increase in seawater $^{87}Sr/^{86}Sr$ towards more radiogenic values over the past 40 Mya.

Regarding the construction of $\delta^{88/86}Sr$ marine records, beyond that of the past 40 Myr increase in radiogenic ratios, future work should apply the $\delta^{88/86}Sr$ proxy specifically to investigations of changing oceanic carbonate chemistry over periods longer than the residence time of Sr in the ocean such as the mass carbonate dissolution events at the Paleocene-Eocene Thermal Maximum (PETM) ~55 million years ago (e.g Zachos et al., 2005) or the Caribbean carbonate crash (CCC) ~12-10 Myr (e.g. Roth et al., 2000).

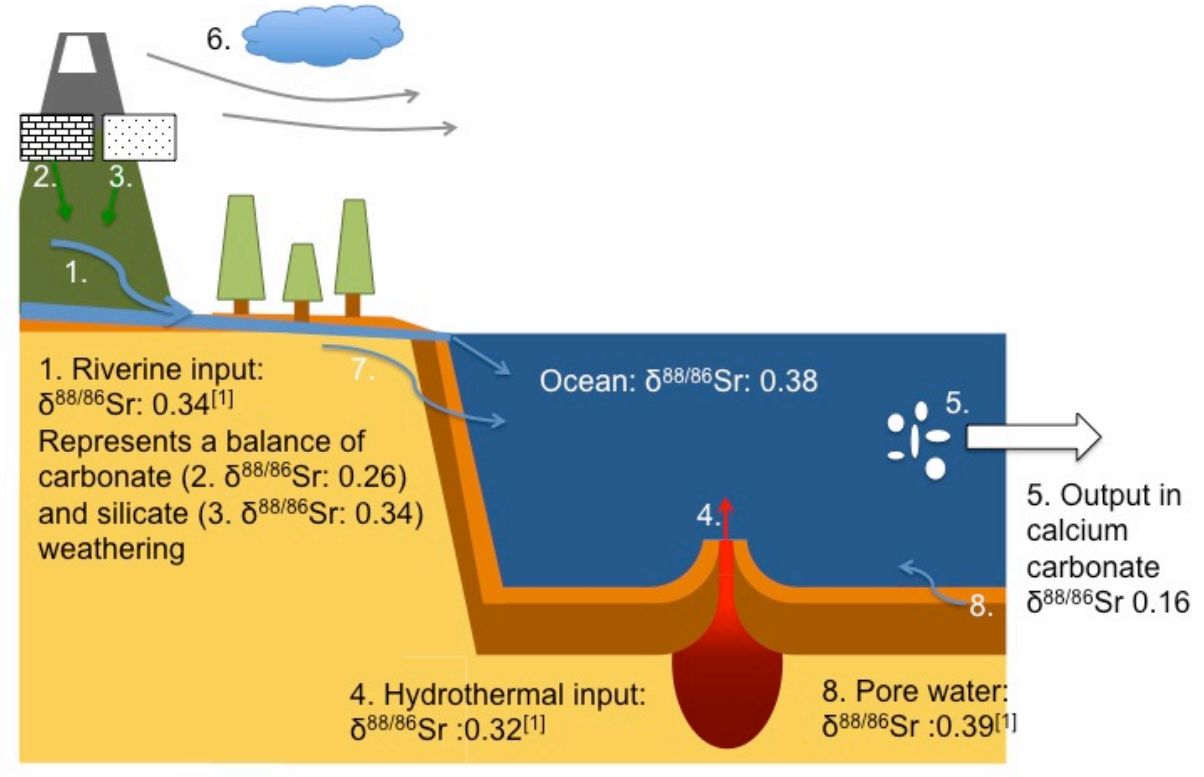

Figure 7.3 The modern day $\delta^{88/86}Sr$ cycle, including the data produced in this thesis of carbonate output, and the contribution of carbonate and silicate draining rivers to the global river $\delta^{88/86}Sr$ average. Inputs such as the global river average, hydrothermal input and pore-water/diagenic input are from a collation by Pearce et al. (2011), while inputs of precipitation (e.g. 6), dust (e.g. 6), groundwater (7) and other aspects of the hydrological cycle (e.g. 6) remain to be quantified, we are beginning to create the emerging picture of the $\delta^{88/86}Sr$ cycle geochemical cycle.

REFERENCES

References

Albarede, F., Beard, B. (2004). Analytical methods for non-traditional isotopes. *Reviews in Mineralogy and Geochemistry*, volume *55,* pages 113-152.

Allegre, C.J., Louvat, P., Gaillardet, J., Meynadier, L., Rad, S., Capmas, F. (2010). The fundamental role of island arc weathering in the oceanic Sr isotope budget. *Earth and Planetry Science Letters,* 292:51-56.

Amakawa, H., Alibo, D.S., Nozaki, Y. (2000). Nd isotopic composition and REE pattern in the surface waters of the eastern Indian Ocean and its adjacent seas. *Geochimica et Cosmochimica Acta,* 64:1715-1727.

An, Y., Jian, Z-M., (2009). Pulleniatina Minimum Event during the last deglaciation in the southern South China Sea. *Chinese Science Bulletin*, 54:4514-4519.

Anand, P., Elderfield, H. (2005). Variability of Mg/Ca and Sr/Ca between and within the planktonic foraminifers Globigerina bulloides and Globorotalia truncatulinoides. *Geochemistry, Geophysics, Geosystems*, (6)11: Q11D15

Anand, P., Elderfield, H., Conte, M.H. (2003). Calibration of Mg/Ca thermometry in planktonic foraminifera from a sediment trap time series. *Paleoceanograph,y* (18)2:1050-1065

Andermann, C., Longuevergne, L., Bonnet, S., Crave, A., Davy, P., Gloaguen, R. (2012). Impact of transient groundwater storage on the discharge of Himalayan rivers. *Nature Geoscience,* 5:127-132.

Ando, A., Nakano, T., Kawahata, H., Yokoyama, Y., Khim, B.K. (2010). Testing seawater Sr isotopic variability on a glacial interglacial timescale: An application of latest high-precision thermal ionization mass spectrometry. *Geochemistry Journal,* 44:347-357.

Archer, D.E., Eshel, G., Winguth, A., Broecker, W., Pierrehumbert, R., Tobis, M., Jacob, R. (2000). Atmospheric pCO(2) sensitivity to the biological pump in the ocean. *Global Biogeochemical Cycles*, 14:1219-1230.

Armstron. R.L. (1971). Glacial Erosion and Variable Isotopic Composition of Strontium in Sea Water. *Nature-Physical Science*, 230:132-133.

Aurasschudnagies, A., Kroon, D., Ganssen, G., Hemleben, C., Vanhinte, J.E. (1989). Distributional Pattern of Planktonic Foraminifers and Pteropods in Surface Waters and Top Core Sediments of the Red-Sea, and

Adjacent Areas Controlled by the Monsoonal Regime and Other Ecological Factors. *Deep-Sea Research Part a-Oceanographic Research Papers,* 36:1515-1533.

Barker, S., Greaves, M., Elderfield, H. (2003). A study of cleaning procedures used for foraminiferal Mg/Ca paleothermometry. *Geochemistry Geophysics Geosystems* 4(9)**:**GC000559.

Basu, A.R., Jacobsen, S.B., Poreda, R.J., Dowling, C.B., Aggarwal, P.K. (2001). Large groundwater strontium flux to the oceans from the bengal basin and the marine strontium isotope record. *Science,* 293:1470-1473.

Baumann, K.H., Bockel, B., Frenz, M. (2004). Coccolith contribution to south Atlantic carbonate sedimentation. *Coccolithophores: From Molecular Processes to Global Impact*, pages 367-402.

Be, A.W.H. (1980). Gametogenic Calcification in a Spinose Planktonic Foraminifer, Globigerinoides-Sacculifer (Brady). *Marine Micropaleontology*, 5:283-310.

Bentov, S., Erez, J. (2005). Novel observations on biomineralization processes in foraminifera and implications for Mg/Ca ratio in the shells. *Geology* 33:841-844.

Berger, W.H. (1968). Planktonic Foraminifera - Selective Solution and Paleoclimatic Interpretation. Deep-Sea Research 15, 31-&.

Berner, R.A. (2003). The long-term carbon cycle, fossil fuels and atmospheric composition. *Nature* 426:323-326.

Berner, R.A., Rye, D.M. (1992). Calculation of the Phanerozoic Strontium Isotope Record of the Oceans from a Carbon-Cycle Model. *American Journal of Science,* 292:136-148.

Bickle, M.J. (1996). Metamorphic decarbonation, silicate weathering and the long-term carbon cycle. *Terra Nova*, 8:270-276.

Bickle, M.J., Harris, N.B.W., Bunbury, J.M., Chapman, H.J., Fairchild, I.J., Ahmad, T. (2001). Controls on the Sr-87/Sr-86 ratio of carbonates in the Garhwal Himalaya, headwaters of the Ganges. *Journal of Geology*, 109: 737-753.

Bigeleisen. J. (1965). Chemistry of Isotopes. *Science* 147, 463-471.

Blum, J.D., Erel, Y. (1995). A Silicate Weathering Mechanism Linking Increases in Marine Sr-87/Sr-86 with Global Glaciation. *Nature,* 373:415-418.

Blum, J.D., Gazis, C.A., Jacobson, A.D., Chamberlain, C.P. (1998). Carbonate versus silicate weathering in the Raikhot watershed within the high Himalayan crystalline series. *Geology,* 26:411-414.

Bluth, G.J.S., Kump, L.R. (1994). Lithologic and Climatologic Controls of River Chemistry. *Geochimica et Cosmochimica Acta,* 58:2341-2359.

Bohm, F., Gussone, N., Eisenhauer, A., Dullo, W.C., Reynaud, S., Paytan, A. (2006). Calcium isotope fractionation in modern scleractinian corals. *Geochimica et Cosmochimica Acta,* 70:4452-4462.

Bohm, F., Eisenhauer, A., Tang, J., Dietzel, M., Krabbenhoft, A., Kisakurek, B., Horn, C. (2012). Strontium isotope fractionation of planktic foraminifera and inorganic calcite. *Geochimica et Cosmochimica Acta, In press*

Brass, G.W. (1976). Variation of Marine Sr-87-Sr-86 Ratio during Phanerozoic Time - Interpretation Using a Flux Model. *Geochimica et Cosmochimica Acta,* 40:721-730.

Broccoli, A.J., Dahl, K.A., Stouffer, R.J. (2006). Response of the ITCZ to Northern Hemisphere cooling. *Geophysical Research Letters*, 33:GL024546

Brookhagen, B. (2012). Hydrology: Himalayan groundwater. *Nature Geoscience,* 5:97-98.

Brown, S.J., Elderfield, H. (1996). Variations in Mg/Ca and Sr/Ca ratios of planktonic foraminifera caused by postdepositional dissolution: Evidence of shallow Mg-dependent dissolution. *Paleoceanography*,11:543-551.

Burke, W.H., Denison, R.E., Hetherington, E.A., Koepnick, R.B., Nelson, H.F., Otto, J.B. (1982). Variation of Sea-Water 87sr/86sr Throughout Phanerozoic Time. *Geology,* 10:516-519.

Burton, K.W. (2006). Global weathering variations inferred from marine radiogenic isotope records. *Journal of Geochemical Exploration*, 88:262-265.

Burton, K.W., Gannoun, A., Parkinson, I.J. (2010). Climate driven glacial-interglacial variations in the osmium isotope composition of seawater recorded by planktic foraminifera. *Earth and Planetry Science Letters,* 295:58-68.

Burton, K.W., Parkinson, I.J., Mokadem, F. (2008). Strontium stable isotope variations accompanying continental weathering with implications for the marine radiogenic strontium record. *Geochimica et Cosmochimica Acta,* 72:A123-A123.

Burton, K.W., Vance, D. (2000). Glacial-interglacial variations in the neodymium isotope composition of seawater in the Bay of Bengal recorded by planktonic foraminifera. *Earth and Planetry Science Letters,* 176: 425-441.

Capo, R.C., Depaolo, D.J. (1990). Seawater Strontium Isotopic Variations from 2.5 Million Years Ago to the Present. *Science,* 249:51-55.

Charlier, B.L.A., Ginibre, C., Morgan, D., Nowell, G.M., Pearson, D.G., Davidson, J.P., Ottley, C.J. (2006). Methods for the microsampling and high-precision analysis of strontium and rubidium isotopes at single crystal scale for petrological and geochronological applications. *Chemical Geology,* 232:114-133.

Charlier, B.L.A, Nowell, G., Parkinson, I.J., Kelley, S.P., Pearson, D.G., Burton, K.W. (2012). High temperature strontium stable isotope behaviour in the early solar system and planetary bodies. *Earth and Planetry Science Letters*, *In Press*

Chen, M-T. and Farrell, J. (1991). Planktonic foraminiferal faunal variations in the Northeastern Indian Ocean: A high resolution record of the past 800,000 years from the site 758. *In* Weissel, J., Peirce, J., Taylor, E., Alt, J., et al., *Proc. ODP, Sci. Results*, 121: College Station, TX (Ocean Drilling Program), 125-139

Chiang, J.C.H., Bitz, C.M. (2005). Influence of high latitude ice cover on the marine Intertropical Convergence Zone. *Climate Dynamics*, 25:477-496.

Clemens, S.C., Farrell, F.W., Gromet, L.P. (1993). Synchronous changes in seawater strontium isotope composition and global climate. *Nature*, 363:607–610.

Colin, C., Turpin, L., Bertaux, J., Desprairies, A., Kissel, C. (1999). Erosional history of the Himalayan and Burman ranges during the last two glacial-interglacial cycles. *Earth and Planetry Science Letters,* 171:647-660.

Colin, C., Turpin, L., Blamart, D., Frank, N., Kissel, C., Duchamp, S. (2006). Evolution of weathering patterns in the Indo-Burman Ranges over the last 280 kyr: Effects of sediment provenance on Sr-87/Sr-86 ratios tracer. *Geochemistry Geophysics Geosystems*, 7(3):GC000962

Cullen, J.L. (1981). Microfossil Evidence for Changing Salinity Patterns in the Bay of Bengal over the Last 20000 Years. Palaeogeography Palaeoclimatology Palaeoecology, 35:315-356.

Cullen, J.L., Prell, W.L. (1984). Planktonic-Foraminifera of the Northern Indian-Ocean - Distribution and Preservation in Surface Sediments. *Marine Micropaleontology*, 9:1-52.

Davis, A.C., Bickle, M.J., Teagle, D.A.H. (2003). Imbalance in the oceanic strontium budget. *Earth and Planetry Science Letters,* 211:173-187.

De La Rocha, C.L., DePaolo, D.J. (2000). Isotopic evidence for variations in the marine calcium cycle over the cenozoic. *Science,* 289:1176-1178.

de Souza, G.F., Reynolds, B.C., Kiczka, M., Bourdon, B. (2010). Evidence for mass-dependent isotopic fractionation of strontium in a glaciated granitic watershed. *Geochimica et Cosmochimica Acta,* 74:2596-2614.

de Villiers, S., Greaves, M., Elderfield, H. (2002). An intensity ratio calibration method for the accurate determination of Mg/Ca and Sr/Ca of marine carbonates by ICP-AES. Geochemistry Geophysics Geosystems, 3(1):GC000169

Deniel, C., Pin, C. (2001). Single-stage method for the simultaneous isolation of lead and strontium from silicate samples for isotopic measurements. *Analytica Chimica Acta*, 426:95-103.

DePaolo, D.J. (2011). Surface kinetic model for isotopic and trace element fractionation during precipitation of calcite from aqueous solutions. *Geochimica et Cosmochimica Acta,* 75:1039–1056

Derry, L.A., FranceLanord, C. (1996). Neogene Himalayan weathering history and river Sr-87/Sr-86: Impact on the marine Sr record. *Earth and Planetry Science Letters,* 142:59-74.

Dessert, C., Dupre, B., Gaillardet, J., Francois, L.M., Allegre, C.J. (2003). Basalt weathering laws and the impact of basalt weathering on the global carbon cycle. *Chemical Geology*, 202:257-273.

Dia, A.N., Cohen, A.S., O'Nions, R.K., Shackelton, N.J. (1991). Seawater Sr-isotope variations over the last 300ka and global climate change. *Nature*, 356:786–789.

Duplessy, J.C. (1982). Glacial to Interglacial Contrasts in the Northern Indian-Ocean. *Nature,* 295:494-498.

Durkop, A., Holbourn, A., Kuhnt, W., Zuraida, R., Andersen, N., Grootes, P.M. (2008). Centennial-scale climate variability in the Timor Sea during Marine Isotope Stage 3. *Marine Micropaleontology*, 66:208-221.

Eggins, S., De Deckker, P., Marshall, J. (2003). Mg/Ca variation in planktonic foraminifera tests: implications for reconstructing palaeo-seawater temperature and habitat migration. *Earth and Planetry Science Letters,* 212: 291-306.

Eiriksdottir, E.S., Gislason, S.R., Oelkers, E.H. (2009). What causes the positive feedback between climate and chemical weathering rates? *Geochimica et Cosmochimica Acta,* 73:A323-A323.

Eisenhauer, A., Boehm, F., Fietzke, J., Liebetrau, V., Amini, M., Kisakurek, B., Heuser, A., Tang, J., Dietzel, M. (2008). The application of natural divalent cation isotope (Ca, Sr, Mg) fractionation (DCIF) in earth system research. *Geochimica et Cosmochimica Acta,* 72:A241-A241.

Eisenhauer, A., Kisakurek, B., Bohm, F. (2009). Marine Calcification: An Alkaline Earth Metal Isotope Perspective. *Elements,* 5:365-368.

Elderfield, H. (1986). Strontium Isotope Stratigraphy. Palaeogeography Palaeoclimatology Palaeoecology, 57: 71-90.

Elderfield, H., Rickaby, R., Henderiks, J. (2006). How do marine carbonate Mg/Ca and Sr/Ca proxies constrain Cenozoic ocean history. *Geochimica et Cosmochimica Acta,* 70:A158-A158.

Elderfield, H., Vautravers, M., Cooper, M. (2002). The relationship between shell size and Mg/Ca, Sr/Ca, delta O-18, and delta C-13 of species of planktonic foraminifera. *Geochemistry Geophysics Geosystems* 3(8): GC000194.

Fairbanks, R.G., Sverdlove, M., Free, R., Wiebe, P.H., Be, A.W.H. (1982). Vertical-Distribution and Isotopic Fractionation of Living Planktonic-Foraminifera from the Panama Basin. *Nature,* 298:841-844.

Farrell, J.W., and Janecek, T.P. (1991). Late Neogene paleoceanography and paleoclimatology of the northeast Indian Ocean (site 758). *In* Weissel, J., Peirce, J., Taylor, E., Alt, J., et al., *Proc. ODP, Sci. Results*, 121: College Station, TX (Ocean Drilling Program), 297-358.

Fietzke, J., Eisenhauer, A. (2006). Determination of temperature-dependent stable strontium isotope (Sr-88/Sr-86) fractionation via bracketing standard MC-ICP-MS. *Geochemistry Geophysics Geosystems*, 7(8)**:**GC001243.

Foster, G.L., Vance, D. (2006). Negligible glacial-interglacial variation in continental chemical weathering rates. *Nature,* 444:918-921.

Frank, M. (2002). Radiogenic isotopes: Tracers of past ocean circulation and erosional input. Rev Geophys 40.
Gaillardet, J., Dupre, B., Allegre, C.J., 1999a. Geochemistry of large river suspended sediments: Silicate weathering or recycling tracer? *Geochimica et Cosmochimica Acta,* 63:4037-4051.

Gaillardet, J., Dupre, B., Louvat, P., Allegre, C.J. (1999b). Global silicate weathering and CO2 consumption rates deduced from the chemistry of large rivers. *Chemical Geology*, 159:3-30.

Gaillardet, J., Viers, J., Dupre, B. (2003). Trace Elements in River waters. *In Surface and groundwater, weathering and soils* (ed. Drever, J.I.) Vol. 5 *Treatise on Geochemistry* (eds. Holland, H.D. and Turekian, K.K), Elsevier-Pergamon, Oxford. *pages* 255-272

Galer, S.J.G. (1999). Optimal double and triple spiking for high precision lead isotopic measurement. *Chemical Geology*, 157:255-274.

Galer, S.J.G., Krabbenhōft, A., Abouchami, W., Borggässer, G., Feldmann, H. (2011). Stable Sr isotopes in seawater. *Mineralogical Magazine*, 75(3):A883

Galy, A., France-Lanord, C. (1999). Weathering processes in the Ganges-Brahmaputra basin and the riverine alkalinity budget. *Chemical Geology*, 159:31-60.

Galy, A., France-Lanord, C., Derry, L.A. (1999). The strontium isotopic budget of Himalayan Rivers in Nepal and Bangladesh. *Geochimica et Cosmochimica Acta,* 63:1905-1925.

Gibbs, M.T., Kump, L.R. (1994). Global Chemical Erosion during the Last Glacial Maximum and the Present - Sensitivity to Changes in Lithology and Hydrology. *Paleoceanography,* 9:529-543.

Gislason, S.R., Oelkers, E.H., Eiriksdottir, E.S., Kardjilov, M.I., Gisladottir, G., Sigfusson, B., Snorrason, A., Elefsen, S., Hardardottir, J., Torssander, P., Oskarsson, N. (2009). Direct evidence of the feedback between climate and weathering. *Earth and Planetry Science Letters,* 277:213-222.

Goldstein, S.J., Jacobsen, S.B. (1987). The Nd and Sr Isotopic Systematics of River-Water Dissolved Material - Implications for the Sources of Nd and Sr in Seawater. *Chemical Geology*, 66:245-272.

Goldstein, S.L., Onions, R.K., Hamilton, P.J. (1984). A Sm-Nd Isotopic Study of Atmospheric Dusts and Particulates from Major River Systems. *Earth and Planetry Science Letters,* 70:221-236.

Gordon, A.L., Susanto, R.D., Vranes, K. (2003). Cool Indonesian throughflow as a consequence of restricted surface layer flow. *Nature,* 425:824-828.

Griffith, E.M., Paytan, A., Kozdon, R., Eisenhauer, A., Ravelo, A.C. (2008). Influences on the fractionation of calcium isotopes in planktonic foraminifera. *Earth and Planetry Science Letters,* 268:124-136.

Guillard, R.R.L. and Ryther, J.H (1962). Studies of marine planktonic diatoms. I. *Cyclotella nana* Hustedt and *Detonula confervacea. Canadian Journal of Microbiology*, 8(2):229-239

Gussone, N., Eisenhauer, A., Heuser, A., Dietzel, M., Bock, B., Bohm, F., Spero, H.J., Lea, D.W., Bijma, J., Nagler, T.F. (2003). Model for kinetic effects on calcium isotope fractionation (delta Ca-44) in inorganic aragonite and cultured planktonic foraminifera. *Geochimica et Cosmochimica Acta,* 67:1375-1382.

Gussone, N., Honisch, B., Heuser, A., Eisenhauer, A., Spindler, M., Hemleben, C. (2009). A critical evaluation of calcium isotope ratios in tests of planktonic foraminifers. *Geochimica et Cosmochimica Acta,* 73:7241-7255.

Gussone, N., Langer, G., Thoms, S., Nehrke, G., Eisenhauer, A., Riebesell, U., Wefer, G. (2006). Cellular calcium pathways and isotope fractionation in Emiliania huxleyi. *Geology,* 34:625-628.

Halicz, L., Segal, I., Fruchter, N., Stein, M., Lazar, B. (2008). Strontium stable isotopes fractionate in the soil environments? *Earth and Planetry Science Letters,* 272:406-411.

Hathorne, E.C., James, R.H., Lampitt, R.S. (2009). Environmental versus biomineralization controls on the intratest variation in the trace element composition of the planktonic foraminifera G. inflata and G. scitula. *Paleoceanography* 24(4):PA001742

Hemleben, Ch., Spindler, M., Anderson, O.R. (1989). Modern Planktonic Foraminifera. Springer-Verlag New York Inc. page 25

Henderson, G.M., Matrel, D.J., O'Nions, R.K., Shackelton, N.J. (1994). Evolution of seawater 87Sr/86Sr over the last 400 ka: the absence of glacial/interglacial cycles. *Earth and Planetry Science Letters,* 128:643-651.

Henderson, G.M. (2002). New oceanic proxies for paleoclimate. *Earth and Planetry Science Letters,* 203:1-13.

Hess, J., Bender, M., Schilling, J.G. (1991). Assessing Seawater Basalt Exchange of Strontium Isotopes in Hydrothermal Processes on the Flanks of Midocean Ridges. *Earth and Planetry Science Letters,* 103:133-142.

Hess, J., Bender, M.L., Schilling, J.G. (1986). Evolution of the Ratio of Sr-87 to Sr-86 in Seawater from Cretaceous to Present. *Science,* 231:979-984.

Hintz, C.J., Shaw, T.J., Chandler, G.T., Bernhard, J.M., McCorkle, D.C., Blanks, J.K. (2006). Trace/minor element : calcium ratios in cultured benthic foraminifera. Part I: Inter-species and inter-individual variability. *Geochimica et Cosmochimica Acta,* 70:1952-1963.

Hodell, D.A., Kamenov, G.D., Ed, C.H.D.O.E.S.O.U., Zachos, J.C., Rohl, U., Westerhold, T. (2007). Variations in the strontium isotope composition of seawater during the Paleocene and early Eocene from ODP Leg 208 (Walvis Ridge). *Geochemistry Geophysics Geosystems*, 8.

Hodell, D.A., Mead, G.A., Mueller, P.A. (1990). Variation in the Strontium Isotopic Composition of Seawater (8 Ma to Present) - Implications for Chemical-Weathering Rates and Dissolved Fluxes to the Oceans. *Chemical Geology*, 80:291-307.

Hodges, K.V. (2000). Tectonics of the Himalaya and southern Tibet from two perspectives. *Geological Society of America Bulletin*, 112:324-350.

Holbourn, A., Kuhnt, W., Kawamura, H., Jian, Z.M., Grootes, P., Erlenkeuser, H., Xu, J., (2005) Orbitally paced paleoproductivity variations in the Timor Sea and Indonesian Throughflow variability during the last 460 kyr. *Paleoceanography* 20(3):PA001094

Honisch, B., Hemming, N.G. (2004). Ground-truthing the boron isotope-paleo-pH proxy in planktonic foraminifera shells: Partial dissolution and shell size effects. *Paleoceanography* 19(4):PA001026

Imbrie, J., Hays, J.D., Martinson, D.G., McIntyre, A., Mix, A.C., Morley, J.J., Pisias, N.G., Prell, W.L. and Shackelton, N.J. (1984). The orbital theory of Pleistocene climate: Support from a revised chronology of the marine $\delta^{18}O$ record. *In* Berger, A.L., et al. (Ed.) Milankovitch and Climate (Pt. 1) Reidel, D., Dodrecht. *pages* 269-305

Imbrie, J. (1985). A Theoretical Framework for the Pleistocene Ice Ages. *Journal of the Geological Society*, 142:417-432.

Jacobson, A.D., Blum, J.D., Walter, L.M. (2002). Reconciling the elemental and Sr isotope composition of Himalayan weathering fluxes: Insights from the carbonate geochemistry of stream waters. *Geochimica et Cosmochimica Acta,* 66:3417-3429.

Jacobson, A.D., Zhang, Z., Lundstrom, C., Huang, F. (2012). Behaviour of Mg isotopes during dedolomitization in the Madison Aquifer, South Dakota. *Earth and Planetry Science Letters,* 297:446-452.

James, R.H., Kisakurek, B., Pogge Von Strandmann, P.A.E., Hathorne, E.C. (2006). Utility of Li and Li isotopes as tracers of silicate weathering. *Geochimica et Cosmochimica Acta,* 70:A288-A288.

Kasemann, S.A., Schmidt, D.N., Pearson, P.N., Hawkesworth, C.J. (2008). Biological and ecological insights into Ca isotopes in planktic foraminifers as a palaeotemperature proxy. *Earth and Planetry Science Letters,* 271: 292-302.

Keller, M.D., Selvin, R.C., Claus, W., Guillard, R.R.L. (1987). Media for the Culture of Oceanic Ultraphytoplankton. *Journal of Phycology*, 23:633-638.

Kisakurek, B., Eisenhauer, A., Bohm, F., Garbe-Schonberg, D., Erez, J. (2008). Controls on shell Mg/Ca and Sr/Ca in cultured planktonic foraminiferan, Globigerinoides ruber (white). *Earth and Planetry Science Letters,* 273:260-269.

Kisakurek, B., Eisenhauer, A., Bohm, F., Hathorne, E.C., Erez, J. (2011). Controls on calcium isotope fractionation in cultured planktic foraminifera, Globigerinoides ruber and Globigerinella siphonifera. *Geochimica et Cosmochimica Acta,* 75:427-443.

Kisakurek, B., Niedermayr, A., Muller, M.N., Taubner, I., Eisenhauer, A., Dietzel, M., Buhl, D., Fietzke, J., Erez, J. (2009). Magnesium isotope fractionation in inorganic and biogenic calcite. *Geochimica et Cosmochimica Acta,* 73:A663-A663.

Kisakurek, B., James, R.H., Harris, N.B.W. (2005). Li and delta Li-7 in Himalayan rivers: Proxies for silicate weathering? *Earth and Planetry Science Letters,* 237:387-401.

Kisakurek, B. (2005). Utility of Lithium and Magnesium Isotopes as Tracers of Continental Weathering Processes, PhD, The Open University.

Kisakurek, B., Eisenhauer, A., Erez, J., Bohm, F., Garbe-Schonberg, D. (2007). Paired delta Ca-44/40, Mg/Ca and Sr/Ca in cultured G-ruber. *Geochimica et Cosmochimica Acta,* 71:A487-A487.

Kisakurek, B., James, R.H., Harris, N.B.W. (2004a). Utility of lithium isotopes as tracers of continental weathering processes. *Geochimica et Cosmochimica Acta,* 68:A420-A420.

Kisakurek, B., Widdowson, M., James, R.H. (2004b). Behaviour of Li isotopes during continental weathering: the Bidar laterite profile, India. *Chemical Geology*, 212:27-44.

Knudson, K.J., Williams, H.M., Buikstra, J.E., Tomczak, P.D., Gordon, G.W., Anbar, A.D. (2010). Introducing delta(88/86)Sr analysis in archaeology: a demonstration of the utility of strontium isotope fractionation in paleodietary studies. *Journal of Archaeological Science*, 37:2352-2364.

Krabbenhoft, A., Eisenhauer, A., Bohm, F., Vollstaedt, H., Fietzke, J., Liebetrau, V., Augustin, N., Peucker-Ehrenbrink, B., Muller, M.N., Horn, C., Hansen, B.T., Nolte, N., Wallmann, K. (2010). Constraining the marine strontium budget with natural strontium isotope fractionations ((87)Sr/(86)Sr*, delta(88/86)Sr) of carbonates, hydrothermal solutions and river waters. *Geochimica et Cosmochimica Acta,* 74:4097-4109.

Krabbenhoft, A., Fietzke, J., Eisenhauer, A., Liebetrau, V., Bohm, F., Vollstaedt, H. (2009). Determination of radiogenic and stable strontium isotope ratios ((87)Sr/(86)Sr; delta(88/86)Sr) by thermal ionization mass spectrometry applying an (87)Sr/(84)Sr double spike. *Journal of Analytical Atomic Spectrometry,* 24:1267-1271.

Krishnaswami, S., Trivedi, J.R., Sarin, M.M., Ramesh, R., Sharma, K.K. (1992). Strontium Isotopes and Rubidium in the Ganga Brahmaputra River System - Weathering in the Himalaya, Fluxes to the Bay of Bengal and Contributions to the Evolution of Oceanic Sr-87/Sr-86. *Earth and Planetry Science Letters,* 109:243-253.

Kump, L.R. and Alley, R.B. (1994). In: Usseleman, T. M., Hay, W. W. (Eds.), Material Fluxes on the Surface of the Earth. National Academy Press, Washington DC, *pages* 46-60

Langer, G., Gussone, N., Nehrke, G., Riebesell, U., Eisenhauer, A., Kuhnert, H., Rost, B., Trimborn, S., Thoms, S. (2006). Coccolith strontium to calcium ratios in Emiliania huxleyi: The dependence on seawater strontium and calcium concentrations. *Limnology and Oceanography*, 51:310-320.

Lea, D.W., Mashiotta, T.A., Spero, H.J. (1999). Controls on magnesium and strontium uptake in planktonic foraminifera determined by live culturing. *Geochimica et Cosmochimica Acta,* 63:2369-2379.

Lea, D.W. (1999) Trace elements in foraminiferal calcite. *In* Modern Foraminifera edited by Barun K. Sen Gupta, *Kluwer*, 1999. pages 259-277.

Lear, C.H., Elderfield, H., Wilson, P.A. (2003). A Cenozoic seawater Sr/Ca record from benthic foraminiferal calcite and its application in determining global weathering fluxes. *Earth and Planetry Science Letters,* 208:69-84.

Levasseur, S., Birck, J.L., Allegre, C.J. (1999). The osmium riverine flux and the oceanic mass balance of osmium. *Earth and Planetry Science Letters,* 174:7-23.

Liebetrau, V., Haeckel, M., Eisenhauer, A., Scholz, F., Hansen, C., Reitz, A. (2011). Paired Sr isotope ($^{87}Sr/^{86}Sr$, $\delta^{88/86}Sr$) Systematic of pore water Profiles: A New Perspective in Marine Weathering and Seapage Studies. *Mineralogical Magazine*, 75(3):A1326

Liu, H. C., You, C. F., Huang K. F. and Chung, C. H. (2012). Precise determination of triple Sr isotopes ($\delta^{87}Sr$ and $\delta^{88}Sr$) using MC-ICP-MS. *Talanta,* 88:338-344.

Lohmann, G.P. (1995). A model for variation in the chemistry of planktonic formainifera due to secondary calcification and selectivr dissolution. Paleoceanography, 10(3) PA00059.

Lombard, F., Labeyrie, L., Michel, E., Spero, H.J., Lea, D.W. (2009). Modelling the temperature dependent growth rates of planktic foraminifera. *Marine Micropaleontology*, 70:1-7.

Lorens, R.B. (1981). Sr, Cd, Mn and Co Distribution Coefficients in Calcite as a Function of Calcite Precipitation Rate. *Geochimica et Cosmochimica Acta,* 45:553-561.

Lowenstam HA, Weiner S (1989) On Biomineralization. Oxford University Press, New York. Page 68

Martin, R.E. (1999). Taphonomy and temporal resolution of foraminiferal assemblages. *In*: Modern foraminifera. Sen Gupta, B.K., (Ed.) Kluwer Academic Publishers. pages 281-299.

McArthur, J.M., Howarth, R.J., Bailey, T.R. (2001). Strontium isotope stratigraphy: LOWESS version 3: Best fit to the marine Sr-isotope curve for 0-509 Ma and accompanying look-up table for deriving numerical age. *Journal of Geology*, 109:155-170.

Minoletti, F., Hermoso, M., Gressier, V. (2009). Separation of sedimentary micron-sized particles for palaeoceanography and calcareous nannoplankton biogeochemistry. Nature Protocols, 4:14-24.

Mokadem, F., Burton, K.W., Parkinson, I.J., Hathorne, E.C., Anand, P., Allen, J.T. (2012) High-precision radiogenic strontium isotope measurements of the modern and glacial ocean: limits on glacial-interglacial variations in continental weathering. *submitted to Earth and Planetry Science Letters*

Mortyn, P.G., Elderfield, H., Anand, P., Greaves, M. (2005). An evaluation of controls on planktonic foraminiferal Sr/Ca: Comparison of water column and core-top data from a North Atlantic transect. *Geochemistry Geophysics Geosystems*, 6(12):GC001047

Moynier, F., Agranier, A., Hezel, D.C., Bouvier, A. (2010). Sr stable isotope composition of Earth, the Moon, Mars, Vesta and meteorites. *Earth and Planetry Science Letters,* 300:359-366.

Muller, M.N., Kisakurek, B., Buhl, D., Gutperlet, R., Kolevica, A., Riebesell, U., Stoll, H., Eisenhauer, A. (2011). Response of the coccolithophores Emiliania huxleyi and Coccolithus braarudii to changing seawater Mg2+ and Ca2+ concentrations: Mg/Ca, Sr/Ca ratios and delta Ca-44/40, delta Mg-26/24 of coccolith calcite. *Geochimica et Cosmochimica Acta,* 75:2088-2102.

Nagler, T.F., Eisenhauer, A., Muller, A., Hemleben, C., Kramers, J. (2000). The delta 44Ca-temperature calibration on fossil and cultured Globigerinoides sacculifer: New tool for reconstruction of past sea surface temperatures. *Geochemistry Geophysics Geosystems* 1(9):GC000091

Niedermayr, A., Dietzel, M., Kohler, S.J., Kisakurek, B., Bohm, F., Eisenhauer, A. (2009). Mg-, Sr-incorporation and calcium isotopic fractionation during calcium carbonate precipitation. *Geochimica et Cosmochimica Acta,* 73:A941-A941.

Nier, A. O. (1938). The isotopic constitution of strontium, barium, bismuth, thallium and mercury. *Physical Reviews*, **5**:275-279

Nowell, G.M., Charlier, B.L.A., Pearson, D.G., Burton, K.W. (2007). Quantification of stable strontium isotope variability in nature by MC-ICP-MS. *Geochimica et Cosmochimica Acta,* 71:A725-A725.

Ohno, T., Hirata, T. (2007). Simultaneous determination of mass-dependent isotopic Fractionation and radiogenic isotope variation of strontium in geochemical samples by multiple collector-ICP-mass spectrometry. *Analytical Sciences*, 23:1275-1280.

Ohno, T., Komiya, T., Ueno, Y., Hirata, T., Maruyama, S. (2008). Determination of Sr-88/Sr-86 mass-dependent isotopic and radiogenic isotope variation of Sr-87/Sr-86 in the Neoproterozoic Doushantuo Formation. *Gondwana Research*, 14:126-133.

Oliva, P., Dupre, B., Martin, F., Viers, J. (2004). The role of trace minerals in chemical weathering in a high-elevation granitic watershed (Estibere, France): Chemical and mineralogical evidence. *Geochimica et Cosmochimica Acta,* 68:2223-2243.

Oliver, L., Harris, N., Bickle, M., Chapman, H., Dise, N., Horstwood, M. (2003). Silicate weathering rates decoupled from the Sr-87/Sr-86 ratio of the dissolved load during Himalayan erosion. Chemical Geology, 201: 119-139.

Opfergelt, S., Georg, B., Burton, K., Delvaux, B., Siebert, C., Guicharnaud, R., Cabidoche, Y., Halliday, A. (2010). Magnesium isotope fractionation in volcanic soils controlled by clay mineralogy and exchangeable Mg. In: American Geophysical Union, Fall Meeting 2010., 13-17 December 2010., San Francisco. B23K-05

Oxburgh, R. (1998). Variations in the osmium isotope composition of sea water over the past 200,000 years. *Earth and Planetry Science Letters,* 159:183-191.

Oxburgh, R., Pierson-Wickmann, A.C., Reisberg, L., Hemming, S. (2007). Climate-correlated variations in seawater Os-187/Os-188 over the past 200,000 yr: Evidence from the Cariaco Basin, Venezuela. *Earth and Planetry Science Letters,* 263:246-258.

Page, B.D., Bullen, T.D., Mitchell, M.J. (2008). Influences of calcium availability and tree species on Ca isotope fractionation in soil and vegetation. *Biogeochemistry,* 88:1-13.

Palmer, M.R., Edmond, J.M. (1989). The Strontium Isotope Budget of the Modern Ocean. *Earth and Planetry Science Letters,* 92:11-26.

Palmer, M.R., Edmond, J.M. (1992). Controls over the Strontium Isotope Composition of River Water. *Geochimica et Cosmochimica Acta,* 56:2099-2111.

Pankhurst, D.L., Appelo, C.A.J. (1999). User's guide to PHREEQC (version 2) – a computer program for speciation, batch-reaction, one-dimensional transport, and inverse geochemical calculations.

Papanastassiou, D.A., Wasserburg, G.J. (1978). Strontium Isotopic Anomalies in Allende Meteorite. Geophysical Research Letters, 5:595-598.

Parkinson, I.J., Burton, K.W., Mokadem, F., Charlier, B.L.A. (2007). High-precision double spike Sr isotope measurements: Applications to geochemistry and geochronology. EOS, transactions of the American Geophysoical Union 88, V41E-07

Parkinson, I.J., Burton, K.W. and Mokadem, F. (2008). High-Precision measurement of radiogenic and stable Sr isotopes; applications to the marine Sr record. EOS, transactions of the American Geophysical Union 89, B14B-08

Patchett, P.J. (1980a). Sr Isotopic Fractionation in Allende Chondrules - a Reflection of Solar Nebular Processes. *Earth and Planetry Science Letters,* 50:181-188.

Patchett, P.J. (1980b). Sr Isotopic Fractionation in Ca-Al Inclusions from the Allende Meteorite. *Nature,* 283: 438-441.

Payne, V.E., Rickaby, R.E.M., Benning, L.G., Shaw, S. (2008). Calcite crystal growth orientation: implications for trace metal uptake into coccoliths. *Mineralogical Magazine*, 72:269-272.

Pearce, C. R.; Parkinson, I. J.; Burton, K. and Gaillardet, J. (2010). The strontium stable isotope composition of global rivers and the implications for the marine δ^{88}Sr record. In: American Geophysical Union, Fall Meeting 2010., 13-17 December 2010., San Francisco.

Pearce, C.R., Parkinson, I.J., Burton, K.W. (2011). A reconsideration of marine strontium budgets using both stable (δ^{88}Sr) and radiogenic (^{87}Sr/^{86}Sr) systems. In: American Geophysical Union, Fall Meeting 2011., 5-9 December 2011., San Francisco.

Peucker-Ehrenbrink, B. (2002). Comment on "Residence time of osmium in the oceans" by Rachel Oxburgh. *Geochemistry Geophysics Geosystems*, 3(10)**:**GC000297.

Pogge von Strandmann, P.A.E. (2008). Precise magnesium isotope measurements in core top planktic and benthic foraminifera. *Geochemistry Geophysics Geosystems*, 9(10)**:**GC002209.

Pogge von Strandmann, P.A.E., Burton, K.W., James, R.H., van Calsteren, P., Gislason, S.R., Sigfusson, B. (2008). The influence of weathering processes on riverine magnesium isotopes in a basaltic terrain. *Earth and Planetry Science Letters,* 276:187-197.

Prell, W.L., Hutson, W.H., Williams, D.F., Be, A.W.H., Geitzenauer, K., Molfino, B. (1980). Surface Circulation of the Indian-Ocean during the Last Glacial Maximum, Approximately 18,000 Yr Bp. *Quaternary Research*, 14:309-336.

Probert, I., Houdan, A. (2004). The laboratory culture of coccolithophores. *Coccolithophores: From Molecular Processes to Global Impact*, 217-249.

Quade, J., English, N., DeCelles, P.G. (2003). Silicate versus carbonate weathering in the Himalaya: a comparison of the Arun and Seti River watersheds. *Chemical Geology,* 202:275-296.

Ra, K., Kitagawa, H., Shiraiwa, Y. (2010). Mg isotopes and Mg/Ca values of coccoliths from cultured specimens of the species Emiliania huxleyi and Gephyrocapsa oceanica. *Marine Micropaleontology*, 77:119-124.

Raymo, M.E., Ruddiman, W.F. (1992). Tectonic Forcing of Late Cenozoic Climate. *Nature,* 359:117-122.

Raymo, M.E., Ruddiman, W.F., Froelich, P.N. (1988). Influence of Late Cenozoic Mountain Building on Ocean Geochemical Cycles. *Geology,* 16:649-653.

Richter, F.M., Rowley, D.B., Depaolo, D.J. (1992). Sr Isotope Evolution of Seawater - the Role of Tectonics. *Earth and Planetry Science Letters,* 109:11-23.

Richter, F.M., Turekian, K.K. (1993). Simple-Models for the Geochemical Response of the Ocean to Climatic and Tectonic Forcing. *Earth and Planetry Science Letters,* 119:121-131.

Rickaby, R.E.M., Bard, E., Sonzogni, C., Rostek, F., Beaufort, L., Barker, S., Rees, G., Schrag, D.P. (2007). Coccolith chemistry reveals secular variations in the global ocean carbon cycle? *Earth and Planetry Science Letters*, 253:83-95.

Rickaby, R.E.M., Schrag, D.P., Zondervan, I., Riebesell, U. (2002). Growth rate dependence of Sr incorporation during calcification of Emiliania huxleyi. *Global Biogeochemical Cycles* 16(1):GB001408

Robinson, L.F., Belshaw, N.S., Henderson, G.M. (2004). U and Th concentrations and isotope ratios in modern carbonates and waters from the Bahamas. *Geochimica et Cosmochimica Acta,* 68:1777-1789.

Rosenthal, Y., Perron-Cashman, S., Lear, C.H., Bard, E., Barker, S., Billups, K., Bryan, M., Delaney, M.L., deMenocal, P.B., Dwyer, G.S., Elderfield, H., German, C.R., Greaves, M., Lea, D.W., Marchitto, T.M., Pak, D.K., Paradis, G.L., Russell, A.D., Schneider, R.R., Scheiderich, K., Stott, L., Tachikawa, K., Tappa, E., Thunell, R., Wara, M., Weldeab, S., Wilson, P.A. (2004). Interlaboratory comparison study of Mg/Ca and Sr/Ca measurements in planktonic foraminifera for paleoceanographic research. *Geochemistry Geophysics Geosystems*, 5(4)**:**GC000650.

Roth, J.M., Droxler, A.W., Kameo, K. (2000). The Caribbean carbonate crash at the middle to late Miocene transition: linkage to the establishment of the modern global ocean conveyor. Leckie, R.M., Sigurdsson, H., Acton, G.D., and Draper, G. (Eds.), 2000. *Proceedings of the Ocean Drilling Program, Scientific Results*, Vol. 165-249

Rudge, J.F., Reynolds, B.C., Bourdon, B. (2009). The double spike toolbox. Chem Geol 265, 420-431.

Ruggeberg, A., Fietzke, J., Liebetrau, V., Eisenhauer, A., Dullo, W.C., Freiwald, A., 2008. Stable strontium isotopes (delta Sr-88/86) in cold-water corals - A new proxy for reconstruction of intermediate ocean water temperatures. *Earth and Planetry Science Letters,* 269:569-574.

Russell, W.A., Papanastassiou, D.A., Tombrello, T.A. (1978). Ca Isotope Fractionation on Earth and Other Solar-System Materials. *Geochimica et Cosmochimica Acta,* 42:1075-1090.

Schiebel, R. (2002). Planktic foraminiferal sedimentation and the marine calcite budget. Global Biogeochem Cy 16.

Schmidt, D.N., Renaud, S., Bollmann, J. (2003). Response of planktic foraminiferal size to late Quaternary climate change (vol 18, pg 1066, 2003). *Paleoceanography* 18.

Schmidt, D.N., Renaud, S., Bollmann, J., Schiebel, R., Thierstein, H.R. (2004a). Size distribution of Holocene planktic foraminifer assemblages: biogeography, ecology and adaptation. Mar Micropaleontol 50, 319-338.

Schmidt, D.N., Thierstein, H.R., Bollmann, J., Schiebel, R. (2004b). Abiotic forcing of plankton evolution in the Cenozoic. *Science,* 303:207-210.

Sharma, M., Wasserburg, G.J., Hoffmann, A.W., Chakrapani, G.J. (1999). Himalayan uplift and osmium isotopes in oceans and rivers. *Geochimica et Cosmochimica Acta,* 63:4005-4012.

Siebert, C., Nagler, T.F., Kramers, J.D. (2001). Determination of molybdenum isotope fractionation by double-spike multicollector inductively coupled plasma mass spectrometry. *Global Biogeochemical Cycles,* 2(7): GC000124.

Sime, N.G., De La Rocha, C.L., Galy, A. (2005). Negligible temperature dependence of calcium isotope fractionation in 12 species of planktonic foraminifera. *Earth and Planetry Science Letters,* 232:51-66.

Spero, H.J., Bijma, J., Lea, D.W., Bemis, B.E. (1997). Effect of seawater carbonate concentration on foraminiferal carbon and oxygen isotopes. *Nature,* 390:497-500.

Stefansson, A., Gislason, S.R., Arnorsson, S. (2001). Dissolution of primary minerals in natural waters - II. Mineral saturation state. Chemical Geology, 172:251-276.

Stoll, H.M., Klaas, C.M., Probert, I., Encinar, J.R., Alonso, J.I.G. (2002a). Calcification rate and temperature effects on Sr partitioning in coccoliths of multiple species of coccolithophorids in culture. *Global and Planetary Change*, 34:153-171.

Stoll, H.M., Rosenthal, Y., Falkowski, P. (2002b). Climate proxies from Sr/Ca of coccolith calcite: Calibrations from continuous culture of Emiliania huxleyi. *Geochimica et Cosmochimica Acta,* 66:927-936.

Stoll, H.M., Schrag, D.P. (1998). Effects of Quaternary sea level cycles on strontium in seawater. *Geochimica et Cosmochimica Acta,* 62:1107-1118.

Stoll, H.M., Schrag, D.P. (2000). Coccolith Sr/Ca as a new indicator of coccolithophorid calcification and growth rate. *Geochemistry Geophysics Geosystems* 1(5):GC000015.

Stoll, H.M., Schrag, D.P., Clemens, S.C. (1999). Are seawater Sr/Ca variations preserved in Quaternary foraminifera? *Geochimica et Cosmochimica Acta,* 63:3535-3547.

Stoll, H.M., Ziveri, P. (2002a). Controls over the chemistry of coccolith calcite. *Geochimica et Cosmochimica Acta,* 66:A744-A744.

Stoll, H.M., Ziveri, P. (2002b). Separation of monospecific and restricted coccolith assemblages from sediments using differential settling velocity. Marine Micropaleontology, 46:209-221.

Stoll, H.M., Ziveri, P., Geisen, M., Probert, I., Young, J.R. (2002c). Potential and limitations of Sr/Ca ratios in coccolith carbonate: new perspectives from cultures and monospecific samples from sediments. *Philosophical Transactions of the Royal Society of London Series a-Mathematical Physical and Engineering Sciences*, 360: 719-747.

Stoll, H.M. and Ziveri, P. (2004). Coccolithophore-based geochemical proxies. in Thierstein, H. and Young, J. Eds. Coccolithophores: From Molecular Processes to Global Impact. Springer Verlag. *pages* 529-562

Stoll, H.M., Ziveri, P., Shimizu, N., Conte, M., Theroux, S. (2007). Relationship between coccolith Sr/Ca ratios and coccolithophore production and export in the Arabian Sea and Sargasso Sea. *Deep-Sea Research Part Ii-Topical Studies in Oceanography*, 54:581-600.

Tang, J.W., Niedermayr, A., Kohler, S.J., Bohm, F., Kisakurek, B., Eisenhauer, A., Dietzel, M. (2012). Sr2+/Ca2+ and Ca-44/Ca-40 fractionation during inorganic calcite formation: III. Impact of salinity/ionic strength. *Geochimica et Cosmochimica Acta,* 77:432-443.

Tesoriero, A.J., Pankow, J.F. (1996). Solid solution partitioning of Sr2+, Ba2+, and Cd2+ to calcite. *Geochimica et Cosmochimica Acta,* 60:1053-1063.

Thomas, A.L., Henderson, G.M., Robinson, L.F. (2006). Interpretation of the Pa-231/Th-230 paleo circulation proxy: New water-column measurements from the southwest Indian Ocean. *Earth and Planetry Science Letters,* 241:493-504.

Tipper E.T., Bickle M.J., Galy A., West A.J., Pomi`es C., Chapman H.J. (2006a). The short term climatic sensitivity of carbonate and silicate weathering fluxes: Insight from seasonal variations in river chemistry. *Geochimica et Cosmochimica Acta,* 70, 11:2737-2754.

Tipper E.T., Galy A., Bickle M.J. (2006b). Riverine evidence for a fractionated reservoir of Ca and Mg on the continents: Implications for the oceanic Ca cycle. *Earth and Planetry Science Letters,* 247:267-279.

Tipper E.T., Galy A., Gaillardet J., Bickle M.J., Elderfield H., Carder E.A. (2006c). The Mg isotope budget of the modern ocean: Constraints from riverine Mg isotope ratios. *Earth and Planetry Science Letters,* 250:241-253.

Tipper, E.T., Lemarchand, E., Hindshaw, R.S., Reynolds, B.C., Bourdon, B. (2012). Seasonal sensitivity of weathering processes: Hints from magnesium isotopes in a glacial stream. *Chemical Geology, accepted manuscript.*

Urey, H.C. (1947). The Thermodynamic Properties of Isotopic Substances. *Journal of the Chemical Society*, 562-581.

Vance, D., Teagle, D.A.H., Foster, G.L. (2009). Variable Quaternary chemical weathering fluxes and imbalances in marine geochemical budgets. *Nature,* 458:493-496.

Veizer, J. (1989). Strontium Isotopes in Seawater through Time. *Annual Review of Earth and Planetary Sciences*, 17:141-167.

Veizer, J., Mackenzie, F.T. (2003). Evolution of sedimentary rocks. T*reatise on Geochemistry*, Vol. 7: 369–407.

Viers, J., Oliva, P., Dandurand, B., Dupré, B., Gaillardet, J. (2003). Chemical weathering rates, CO_2 consumption and control parameters deduced from the chemical composition of rivers. *Treatise on Geochemistry*, Vol. 5:1-25

Walker, J.C.G., Hays, P.B., Kasting, J.F. (1981). A Negative Feedback Mechanism for the Long-Term Stabilization of Earths Surface-Temperature. J*ournal of Geophysical Research-Oceans and Atmospheres*, 86,:9776-9782.

Westbroek, P., Brown, C.W., Vanbleijswijk, J., Brownlee, C., Brummer, G.J., Conte, M., Egge, J., Fernandez, E., Jordan, R., Knappertsbusch, M., Stefels, J., Veldhuis, M., Vanderwal, P., Young, J. (1993). A Model System Approach to Biological Climate Forcing - the Example of Emiliania-Huxleyi. *Global and Planetary Change*, 8:27-46.

White, A.F., Blum, A.E. (1995). Effects of Climate on Chemical-Weathering in Watersheds. *Geochimica et Cosmochimica Acta,* 59:1729-1747.

White, A.F., Blum, A.E., Bullen, T.D., Vivit, D.V., Schulz, M., Fitzpatrick, J. (1999). The effect of temperature on experimental and natural chemical weathering rates of granitoid rocks. *Geochimica et Cosmochimica Acta,* 63:3277-3291.

White, A.F., Brantley, S.L. (1995). Chemical weathering rates of silicate minerals: An overview. Rev Mineral 31, pages 1-22.

Wombacher, F., Eisenhauer, A., Bohm, F., Gussone, N., Regenberg, M., Dullo, W.C., Ruggeberg, A. (2011). Magnesium stable isotope fractionation in marine biogenic calcite and aragonite. *Geochimica et Cosmochimica Acta,* 75:5797-5818.

Woodhouse, O.B., Ravizza, G., Kenison-Falkner, K., Statham, P.J., Peucker-Ehrenbrink, B. (1999). Osmium in seawater: vertical profiles of concentration and isotopic composition in the eastern Pacific Ocean. *Earth and Planetry Science Letters,* 173:223-233.

Wyrtki, K. (1973). Physical Oceanography of the Indian Ocean, in: B. Zeitschel, S. A. Gerlach (EDs.), The Biology of the Indian Ocean, Vol. 3, Springer-Verlag, New York, pages, 18-36.

Yang, L., Peter, C., Panne, U., Sturgeon, R.E. (2008). Use of Zr for mass bias correction in strontium isotope ratio determinations using MC-ICP-MS. *Journal of Analytical Atomic Spectrometry*, 23:1269-1274.

Young, E.D., Galy, A., Nagahara, H. (2002). Kinetic and equilibrium mass-dependent isotope fractionation laws in nature and their geochemical and cosmochemical significance. *Geochimica et Cosmochimica Acta,* 66:1095-1104.

Zachos, J.C., Rohl, U., Schellenberg, S.A., Sluijs, A., Hodell, D.A., Kelly, D.C., Thomas, E., Nicolo, M., I, R., Lourens, L.J., McCarren, H., Kroon, D. (2005). Rapid acidification of the ocean during the Paleocene-Eocene thermal maximum. *Science,* 308:1611-1615.

Zuraida, R., Holbourn, A., Nurnberg, D., Kuhnt, W., Durkop, A., Erichsen, A. (2009). Evidence for Indonesian Throughflow slowdown during Heinrich events 3-5. Paleoceanography 24(2):PA001653.

APPENDICES

Appendix 2 (a) Column chemistry, isolation of Sr from interferences.

Figure A2a.1 Column calibration, using 1mg of coralline aragonite run through a Sr Spec™ column loaded with 150 μl of resin (see chapter two, section 2.2.3 for method). Data was collected on the Perkin Elmer Elan 6100 DRC ICP-MS. Arrows represent intensities that are larger than the scale given here; a maximum of 81,000 cps for ^{44}Ca.

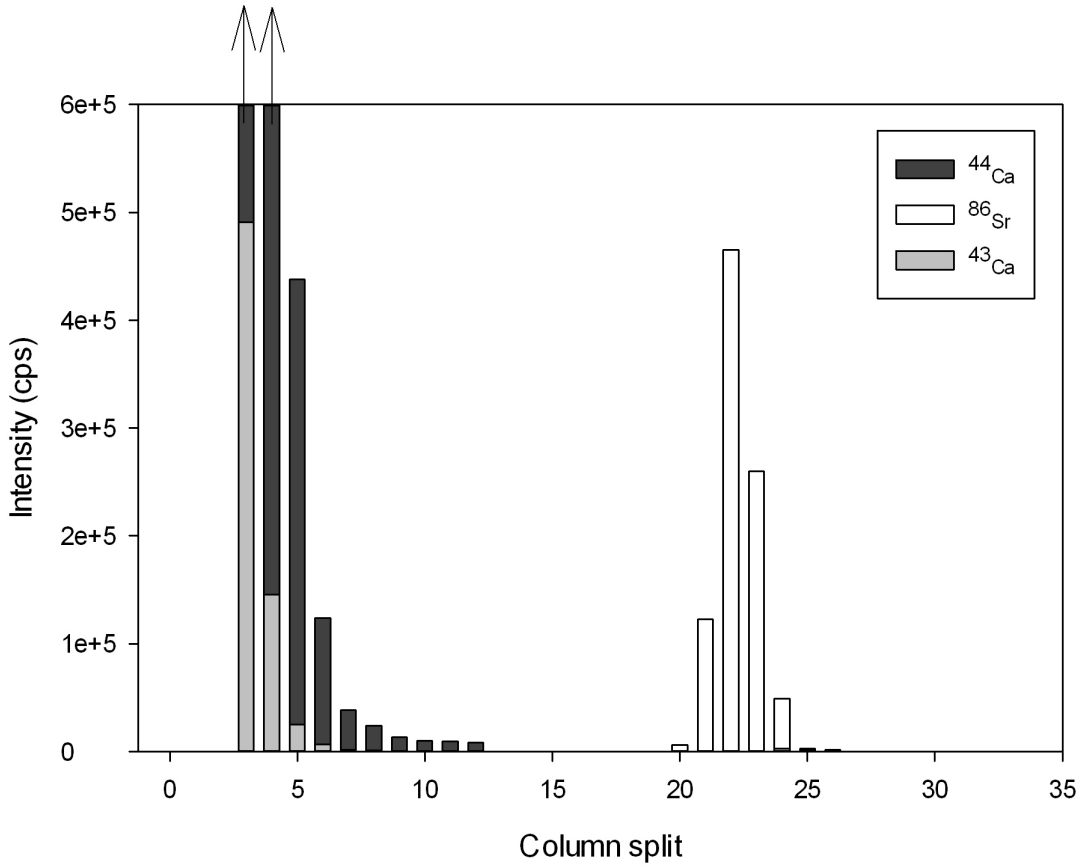

Overleaf: Figure A2a.2 Column calibration, using 1mg of foraminiferal shells. (a) Illustration of Ca contamination in samples from column chemistry. This became apparent during ionization of Sr on filaments for TIMS analysis; Ca present in the Sr column cut hindered Sr ionization therefore a new method for Sr separation was used (b) increasing the Ca elution see text in chapter two section 2.2.3 for new method. Elemental concentrations measured on a Thermo Element 2.

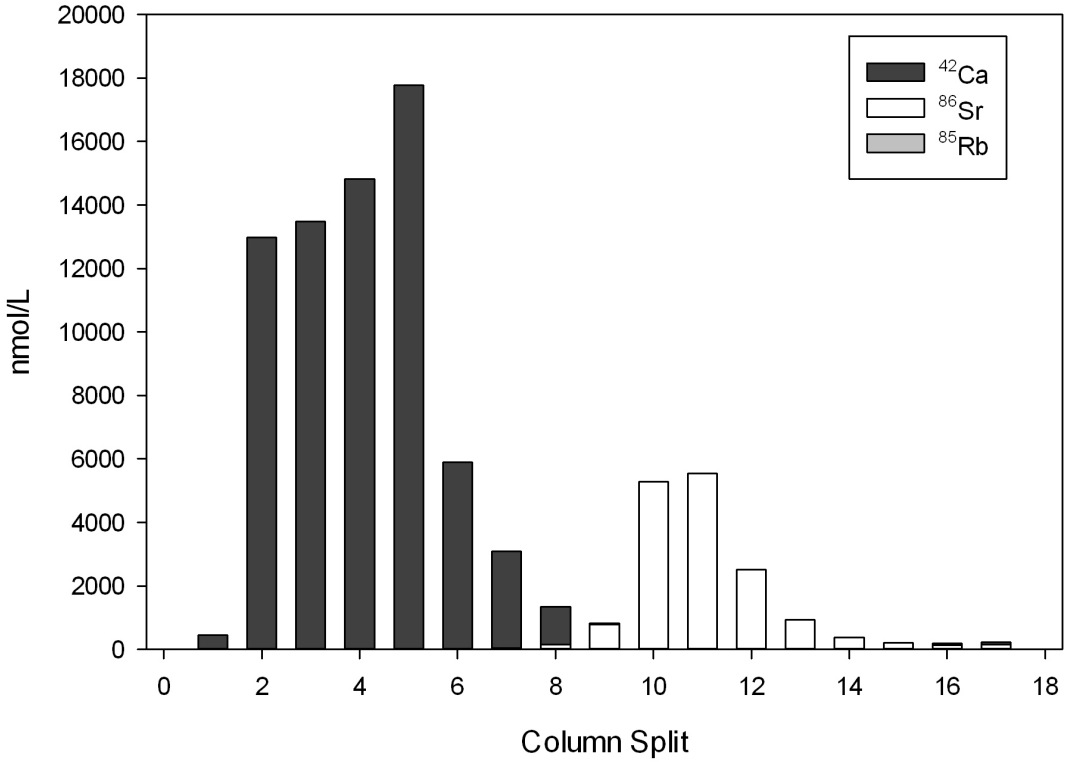
20000
18000
16000
14000
12000
10000
8000
6000
4000
2000
0
nmol/L
0
2
4
6
8
10
12
14
16
18
Column Split
42Ca
86Sr
85Rb

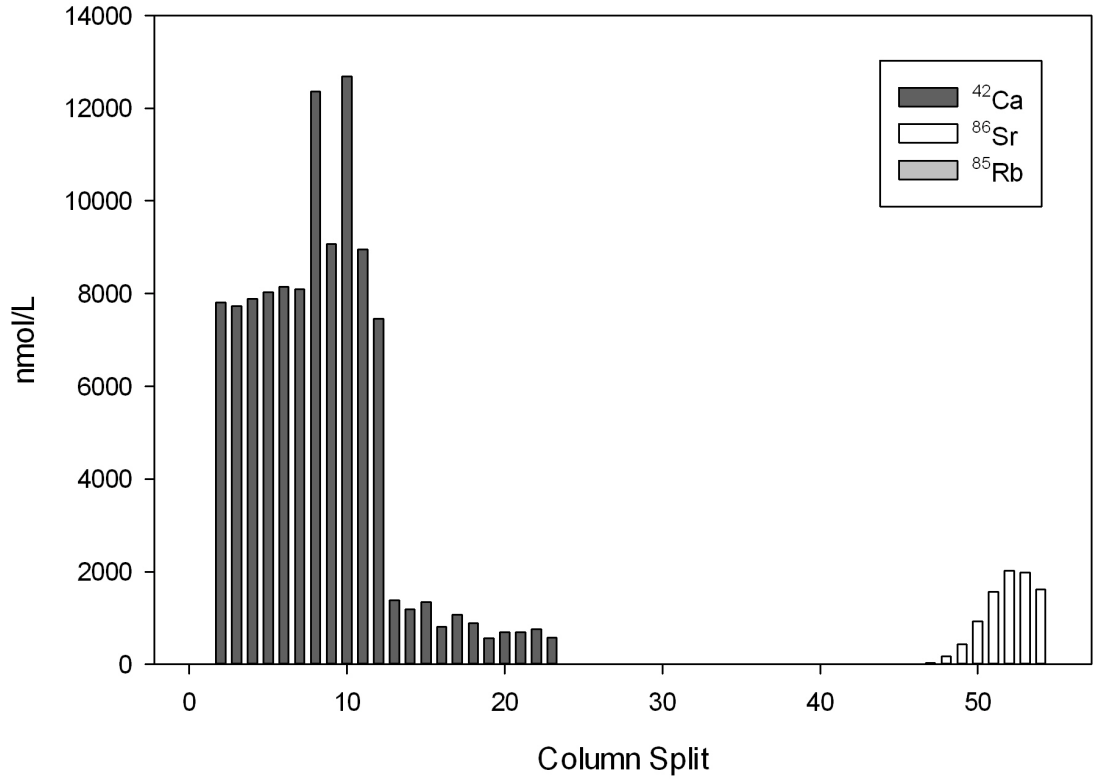
14000
12000
10000
8000
6000
4000
2000
0
nmol/L
0
10
20
30
40
50
Column Split
42Ca
86Sr
85Rb

Appendix 2 (b) Coral data

Coral species	Calcite Polymorph	Temperature ^{O}C*	Sr/Ca µmol/mol	$\delta^{88/86}Sr$ ‰	2.s.e ‰
Thicket Algae	High Mg calcite	26	3.45	0.174	0.009
Acropora Palmata	Aragonite	26	9.09	0.201	0.009
Porites Asteroides	Aragonite	26	8.69	0.201	0.011
Porites Porites	Aragonite	26	8.56	0.191	0.008
Madrepora Oculata	Aragonite	4	11.27	0.166	0.008

The five corals analysed in this study, from the suite collected by Robinson et al. (2004); four aragonite and one high-Mg calcite. The corals were cleaned and run for trace element analysis by T. Horner. The warm water corals were precipitated at ~26°C where as the cold water coral was precipitated at ~4°C, (Sea surface temperatures were obtained from the world ocean atlas 2005; http://www.nodc.noaa.gov/OC5/WOA05/pr_woa05.html).

Appendix A3 (a): Geographical locations, depth, SST's and variation of $\delta^{88/86}Sr$ in *G. sacculifer* from South Atlantic Core-top samples

Sample	Latitude	Longitude	Depth, m	Temp, °C	$^{88}Sr/^{86}Sr$	2.s.e.	$\delta^{88}Sr$, ‰	2.s.e. , ‰
1726-2	30.5 S	2.5 E	1006	19.5	8.37608	0.00026	0.104	0.031
1728-3	29.5 S	1.5 E	2887	19.87	8.37620	0.00005	0.119	0.006
6220-1	33.5 S	49.5 E	2277	20.34	8.37631	0.00030	0.131	0.036
6204-2	28.5 S	47.5 W	578	23.11	8.37627	0.00006	0.127	0.008
2106-1	27.5 S	46.5 W	502	23.22	8.37547	0.00007	0.032	0.008
2119-2	21.5 S	38.5 W	2958	25.47	8.37548	0.00016	0.033	0.019
2204-1	8.5 S	34.5 W	2080	27.58	8.37587	0.00010	0.079	0.012

Appendix A3 (b) $\delta^{88/86}Sr$ composition of test sizes for different species of foraminifera.

Size Fraction, μm	$^{88}Sr/^{86}Sr$	2.s.e.	$\delta^{88/86}Sr$, ‰	2.s.e. , ‰
	G. sacculifer			
250-355	8.37516	0.00028	-0.006	0.033
355-400	8.37556	0.00027	0.042	0.032
400-500	8.37626	0.00025	0.126	0.030
500-1000	8.37650	0.00019	0.154	0.022
	G. menardaii			
355-400	8.37262	0.00022	-0.309	0.026
400-500	8.37567	0.00016	0.056	0.019
500-1000	8.37754	0.00007	0.279	0.008
	G. ruber			
250-355	8.37534	0.00023	0.016	0.027
355-400	8.37422	0.00063	-0.118	0.075
400-500	8.37465	0.00013	-0.067	0.016
	G. aequlateralis			
250-355	8.37510	0.00082	-0.014	0.097
355-400	8.37496	0.00026	-0.029	0.031
500-1000	8.37499	0.00018	-0.026	0.022

Appendix 4 (a) Mg/Ca temperature data

Age, ky	Mg/Ca, mmol/mol	Temp °C	δT °C
Nq. dutertrei			
2.7	1.02	12.14	0.00
6.4	1.09	12.92	0.78
10.8	1.14	13.38	1.24
15.1	1.13	13.31	1.17
19.7	0.93	11.17	-0.97
24.3	1.13	13.25	1.11
28.7	1.16	13.58	1.44
34.3	1.08	12.77	0.63
38.9	1.24	14.35	2.21
43.8	1.21	14.01	1.87
G. conglobatus			
2.7	1.66	17.37	0.00
6.4	1.85	18.58	1.21
10.8	1.80	18.27	0.90
15.1	1.78	18.16	0.79
19.7	1.52	16.39	-0.98
24.3	1.51	16.33	-1.04
28.7	1.45	15.89	-1.48
34.3	1.53	16.48	-0.89
38.9	1.49	16.22	-1.16
43.8	1.58	16.85	-0.52
G. menardii			
2.7	0.90	10.79	0.00
6.4	0.93	11.15	0.36
10.8	0.89	10.69	-0.10
15.1	0.97	11.61	0.83
19.7	0.83	9.87	-0.92
24.3	0.84	10.00	-0.79
28.7	0.78	9.12	-1.67
34.3	0.80	9.43	-1.36
38.9	0.84	10.02	-0.77
43.8	0.76	8.90	-1.88

Table A4a.1; data is from Burton (unpublished). The temperatures were calculated using the formula given in Anand et al. (2003).

Appendix 4(b) Trace element data for clean and unclean foraminifera, and as sediment concentrations

Age	Clean				Unclean				Bulk sediment
ka	Mg ppm	Sr ppm	Fe ppm	Mn ppm	Mg ppm	Sr ppm	Fe ppm	Mn ppm	Mn* ppm
6.4	1830.8	1283.9	10.8	18.3	1963.0	1364.2	21.9	30.6	559
10.8	1475.4	1306.9	7.2	7.3	2281.3	1378.3	7.3	106.1	1943
15.1	1603.5	1341.3	7.2	5.5	1868.0	1398.6	129.5	185.3	2140
19.7	1370.4	1352.7	16.2	7.3	1665.5	1341.3	120.7	102.5	2469
24.3	1386.2	1352.7	10.8	38.4	1491.9	1295.4	7.3	66.6	1065
28.7	1281.1	1375.7	14.4	34.7	2054.0	1283.9	82.8	50.0	260
34.3	1317.5	1376.9	14.4	9.1	2529.2	1306.9	14.6	64.8	417
38.9	1389.5	1375.7	10.8	42.1	1686.2	1333.0	162.7	95.3	419
43.8	1256.4	1352.7	7.2	32.9	1520.8	1287.1	7.3	88.1	300
79	1599.4	1334.4	50.4	67.6	1843.2	1244.4	181.7	184.7	264
81.4	1669.6	1355.1	45.0	82.3	2008.5	1194.5	187.1	190.1	266
107.8	1684.5	1347.3	55.8	43.9	2459.0	1202.6	134.9	137.1	294
115.9	1647.3	1365.3	41.4	36.6	1711.0	1199.1	131.3	133.5	271
122.9	1797.7	1351.6	46.8	69.5	1657.2	1208.3	151.1	153.6	260
127.2	1899.4	1398.9	46.1	54.9	1971.3	1256.6	194.3	197.5	272
132	1958.9	1426.1	42.7	76.8	2628.4	1277.1	228.4	232.2	306
135.7	1921.7	1474.2	41.4	85.9	2301.9	1360.8	289.6	294.4	311
142.9	1855.6	1383.7	37.8	64.6	2301.9	1247.3	223.0	226.7	289

Table A4b.1 Trace element concentrations measured on tests of the foraminifera *G. menardii* for either cleaned (pale grey) or uncleaned (dark grey), which includes secondary Fe-Mn coatings (Burton, unpublished). *Bulk sediment data from Burton et al. (2010).

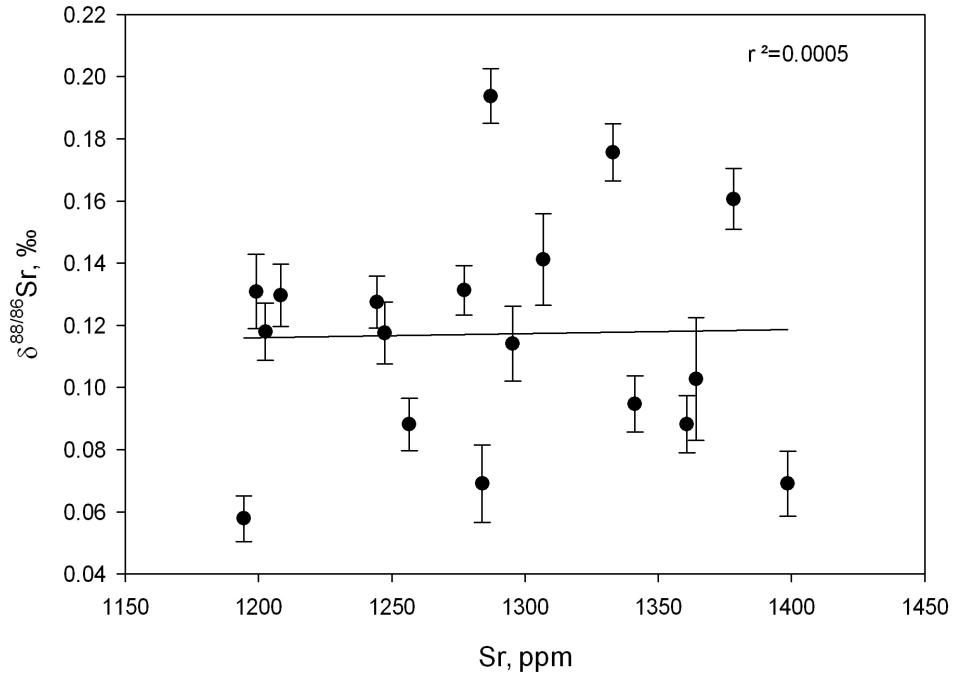

Figure A4b.1 Plot of Sr (ppm) in unclean foraminiferal shells (*G. menardii*; Burton, unpublished) with $\delta^{88/86}$Sr from a downcore record for G. ruber from ODP 758 A.

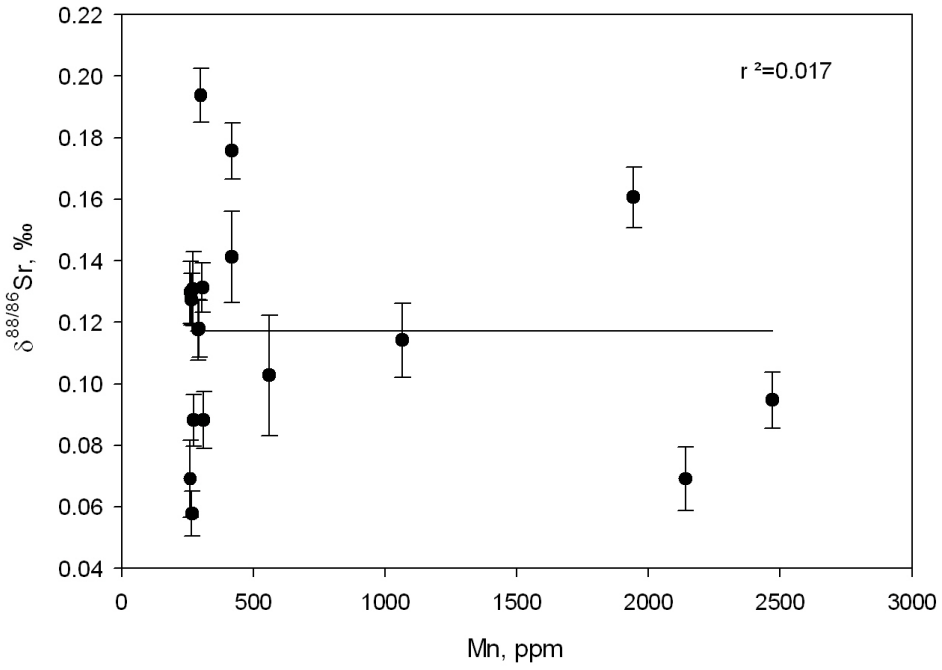

Figure A4b.2 Plot of Mn (ppm) in sediment (Burton et al., 2010) with $\delta^{88/86}$Sr from a downcore record for G. ruber from ODP 758 A.

Appendix 4 (c) Magnetic susceptibility for ODP 758 A

Age Ka†	Interpolated MS k (10-6) (CGS) †	Clean foraminiferal Sr§ ppm	Bulk sediment Sr* ppm
6	5.23	1283.9	756.34
10.33	6.2	1306.9	519.81
14.67	8.07	1341.3	572.36
19	9.77	1352.7	700.49
23.86	8.9	1352.7	661.72
28.71	10.53	1375.7	741.03
33.57	10.53	1376.9	710.40
38.43	6.7	1375.7	769.05
43.29	7.57	1352.7	812.69
78.71	5.57	1334.4	739.46
80	5.07	1355.1	851.12
106.67	13.63	1347.3	848.08
114.33	13.8	1365.3	984.58
122	11.53	1351.6	781.84
126.33	12.83	1398.9	728.55
130.67	14.4	1426.1	809.18
135	10.9	1474.2	826.87
142.2	11.53	1383.7	793.72

Table A4c.1 †data from Farrell and Janacek, (1991), § data from Burton (unpublished) * data from Burton et al. (2010).

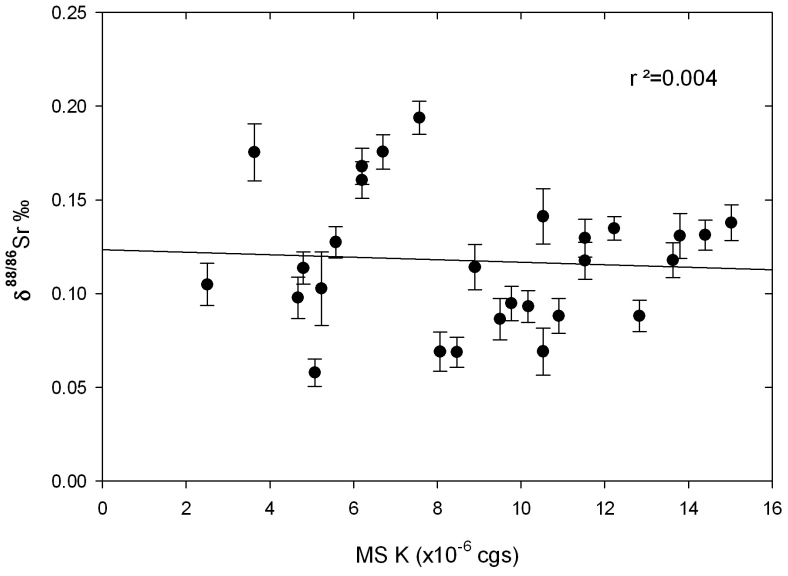

Figure A4c.1 Magnetic susceptibility data from Farrell and Janacek, (1991). They use magnetic susceptibility as a proxy for the presence of ash, however, there is no covariation of $\delta^{88/86}$Sr isotope composition suggesting that this isotope ratio is not strongly influenced by the presence of volcanic ash.

Appendix 5 (a): Composition of coccolithophore culture media (K, trace metals and f/2)

1. K Medium

Keller and Guillard 1985, Keller *et al.* 1987

To 950 mL of filtered natural seawater (sourced from Plymouth, aged for X years), the following components were added. The final volume was then topped up to 1 liter with filtered natural seawater (as above)

Component	Stock Solution	Quantity	Molar Concentration in Final Medium
$NaNO_3$	75.00 g /L dH_2O	1 mL	8.82 x 10^{-4} M
NH_4Cl	2.67 g/ L dH_2O	1 mL	5.00 x 10^{-5} M
Na_2 b-glycerophosphate*	2.16 g/ L dH_2O	1 mL	1.00 x 10^{-5} M
$Na_2SiO_3 \bullet 9H_2O$	15.35 g/ L dH_2O	1 mL	5.04 x 10^{-4} M
H_2SeO_3	1.29 mg/ L dH_2O	1 mL	1.00 x 10^{-8} M
Tris-base (pH 7.2)	121.10 g/ L dH_2O	1 mL	1.00 x 10^{-3} M
trace metal solution	(see recipe below)	1 mL	---
vitamin solution	(see recipe below)	0.5 mL	---

2. Trace Metal Solution

To prepare, the following components were dissolved in to 950 mL of Milli Q H_2O. The pH was adjusted up with sodium hydroxide until all the components were in solution. The final volume was made to 1 litre using Milli Q H_2O.

Component	Stock Solution	Quantity	Molar Concentration in

			Final Medium
$Na_2EDTA \cdot 2H_2O$	---	41.60g	1.11×10^{-4} M
$FeCl_3 \cdot 6\ H_2O$	---	3.150 g	1.17×10^{-5} M
$MnCl_2 \cdot 4H_2O$	---	0.178 g	9.00×10^{-7} M
$ZnSO_4 \cdot 7H_2O$	23.00 g/ L dH_2O	1 mL	8.00×10^{-8} M
$CoCl_2 \cdot 6\ H_2O$	10.00 g/ LdH_2O	1 mL	5.00×10^{-8} M
$Na_2MoO_4 \cdot 2H_2O$	6.3 g/L dH_2O	1 mL	2.60×10^{-8} M
$CuSO_4 \cdot 5H_2O$	2.50 g/ L dH_2O	1 mL	1.00×10^{-8} M

3. f/2 Vitamin Solution

(Guillard and Ryther 1962, Guillard 1975)

To prepare the vitamin solution, to 950 mL of Milli Q H_2O firstly dissolve the thiamine, then the primary stocks as indicated in the quantity column below. The final volume is made to 1 liter with dH_2O. This media was stored in either the refrigerator or freezer.

Component	PrimaryStock Solution	Quantity	Molar Concentration in Final Medium
thiamine · HCl (vit. B_1)	---	200 mg	2.96×10^{-7} M
biotin (vit. H)	0.1 g/ L dH_2O	10 mL	2.05×10^{-9} M
cyanocobalamin (vit. B_{12})	1.0 g/ L dH_2O	1 mL	3.69×10^{-10} M

Guillard, R.R.L. 1975. Culture of phytoplankton for feeding marine invertebrates. pp 26-60. *In* Smith W.L. and Chanley M.H (Eds.) *Culture of Marine Invertebrate Animals*. Plenum Press, New York, USA.

Guillard, R.R.L. and Ryther, J.H. 1962. Studies of marine planktonic diatoms. I. *Cyclotella nana* Hustedt and *Detonula confervacea* Cleve Can J Microbio. 8**,** 229-239.

Keller, M.D. and Guillard, R.R.L. 1985. Factors significant to marine diatom culture. pp. 113-6. *In* Anderson, D.M., White, A.W. and Baden, D.G. (eds.) *Toxic Dinoflagellates*. Elsevier, New York.

Keller, M.D., Selvin, R.C., Claus, W. and Guillard, R.R.L. 1987. Media for the culture of oceanic ultraphytoplankton. *J. Phycol.* **23:** 633-638.

Appendix 5 (b) All Sr/Ca data

Coccolithophore species	Temperature °C	Nutrients*	Repeat	Sr/Ca mmol/mol	K_{DSr}
Emiliania huxleyi	15	K	R1	2.72	-6.11
	15	K	R2	2.69	-6.14
	15	K/6	R1	2.83	-5.97
	15	K/6	R2	2.86	-5.94
	20	K	R1	2.90	-5.93
	20	K	R2	2.90	-5.93
	20	K/6	R1	3.11	-5.69
	20	K/6	R2	3.05	-5.75
	25	K	R1	3.08	-5.75
	25	K	R2	3.06	-5.77
	25	K/6	R1	3.18	-5.62
	25	K/6	R2	3.25	-5.55
Gephryocapsa oceanica	10	K	R1	2.02	-6.81
	10	K	R2	2.04	-6.79
	10	K/6	R1	2.20	-6.60
	10	K/6	R2	2.18	-6.62
	15	K	R1	2.32	-6.51
	15	K	R2	2.34	-6.49
	15	K/6	R1	2.48	-6.32
	15	K/6	R2	2.49	-6.31
	20	K	R1	2.67	-6.16
	20	K	R2	2.84	-5.99
	20	K/6	R1	2.82	-5.98
	20	K/6	R2	2.80	-6.00
	25	K	R1	2.96	-5.87
	25	K	R2	2.90	-5.93
	25	K/6	R1	3.08	-5.72
	25	K/6	R2	3.16	-5.64
Coccolithicus pelagicus	10	K	R1	2.40	-6.43
	10	K	R2	2.49	-6.34
	10	K/6	R1	2.64	-6.16
	10	K/6	R2	2.73	-6.07
	15	K	R1	2.93	-5.90
	15	K	R2	3.00	-5.83
	15	K/6	R1	3.00	-5.80
	15	K/6	R2	3.13	-5.67
	20	K	R1	3.17	-5.66
	20	K	R2	3.22	-5.61
	20	K/6	R1	3.30	-5.50
	20	K/6	R2	3.41	-5.39
Seawater medium		K		8.83	0
		K/6		8.80	0

*K media – see chapter 5 text and appendix 5.1 for details

Appendix 5 (c) stable isotope data for coccoliths

Species	Temperature	Nutrients	$\delta^{18}O_{carb}$	$\delta^{18}O_{sw}$	$\delta^{18}O_c - \delta^{18}O_{sw}$	$\delta^{18}O_{PDB}$ Eq calcite
G. oceanica	10	K	2.6	0.53	2.07	1.2254
	10	K	2.27	0.53	1.74	1.2254
	10	K/6	2.49	0.53	1.96	1.2254
	10	K/6	2.49	0.53	1.96	1.2254
C. pelagicus	10	K	1.32	0.53	0.79	1.2254
	10	K	1.33	0.53	0.8	1.2254
	10	K/6	1.22	0.53	0.69	1.2254
	10	K/6	1.15	0.53	0.62	1.2254
G. oceanica	15	K	1.12	0.53	0.59	0.1039
	15	K	1.65	0.53	1.12	0.1039
	15	K/6	1.67	0.53	1.14	0.1039
	15	K/6	1.45	0.53	0.92	0.1039
E. huxleyi	15	K	1.77	0.53	1.24	0.1039
	15	K	1.75	0.53	1.22	0.1039
	15	K/6	1.23	0.53	0.7	0.1039
	15	K/6	1.83	0.53	1.3	0.1039
C. pelagicus	15	K	0.19	0.53	-0.34	0.1039
	15	K	-0.36	0.53	-0.89	0.1039
	15	K/6	0.12	0.53	-0.41	0.1039
	15	K/6	0.14	0.53	-0.39	0.1039
G. oceanica	20	K	0.75	0.53	0.22	-0.9726
	20	K	0.52	0.53	-0.01	-0.9726
	20	K/6	0.74	0.53	0.21	-0.9726
	20	K/6	0.69	0.53	0.16	-0.9726
E. huxleyi	20	K	0.89	0.53	0.36	-0.9726
	20	K	0.88	0.53	0.35	-0.9726
	20	K/6	0.58	0.53	0.05	-0.9726
	20	K/6	0.86	0.53	0.33	-0.9726
C. pelagicus	20	K	-0.38	0.53	-0.91	-0.9726
	20	K	-0.5	0.53	-1.03	-0.9726
	20	K/6				
	20	K/6	-0.52	0.53	-1.05	-0.9726
G. oceanica	25	K	-0.59	0.53	-1.12	-2.0041
	25	K	-0.62	0.53	-1.15	-2.0041
	25	K/6	-0.08	0.53	-0.61	-2.0041
	25	K/6	-0.56	0.53	-1.09	-2.0041
E. huxleyi	25	K	-0.09	0.53	-0.62	-2.0041
	25	K	0.13	0.53	-0.4	-2.0041
	25	K/6				
	25	K/6	0.05	0.53	-0.48	-2.0041

$\alpha^{18}O$	$\delta^{13}C_{carb}$	$\delta^{13}C_{DIC}$	$\delta^{13}C_c - \delta^{13}C_{DIC}$	$\alpha^{13}C$	Biomass (mg)	Nr of days
1.033	0.77	0	0.77	1.001	17.425	25
1.0327	0.98	0	0.98	1.001	21.14	22
1.0329	0.65	0	0.65	1.001	16.3	18
1.0329	0.89	0	0.89	1.001	16.81	18
1.0317	-1.69	0	-1.69	0.998	22.355	19
1.0317	-1.95	0	-1.95	0.998	19.835	19
1.0316	-1.31	0	-1.31	0.999	24.805	19
1.0315	-1.07	0	-1.07	0.999	23.345	19
1.0315	-0.66	0	-0.66	0.999	16.82	7
1.0321	-0.14	0	-0.14	1	20.32	7
1.0321	-2.52	0	-2.52	0.997	15.48	11
1.0319	-0.32	0	-0.32	1	16.48	7
1.0322	-0.23	0	-0.23	1	18.61	11
1.0322	-0.31	0	-0.31	1	22.07	11
1.0316	0.2	0	0.2	1	28.72	13
1.0322	-0.27	0	-0.27	1	16.14	13
1.0306	-2.72	0	-2.72	0.997	24.505	13
1.03	-3.28	0	-3.28	0.997	20.69	13
1.0305	-1.89	0	-1.89	0.998	32.96	13
1.0305	-2.17	0	-2.17	0.998	31.68	13
1.0311	0.12	0	0.12	1	23.57	8
1.0309	0.63	0	0.63	1.001	26.06	8
1.0311	0.45	0	0.45	1	22.25	8
1.0311	0.22	0	0.22	1	21.05	6
1.0313	-0.19	0	-0.19	1	20.92	8
1.0313	-0.07	0	-0.07	1	21.25	7
1.031	0.12	0	0.12	1	25.88	7
1.0312	-0.42	0	-0.42	1	12.43	8
1.03	-3.44	0	-3.44	0.997	39.19	17
1.0298	-3.93	0	-3.93	0.996	18.51	17
					33.35	17
1.0298	-3.83	0	-3.83	0.996	37.23	17
1.0298	-0.88	0	-0.88	0.999	25.18	6
1.0297	-2.46	0	-2.46	0.998	12.25	6
1.0303	-0.71	0	-0.71	0.999	23.33	6
1.0298	0.89	0	0.89	1.001	25	6
1.0303	-1.75	0	-1.75	0.998	19.68	8
1.0305	-1.71	0	-1.71	0.998	18.55	8
					5.92	13
1.0304	-1.65	0	-1.65	0.998	14.34	8

G. rate (mass/No days)
0.7
1
0.9
0.9
1.2
1
1.3
1.2
2.4
2.9
1.4
2.4
1.7
2
2.2
1.2
1.9
1.6
2.5
2.4
2.9
3.3
2.8
3.5
2.6
3
3.7
1.6
2.3
1.1
2
2.2
4.2
2
3.9
4.2
2.5
2.3
0.5
1.8

Appendix A6 (a)
Graphical locations and lithological details of samples selected from the suite by Kisakürek et al, (2005)

Sample	Latitude (N)	Longitude (E)	Collection date	Lithology	Altitude (m)	Temperature (°C)	pH
Dudh Khosi and its tributaries							
S3*	27°47.42	86°43.12	12-Apr	FI (HHCS)	2876	4.8	6.81
A15*	27°47.37	86°43.07	14-Oct	FI (HHCS)	3050	6.3	7.65
S1	27°45.71	86°42.89	10-Apr	FI (HHCS)	2784	8.5	6.13
S4	27°46.92	86°43.38	12-Apr	FI (HHCS)	2843	8.7	5.98
S5	27°43.12	86°42.99	13-Apr	FI (HHCS)	2567	7.6	7.32
A13	27°51.01	86°46.76	12-Oct	FI (HHCS)	3809	8.1	8.11
A14	27°49.92	86°44.70	13-Oct	FI (HHCS)	3380	10.8	7.48
A18	27°43.07	86°43.01	15-Oct	FI (HHCS)	2600	9.4	7.3
Indrawati and its tributaries							
S6*	27°50.09	85°34.62	16-Apr	FI (HHCS)	822	na	7.5
A10*	27°50.11	85°34.63	01-Oct	FI (HHCS)	848	17.8	7.62
S7	27°50.85	85°34.76	16-Apr	FI (HHCS)	850	23.5	7.27
S8	27°50.57	85°33.38	16-Apr	FI (HHCS)	925	23.1	6.72
A11	27°50.32	85°34.62	01-Oct	FI (HHCS)	800	27.6	8.25
A12	na	na	01-Oct	FI (HHCS)	800	24.5	8.1
Tributaries of the Marsyangdi							
S17	28°38.71	84°04.19	27-Apr	TSS	3448	11.7	8.42
S18	28°39.80	84°01.66	27-Apr	TSS	3525	11.3	8.44
S19	28°41.97	83°59.42	28-Apr	TSS	3961	6.9	8.56
S20	28°36.65	84°09.31	30-Apr	TSS	3210	8.6	8.24
S21	28°33.85	84°11.15	01-May	TSS	2900	na	8.4
S22	28°31.79	84°18.62	02-May	FII (HHCS)	2359	14.9	8.28
S24	28°31.08	84°21.55	03-May	FII (HHCS)	1999	11.8	8.07
S25	28°23.16	84°24.10	04-May	FI (HHCS)	1087	16.9	6.53
Tributaries of the Modi Khola							
A1	28°31.12	83°54.45	20-Sep	TSS	3590	1.7	8.3
A2	28°29.52	83°53.39	21-Sep	TSS	3082	11.2	8.32
A3	28°28.39	83°52.42	21-Sep	TSS and FII	2540	14.9	8.32
Tributaries of the Bhote Khosi							
S9	27°52.68	85°55.01	17-Apr	LHS	825	17.9	7.76
S10	27°52.54	85°53.88	17-Apr	LHS	1228	19.7	8.27
S11	27°51.34	85°52.60	17-Apr	LHS	1026	8.3	8.15
S12	27°49.76	85°51.98	17-Apr	LHS	966	21.3	7.77
A6	27°49.77	85°52.01	28-Sep	LHS	972	21.8	8.54
A7	27°53.01	85°54.91	29-Sep	LHS	1225	17.5	8.2
A8	27°52.79	85°54.50	29-Sep	LHS	1283	21.4	8.62
A9	27°51.34	85°52.60	29-Sep	LHS	1060	22.8	8.6
Likhu Khola							
S26	27°53.87	85°13.15	08-May	FI (HHCS)	572	29.1	8.2

Appendix 6 (b) PHREEQC calculations and mineral saturation states

PHREEQC is a computer program that is designed to perform a wide variety of low-temperature aqueous geochemical calculations using a basis of thermodynamic equations. For the purposes of my project I used PHREEQC to calculate mineral saturation states (Pankhurst and Appelo, 1999).

For a given reaction (A6.1) the equilibrium constant (K_{eq}) is given by Equation A6.2 below;

$$aA + bB \leftrightarrow cC + dD \qquad [A6.1]$$

$$K_{eq} = \frac{[C]^c[D]^d}{[A]^a[B]^b} \qquad [A6.2]$$

At equilibrium K_{eq} is equal to a Gibbs free energy (ΔG) of zero and are related by Equation A6.3;

$$\Delta G = -RT \ln K_{eq} \qquad [A6.3]$$

Where R is the gas constant and T is the temperature.

PHREEQC calculates the saturation index (SI) of mineral phases via the input of measured elemental concentration data and in-situ measurements such as pH and temperature. The SI is calculated from the predicted K_{eq} from Equation A6.4 where IAP is the ion activity product.

$$\mathrm{SI} = \log_{10}\left(\frac{\mathrm{IAP}}{\mathrm{K_{eq}}}\right) \qquad [A6.4]$$

The SI is give on a log scale where SI = 0 at equilibrium (at saturation) of the mineral with solution, negative values (<0) are undersaturated and positive values (>0) are oversaturated with respect to the mineral in solution. Overall uncertainties are on the order of 1-2 SI units (Stefansson et al., 2001). PHREEQC relies upon elemental data and thermodynamic interpretations therefore it has to be recognised that perhaps not all the mineral phases predicted by PHREEQC will be present in the river catchments themselves.

For this project elemental data (in ppm) was inputted into the PHREEQC program as well as pH, temperature and $^{87}Sr/^{86}Sr$ data from Kisakürek (2005)

	Sample	**A1**	**A2**	**A3**	**A6**
	Lithology	**TSS HA**	**TSS HA**	**TSS FII HA**	**LHS**
Mineral phase	**Chemical formula**				
Al(OH)3(a)	$Al(OH)_3$	-1.79	-2.39	-2.72	-2.85
Albite	$NaAlSi_3O_8$	-6.27	-6.3	-5.69	-6.12
Alunite	$KAl_3(SO_4)_2(OH)_6$	-6.29	-11.38	-11.45	-14.67
Anhydrite	$CaSO_4$	-2.68	-3.66	-3.11	-4.14
Anorthite	$CaAl_2Si_2O_8$	-5.52	-5.64	-5.37	-5
Aragonite	$CaCO_3$	-0.31	-0.13	0.04	0.33
Ca-Montmorillonite	$Ca_{0.165}Al_{2.33}Si_{3.67}O_{10}(OH)_2$	-1.52	-2.71	-2.38	-3.05
Calcite	$CaCO_3$	-0.15	0.03	0.2	0.48
Celestite	$SrSO_4$	-3.12	-3.89	-3.86	-5.43
Chalcedony	SiO_2	-1.12	-1.05	-0.74	-0.84
Chlorite(14A)	$Mg_5Al_2Si_3O_{10}(OH)_8$	-7.74	-6.05	-7.7	1.22
Chrysotile	$Mg_3Si_2O_5(OH)_4$	-7.08	-5.54	-6.15	-0.8
Dolomite	$CaMg(CO_3)_2$	-1.13	-0.77	-0.99	0.89
Gibbsite	$Al(OH)_3$	1.13	0.43	0.07	-0.13
Gypsum	$CaSO_4{:}2H_2O$	-2.42	-3.41	-2.87	-3.91
Halite	NaCl	-11.53	-13.43	-11.57	-11.56
Illite	$K_{0.6}Mg_{0.25}Al_{2.3}Si_{3.5}O_{10}(OH)_2$	-1.78	-3.14	-2.9	-2.98
K-feldspar	$KAlSi_3O_8$	-2.96	-3.69	-2.97	-3.05
K-mica	$KAl_3Si_3O_{10}(OH)_2$	4.79	2.71	2.72	2.29
Kaolinite	$Al_2Si_2O_5(OH)_4$	1.76	0.49	0.36	-0.23
Quartz	SiO_2	-0.61	-0.58	-0.29	-0.42
Sepiolite	$Mg_2Si_3O_{7.5}OH{:}3H_2O$	-5.87	-5.11	-5.16	-2.02
Sepiolite(d)	$Mg_2Si_3O_{7.5}OH{:}3H_2O$	-8.1	-7.63	-7.79	-4.84
SiO2(a)	SiO_2	-2.04	-1.93	-1.62	-1.69
Strontianite	$SrCO_3$	-1.97	-1.63	-1.99	-2.28
Talc	$Mg_3Si_4O_{10}(OH)_2$	-5.96	-4.12	-4.08	1.18
$\delta^{88/86}$Sr,‰		0.3136	0.3475	0.3542	0.3784

	Sample	**A7**	**A8**	A9	**A10**
	Lithology	**LHS**	**LHS**	**LHS**	**HHCS LA**
Mineral phase	**Chemical formula**				
Al(OH)3(a)	$Al(OH)_3$	-2.26	-3.37	-3.19	-1.48
Albite	$NaAlSi_3O_8$	-5.42	-6.16	-6.23	-4.38
Alunite	$KAl_3(SO_4)_2(OH)_6$	-9.79	-13.77	-15.8	-7.4
Anhydrite	$CaSO_4$	-3.46	-2.8	-4.06	-4.5
Anorthite	$CaAl_2Si_2O_8$	-4.86	-5.53	-5.34	-4.46
Aragonite	$CaCO_3$	-0.59	0.76	0.68	-1.92
Ca-Montmorillonite	$Ca_{0.165}Al_{2.33}Si_{3.67}O_{10}(OH)_2$	-1.43	-3.81	-3.72	0.71
Calcite	$CaCO_3$	-0.44	0.91	0.82	-1.77
Celestite	$SrSO_4$	-4.44	-3.95	-5.36	-5.07
Chalcedony	SiO_2	-0.74	-0.72	-0.81	-0.58
Chlorite(14A)	$Mg_5Al_2Si_3O_{10}(OH)_8$	-2.96	2.36	2.48	-11.94
Chrysotile	$Mg_3Si_2O_5(OH)_4$	-3.91	0.54	0.36	-10.21
Dolomite	$CaMg(CO_3)_2$	-0.99	1.81	1.68	-4.37
Gibbsite	$Al(OH)_3$	0.5	-0.65	-0.48	1.28
Gypsum	$CaSO_4{:}2H_2O$	-3.22	-2.56	-3.83	-4.26
Halite	NaCl	-11.58	-11.62	-11.34	-10.89
Illite	$K_{0.6}Mg_{0.25}Al_{2.3}Si_{3.5}O_{10}(OH)_2$	-1.72	-3.45	-3.44	-0.44
K-feldspar	$KAlSi_3O_8$	-2.54	-2.83	-3.05	-2.15
K-mica	$KAl_3Si_3O_{10}(OH)_2$	4.03	1.46	1.59	5.98
Kaolinite	$Al_2Si_2O_5(OH)_4$	1.22	-1.05	-0.89	3.09
Quartz	SiO_2	-0.3	-0.3	-0.39	-0.15
Sepiolite	$Mg_2Si_3O_{7.5}OH{:}3H_2O$	-3.76	-0.92	-1.23	-7.72
Sepiolite(d)	$Mg_2Si_3O_{7.5}OH{:}3H_2O$	-6.46	-3.73	-4.08	-10.42
SiO2(a)	SiO_2	-1.6	-1.58	-1.65	-1.45
Strontianite	$SrCO_3$	-2.86	-1.71	-1.95	-3.79
Talc	$Mg_3Si_4O_{10}(OH)_2$	-1.79	2.74	2.42	-7.78
$\delta^{88/86}$Sr,‰		0.3379	0.2074	0.0499	0.3904

	Sample **Lithology**	**A11** **HHCS** **LA**	**A12** **HHCS** **LA**	**A13** **HHCS** **HA**	**A14** **HHCS** **HA**
Mineral phase	**Chemical formula**				
Al(OH)3(a)	$Al(OH)_3$	-2.72	-2.82	-2.24	-1.43
Albite	$NaAlSi_3O_8$	-2.72	-2.9	-4.72	-4.21
Alunite	$KAl_3(SO_4)_2(OH)_6$	-12.74	-13.4	-14.19	-7.41
Anhydrite	$CaSO_4$	-3.94	-4.49	-6.05	-5.4
Anorthite	$CaAl_2Si_2O_8$	-3.8	-4.44	-5.59	-5.45
Aragonite	$CaCO_3$	-0.57	-0.67	-1.38	-2.89
Ca-Montmorillonite	$Ca_{0.165}Al_{2.33}Si_{3.67}O_{10}(OH)_2$	-0.27	-0.4	-0.66	1.11
Calcite	$CaCO_3$	-0.43	-0.53	-1.22	-2.73
Celestite	$SrSO_4$	-4.4	-4.92	-6.85	-5.84
Chalcedony	SiO_2	-0.1	-0.06	-0.54	-0.49
Chlorite(14A)	$Mg_5Al_2Si_3O_{10}(OH)_8$	-0.92	-3.59	-11.56	-14.76
Chrysotile	$Mg_3Si_2O_5(OH)_4$	-2.2	-3.61	-8.85	-11.79
Dolomite	$CaMg(CO_3)_2$	-1.16	-1.45	-3.61	-5.92
Gibbsite	$Al(OH)_3$	-0.06	-0.13	0.61	1.39
Gypsum	$CaSO_4{:}2H_2O$	-3.73	-4.27	-5.79	-5.15
Halite	NaCl	-9.13	-9.79	-11.12	-10.29
Illite	$K_{0.6}Mg_{0.25}Al_{2.3}Si_{3.5}O_{10}(OH)_2$	-0.6	-0.83	-1.77	-0.23
K-feldspar	$KAlSi_3O_8$	-0.98	-1.05	-2.73	-2.12
K-mica	$KAl_3Si_3O_{10}(OH)_2$	4.53	4.3	4.01	6.2
Kaolinite	$Al_2Si_2O_5(OH)_4$	1.37	1.3	1.85	3.53
Quartz	SiO_2	0.3	0.34	-0.07	-0.02
Sepiolite	$Mg_2Si_3O_{7.5}OH{:}3H_2O$	-1.93	-2.71	-6.36	-8.33
Sepiolite(d)	$Mg_2Si_3O_{7.5}OH{:}3H_2O$	-4.9	-5.59	-8.79	-10.84
SiO2(a)	SiO_2	-0.93	-0.91	-1.44	-1.38
Strontianite	$SrCO_3$	-2.38	-2.44	-3.44	-4.59
Talc	$Mg_3Si_4O_{10}(OH)_2$	1.34	-0.05	-6.48	-9.27
$\delta^{88/86}$Sr,‰		0.2743	0.2944	0.342	0.3617

	Sample	**A15 HHCS HA**	**A18 HHCS HA**
	Lithology		
Mineral phase	**Chemical formula**		
Al(OH)3(a)	$Al(OH)_3$	-0.64	-1.16
Albite	$NaAlSi_3O_8$	-3.98	-5.35
Alunite	$KAl_3(SO_4)_2(OH)_6$	-2.74	-4.15
Anhydrite	$CaSO_4$	-3.73	-4.17
Anorthite	$CaAl_2Si_2O_8$	-3.75	-5.71
Aragonite	$CaCO_3$	-2.06	-3.02
Ca-Montmorillonite	$Ca_{0.165}Al_{2.33}Si_{3.67}O_{10}(OH)_2$	2.47	0.65
Calcite	$CaCO_3$	-1.9	-2.86
Celestite	$SrSO_4$	-4.5	-4.91
Chalcedony	SiO_2	-0.67	-0.78
Chlorite(14A)	$Mg_5Al_2Si_3O_{10}(OH)_8$	-13.63	-17.82
Chrysotile	$Mg_3Si_2O_5(OH)_4$	-12	-13.98
Dolomite	$CaMg(CO_3)_2$	-4.91	-6.58
Gibbsite	$Al(OH)_3$	2.23	1.68
Gypsum	$CaSO_4{:}2H_2O$	-3.47	-3.91
Halite	NaCl	-10.88	-11.24
Illite	$K_{0.6}Mg_{0.25}Al_{2.3}Si_{3.5}O_{10}(OH)_2$	1.23	-0.94
K-feldspar	$KAlSi_3O_8$	-1.55	-3.06
K-mica	$KAl_3Si_3O_{10}(OH)_2$	8.41	5.83
Kaolinite	$Al_2Si_2O_5(OH)_4$	4.85	3.51
Quartz	SiO_2	-0.18	-0.31
Sepiolite	$Mg_2Si_3O_{7.5}OH{:}3H_2O$	-8.59	-10.23
Sepiolite(d)	$Mg_2Si_3O_{7.5}OH{:}3H_2O$	-10.96	-12.7
SiO2(a)	SiO_2	-1.57	-1.68
Strontianite	$SrCO_3$	-4.07	-5.02
Talc	$Mg_3Si_4O_{10}(OH)_2$	-9.9	-12.07
$\delta^{88/86}$Sr,‰		0.3647	0.3862

Figure A6b.1 PHREEQC calculation of saturation index versus stable strontium isotopes for carbonate minerals

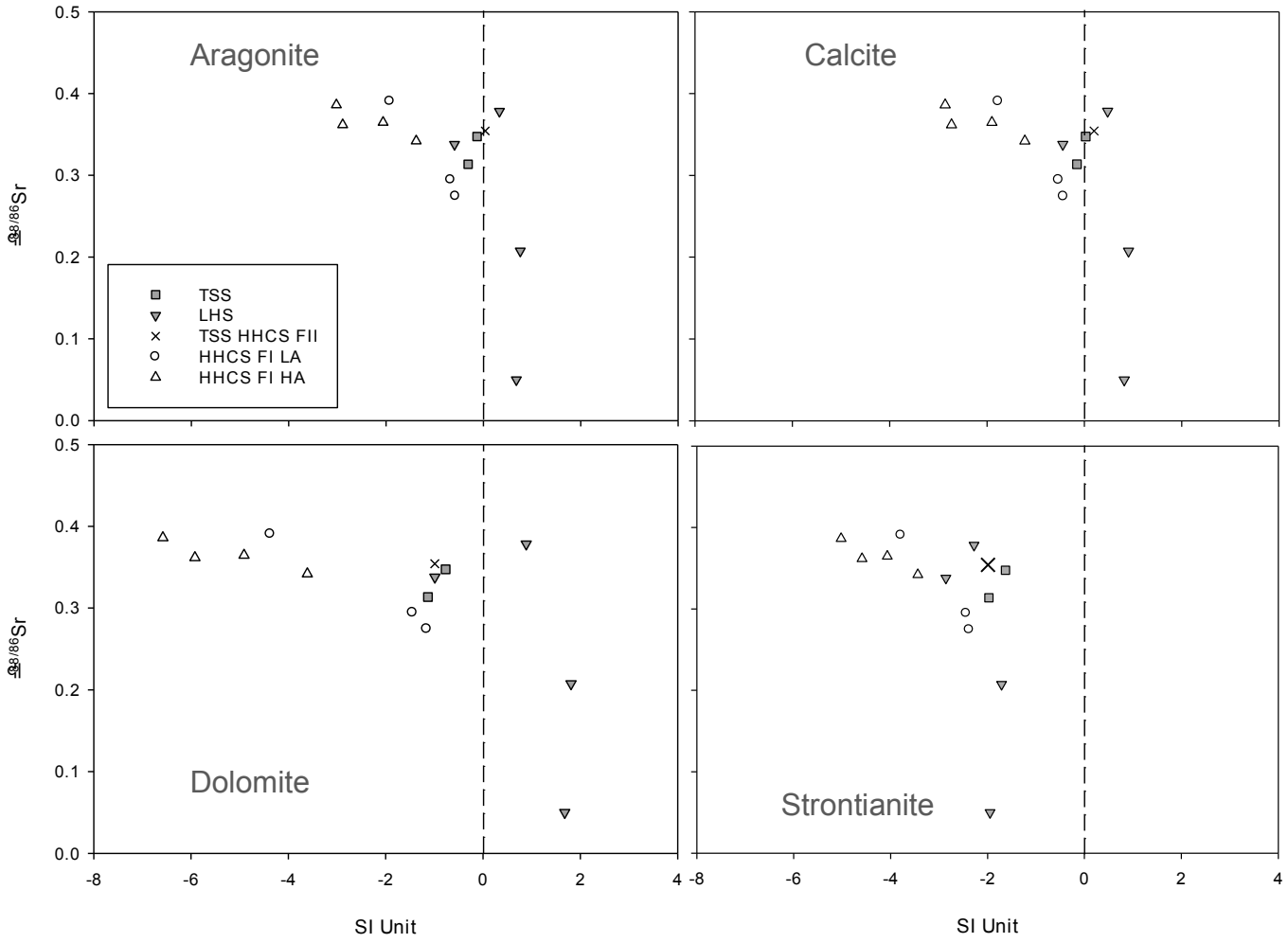

Figure A6b.2 PHREEQC calculation of saturation index versus stable strontium isotopes for Al- bearing silicate minerals and clays

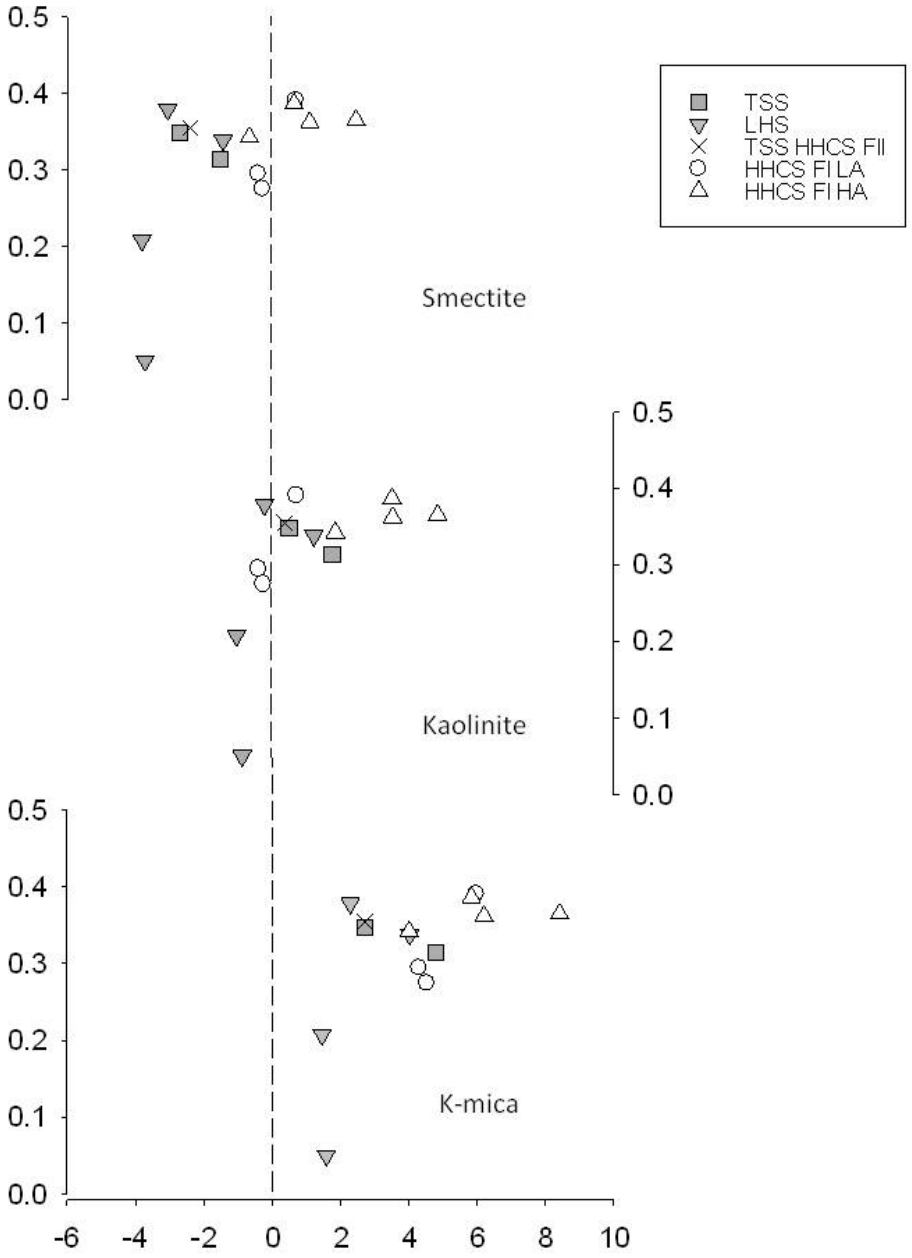

Figure A6b.3 PHREEQC calculation of saturation index versus stable strontium isotopes for Mg- bearing silicate minerals and clays

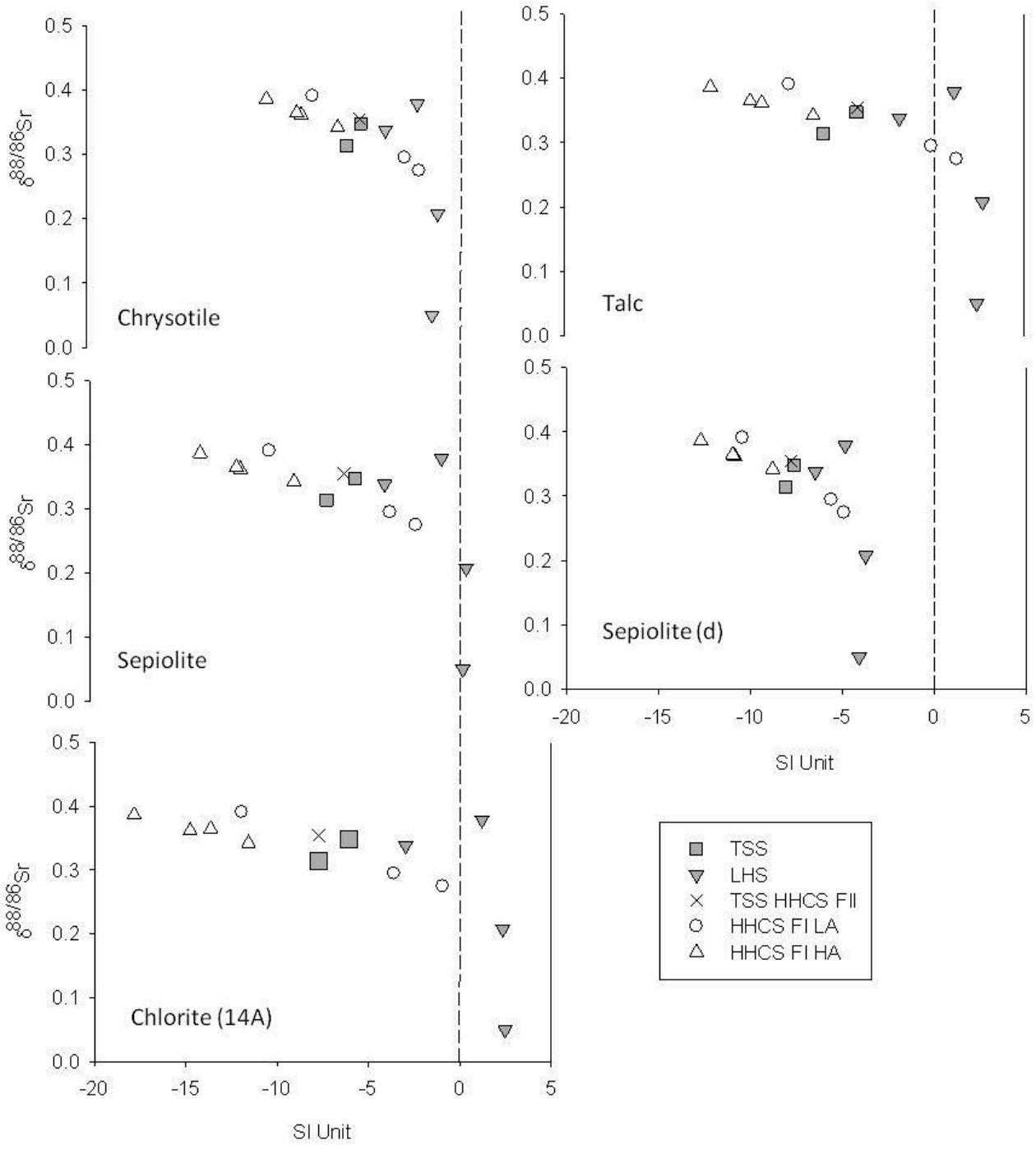

Appendix 7: Calcite precipitation experiments

In 2009, attempts were made to establish the equilibrium fractionation of $\delta^{88/86}Sr$ in inorganically precipitated calcite at the Laboratoire des Mécanismes et Transferts en Géologie (LMTG) at the Université de Paul Sabatier in Toulouse, France, under the supervision of Dr Eric Oelkers and Dr Therese Flaathen-Loe.

Due to personal reasons I was unable to complete the work but attempts were made to follow up the preliminary experiments by Dr Allison Stephenson-Haus. The experimental set up she used is summarised in Figure A8.1, and the experiments she performed in Table A7.1 and is as follows:

Calcite precipitation experiments were performed on the calcite seeds in a mixed flow polypropylene reactor system at pH 9.1. The electrode used was regularly calibrated with NBS standards at pH 4.01, 6.86 and 9.22, with an average error of less than 0.05 pH units.

Calcite seed was placed in a circular Teflon reactor (30mL volume) and once the experiment started, was continuously stirred with floating Teflon stirring bars. Calcite precipitation was induced by using two Gilson peristaltic pumps to inject simultaneously two distinct solutions into the reactor; firstly a 5L $NaHCO_3$-Na_2CO_3 mixed solution and secondly a 5L $CaCL_2$ solution doped with $SrCl_2$ at identical flow rates. The solution left the reactor through a 2.5 μm filter. No additional filtering was performed on outlet fluid samples obtained from the reactor before chemical analysis. Each experiment was performed on a single batch of calcite seed powder. The computer code PHREEQC (Parkhurst and Appelo, 1999) was used to calculate saturation states (Ω) which were close to 2.88 (for calcite) for each experiment. The experiments were performed at 4, 25 or 40 °C. The concentration of Ca was kept the same but the Sr concentration was varied from 0 to 150, 300 and 600ppb.The Ca and Sr content of the inlet and outlet solutions was determined using atomic adsorption spectroscopy (Perkin Elmer Zeeman 5000).

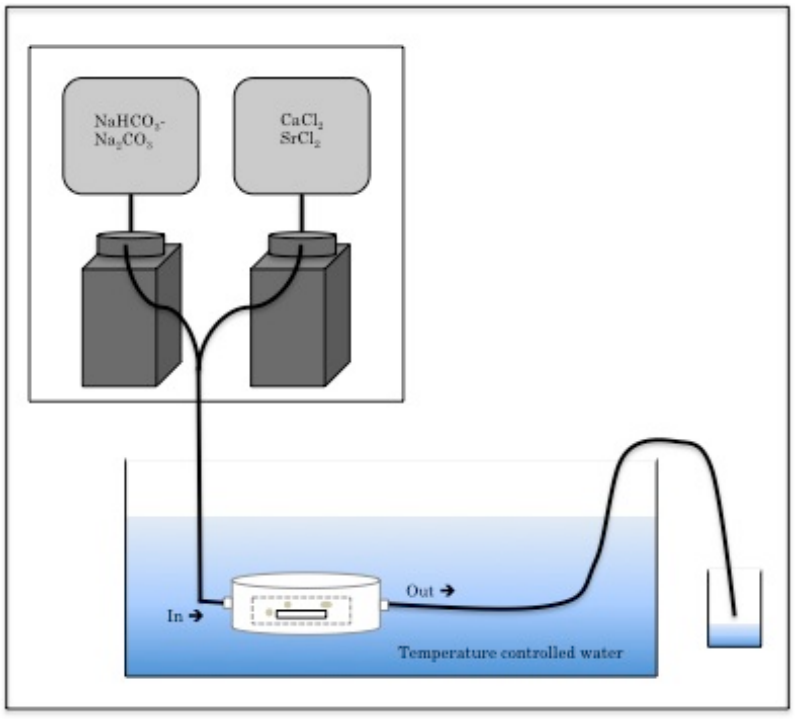

Figure A8.1 Schematic of the calcite precipitation experiments. The aqueous output was collected for analysis after being acidified with HCl.

All experiments performed are summarised in Table A8.1 below.

name	**[Sr]** estimate	**Sample name**	**sample**	**date**
1i		beta1-4	initial	27.01.10
1ss		beta1-4	steady sate	16.02.10
2i		gamma1-4	intial	27.01.10
2ss		gamma1-4	steady sate	15.02.10
3i	150	beta2-4 (150 ppb)	initial	16.03.10
3ss	60	beta2-4 (150 ppb)	steady state	03.04.10
4i1	600	beta 2-4 (600 ppb Sr)	initial	25.02.10
4ss1	400	beta2-4 (600 ppb)	steady state	09.03.10
4i2	400	beta2-4	initial	
4ss2	400	beta2-4	steadystate	24.03.10
5i1	0	gamma2-4 (no Sr)	initial	16.03.10
5ss1	0	gamma2-4	steady state	24.03.10
5i2	300	gamma (300 ppb Sr)	initial	25.02.10
5ss2	150	gamma2-4	steady state	03.04.10
6i	300	A1-25	initial	
6ss	150	A1-25	steady state	
		B2-25a	initial	11.12.09
7i	300	A2-25a	initial	11.12.09
7ss	150	A2-25b	steady state	16.12.09
8i	300	Br5-25	initial	24.02.10
8m	150	Br5-25		01.03.10
8ss	150	B5-25	steady state	10.03.10
9i	300	At5-25	initial	24.02.10
9m	150	At5-25		01.03.10
9ss	150	A5-25	steady state	10.03.10
10i	150	C6-25	initial	24.02.10 (11.03.10)
10m	150	C6-25		02.03.10
10ss	150	C6-25	steady state	10.03.10
		At5-40 (control)	initial	18.03.10
		At5-40 (control)	steady state	24.03.10
		C5-40 (control)	initial	18.03.10
		C5-40 (control)	steady state	24.03.10
12i1	150	Br5-40 (150)	initial	18.03.10
12ss1	60	Br5-40 (150)	steady state	24.03.10
12i2	300	Br5-40 (150)		02.02.10
12ss2	150	Br5-40 (150)	end	09.02.10
13i	300	At4-40		02.02.10
13ss	150	At4-40	end	09.02.10
14i	300	Br4-40		02.02.10
14ss	150	Br4-40	end	09.02.10
15i	300	BA3-40	initial	19.01.10
15mB	150	B3-40	middle	21.01.10
15mA	150	A3-40	middle	20.01.10
15ssB	150	B3-40	steady state	28.01.10
16i1	150	D5-40 (150 ppb)	initial	18.03.10
16ss1	60	D5-40 (150 ppb)	steady state	24.03.10
16i2	600	D5-40 (600 ppb)	initial	
16ss2	300	D5-40 (600 ppb)	steady state	
17i	300	A2-40	inflow initial	25.11.09

17ss	150	A2 40	steady state	02.12.09
18i	300	B40-1	initial inflow	14.11.09
18ss	150	B40-1	steady state	28.11.09
19i	300	At5-40	inflow initial	
19ss	150	At5-40	steady state	
20i	300	C5-40	initial inflow	
20ss	150	C5-40	steady state	

Ah, mastery... what a profoundly satisfying feeling when one finally gets on top of a new set of skills... and then sees the light under the new door those skills can open, even as another door is closing.

Gail Sheehy